MATHEMATICAL MODELLING OF DEFORMATION AND MICROSTRUCTURE EVOLUTION DURING HOT ROLLING OF AA5083 ALUMINUM ALLOY

by

HANY AHMED

B. Sc., The American University in Cairo, Egypt, 1999

M.Sc., The American University in Cairo, Egypt, 2001

A THESIS SUBMITTED IN PARTIAL FULFILMENT OF
THE REQUIREMENTS FOR THE DEGREE OF

DOCTOR OF PHILOSOPHY

in

THE FACULTY OF GRADUATE STUDIES

(Materials Engineering)

THE UNIVERSITY OF BRITISH COLUMBIA

October 2005

Abstract

Hot rolling, a critical process in the manufacturing of aluminum sheet, can significantly impact the final properties of the cold rolled sheet. The control of the thermo-mechanical conditions during hot rolling and the resulting microstructure of aluminum sheets is critical in order to determine the final sheet properties. Several complexities are associated with controlling microstructure evolution especially during multi-pass hot rolling. Firstly, the microstructure evolution is a result of the complex interaction between the deformation history that the material experiences during rolling and the resulting material changes that occur during rolling. Moreover, the multi-pass aspect of the rolling process adds to the complexity of the process as the prior thermo-mechanical history can influence the material stored energy and response to subsequent deformation. This calls for further understanding of the way the stored energy is accumulated in situations where various recrystallizations levels may occur in the inter-pass region to be able to follow and track microstructure changes.

In this research, a comprehensive mathematical model has been developed to predict through-thickness thermal and deformation history of AA5083 aluminum sheet undergoing single-pass and multi-pass hot rolling using the commercial finite element package, ABAQUS. A physically based internal state variable microstructure model was employed to calculate the material stored energy and subsequent recrystallization kinetics as a function of deformation conditions. A new more physically-based approach to account for the non-isothermal cooling in the inter-pass region was applied to capture and track the accumulation of the material stored energy during multi-pass hot rolling.

The model has been extensively validated against experimental measurements conducted using Corus' pilot scale rolling facility located in IJmuiden, the Netherlands for AA5083 aluminum alloy sheet under a wide variety of industrially relevant single-pass and multi-pass hot rolling conditions. The model was able to predict the

temperature, strain profile and the rolling load reasonably well for both single-pass and multi-pass rolling cases. The model was able to predict the fraction recrystallized relatively well for all the cases. The model predicted recrystallized grain size was in reasonable agreement with the measurements for single-pass rolling cases while a constant deviation of ~ 11 μm was observed for multi-pass ones. The validated model was further utilized to determine the sensitivity of the predicted fraction recrystallized to changes in the rolling process. The model was also applied to achieve further understanding and optimization of the rolling process such as the way the strain is partitioned. The results indicate the merit and usefulness of the model as a powerful tool to further understand the complex interactions between the thermo-mechanical and microstructure changes during rolling and thus achieve process optimization and control.

TABLE OF CONTENTS

List of Tables

List of Figures

List of Symbols

Latin Symbols	Description	Units
A	Material constant in the hyperbolic sin equation	---
b	Burgers vector	m
$\lfloor C^e \rfloor$	The elemental heat capacitance matrix	J $kg^{-1}K^{-1}$
C_p	Specific heat capacity	J kg^{-1} $°C^{-1}$
D	Diffusion coefficient	---
d_1	Grain length in the y-direction	μm
d_2	Grain width in the x-direction	μm
d_o	Initial grain size	μm
d_{rex}	Recrystallized grain size	μm
E_ρ	Dislocation network energy	---
E_δ	Stored energy in the subgrain boundary	---
$[F]$	Force matrix per unit volume	N m^{-3}
$\dot{G}$	Growth rate	---
G	Shear modulus	Pa
h	Interface heat transfer coefficient	W m^{-2} $°C^{-1}$
k	Thermal conductivity	W m^{-1} K^{-1}
$\lfloor K^e \rfloor$	The elemental heat conduction matrix	W m^{-1} K^{-1}
L_c	Length of dislocation annihilated	μm
M	Taylor Factor	---
M_{gb}	Grain boundary mobility	---

n	Avrami exponent	---
$\dot{N}$	Nucleation rate	---
N_i	Shape function	---
N_C	Cube nucleation	m^{-3}
N_{GB}	Grain boundary nucleation	m^{-3}
N_{Lv}	Grain lines per unit volume nucleation	m^{-3}
N_{PSN}	Particle stimulated nucleation	m^{-3}
$N_{P\theta}$	Grain interior nucleation	m^{-3}
N_{Pv}	Grain corners per unit volume nucleation	m^{-3}
N_{Sv}	Grain surface per unit volume nucleation	m^{-3}
N_v	Grain boundary surface nucleation	m^{-3}
N_v	Nucleation density	m^{-3}
P	Interface pressure	Pa
P_D	Driving pressure	Pa
$\dot{q}$	Heat released due to plastic work per unit volume	$W\ m^{-3}$
Q_{def}	Activation energy for deformation	$J\ mole^{-1}$
Q_{rex}	Activation energy for recrystallization	$J\ mole^{-1}$
r	Radial position through the work roll, mm	mm
R	Universal gas constant	$J\ mole^{-1}\ °C^{-1}$
$\frac{1}{R}$	Local lattice curvature	m^{-1}
$\{R^e\}$	Heat flux (load) vector arising from internal heat generation	$W\ m^{-1}$
S_V	Grain boundary area per unit volume	μm^{-1}

t	Time	s
δt	Time increment	s
$t_{0.5}$	Time required to achieve 50% recrystallization	s
$\{T\}$	The temperature vector	°C
T_{def}	Deformation Temperature	°C, K
$[\delta u]$	Displacement field matrix	m
w	Temperature compensated time parameter	s
δW_{ext}	The change in the external virtual work	---
δW_{int}	The change in the internal virtual work	---
x	Position along the length of the strip	mm
$[x]$	The direction matrix (i.e. x, y, z directions)	m
X_v	Fraction transformed	%
y	Position through the thickness of the strip	mm
Z	Zener Hollomon parameter	S^{-1}

Greek Symbols

β	Drag Force	N
$d\delta$	Average subgrain size increment	---
δ	Average subgrain size	m
δ_o	Staring average subgrain size	m
δ_{ss}	Steady state subgrain size	m
$\delta\varepsilon$	Strain increment	---
ε	Strain	---

$\dot{\varepsilon}$	Strain rate	s^{-1}
$d\theta$	Misorientation angle between sub grains increment	---
θ	Average misorientation angle between subgrains	°
θ_o	Staring average misorientation angle	°
θ_c	Critical misorientation angle	°
θ_{ss}	Steady state misorientation angle	°
Λ_r	Dislocation mean free Path	μm
μ	Coefficient of friction	---
ν	Poisson's ratio	---
v_m	Mean velocity of a mobile dislocation	$m\ s^{-1}$
σ	Stefan- Boltzmann constant (5.6696×10^{-8})	$W\ m^{-2}\ K^{-4}$
$[\sigma]$	True stress matrix	Pa
σ_f	Frictional stress	Pa
σ_{ss}	Steady state flow stress	Pa
ρ	Density	$kg\ m^{-3}$
ρ_o	Starting total dislocation density	m^{-2}
ρ_g	Geometrical necessary dislocation density	m^{-2}
ρ_i	Internal dislocation density	m^{-2}
ρ_r	Random dislocation density	m^{-2}
$d\rho_r$	Random dislocation density increment	---
τ	Shear stress	Pa
$\hat{\phi}(x,y)$	Approximate solution	---

$\phi(x,y)$	Exact solution	---
Ω	Problem domain	---

Acknowledgements

I would like to thank my research supervisors, Dr. Mary Wells and Dr. Daan Maijer, for their continued guidance and support and their unlimited patience during the course of my research program. They have been true mentors and have contributed significantly to my personal and professional development in UBC. Their opinions and insights are highly valued and often sought. I am especially thankful to Dr. Wells for providing the background, technical expertise and helpful suggestions for the microstructure work and for her genuine interest and continued support and encouragement throughout different stages of this project. A special thanks to Dr. Maijer for his help, support and many interesting discussions of the modeling work and for being a very critical reviewer of my work.

I am truly grateful to Dr. Menno van der Winden and Dr. Andy Norman of Corus' research, development and technology (RD & T) center for their commitment to the academic research program investigating this industrial problem and their support and help and many useful discussions during the course of my experimental research program. I would also like to acknowledge Dr. Cheng liu of Corus' RD&T for his helpful discussion and suggestions. The interesting discussions that I shard with Dr. Duan of McMaster University was of great help to me as well. I am also grateful for the useful discussions and ideas that I shared with prof. Hugh Shercliff and prof. John Humphreys during my very short visit to England.

I am especially grateful to Mr. Gary Lockhart of UBC, his expertise in conducting experimental rolling trials were instrumental to the success of the experimental program. I am also thankful to Jan Wormann and Jan Brussel of Corus' RD&T for making sure that all industrial experiments were carried out smoothly.

I also gratefully acknowledge the expertise of Dr. Chad Sinclair and Dr. Matthias Militzer, who as member of my doctoral supervisory committee provided a critical feedback and many useful discussions. I am specifically thanks to Dr. Sinclair for his help on using EBSD. The in kind financial support of Natural Science and Engineering Research Council (NSERC) in a form of postgraduate scholarship, which supported me financially for two years during my research program is gratefully acknowledged. I am

also thankful to Corus for providing the material and access to their experimental rolling facility and their financial support.

I am thankful to my parents for the love and support that they constantly shower on me without which this work would not have been possible. I also acknowledge my friends in the department for the good times I shared with them in Vancouver. This thesis is dedicated to the soul of my grandmother, Fatima El-Mekkawy.

CHAPTER 1

INTRODUCTION

1.1 The Importance of Aluminum Sheet Alloys

Metal forming operations are used extensively in industry to alter the shape of the metal through plastic deformation. During these forming operations, control of the evolved microstructure is critical, as it will have a direct impact on the final properties of the product. One example of this is in aluminum alloy sheet production, where controlling recrystallization and grain size represents the very heart of quality control and improvement[1]. The demand by customers for stringent property specifications along with maximizing production to remain efficient and economically viable in an increasingly competitive market is continuously driving aluminum sheet manufacturers forward.

The usage of aluminum sheet is expected to increase dramatically over the next few years due to their lightweight and unique mechanical and corrosion properties[2]. In fact, Canadian primary aluminum production has increased by 19% from 2,347,118 metric tons in 1998 to 2,791,916 metric tons in 2003[3]. The annual growth of aluminum consumption in transport applications averaged 8% during the 1990s. In fact, the transportation sector was the largest aluminum consumer in the form of sheets and coils for a wide variety of applications in North America during 1999[4]. Typical applications of aluminum sheets are in the automobile industry, the aircraft and aerospace industry and in the shipbuilding industry. Aluminum is increasingly used for the construction of ship hulls and deck sections. Specifically, high speed boats and fast ferries constructed using aluminum hulls mark a new era of passenger safety and comfort[5]. This prospect for aluminum usage has initiated research programs focusing on understanding wrought Al-Mg alloys material behavior during processing, which is the primary candidate material used in the ship building industry. Specifically, Corus Research Development and Technology, a major aluminum producer in Europe, initiated a project focusing on understanding the material behavior during processing of high strength AA5XXX aluminum alloys[6]. This further understanding of sheet properties during processing will aid ship

designers and manufacturers in selecting aluminum alloys to obtain higher strength, good formability, good weldability and high corrosion resistance at significantly reduced weight compared to conventional steel hulls[7].

1.2 Hot Rolling of Aluminum Alloys

Typically, commercial production of aluminum sheet for the transportation industry encompass various manufacturing steps. Ingots produced by direct chill (DC) casting are scalped and homogenized prior to rolling. Hot rolling of aluminum alloys starts by breaking down the homogenized cast ingot (550mm) to slab-gauge (30mm) in a hot breakdown-reversing mill. The number of passes required to achieve this reduction can vary from 9 to 25 passes based on the mill size[8] . This process is usually followed by rolling in a continuous hot tandem-rolling mill, which reduces the slab gauge material to the required final sheet thickness (1-3mm)[8]. The sheet produced may be annealed and then cold rolled to the final sheet with or without intermediate annealing. A final heat treatment process (anneal) may be applied depending on the temper requirements[1]. A typical aluminum production flow chart is shown in **Figure 1.1**.

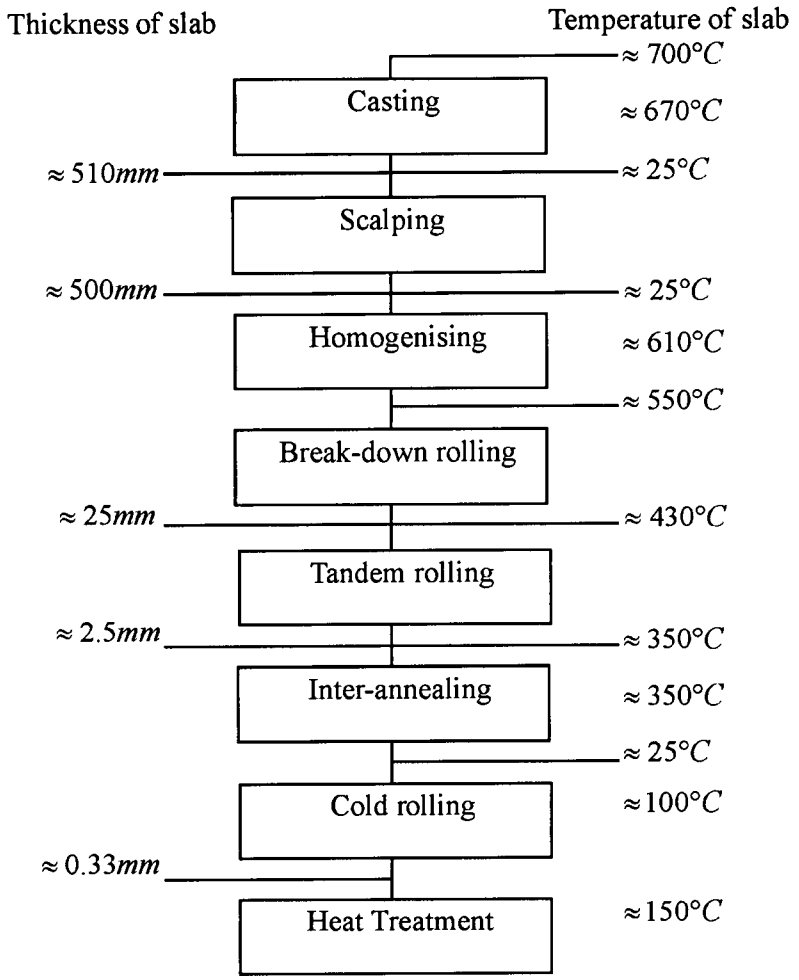

Figure 1.1 – Typical aluminum production flow chart[8].

A critical aspect in the manufacturing of sheet products is hot rolling where the thickness of the ingot is reduced. During industrial hot tandem rolling, a sheet with an initial thickness of 15-25 mm and temperatures of 400-450°C is rolled through two to four rolling stands to a strain between 0.6 to 1.0 per pass with strain rates between 10-100 s^{-1} before exiting with a thickness of 1-3 mm and a temperature of 350°C[1, 8]. The reason hot rolling is so important is that the sheet properties and microstructure that develop during this stage can significantly impact the final sheet microstructure and material properties of the cold rolled sheet[2, 9]. A schematic diagram of the hot rolling operation showing both breakdown rolling and tandem rolling and an image showing the hot rolling process are shown in **Figure 1.2** and **Figure 1.3**, respectively.

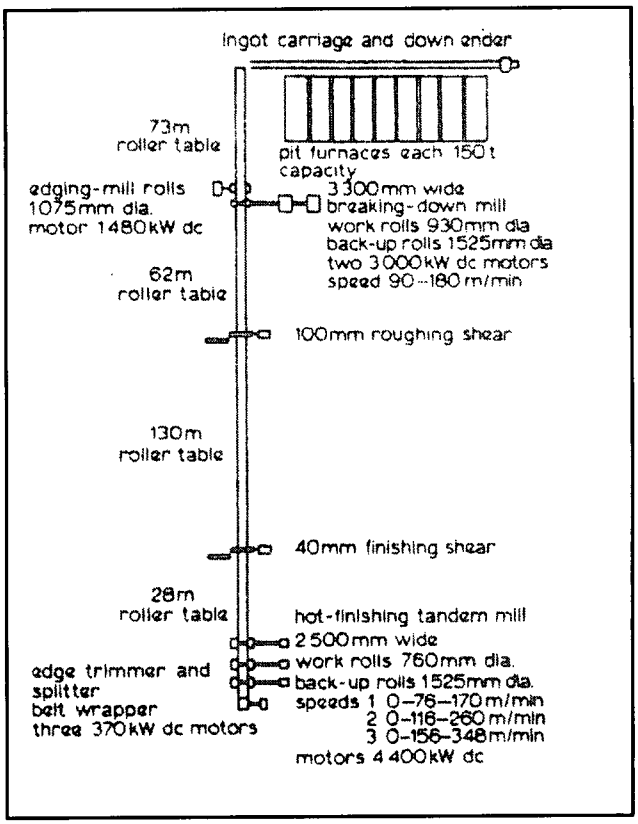

Figure 1.2 – Schematic of industrial hot rolling operation for aluminum alloys[10].

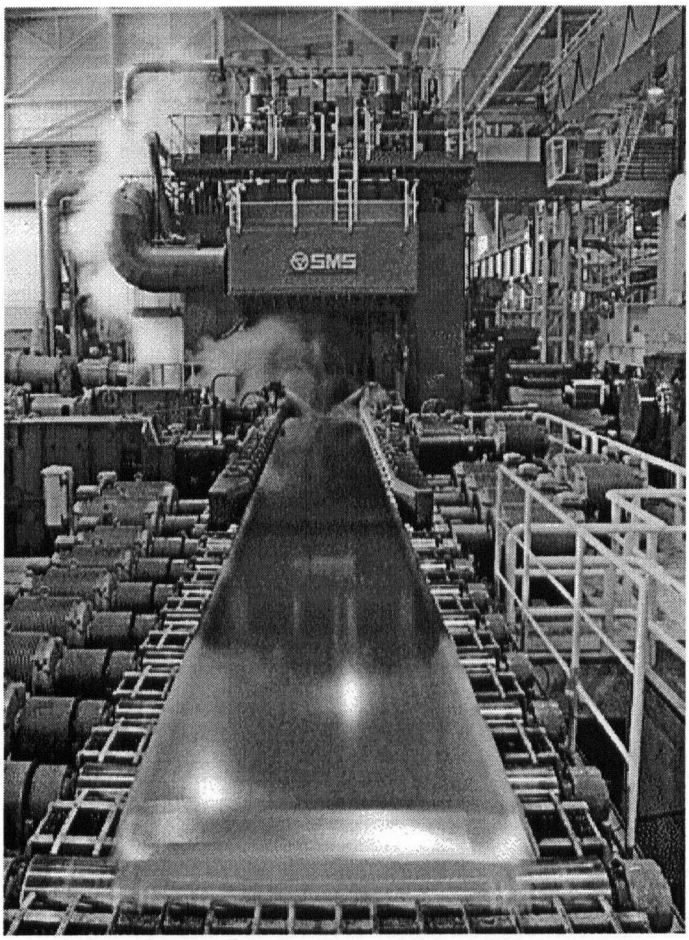

Figure 1.3 – An image showing sheet hot rolling operation[11].

1.2.1 Microstructure Evolution During Hot Rolling of Aluminum Alloys

In addition to dimensional change occurring during the hot rolling process, the rolling process imparts thermo-mechanical changes that affect the final material properties. Thus, a close control of the process conditions and properties is needed to achieve the desired microstructure. For example, a grain size that is too large may be undesirable for a number of reasons related to strength and ductility[9]. The key microstructure features that describe a hot deformed structure include: (i) the size and shape of the deformed grains and (ii) the substructure within the deformed grains. The factors which influence the formation of the microstructure during hot rolling include both the thermal and deformation history (strain, strain rate and temperature) experienced by the material during rolling as well as the starting microstructure and the alloy chemistry. These key features, in turn, define microstructure changes such as

recovery, recrystallization, and grain growth which are the main factors that determine the resulting microstructure and thus the final sheet properties.

The microstructure changes that occur during hot rolling include both dynamic and static changes. Dynamic changes, namely dynamic recovery and recrystallization, are those microstructure changes that occur during the deformation process. Metadynamic changes are initiated during rolling and continue between rolling passes. For example, if straining of the material has stopped but annealing continued, the available nuclei in he material will grow with no incubation period into heterogeneous, partly dynamically recrystallized matrix[12]. Static changes, namely static recovery and recrystallization, occur in the inter-pass region, and after rolling is completed[12, 13]. A schematic of microstructure changes that occur during hot rolling is shown in **Figure 1.4.**

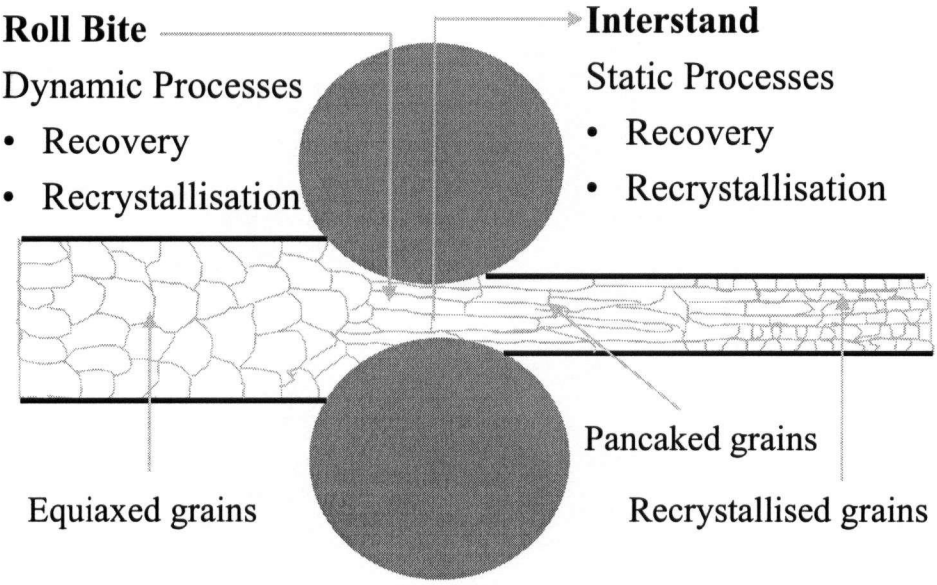

Figure 1.4- Schematic of a strip microstructure changes during the hot rolling process.

Recovery involves grain restoration both during and after deformation processes to minimize energy without the formation of any new grains[12]. Recrystallization involves the formation of new strain free grains in the deformed matrix through the processes of nucleation and growth[12, 14]. Grain growth involves the growth of the recrystallized grains so that the surface energy is minimized. In AA5XXX series alloys, grain growth does not occur readily, because precipitates act as pinning particles that limit grain growth[12]. Thus, the recovery and recrystallization

processes become the major microstructure changes occurring to relieve the material of most of its stored energy.

1.2.2 Modelling of Microstructure Evolution During Hot Rolling of Aluminum Alloys

The development of thermo-mechanical process modelling for the optimization of steel alloy properties during industrial hot rolling has been a steady trend during the past few decades[10, 14-16]. The ultimate goal of these models was to relate the process parameters to the final material properties through a quantitative description of the microstructure evolution and control the manufacturing process to achieve the desired properties. Unfortunately, the modelling activities in the aluminum industry are at a much earlier stage of development than for steel[1, 17]. In spite of the importance of these modelling activities in aluminum manufacturing, to date, only a few mathematical models have been developed to link the microstructure changes that occur during hot rolling of aluminum alloys to the thermo-mechanical history of the material during hot rolling[8]. Most of the relationships that describe microstructure evolution are based on laboratory measurements which have been used to develop empirical equations to predict the microstructure evolution after hot deformation including, recrystallization kinetics, final grain size, and to a lesser extent texture evolution[8, 18].

Thus, it appears that a more sophisticated and fundamental description of microstructure evolution for aluminum alloys is required[14, 17]. The main reason behind the difficulty in developing a fundamentally based microstructure model is due to the lack of understanding of the effect of the rolling parameters on the deformed microstructure and subsequent recrystallization process[19]. A schematic diagram showing the interaction between various hot rolling process parameters and microstructure evolution is shown in **Figure 1.5.**

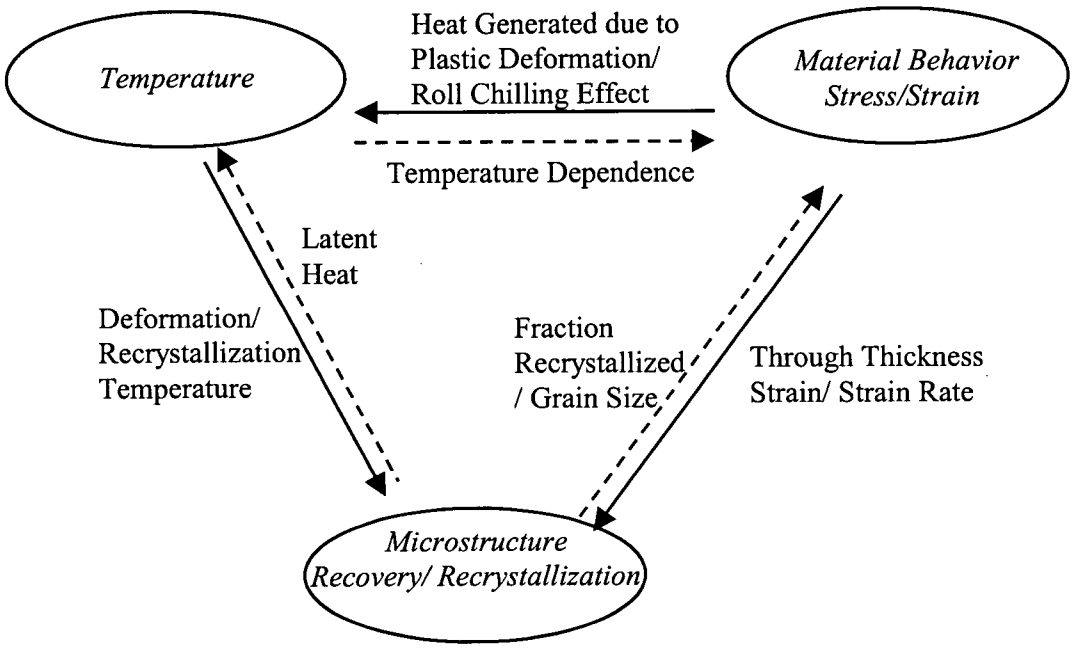

Figure 1.5- A schematic diagram of the interaction between rolling process parameters and microstructure.

The complexity of the interactions between the material thermo-mechanical behavior during hot rolling and the resulting microstructure evolution, shown in **Figure 1.5**, indicates the challenging nature of the development of a model that can capture this interaction and link the process parameters to microstructure evolution during hot rolling. In order to develop a representative hot rolling model, it is essential to track the changes in a number of appropriate material-related state variables through the different stages of the hot rolling process to be able to understand the through-process microstructure changes and dependencies[19-21]. With the development of sophisticated commercial finite element software, mathematical models can be developed to predict through-thickness temperature, strain and strain rate distribution during hot rolling process. These data can be coupled to a microstructure model to track the change in different state variables and predict the resulting microstructure. This approach not only eliminates immense experimental trials required to optimize the process to achieve the desired results, but also addresses the crux of the problem by analyzing the thermo-mechanical and microstructure changes occurring during multi-pass hot rolling.

Moreover, most of the model validation work completed to date was carried out using laboratory scale experiments[22]. Although there are great advantages to using lab scale validation, it is necessary to validate the model using measurements that simulate the industrial rolling more clearly[23]. To date, very few of the models developed so far have been properly validated against measurements of this nature[21, 24, 25].

As part of an on-going effort to optimize the hot rolling process to achieve desired material properties, Corus Group plc. has entered into a collaborative research project with researchers in the Department of Materials Engineering at the University of British Columbia to developed and validate a 2-D mathematical model to describe the thermo-mechanical, and microstructure evolution of AA5083* aluminum sheet during both single and multi-pass industrial hot rolling. This doctoral research project presents a part of this effort towards achieving and implementing a rolling process model. The VIR [*] project is a similar collaborative project between major European aluminum producers (Alcan, Corus, Hydro, Pechiney, Raytek, and Sapa) and many universities in the field of aluminum technology (NTNU and SINTEF in Norway, Immpetus and UMIST in UK, NIMR in Netherlands, SIMR in Sweden and RWTH in Germany) with a total budget of 17.4 million euros[18, 21, 23, 26]. Models of the hot rolling process are currently being developed as coupled thermo-mechanical models using finite element commercial code, mainly MARC** and ABAQUS***, and microstructure/ texture models[18, 21].

In the following chapter, the thermo-mechanical and microstructure changes that occur during hot rolling as well as the microstructure evolution modelling approaches are presented and reviewed.

* AA5083 is a non-heat treatable aluminum alloy containing a nominal composition of 4.5 wt% magnesium, a small percentage of manganese (0.7 wt%) which increases the strength and reduces corrosion susceptibility and a low level of chromium (< 0.1%) added to raise the recrstallization temperature. Magnesium is largely present in solid solution in this alloy. The two-phase boundary is crossed only at relatively low temperature where diffusion constrains may limit the precipitation of Mg_2Al_3 at grain boundaries or within the grain. Thus, AA5083 is primarily strengthened by work hardening rather than second phase particle (Mg_2Al_3) precipitation[27].

** Trademark of MARC Analysis Research Corporation, Palo Alto, USA.

*** Trademark of Hibbit, Karlsson and Sorensen, Inc. Rhode Island, USA.

References

1. Wells, M.A., *Mathematical modelling of the microstructure and texture changes during hot tandem rolling of AA5182 and AA5052 aluminum alloys, Ph. D Thesis*. 1995, University of British Columbia: Vancouver, Canada.

2. van der Winden, M.R., H.E. Vatne, and C.M. Sellars. *Modelling the texture evolution during break-down rolling of AA3104 with special attention to the effect of the distribution of second phase particles*. in *Hot deformation of aluminum alloys II*. 1998. Rosemont, Illinois: The minerals, metals, and materials society.

3. Aluminum Association of Canada, *Canadian Primary Aluminum Production*. 2003.

4. Hale, W., *The global light metals sector outlook*. JOM, 2000. **52**(11): p. 26-30.

5. *Alcan rolled products in Europe website*, Alcan Inc., http://www.alcanrolledproducts.com/, 2002.

6. Corus Aluminium Walzprodukte, *Shipbuilding - Aluminium sheet and plate, Newsletter published by Corus*. 2004: Koblenz, Germany.

7. John Simpson, M.S., *Aluminum Boats Prove Their Mettle. Reputation, Innovations Make Aluminum the Material of Choice of a Growing Number of Boat Builders*, in *The aluminum Association, Inc.* 2003.

8. van der Winden, M.R., *Laboratory simulation and modelling of the break-down rolling of AA3104, Ph.D thesis*. 1999, Sheffield university: Sheffield, U.K.

9. Vatne, H.E., T. Furu, R. Orsund, and E. Nes, *Modelling recrystallization after hot deformation of aluminum*. Acta Mater., 1996. **44**: p. 4463-4473.

10. Sellars, C.M. and J.A. Whiteman, *Recrystallization and grain growth in hot rolling*. Metal Sciene, 1979. **13**: p. 187-194.

11. *Aluminum casting and fabrication*, The Metallurgical Society , CIM, http://www.metsoc.org/virtualtour/processes/aluminum/AlumCastFabri.asp.

12. Humphreys, F.J. and M. Hatherly, *Recrystallization and related annealing phenomena*. 1996, NewYork: Pergamon Press. 363.

13. Cotterill, P. and P.R. Mould, *Recrystallization and grain growth in metals*. 1976, London: Surrey university press. 408.

14. Sellars, C.M., *Modelling microstructural development during hot rolling*. Mater. Sci. Technol., 1990. **6**: p. 1072-1081.

15. Beynon, J.H. and C.M. Sellars, *Modelling microstructure and its effects during multipass hot rolling*. ISIJ International, 1992. **32**: p. 359-367.

16. Zurob, H.S., C.R. Hutchinson, Y. Brechet, and G. Purdy, *Modeling recrystallization of microalloyed austenite: effect of coupling recovery, precipitation and recrystallization.* Acta Mater., 2002. **50**: p. 3075-3092.

17. Vatne, H.E., K. Marthinsen, R. Orsund, and E. Nes, *Modeling recrystallization kinetics, grain sizes, and textures during multipass hot rolling.* Metall. Mater. Trans. A, 1996. **27A**: p. 4133-4144.

18. Hirsch, J., *VIRFAB- What was achieved from an industrial perspective?* Aluminium, 2004. **80**(6): p. 553-559.

19. Vatne, H.E. and M.A. Wells. *Microstructure modelling in industrial aluminum hot-rolling processes - the state of the art and the challenges ahead.* in *Light Metals 1999.* 1999. Quebec City, Canada: CIM.

20. Furu, T., K. Marthinsen, and E. Nes, *Modelling recrystallization.* Mater. Sci. Technol., 1990. **6**: p. 1093-1102.

21. Marthinsen, K., S. Abtahi, K. Sjolstad, B. Holmedal, E. Nes, A. Johansen, J.A. Saeter, T. Furu, O. Engler, Z.J. Lok, J. Talamantes-Silva, C. Allen, and C. Liu, *Modelling the evolution of microstructure and mechanical properties during processing of AA3103.* Aluminium, 2004. **80**(6): p. 729-738.

22. Wells, M.A., D.J. Lloyd, I.V. Samarasekera, J.K. Brimacombe, and E.B. Hawbolt, *Modelling the microstructural changes during hot tandem rolling of AA5XXX aluminum alloys: part I.* Metall. Mater. Trans. B, 1998. **29B**: p. 611-620.

23. van der Winden, M.R., G.U. Grun, T. Furu, K. Asboell, and C. Leroy, *The three VIR [*] projects and the final VIR [*]-conference.* Aluminium, 2004. **80**(6): p. 566-570.

24. Timothy, S.P., H.L. Yiu, J.M. Fine, and R.A. Ricks, *imulation of single pass of hot rolling deformation of aluminum alloy by plane strain compression.* Mater. Sci. Technol., 1991. **7**(3): p. 255-261.

25. Wells, M.A., D.M. Maijer, S. Jupp, G. Lockhart, and M.R. van der Winden, *Mathematical model of deformation and microstructural evolution during hot rolling of aluminum alloy 5083.* Mater. Sci. Technol., 2003. **19**(4): p. 467-476.

26. van der Winden, M.R., *A joint European approach towards through process modelling of hot deformation of aluminum alloys*, in *JOM.* 2002. p. 238.

27. Hatch, J.E.E., *Aluminum: properties and physical metallurgy.* 1999, Materials Park, Ohio: American Society for Metals.

CHAPTER 2

LITERATURE REVIEW

2.1 Introduction

Over the past two decades, computer simulations capable of modelling the microstructure evolution during industrial hot rolling operations in many steel alloys have been developed and used successfully to improve the scientific understanding of the influence of the hot rolling process parameters on the resulting microstructure[1]. Several of the empirical microstructure equations that were originally developed for steels have been applied to predict similar microstructure changes in aluminum alloys during hot deformation after the appropriate material-dependent constants were identified based on laboratory experiments[2, 3]. However, the modelling activities focused on microstructure evolution in aluminum alloys are still at a much earlier research stage compared to microstructure modelling of steel.

2.2 Microstructure Evolution During Hot Rolling

The key microstructure features that describe a hot deformed structure include: (i) the size and shape of the deformed grains and (ii) the substructure within the deformed grains. The factors which influence the formation of the deformed structure include both the thermal and deformation history experienced by the material during rolling as well as the starting microstructure and alloy chemistry. The microstructure changes that occur during rolling are referred to as dynamic changes, and those taking place between rolling passes and after rolling as static[4, 5]. Recovery and recrystallization are two key fundamental processes that control microstructure changes. Recovery involves grain restoration both during and after deformation processes to minimize energy without the formation of any new grains. Specifically, in high stacking fault energy materials, dislocation movement is relatively easy and may occur by cross slip and climb which allow the annihilation of dislocations that have opposite signs and rearrangement of like dislocations to a configuration of minimum energy[4, 6, 7]. Recrystallization involves the formation of new strain free grains in the deformed matrix through the processes of nucleation and growth[4].

Instead of reviewing the literature with a view towards all the microstructure changes that may occur during hot rolling of aluminum alloys, the following section discusses the key microstructure processes that take place during hot rolling and after rolling is complete for the non-heat treatable AA5XXX aluminum alloy series. Thereafter, the rest of the literature review will focus on presenting and analyzing the modeling approaches reported to model deformation and microstructure evolution during hot rolling of aluminum alloys and discuss their advantages and short comings as well as investigate the validation of these models to date.

2.2.1 Dynamic Microstructural Changes

2.2.1.1 Dynamic recovery

In metals of high stacking fault energy like aluminum (166 mJ m^{-2})[8, 9], dislocations can easily climb and cross slip out of their plane, which means dynamic recovery tends to be the main softening mechanism during deformation. Sheppard *et al.* indicated that dynamic recovery is one of the primary high temperature softening mechanism for Al alloys[6]. Recovery comprises all the processes that lead to a reduction in dislocation density and rearrangement of the remaining dislocations in the form of cell/subgrain structure. The importance of dynamic recovery stems from the fact that it controls the amount of stored energy in the material which provides the driving pressure for subsequent recrystallization. A typical stress strain curve of a material undergoing dynamic recovery during hot working is shown in **Figure 2.1**[1, 4].

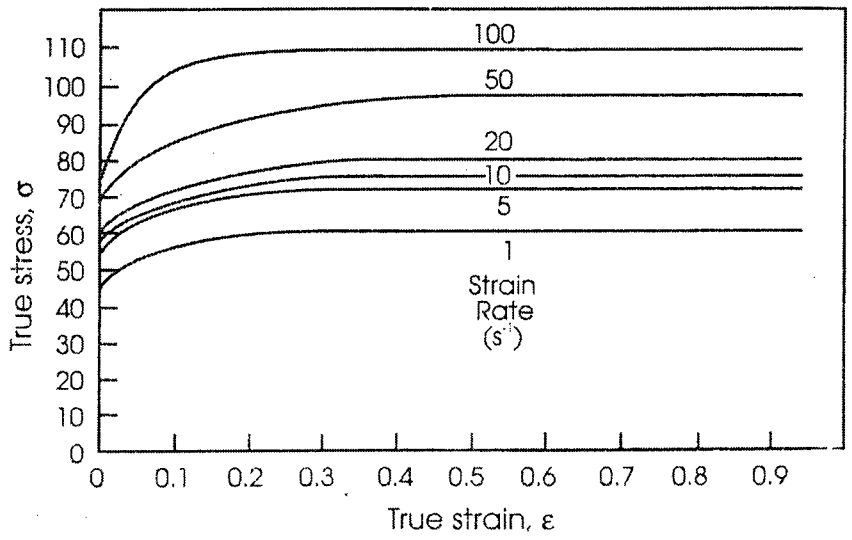

Figure 2.1 – Stress-strain curves for Al-1%Mg during hot deformation[1].

Dynamic recovery is a thermally activated process which results in dislocation movement and rearrangement. Both the strain rate and deformation temperature influence the dynamic recovery rate which in turn determines the steady state flow stress. The softening effect due to dynamic recovery is significant at high temperature and low strain rate. These conditions promote dislocation annihilation and rearrangement due to the high temperatures for a prolonged time period resulting in significant recovery. During the early stages of the deformation process, work hardening occurs which leads to an increase in dislocation density and flow stress. As the dislocation density increases, dynamic recovery occurs and leads to softening by annihilation of some of the dislocations and rearrangement of others to form sub-grain cells[10]. Beyond a certain strain, the rates of dislocation generation and annihilation are equal; i.e., the rate of work hardening and recovery reach a dynamic equilibrium which results in a steady state flow stress[4]. When the steady state stress regime is attained, a well-developed subgrain structure has been developed which is characterized by an average subgrain size (δ) and an average misorientation angle between subgrains (θ). Also, there is a three dimensional dislocation network inside these subgrains. Nes *et al.* found that as the strain increases above a critical strain value, grains become elongated but the mean dislocation structure remains constant as a result of the dynamic balance between the generation and the annihilation rates of dislocations for Al- 1%Mg alloys[7]. This results in a constant dislocation density

within subgrains, a constant subgrain size and misorientation angle within the deformed structure[4]. This agrees with the findings of MC Queen *et al.* who indicated that the misorientation between subgrains is found to remain constant at a few degrees when the steady state is reached for pure aluminum[11].

Several models have been adopted in the literature to describe the subgrain formation, and the rate of dislocation annihilation during deformation by dynamic recovery. Sellars *et al.* adopted an empirical approach to describe microstructure evolution for commercial purity aluminum alloys, where subgrain boundaries were assumed to move under the influence of stress [12-15]. The subgrain size has been shown by many researchers to be related to the Zener Hollomon parameter through a relation of the following form[14, 16, 17]:

$$d^{-1} = a + b\ln Z \tag{2.1}$$

where a and b are material related constants and Z (the Zener Hollomon Parameter) is the temperature compensated strain rate of the form:

$$Z = \dot{\varepsilon}\exp\left(\frac{Q_{def}}{RT_{def}}\right) \tag{2.2}$$

where Q_{def} is the activation energy for deformation, T_{def} is the deformation temperature, $\dot{\varepsilon}$ is the average strain rate during the deformation and R is the universal gas constant.

Humphreys simulated dynamic recovery using a cellular microstructure approach, where microstructure was assumed to consist of cellular regions, which could be grains, or subgrains[18]. The results of the analysis indicated that under large strain deformation conditions that is higher than 2, a stable microstructure forms[18] which agrees with findings of Nes *et al.*[19] and McQueen *et al.*[11].

2.2.1.2 Dynamic recrystallization

During hot rolling of metals with low or medium stacking fault energy, the ability of dislocations to climb and cross slip diminishes which in turn reduces the recovery processes. Thus, dynamic recrystallization may occur when critical deformation conditions are reached. Since aluminum is a high stacking fault energy material, dynamic recrystallization is unlikely to occur[4]. However, yjere have been

some observations of dynamic recrystallization in AA5XXX aluminum alloys[17, 20, 21]. For example, McQueen *et al.* found that increasing the Mg content up to 5% in aluminum alloys reduced dynamic recovery and increased dynamic recrystallization due to the formation of Al_6Mn particles for AA5XXX alloys[21]. Thus, it was concluded that that dynamic recrystallization can occur due to the presence of large second phase particles in aluminum alloys during hot rolling[21, 22]. Another study conducted by Sheppard *et al.* shows that dynamic recrystallization was more visible in higher magnesium containing aluminum alloys where it was argued that second phase particles are required to nucleate recrystallization[23].

Other researchers believe that magnesium in aluminum alloys lowers the stacking fault energy which in turn inhibits cross slip and climb of the dislocations and facilitates dynamic recrystallization[24]. Sheppard disagrees with this explanation because low stacking fault energy values have not been observed for Al-Mg alloys[17]. Humphreys indicates that for Al-5%Mg, new grains with high angle boundaries may be formed by progressive rotation of subgrains adjacent to the grain boundaries during deformation with little accompanying boundary migration[25]. The mechanism by which this subgrain rotation occurs is not yet clear[4].

The previous discrepancies between researchers show that the mechanism that causes dynamic recrystallization is not well understood for the AA5XXX aluminum alloy series. It is also hard to assess if the recrystallized grains are produced due to static or dynamic changes during the rapid quenching after deformation is complete. Several models of dynamic recrystallization have been proposed to understand and simulate the growth conditions of the dynamically recrystallized material[4, 26]. It was found that recovery occurs rapidly in aluminum alloys especially in AA5083 aluminum alloy and that the critical conditions for dynamic recrystallization to occur are dependent on the distribution and density of dislocations and occur when a critical value is reached which rarely happens in AA5083 aluminum alloy[4].

2.2.2 Static Microstructure Changes

2.2.2.1 Static recovery

In general, static recovery mechanisms involve changes in dislocation tangles within subgrains into neat arrays, which can lead to subgrain boundary growth, and subsequent disappearance[4]. Dislocations are attracted into arrays of similar dislocations, which increase the misorientation angle. Eventually, the boundaries become sharper and subgrain interiors become nearly dislocation free and the subgrain structure starts to coarsen through boundary migration. These boundaries may serve as nucleation sites during subsequent static recrystallization[27, 28]. A study has measured an overall softening index after double deformations tests as a measure of static recovery termed "restoration index"[29].

Dynamic recovery takes place during hot deformation, thus static recovery has a negligible effect on causing further microstructure changes for an AA5083 aluminum alloy [4, 5] and hence will not be discussed further in this review.

2.2.2.2 Static recrystallization

Compared with static recovery, static recrystallization has a marked softening effect and is easily observed for Al-Mg alloys in hot rolling process[30]. Static recrystallization influences the final grain size and hence the mechanical properties of the material which in turn may affect the rolling load[30]. Static recrystallization occurs by nucleation and growth of new grains in the deformed microstructure. In the case of aluminum alloys that have been deformed at high temperature, dynamic recovery occurs during deformation, which reduces the material dislocation density and thus lower the driving pressure available for static recrystallization. Of importance to the static recrystallization process is the stored energy in the material due to hot deformation as well as the thermal history experienced by the material after hot rolling is complete. Both of these parameters can influence the recrystallization kinetics[31]. In fact, static recrystallization constitutes one of the most important restoration mechanisms during multi-pass rolling in aluminum alloys, and is considered to be the most important process in terms of grain size control[10].

In aluminum, nucleation of grains is favored due to the relatively large grain surface area. Rolling induces the formation of deformations bands which act as effective nucleation sites for grains[4, 32]. Several theories were suggested to understand the recrystallization initiation process via nucleation and subsequent growth to form recrystallized grains. Beck *et al.* suggested a strain induced boundary migration mechanism which involves bulging of a preexisting grain/ subgrain boundary due to differences in energy levels between two regions, leaving behind dislocation free grains[33]. Other theories consider nucleation to occur via discontinuous subgrain growth at sites of high strain energy and orientation gradients[4]. Hurley *et al.*[34] were able to show that recrystallization occurs by a strain induced boundary migration (SIBM) mechanism using an EBSD map for Al-0.13% magnesium, as shown in **Figure 2.2**.

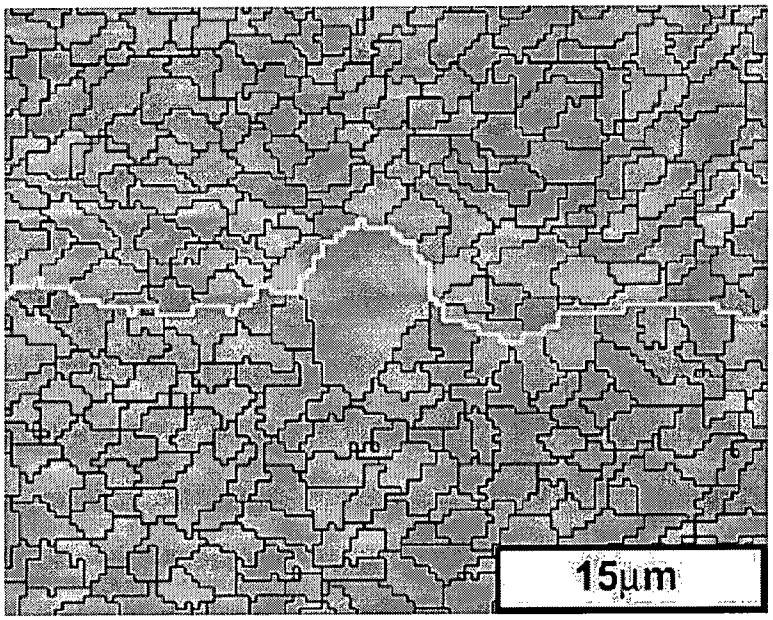

Figure 2.2 – EBSD map showing a subgrain SIBM during early stage of annealing after 50% rolling where bulging of high angle grain boundary HAGB (white line) is shown[34].

Particle stimulated nucleation (PSN) is another mechanism proposed for new grain formation; however, this mechanism becomes less significant at high deformation temperatures[4]. Sellars *et al.* assumed that nucleation may take place at different places within the deformed material, namely: grain corners where four grains meet, grain lines where three grains meet, grain surfaces where two grains meet, and

the grain interior[12, 35]. After employing various nucleation modelling approaches to calculate nucleation density at different strain levels, Sellars *et al.* concluded that grain boundary nucleation is the dominant mechanism for strains typical of hot rolling. This is clearly illustrated in **Figure 2.3** where the highest values of nucleation density was estimated at the grain boundary surface (N_v) and the grain surface area per unit volume (N_{Sv})[12].

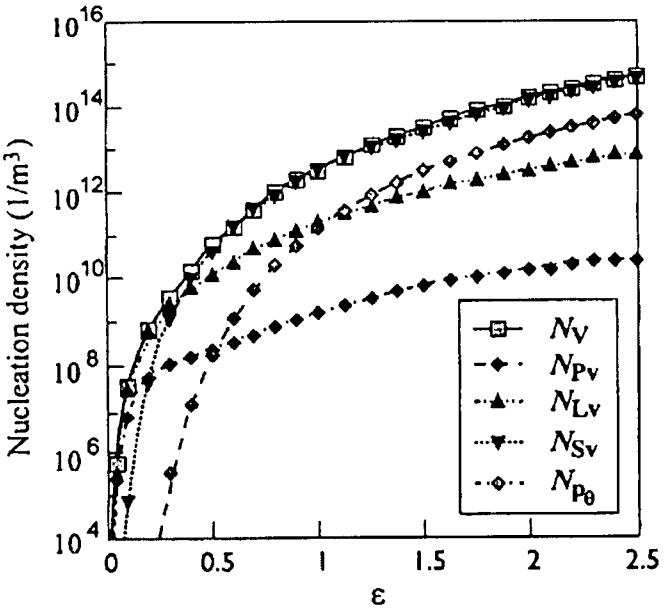

Figure 2.3 – Model predicted contribution of: grain boundary surface nucleation (N_v), grain corners per unit volume (N_{Pv}), grain lines per unit volume (N_{Lv}), grain surface per unit volume (N_{Sv}) and grain interior ($N_{P\theta}$) as a function of strain)[12].

In order to model multi-pass thermo-mechanical processes where partial or no recrystallization occurs between passes, it is important to accumulate stored energy accurately. Thus, the rate of release of stored energy through recovery and recrystallization between passes must be computed to determine the initial microstructure for each successive pass.

2.2.2.2.1 The driving pressure for recrystallization

Most of the work during deformation is dissipated as heat and only a very small amount remains as stored energy in the material. The driving pressure for recrystallization is directly related to the stored energy in the material. During

deformation, a variety of defects are introduced in the crystal lattice such as dislocations, vacancies and stacking faults, which act as energy storage mechanisms. The stored energy is derived from point defects and dislocations generated during deformation. The increase in dislocation density is due to the continued trapping of newly created mobile dislocations by existing ones and their incorporation into various microstructure features that characterize the deformed state[4]. The dislocations generated during deformation are usually accumulated in the substructure boundaries, subgrains, which increases the material stored energy[4]. In addition, grains in polycrystalline material change their shape during deformation which results in an increase in the grain boundary area. The energy associated with this increase in grain boundary area can contribute to the material stored energy[4, 8]. In aluminum alloys, dislocations are considered one of the main factors that contribute to the material stored energy which act as a driving pressure for recrystallization. Roters *et al.* proposed a model that describes the deformation of commercial purity aluminum alloys where dislocation arrangements that develop consist of cell walls with high dislocation density (ρ_w) which enclose cell interiors of low dislocation density (ρ_i)[36]. Dislocation sources inside the material generate mobile dislocations (ρ_m) which interact with the other two types of dislocations based on deformation which can result in the generation and annihilation of dislocations and can in turn affect the material stored energy[36]. A schematic drawing of the arrangement of these dislocations is shown in **Figure 2.4**.

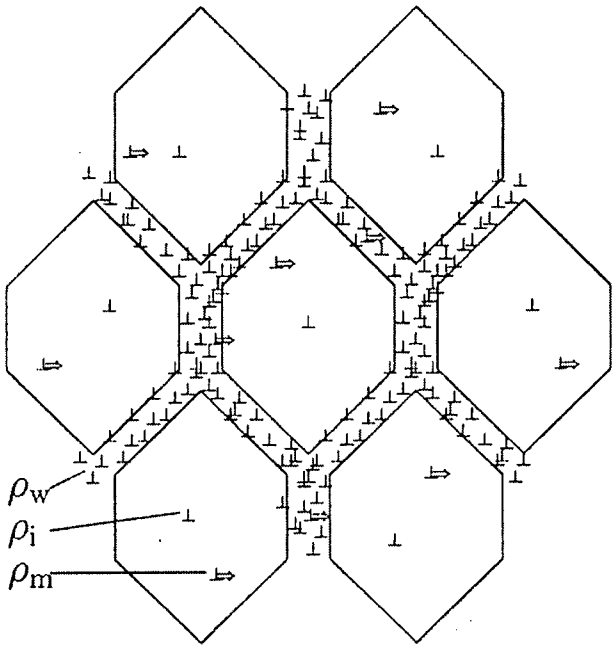

Figure 2.4 – Schematic sketch of different classes of dislocations that can influence the material stored energy[36].

The driving pressure for recrystallization P_D can be calculated based on the following equation[37]:

$$P_D = E_\rho + E_\delta \tag{2.3}$$

where the dislocation network energy E_ρ is equal to $\rho_i \Gamma$ and ρ_i is the dislocation density within the subgrains and Γ equal to $\frac{1}{2}Gb^2$ is the dislocation line tension. The energy stored in the subgrain boundary E_δ can be described as $\frac{\alpha \gamma_{sb}}{\delta}$ where δ is the subgrain size, α is a geometric constant equal to 2. The sub grain boundary energy in a hot deformed structure can be approximated to be[38]:

$$\gamma_{sb} = \frac{Gb}{4\pi(1-\nu)}\theta \ln\left(\frac{e\theta_c}{\theta}\right) \tag{2.4}$$

where G is the shear modulus, b is the Burgers vector, ν is the Poisson's ratio and θ_c is the critical misorientation angle for a boundary to be characterized as a high angle boundary.

By combining the previous two relations, the driving pressure for recrystallization can be rearranged to be:

$$P_D = Gb^2 \frac{\rho_i}{2} + \frac{\alpha G b}{4\pi(1-\nu)} \frac{\theta}{\delta} \ln\left(\frac{e\theta_c}{\theta}\right) \tag{2.5}$$

2.2.3 Grain Growth

Grain growth occurs after recrystallization to reduce the amount of grain boundary energy. In general, the average grain size will increase with time at all temperatures[4]. Also, for smaller strain conditions before recrystallisation, the growth rate during the subsequent grain growth stage is slightly lower[39]. A study carried out by Raghunathan *et al.*[39] to investigate grain growth in an AA5083 aluminum alloy deformed to 80% strain indicated that grain growth does not occur in AA5083 alloys primarily due to the presence of solute atoms of manganese, iron and silicon and the presence of precipitate's pinning the grain boundaries.

Ryum *et al.* investigated the grain growth for AA5XXX series aluminum alloys and found that the magnesium serves to reduce the rate of grain growth after recrystallisation which was attributed to the larger number of dispersoids formed after recrystallization resulting in pinning and limited grain growth [40]. The effect of Mg on the rate of grain growth is shown in **Figure 2.5**[40].

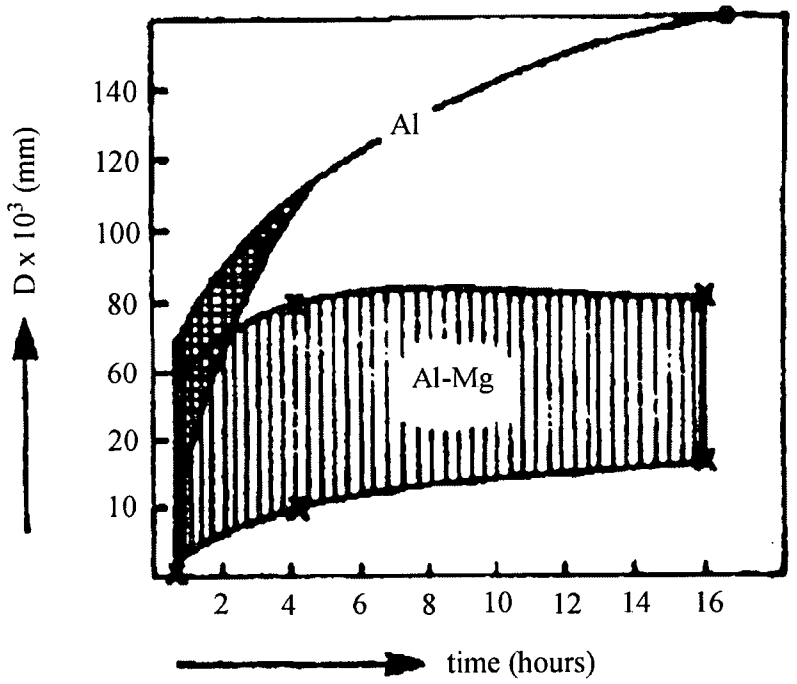

Figure 2.5 – Grain growth in Al and Al-Mg alloys[40].

It is clear from the above figure that grain growth is not a significant process in Al-Mg alloys during the short period of time available for static recrystallization to occur during hot rolling.

2.3 Mathematical Modelling of Microstructure Evolution During Hot Rolling of AA5XXX Aluminum Alloys

Most of the mathematical models developed use the modified JMAK equation to predict the material fraction recrystallized. To date, mathematical models developed to quantify recrystallization during hot deformation and after hot deformation is complete can be divided into three main types: empirical[39, 41-43], semi-empirical physically-based[12, 37, 44], and probabilistic[18, 45-47].

The most commonly used approach to model recrystallization kinetics follows the theory developed by Johnson and Mehl (1939), Avrami (1939) and Kolmogorov (1937), which is usually referred to as the JMAK model. In this model, recrystallization is treated as a thermally activated process comprised of two events,

namely nucleation and growth. Based on the JMAK model, the recrystallized volume fraction (X) as a function of time (t) can be described according to Equation 2.6[4]:

$$X = 1 - \exp\left(-bt^n\right) \tag{2.6}$$

where b is a function of the nucleation rate, $\dot{N}$, and the growth rate, $\dot{G}$. The exponent, n, is commonly referred to as the JMAK or Avrami exponent, which characterizes nucleation conditions, and growth geometries. Some of the assumptions underlying the JMAK relation may not be accurate. Nucleation does not occur homogenously throughout the volume. Also, the growth rate usually decreases as recrystallization progresses. This non-ideal behavior is recognized through the Avrami exponent n. Theoretically, in the limiting case where all nucleation occurs at very early stages of transformation, site saturation, n equals to 3 while it is equal to 4 when nucleation is activated at a constant rate throughout transformation[5]. Experimentally n is found to be in a range between 2-3[4].

Typically when the JMAK equation is used to predict recrystallization after hot deformation, it is modified such that the fraction recrystallized is predicted based on the total holding time, t, as well as the time to achieve 50% recrystallization, $t_{0.5}$, as shown in Equation 2.7:

$$X_v = 1 - \exp\left(-0.693\left(t/t_{0.5}\right)^n\right) \tag{2.7}$$

where t is the annealing time, n is the Avrami exponent, which can range between 2-3 for aluminum alloys, $t_{0.5}$ is the time required to achieve 50% recrystallization, and X_v represents the fraction recrystallized.

Typically this approach has been used to develop equations representing the recrystallization behavior in experimentally deformed materials where the temperature and strain rate during the deformation is constant. Deformation temperature and applied strain rate are employed to calculate the time required to reach fifty percent recrystallization and thus determine the material fraction recrystallized.

However, during industrial rolling, the temperature and the strain rate change during rolling and through the strip thickness. Thus, the choice of temperature and strain rate to represent the deformation behaviour becomes difficult. Some researchers have applied exit values for temperature and strain rate[48] while others used an average temperature and strain rate value during deformation[13].

The empirical models have provided some useful insight into the influence of deformation conditions on the microstructure and property evolution in the material, but the large number of material constants in the model and the relatively simplistic method of representing the deformation history experienced by the material mean that they are of limited use. Another main problem with adapting this modelling approach is the empirical parameters that have to be determined specifically for each material and deformation history[49, 50].

The semi-empirical physically-based models, on the other hand, use fundamentally based equations to predict the stored energy in the material based on the microstructure changes during the deformation[41]. Such models include some physical parameters such as dislocation density, average subgrain size and material stored energy. They are able to model recovery and recrystallization processes and thereafter determine the effect of the rolling process parameters on the final microstructure[34]. Though most of the models developed today contain some material based fitting parameters, they provide better insight into the physics of nucleation and growth during recrystallization.

The probabilistic approaches include the use of Monte-Carlo and Cellular Automaton (CA) techniques. Monte Carlo simulation is based on the fact that the microstructure is developed by growth of nucleated sites during recrystallization. Stored energy is assigned to all sites within those grains. By varying the stored energy within the grain, heterogeneous nucleation rates can be simulated. In the CA method, each cell of the lattice represents a group of atoms, and the movement of individual cells acting in response to their neighborhood describes the microstructure evolution[51]. Cells of CA are characterized by certain attributes, which determine the "state" of the cell[52]. These attributes are variables related to the thermo-mechanical processing. Although CA can be used to model nucleation and grain growth during

recrystallization[34], the main problem in the CA and Monte Carlo approaches is related to their scale of application. Since CA is a computationally intensive technique, it is usually used to simulate only a small number of grains. This simulation of a few grains is not usually sufficient to judge the behavior of the material in a more macroscopic way. Another problem that still persists is the quantification of grain boundary velocity, and the definition of the transient rules which determine the state of the cell in the next time step depending on current cell state, which affects the model's ability to predict the fraction recrystallized.

One of the main aspects that should be considered when modelling recrystallization is the accumulation of stored energy in situations where no or only partial recrystallization occurs between passes. The multi-pass aspect increases the level of modelling complexity due to the partially recrystallized areas in the inter-pass region which receive further deformation and thereafter subsequently recrystallize. Also, continuous cooling occurs in the inter-pass region and after deformation is complete. One of the main challenges is to capture and track the accumulation of stored energy during multi-pass rolling to predict the resulting microstructure during hot rolling.

The recrystallization behavior in the material during hot rolling can be predicted by combining finite element (FE) analysis with either: (1) empirical, (2) or semi-empirical physically-based, (3) or cellular automaton models. In the next section of the literature review, the first two modelling approaches and the multi-pass hot rolling modelling aspects are considered in further detail.

2.3.1 Empirical Modelling Approach

The empirical modelling approach was pioneered by Sellars where the stored energy during hot working and subsequent recrystallization is based on an empirical relationship that relates the time to achieve 50% recrystallization ($t_{0.5}$) to the deformation conditions, as shown in Equation 2.8[13, 42, 50].

$$t_{0.5} = Bd_0^p \varepsilon^{-q} Z^{-r} \exp\left(\frac{Q_{rex}}{RT_a}\right) \tag{2.8}$$

where ε is the von Mises equivalent strain, Q_{rex} is the activation energy for recrystallization, T_a is the holding temperature, d_0 is the initial grain size, R is the universal gas constant and the other parameters are alloy-related empirical constants. This equation can then be integrated into the modified JMAK equation in order to determine the recrystallized fraction as shown in Equation 2.7.

In a similar fashion, the recrystallized grain size, d_{rex}, can be determined as shown in Equation 2.9[37]:

$$d_{rex} = \alpha d_0^a \varepsilon^{-b} Z^c \tag{2.9}$$

where d_0 is the initial grain size, ε is the von Mises equivalent strain, and a,b,c are empirical constants.

Over the years, research has been done to determine the empirical constants necessary to quantify the time required to achieve 50% recrystallization for a number of aluminum alloy systems as shown in Table 2.1.

Table 2.1 - Summary of empirical recrystallization relation for Al alloys.

Researcher	Reference	Alloy	Developed equation for ($t_{0.5}$) (s)
Gutierrez (1988)	[53]	AA1100	$t_{0.5} = 1.5x10^{-4}\varepsilon^{-1.5}Z^{-0.75}\exp\left(\frac{220000}{RT_a}\right)$
Wells (1995)	[54]	AA5182	$t_{0.5} = 8.34x10^{-7}\varepsilon^{-0.93}Z^{-0.73}d_0^{1.35}\exp\left(\frac{200000}{RT_a}\right)$
		AA5052	$t_{0.5} = 1.25x10^{-6}\varepsilon^{-1.023}Z^{-0.66}d_0^{1.35}\exp\left(\frac{200000}{RT_a}\right)$
Dauda (1999)	[55]	Al-3% Mg	$t_{0.5} = A\varepsilon^{-2.7}Z^{-1.1}\exp\left(\frac{205000}{RT_a}\right)$
Sellars (1985)	[29]	Al-1%Mg	$t_{0.5} = 9.8x10^{-6}\varepsilon^{-2.7}Z^{-1.1}d_0^{1.35}\exp\left(\frac{230000}{RT_a}\right)$
Raghunathan (1986)	[39]	AA5083	$t_{0.5} = 2.7x10^{-10}(9.73+3.82\varepsilon^2)^{-1}Z^{-0.58}d_0^{2.45}\exp\left(\frac{183000}{RT_a}\right)$

In general, when using a model of this form to estimate the time required to achieve 50% recrystallization in the material, FE results are processed to calculate a mean Z value, based on the average temperature and strain rate experienced at a specific location in the material during deformation, and the final equivalent strain at various through-thickness locations. Chen *et al.* incorporated the FE output into the aforementioned $t_{0.5}$ relation, where, as expected, the predicted fraction recrystallized fell from surface to center for an Al-1%Mg alloy; the specific predictions were not validated through either lab experimental data or industrial data[16, 56].

The simulation results reported by Dauda *et al.* for an Al-3% Mg alloy also indicated an increasing fraction recrystallization from slab center to surface, but their predicted recrystallized fractions were much greater than the measured ones[55]. Brand *et al.* predicted grain size evolution for AA2024 by combining FE with empirical equations that were initially derived for steel, where the effect of dynamic recovery was neglected. The predicted grain size distribution decreased from surface to center of the strip and decreased with increasing inter-pass time[57]. Mirza *et al.* modeled AA3104 behavior during industrial roughing of aluminum alloys. The thermo-mechanical history, and microstructure development during a 17-pass rolling schedule were simulated. The reported results indicate very small amounts of recrystallization at the surface and relatively high values of fraction recrystallized at the center, which contradicts the expected results. Moreover, the results were not validated against experimental measurements[58]. Wells *et al.* modeled AA5083 behavior during single-pass hot rolling[59]. The adapted microstructure equations were tuned to match the measured fraction recrystallized data for an AA5083 aluminum alloy[59].

The research including observation and modelling of static recrystallization has led to contradicting results in terms of fraction recrystallized, and recrystallized grain size when applied to multi-pass rolling cases as shown by Mirza *et.al*[58]. This can be attributed to the empirical approaches used, which do not account for the substructure evolution during deformation. Though this approach is easy to use, it bypasses the evolution of microstructure; i.e., it does not account for substructure evolution during deformation and its effect on subsequent static recrystallization. In other words, this approach does not reveal the important parameters and the physics behind recrystallization[49]. Another disadvantage of this type of modelling is that it

requires extensive experimental measurements under deformation conditions that encompass the entire range of conditions experienced by the material in the industrial process. Moreover, the equations developed are based on laboratory conditions where the deformation conditions are relatively constant as compared to an industrial process where large transient conditions are experienced by the material through the strip thickness during deformation.

2.3.2 Semi-Empirical Physically-Based State Variable Approach

Microstructure evolution during transient deformation, where the strain, temperature and strain rate change during the deformation process conditions is quite complicated and empirical models are not suitable to predict the complex microstructure evolution due to the fact that they do not account for the structural changes through the strip thickness during rolling[12]. This inability leads to the need to have physically-based models that can describe microstructure evolution during thermo-mechanical processing that have true predictive capabilities in relation to the effect of processing variables on subsequent recrystallization kinetics[60]. More recently semi-empirical physically-based internal state variable approaches have been used to determine recrystallization behavior for an Al-1%Mg aluminum alloys [31, 37, 44]. In this approach, an attempt is made to model the evolution in the microstructure during deformation, based on classical theories of work hardening as well as recovery. Physically-based state variable models have the potential to follow complex process histories and provide the means to track microstructure changes through out the different processing stages[37]. In these models, the dislocation substructure is described using three internal state variables namely: (i) internal dislocation density, (ii) average subgrain size, and (iii) average misorientation angle across subgrain boundaries. Measured as well as model predicted evolution of these variables during hot deformation of an Al- 1%Mg aluminum alloy are shown in **Figure 2.6**.

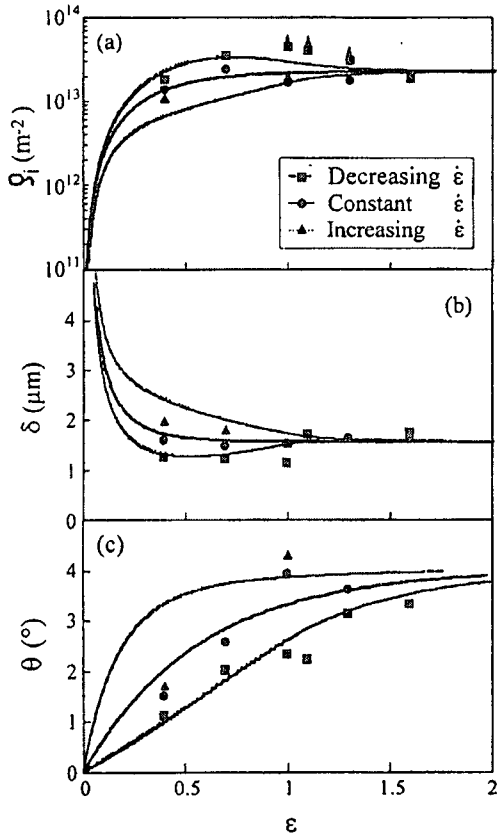

Figure 2.6 – A comparison between calculated and experimental data showing the effect of deformation (strain) on state variables evolution (lines denote calculated results and symbols denote experimental data) for an Al-1%Mg aluminum alloy [12].

Figure 2.6 suggests that during hot deformation, the misorientation angle (θ) increases with increasing strain, while the subgrain size (δ) decreases to a limiting value usually termed the steady state subgrain size (δ_{ss}). In the next section, a description of the state variable approach towards recrystallization modelling is presented.

2.3.2.1 Modelling of evolution of internal state variables

During plastic deformation, internal "random" or statistical dislocations are created by work hardening and annihilated through the dynamic recovery process. The dislocation generation can be linked to incremental plastic strain as shown in Equation 2.10[12]:

$$d\rho_r^+ = \frac{M}{b}\frac{1}{\Lambda_r}d\varepsilon \tag{2.10}$$

where b is the Bugers vector, M is the Taylor factor and Λ_r is the dislocation mean free path which is proportional to $\rho_r^{-1/2}$. The decrease in dislocation density due to recovery can be described through Equation 2.11[61]:

$$d\rho_r^- = -\frac{2L_c v_m \rho_r}{w}dt \tag{2.11}$$

where L_c is the length of dislocation annihilated, w is the length between the sites of cross slip or climb events. For Al-Mg alloys, where dislocation glide is the dominant mechanism of plastic deformation, the mean velocity of a mobile dislocation v_m can be estimated as $v_m = Db\sigma_f / \beta$ where D is the diffusion coefficient, β is the drag force which depends on solute concentration and misfit in atomic size, and σ_f is the effective stress necessary to move dislocations together with the solute atoms surrounding them [62]. The total random internal dislocation density can be estimated based on the balance between strain hardening and recovery as shown in Equation 2.12:

$$d\rho_r = d\rho_r^+ + d\rho_r^- = (C_1\rho_r^{1/2} - C_2\frac{\sigma_f}{Z}\rho_r)d\varepsilon \tag{2.12}$$

where ($C_1 = M/b$) and ($C_2 = 2D_0 b\beta$) are physically-based constants and Z is the Zener Hollomon parameter.

One of the major changes that occurs due to the temperature, strain and transient strain rate during rolling is the change in dislocation density. Baxter *et al.* showed that the dislocation density in a material subject to decreasing strain rate from 25 s^{-1} to 2.5 s^{-1} at a constant strain of 0.6 is higher than the dislocation density in a material subject to constant strain rate of 2.5 s^{-1} for an Al-1%Mg aluminum alloy[63]. Researchers observed that the subgrain structure takes the form of microbands oriented at about 35° to the rolling plane with low misorientation subboundaries within them[63]. Thus, it was concluded that higher misorientation boundaries in the band are geometric boundaries necessary to accommodate local lattice curvature[63], where a unique dependence relationship between lattice curvature and geometrical necessary dislocations can be explained based on **Figure 2.7**.

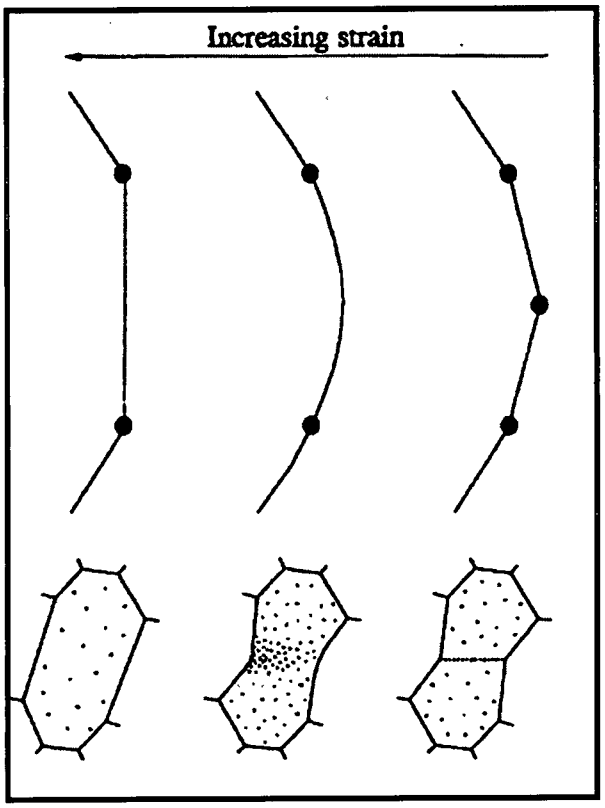

Figure 2.7 – A schematic drawing of dissociation of subgrain boundary and generation of geometrical necessary dislocations to maintain lattice curvature[63].

The initial structure is shown on the top right schematic drawing in **Figure 2.7**. Dissociation of the center boundary (middle schematic drawing) results in the ejection of geometrically necessary dislocations needed to maintain lattice curvature with neighboring subgrains[63, 64]. As the strain increases due to deformation, these geometrically necessary dislocations can join the adjacent subgrain boundaries (left schematic drawing) to increase their misorientation and thus retain local lattice curvature[64].

Based on this mechanism, to estimate the total dislocation density, the geometrically necessary dislocation density (ρ_g) must be considered[64]. For Al-Mg alloys subjected to transient deformation conditions, ρ_g is a major part of the calculated total dislocation density. Baxter *et al.*[63] derived a relationship to calculate local lattice curvature R as a function of geometrically necessary dislocations density, average subgrain size and average misorientation angle between subgrains as shown:

$$\frac{1}{R} = \rho_g b + \frac{\theta}{\delta} \tag{2.13}$$

where δ is the average subgrain size, θ represents the average misorientation angle between subgrains. The calculation of the total stored energy per unit volume during deformation is crucial for every physical model[65]. In order to accurately determine the material stored energy during hot rolling, the calculation of geometrically necessary dislocations needs to be considered in the total dislocation density calculation.

Exponential equations, which are semi-empirical constitutive relations have been successfully developed to model average subgrain size and average misorientation angle between subgrain evolution during hot deformation of aluminum alloys at constant strain rate and temperature[12]. By differentiating these equations, the evolution of substructure, namely average subgrain size and average misorientation angle between subgrains, can be tracked as a function of deformation as shown in Equations 2.14 and 2.15:

$$d\delta = \frac{\delta}{\varepsilon_\delta \delta_{ss}}(\delta_{ss} - \delta)d\varepsilon \tag{2.14}$$

$$d\theta = \frac{1}{\varepsilon_\theta}(\theta_{ss} - \theta)d\varepsilon \tag{2.15}$$

where θ represents the misorientation angle, δ is the subgrain size. ε_δ and ε_θ are characteristic strains, which are functions of the Zener-Hollomon parameter, and the subscript "ss" indicates a steady state condition. The relationships describing the evolution of subgrain size and misorientation angles between subgrains were devised utilizing experimental data for an Al-1%Mg aluminum alloy.

Castro- Fernandez *et al.*[66] devised a relationship between the steady state subgrain size and the instantaneous Zener Hollomon parameters as shown in Equation 2.16:

$$\frac{1}{\delta} = A \ln Z - B \tag{2.16}$$

where δ is the steady state subgrain size and A and B are alloy dependent constants.

2.3.2.2 *Modelling of recrystallization behavior*

As shown in the previous section of this review, nucleation at grain boundary surfaces is the dominant term during large deformation conditions[12]. Based on this finding, Vatne proposed a relationship to estimate nucleation density N_v as shown in Equation 2.17[67].

$$N_v = \left(\frac{C_d}{\delta^2}\right) S_v \tag{2.17}$$

where C_d is a calibration constant and S_v is the grain boundary area per unit volume which can be estimated from simple geometry assuming a cubic grain shape to be: $S_v = \frac{2}{d}\left(\exp(\varepsilon) + \exp(-\varepsilon) + 1\right)$. The recrystallization kinetics are then determined based on the nucleation density and growth rate of nuclei. Assuming site-saturated nucleation, recrystallization kinetics can be represented by the following relation[67]:

$$X = 1 - \exp(X_{ext}) \tag{2.18}$$

where X is the fraction recrystallized and X_{ext} is the corresponding extended volume fraction which is estimated as $\frac{3}{4}\pi N_v (Gxt)^3$. The growth rate G of the recrystallized nuclei is affected by the recovery of the deformed microstructure and the material stored energy[12] and can be described by the following relation:

$$G = M_{gb} P_D \tag{2.19}$$

where M_{gb} is the grain boundary mobility. By combining equations 2.18 and 2.19, the time to achieve 50% recrystallization can then be estimated as shown in Equation 2.20.

$$t_{0.5} = C_3 P_D^{-1} N_v^{-1/3} \tag{2.20}$$

where the material stored energy can be estimated and linked to the state variables based on Equations 2.3 – 2.5[12]. Finally, the fraction recrystallized can be estimated using the modified form of the JMAK equation as shown in Equation 2.7.

For the site saturated cases, the recrystallized grain size can be described based on Equation 2.21[67]:

$$d_{rex} = D(N_v)^{-1/3} \tag{2.21}$$

where D is a geometric parameter equal to 2.347, assuming uniform tetrakaidecahedra (TKD) grain structure.

2.3.2.3 Application of internal state variable model to Al- 4.5 % Mg aluminum alloy (AA5083)

The aforementioned relations describing substructure evolution and recrystallization kinetics were originally applied to an Al-1%Mg aluminum alloys where the constants were tuned based on the available data. The key factors that affect static recrystallization are related to the material stored energy and the number of nucleation sites which depend on the distribution of dispersoids and precipitates [41]. This distribution is determined by the alloy composition and the substructure. In AA5XXX aluminum alloys, the magnesium addition causes a significant lattice distortion, due to the difference in atomic size, leading to substantial solution strengthening, a high work hardening exponent, and the existence of second phase particles [68]. In addition, it was found by Sheppard *et al.*[69] that the fraction recrystallized increases with increase in percentage of magnesium added to aluminum during hot rolling which agrees with the findings of Dauda *et al.*[55].

The current research work aims to utilize and extend the internal state variable model to AA5083 aluminum alloys containing ~ 4.5% Mg. In order to apply the model to an AA5083 aluminum alloy, it is necessary to modify the model by introducing alternative values for the model constants based on experimental measurements.

It can be concluded that the physically-based model has established the level of complexity needed to describe the evolution of state variables, and hence the recrystallization kinetics. However, the model still contains some empirical constants that need to be tuned to fit the experimental results. These fitting parameters need to

be rationalized in order to understand the physics of the recrystallization process which has not been clearly reported so far.

Another approach has been recently proposed by Zurob *et al.* which couples precipitation, recovery and recrystallization along with their interdependencies through the change in one state variable, namely dislocation density[44]. Currently, the model has only been applied to steel where isothermal conditions were assumed, and the compositional effect on precipitation, recovery and recrystallization was not considered[44]. The model has not explored the integration of further state variables such as substructure changes, namely: average subgrain size and average misorientation angle between subgrains, which can play a key role in determining microstructure changes and has been validated against carefully controlled laboratory experiments.

To date, only one researcher has integrated a semi-empirical physically-based state variable model into an FE analysis[41, 70]. However, the predicted microstructure was not satisfactory for a single pass rolling case, where the model under predicted the recrystallized fraction compared to the experimental measurements[41]. During the course of this research work, Ahmed *et al.* have recently presented a successful integration of the model and an experimental validation for a single-pass rolling simulation[71].

To date, no one has attempted to integrate a physically-based model into an FE analysis to predict the recrystallization kinetics in multi-pass rolling cases through the strip thickness. According to Duan and Sheppard[70], the physically-based model in its current form is still not applicable to simulate multi-pass hot rolling with confidence because the effect of static recovery or recrystallization is excluded from the calculation of dislocation density in the inter-pass region and after rolling is complete. The prime challenge in applying a physically-based approach to simulate multi-pass hot rolling is the correct accumulation of the material stored energy [70]. Another challenging aspect is to find an approach to account for the air cooling conditions in the inter-pass region and integrate that effect into the microstructure model.

2.3.3 Modelling of Microstructure Evolution During Multi-Pass Hot Rolling

Hot rolling is a multi-pass process where recrystallization takes place between the passes and after the rolling is complete. The multi pass aspect complicates the modelling approach because of the partially recrystallized regions that occur in the inter-pass region which receive further deformation and subsequent recrystallization[5]. Sellars *et al.* illustrated the major principles of modelling microstructure evolution during multi-pass hot rolling as shown in **Figure 2.8**[13].

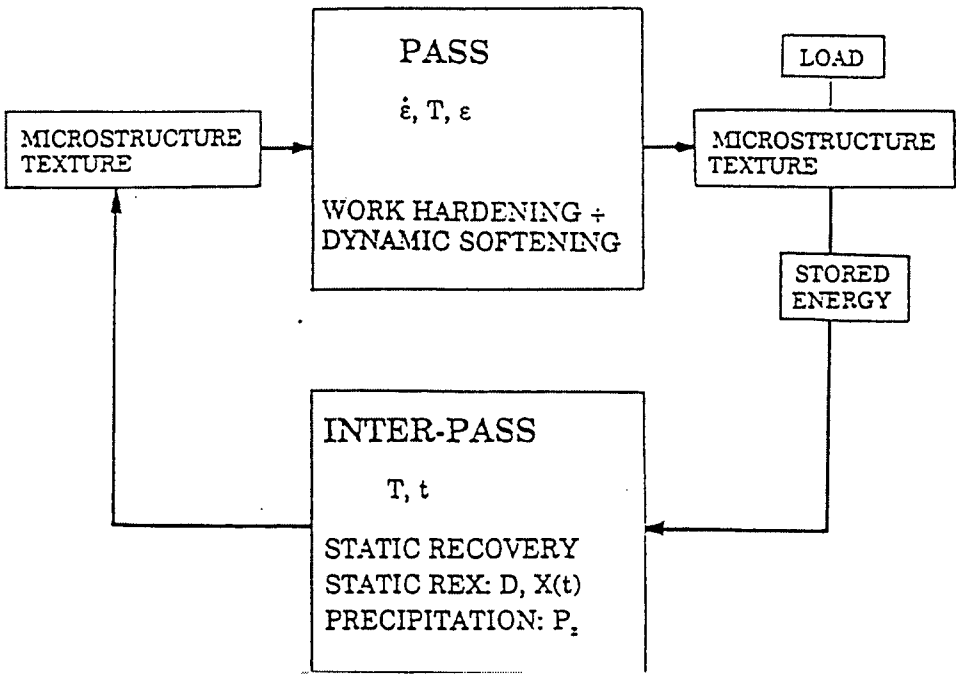

Figure 2.8 – A schematic diagram showing the modelling principles of microstructure evolution during multi-pass hot rolling[13].

During hot rolling, the strip is deformed under certain strain, strain rate and temperature, during which work hardening and dynamic softening take place. This in turn results in a stored energy in the material which provides a driving pressure for recrystallization in the inter-pass region before subsequent rolling passes. The inter-pass reaction will depend on the holding time between passes and the strip thermal profile. One of the main challenges in modelling multi-pass hot rolling is to capture and track the accumulation of stored energy to predict the resulting microstructure

especially during continuous air cooling in the inter-pass region and after rolling is complete.

Several approaches have been reported to model multi-pass hot rolling, differing mainly in effective strain calculation. Van der Winden estimated the driving pressure for recrystallization for AA3004 during break down rolling by calculating an average strain over the first ten passes[2]. The total driving pressure was calculated by averaging the total reduction that occurred during the first 10 passes to a single reduction value that occurred during a single pass rolling [2]. The average values for strain and strain rate were estimated using the strain fraction for each pass as a weighting function[2]. This approach assumes a single average microstructure with an effective strain based on the following relation:

$$\varepsilon_{eff}^{i} = \varepsilon_i - \lambda(1 - X_{i-1})\varepsilon_{i-1} \qquad (2.22)$$

where λ is a constant which varies as a function of the applied strain during rolling and X_{i-1} is the fraction recrystallized between two passes of strain ε_{i-1} and ε_i [2, 49]. Thus, the residual strain is eliminated in the recrystallized fraction and remains the same in the unrecrystallized fraction, so a weighted average representing an effective strain in the strip is calculated. This approach does not account for the variation of strain, strain rate and temperature distribution thorough the thickness of the strip. Another approach that was reported in steel rolling is to subdivide the partially recrystallized region into different sections based on the amount of recrystallization and to follow each new subregion separately during rolling[50, 72].

Vatne *et al.* proposed an approach to model microstructure evolution during multi- pass rolling for an AA3004 aluminum alloy based on JMAK recrystallization kinetics approach and the assumption of random nucleation distribution[49]. Nucleation was assumed to occur from: (i) cube bands, (ii) grain boundary regions and (iii) particles through particle stimulated nucleation (PSN) mechanism. Thus, the total nucleation density was calculated based on the following relationship:

$$N_{TOT} = N_c + N_{GB} + N_{PSN} \tag{2.23}$$

where N_c, N_{GB}, N_{PSN} are the densities of cube, grain boundary sites and particle stimulated nucleation, respectively. Due to partial recrystallization in the inter-pass region, Vatne *et al.* divided the material into two regions, namely X_1 where recrystallization takes place and $(1-X_1)$ where the material remains deformed in the inter-pass region[5, 49]. The total density of nucleation sites after nth pass was calculated based on Equation 2.24[5, 49].

$$N_{TOT}^{n} = N_{PSN}^{n} + X_{X-1}\left(N_C^n + N_{GB}^n\right) + \sum_{i=0}^{n-2} X_i \cdot \left[\prod_{j=i+1}^{n-1}\left(1-X_j\right)\right] \cdot \left[N_C^{i+1,\ldots,n} + N_{GB}^{i+1,\ldots,n}\right] \tag{2.24}$$

where $N_c^{i+1,\ldots,n}$ is the number of cube sites forming from the deformed cube areas which remains deformed between the passes (i+1) to (n-1) without recrystallization, and N_c^n is the cube area that recrystallized before the nth pass. The same naming approach applies to grain boundary (*GB*) nucleation[49]. The microstructure parameters, namely the fraction recrystallized and recrystallized grain size, become a function of the calculated total nucleation density[5].

A limiting factor of this approach is that major nucleation sites were only limited to the previously mentioned three nucleation site types, which may not always be true. For example, particle stimulated nucleation has minimal effect on the recrystallization behavior of AA5083 during hot rolling[4]. The model did not provide a means to track the substructure changes, which contribute significantly to the material stored energy. Another limitation of this approach is that it does not account for the variation in the softening kinetics, nucleation sites and thus the material stored energy through the thickness of the strip, but it rather assumes a unique value of total nucleation density based on Equation 2.24.

It can be seen from the previous review that very little work has been reported on modelling microstructure evolution during multi-pass hot rolling of aluminum alloys. Though a few studies have attempted to track microstructure changes during multi-pass hot rolling, no one has related the changes in the material stored energy to

both the thermo-mechanical and substructure evolution during the different stages of the multi-pass hot rolling process. Moreover, these approaches have not been validated against experimental measurements that simulate industrial hot rolling conditions.

2.4 Mathematical Model Validation for Hot Rolling of Aluminum Alloys

One of the primary aspects which must be considered is the validation of the model predictions against experimental measurements. There exists a considerable difference between the laboratory experiments used to characterize the microstructure evolution and the industrial conditions where these lab-based experimental findings are applied. Most of the laboratory simulations of the hot rolling process involve homogeneous deformation conditions using plane strain compression (PSC) (i.e., constant temperature and strain rate through the strip thickness)[73], which is not the case in industrial rolling mills.

The major problem in carrying out industrial validation of a hot rolling model is not only the major cost associated with such trials but also the difficulty of measuring the rolling parameters (temperatures and loads) due to the high rolling speed and the electrical noisy rolling environment, mainly due to the motors driving the work roll, which may affect the acquired data. Wells *et al.* validated their model predictions of temperatures, rolling load, fraction recrystallized, and recrystallized grain size against industrial measurements[54]. The model temperature predictions match the measurements relatively well; but the predicted rolling loads deviated significantly from the measurements especially in the later stands. Using an empirical approach, Wells *et al.* predicted recrystallized grain sizes that matched the experimental measurements relatively well as shown in **Figure 2.9**[54].

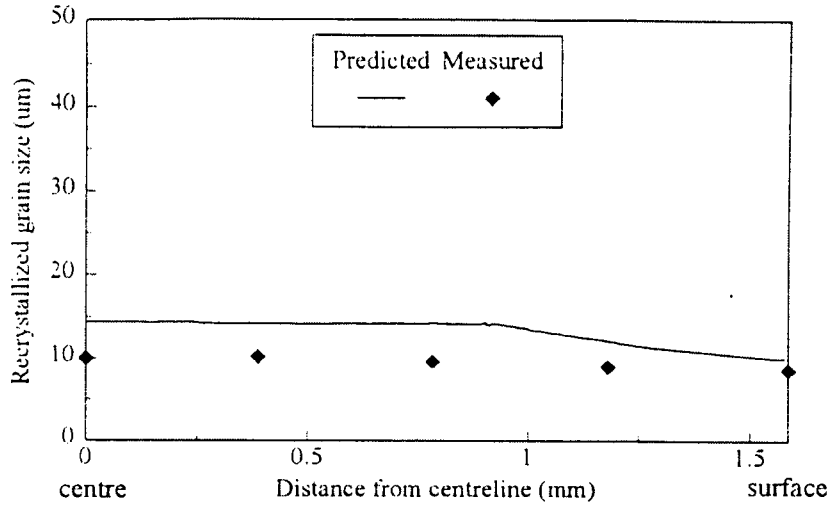

Figure 2.9 – A comparison between the model predicted and measured grain size after hot rolling of AA5182[54].

Timothy *et al.* were one of very few researchers to validate model predictions using industrial hot rolling data for an AA5083 aluminum alloy[74]. The temperature profiles measured during rolling were not physically possible since the recorded peak temperature at the strip centerline was higher than the calculated one assuming perfect insulation, thus the thermal model could not be validated, the measured equivalent strain matched the model predictions relatively well at the center of the strip whereas a considerable deviation occured close to the strip surface. Microstructure validation was not considered in Timothy *et al.* research[74].

Puchi *et al.* developed a mathematical model to predict loads during rolling which was validated based on industrial rolling measurements[1]. The model predictions of rolling load were compared to plant trial measurements where the model predictions were consistently lower than the measured loads as shown in **Figure 2.10**[1]. No microstructure validation was reported in this research.

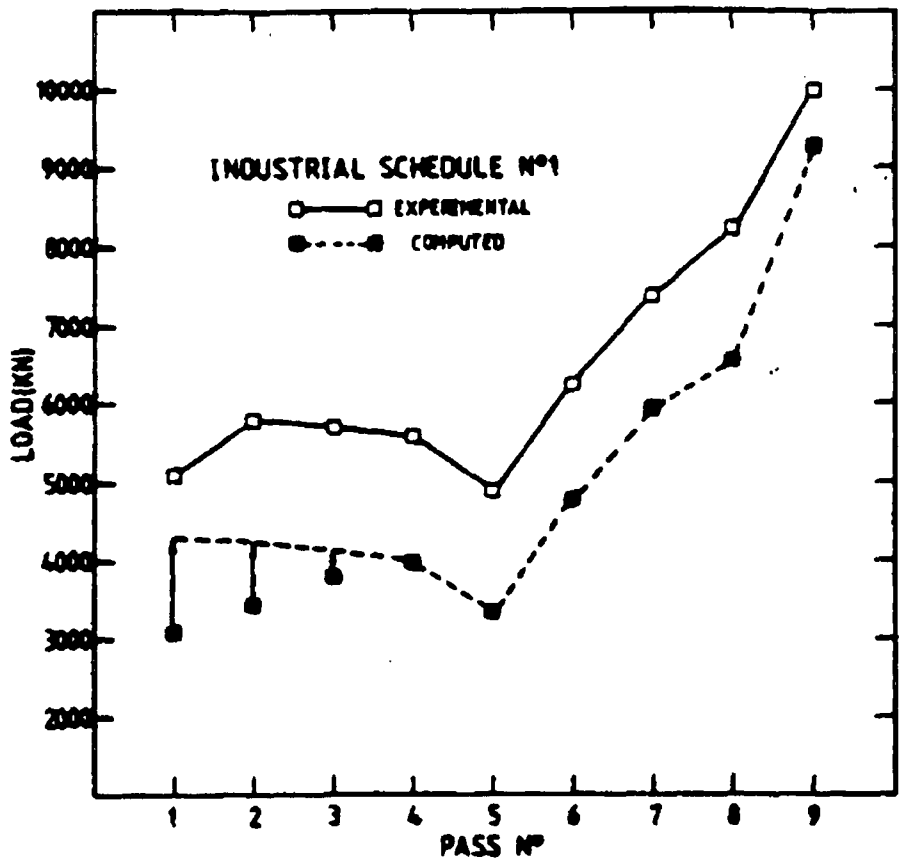

Figure 2.10 – Model predicted vs. experimental measurements of rolling loads[1].

An attempt was carried out to validate the model formulated by Vatne *et al.* for the multi-pass breakdown rolling case of AA3104 using the Sheffield Mill for Aluminium Roughing at Temperature (SMART)[75]. The validation was focused on a 14-pass schedule where the microstructure was studied by quenching specimens at intermediate stages[75]. A comparison between the model predictions after 14 passes ('14') and experimental measurements is shown in **Figure 2.11**.

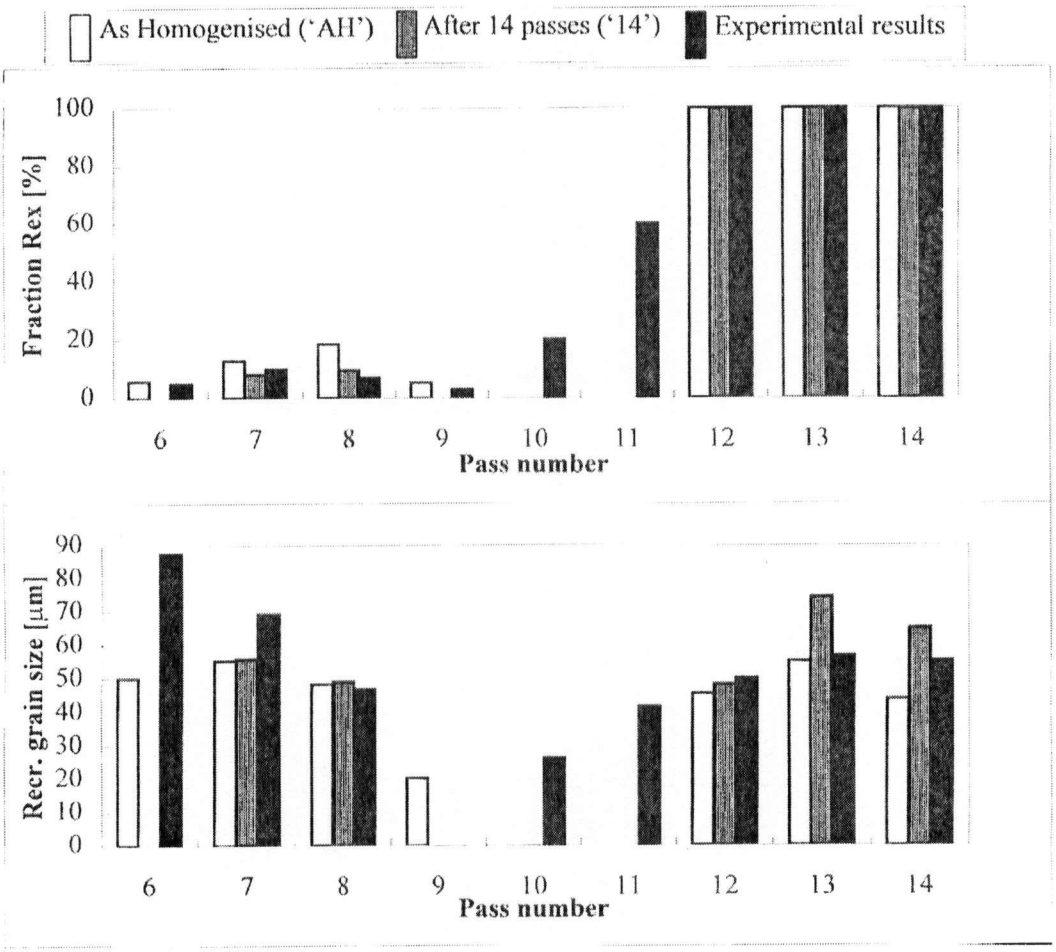

Figure 2.11 – Validation of Vatne's model predicted fraction recrystallized and recrystallized grain size[75].

The model provides reasonable predictions compared to the experimental measurements as can be seen in pass nos. 7,8,12-14[75]. The model predictions were not compared to experimental measurements during the first few rolling passes and has not been extended to tandem rolling cases.

Recently an integrated modelling approach for sheet rolling of commercial AA3103 and AA5182 aluminum alloys was developed during the course of the European VIR [*] project[76]. The main aim of the project was to develop a through process model (TPM) which includes the influence of various processing parameters on microstructure and material properties. To validate the model, the alloys were subjected to two different processing conditions throughout the sheet production

stages[76] . A comparison between the model predicted and measured grain size at different stages during processing for AA3103 is shown in **Figure 2.12**.

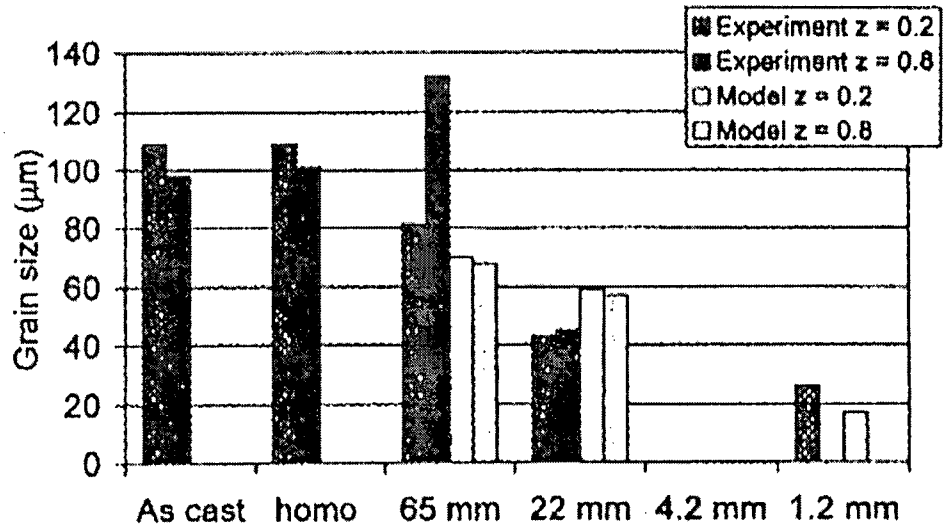

Figure 2.12 – Model predicted vs. measured recrystallized grain size at different processing stages for an AA3103 aluminum alloy[76].

The model predictions match the experimental measurements relatively well, although several major discrepancies occur as shown in **Figure 2.12** for the 65mm stage and 22 mm stage. The results show that the model predictions of recrystallized grain size are within 10-50% of experimental values[76]. The model does not account for the differences in grain size through the thickness of the strip. The model predicted fraction recrystallized during hot rolling at different stages matches the experimental measurements relatively well. The major shortcoming of this validation work is that a qualitative estimate of the model accuracy and reliability is rather difficult due to the fact that only two processing conditions were used to verify the model[76]. Thus the model sensitivity and accuracy at different processing conditions were not studied.

2.5 Summary

The microstructure evolution in aluminum alloy strip during hot rolling is linked to complex interactions between the thermal and mechanical phenomena in the process and the metallurgical response of the material. In order to comprehend these interactions and to develop an optimal processing strategy, it is of prime importance to be able to develop knowledge-based process models which incorporate microstructure equations to provide a scientific understanding of the resulting microstructure during hot rolling. Towards this goal, a trend, driven by industry, has evolved focusing on the development and use of physically-based models to analyze and understand the thermo-mechanical and microstructure behavior during hot rolling.

There are several approaches suggested to understand and model the microstructure evolution and the interaction between thermo-mechanical effect and the resulting microstructure. However, the integration of FE thermo-mechanical models and physically-based microstructure models to simulate industrial multi-pass hot rolling and the tracking of the material stored energy during the various hot rolling stages through the strip thickness to further understand the recrystallization behavior has not been done previously. Based on the literature review, it is clear that extensive industrial validation of a multi-pass hot rolling model is scarce. Industrial validation under a wide range of industrially relevant rolling conditions to verify quantitatively and accurately the thermo-mechanical and microstructure models is still lacking.

References

1. Puchi, E.S., J. Beynon, and C.M. Sellars. in *THERMEC '88, International Conference on Thermomechanical Processing of Steels and Other Materials* . 1988. Tokyo, Japan: Iron and Steel Institute of Japan.

2. van der Winden, M.R., *Laboratory simulation and modelling of the break-down rolling of AA3104, Ph.D thesis*. 1999, Sheffield university: Sheffield, U.K.

3. Vatne, H.E. and M.A. Wells. *Microstructure modelling in industrial aluminum hot-rolling processes - the state of the art and the challenges ahead.* in *Light Metals 1999*. 1999. Quebec City, Canada: CIM.

4. Humphreys, F.J. and M. Hatherly, *Recrystallization and related annealing phenomena*. 1996, NewYork: Pergamon Press. 363.

5. Vatne, H.E. and E. Nes, *Experimental investigation and modelling of recrystallization in two hot deformed aluminum alloys, Ph. D Thesis*. 1995, Norwegian Institute of Technology: Trondheim, Norway.

6. Sheppard, T. *The modern extrusion process; temperature and speed.* in *Modern extrusion: plant, tooling, processes and products*. 1980. Birmingham, U.K.

7. Nes, E., *Recovery Revisited.* Acta Metallurgica Materialia, 1995. **43**(6): p. 2189-2207.

8. Hull, D. and D.J. Bacon, *Introduction to dislocations*. 2001, Oxford: ButterWorth Heinemann. 242.

9. Gallagher, P.C.J., *The influence of alloying, temperature and related effects on stacking fault energy.* Metall. Mater. Trans. A, 1970. **1**: p. 2429-2461.

10. Sellars, C.M. and G.J. Davis. *Hot working and forming processes*. in *International conference organized jointly by the Sheffield Metallurgical and Engineering Association and the University of Sheffield in assocation with The Metals Society*. 1980. London: The Metals Society.

11. McQueen, H.J. and J.J. Jonas, *Recovery and recrystallization during high temperature deformation.* Treatise on Materials Science and Technology, 1975. **6**: p. 393-493.

12. Sellars, C.M. and Q. Zhu, *Microstructureal modelling of aluminum alloys during themomechanical processing.* Mater. Sci. Eng., A, 2000. **280**: p. 1-7.

13. Sellars, C.M., *Modelling microstructural development during hot rolling.* Mater. Sci. Technol., 1990. **6**: p. 1072-1081.

14. Sheppard, T. *Application of Limit Diagrams to Extrusion Process Control.* in *Proceedings of Second International Aluminum Extrusion Technology Seminar*. 1977. Washington, D.C: Aluminum Assoc. Inc.

15. Sellars, C.M., *The Hot worked state.* Mater. Sci. Forum, 1993. **113-115**: p. 29-40.

16. Chen, B.K., P.F. Thomson, and S.K. Choi, *Computer Modelling of microstructure during hot flat rolling of aluminium.* Mater. Sci. Technol., 1992. **8**(1): p. 72-77.

17. Zaidi, M.A. and T. Sheppard, *Development of microstructure throut out roll gap during rolling of aluminum alloys.* Met. Sci., 1982. **16**: p. 229-238.

18. Humphreys, F.J., *A unified theory of recovery, recrystallization and grain growth, based on stability and growth of cellular microstructures - I. The basic model.* Acta Mater., 1997. **45**(10): p. 4231-4240.

19. Nes, E., *Constitutive laws for steady state deformation of metals, a microstructure model.* Scr. Metall., 1995. **33**(2): p. 225-231.

20. McQueen, H.J., O. Knustad, N. Ryum, and J.K. Solberg, *Microstructural Evolution in Al Deformed to Strains of 60 at 400 deg C.* Scr. Metall., 1985. **19**(1): p. 73-78.

21. McQueen, H.J., *Elevated temperature behavior of AA5083.* Journal of Materials Engineering and Performance, 2001. **10**: p. 164-172.

22. McQueen, H.J. and K. Conrod. in *Microstructural Control in Aluminum Alloys: Deformation, Recovery, and Recrystallization.* 1985. New York, USA: TMS.

23. Sheppard, T., M.A. Zaidi, M.G. Tutcher, and N.C. Parson. in *Microstructural control in aluminum alloys: deformation, recovery and recrystallization.* 1985. New York: TMS.

24. Gardner, G.J. and R. Grimes, *Recrystallization during hot deformation of aluminum alloys*, in *Metal Science.* 1979. p. 216-222.

25. Humphreys, F.J. and M.R. Drury. *Formation of High Angle Grain Boundaries and New Grains During Deformation of Al--5%Mg at Elevated Temperatures.* in *Aluminium Technology '86.* 1986. London; UK: The Institute of Metals.

26. Sandstrom, R. and R. Lagneborg, *Controlling factor for dynamic recrystallization.* Scr. Metall., 1975. **9**(1): p. 59-65.

27. Orsund, R. and E. Nes, *Subgrain Growth During Annealing of Heavily Deformed Metals.* Scr. Metall., 1989. **23**(7): p. 1187-1192.

28. Furu, T., R. Orsund, and E. Nes, *Subgrain growth in heavily deformed aluminum--experimental investigation and modelling treatment.* Acta Metall. Mater., 1995. **43**(6): p. 2209-2232.

29. Sellars, C.M., A.M. Irisarri, and E.S. Puchi. in *Microstructural Control in Aluminum Alloys: Deformation, Recovery, and Recrystallization.* 1985. New York, USA: TMS.

30. Sheppard, T. and X.J. Duan, *Modelling of static recrystallization by the combination of empirical models with finite element method.* J. Mat. Sci., 2003. **38**: p. 1747-1754.

31. Sellars, C.M., F.J. Humphreys, E. Nes, and D. Juul Jensen. *Microstructural modeling of industrial thermomechanical processing.* in *Numerical Predictions of Deformation Processes and the Behaviourof Real Materials.* 1994. Roskilde, Denmark.

32. Humphreys, F.J., *A new analysis of recovery, recrystallization and grain growth.* Mater. Sci. Technol., 1999. **15**: p. 37-44.

33. Beck, P.A., H. Hu, and P.R. Sperry, *Rolling texture in face-centered cubic metals.* AIME TRANS., 1952. **194**: p. 76-81.

34. Hurley, P.J. and F.J. Humphreys, *Modelling of recrystallization of single-phase aluminum.* Acta Mater., 2003. **51**: p. 3779-3793.

35. Sellars, C.M. *Microstructure modeling in hot deformation.* in *Thermo-Mechanical Processing in Theory, Modelling & Practice.* 1996. Stockholm; Sweden: Swedish Society for Materials Technology.

36. Roters, F., D. Raabe, and G. Gottstein, *Work hardening in heterogeneous alloys - a microstructural approach based on three internal state variables.* Acta Mater., 2000. **48**: p. 4181-4189.

37. Shercliff, H.R. and A.M. Lovatt, *Modelling of microstructure evolution in hot deformation.* Philos. Trans. R. Soc. London, Ser. A, 1999. **357**: p. 1621-1643.

38. Read, W.T., *Dislocations in crystals.* 1953, New York: McGraw-Hill.

39. Raghunathan, N., M.A. Zaidi, and T. Sheppard, *Recrystallisation kinetics of Al-Mg alloys AA 5056 and AA 5083 after hot deformation.* Mater. Sci. Technol., 1986. **2**: p. 938-945.

40. Ryum, N. and J.D. Embury, *A comment on the recrystallisation behaviour of Al-Mg alloys.* 1982. **11**(2): p. 51-54.

41. Duan, X.J. and T. Sheppard, *Influence of forming parameters on static recrystallization behaviour during hot rolling aluminium alloy 5083.* Modell. Simul. Mater. Sci. Eng., 2002(10): p. 363-380.

42. Raghunathan, N. and T. Sheppard, *Microstructural development during annealing of hot rolled Al-Mg alloys.* Mater. Sci. Technol., 1989. **5**: p. 542-547.

43. Wells, M.A., D.J. Lloyd, I.V. Samarasekera, J.K. Brimacombe, and E.B. Hawbolt, *Modelling the microstructural changes during hot tandem rolling of AA5XXX aluminum alloys: part I.* Metall. Mater. Trans. B, 1998. **29B**: p. 611-620.

44. Zurob, H.S., C.R. Hutchinson, Y. Brechet, and G. Purdy, *Modeling recrystallization of microalloyed austenite: effect of coupling recovery, precipitation and recrystallization.* Acta Mater., 2002. **50**: p. 3075-3092.

45. Davies, C.H.J. and L. Hong, *The cellular automaton simulation of static recrystallization in cold- rolled AA1050.* Scr. Metall., 1999. **1999**: p. 1145-1150.

46. Marx, V., F.R. Reher, and G. Gottstein, *Simulation of primary recrystallization using a modified three-dimentional cellular automation.* Acta Mater., 1999. **47**(4): p. 1219-1230.

47. Geiger, J., A. Roosz, and P. Barkoczy, *Simulation of grain coarsening in two dimensions by cellular-automaton.* Acta Mater., 2001. **49**: p. 623-629.

48. Wells, M.A., D.J. Lloyd, I.V. Samarasekera, J.K. Brimacombe, and E.B. Hawbolt, *Modeling the microstructural changes during hot tandem rolling of AA5XXX aluminum alloys. Part III.* Metall. Mater. Trans. B, 1998. **29B**: p. 709-720.

49. Vatne, H.E., K. Marthinsen, R. Orsund, and E. Nes, *Modeling recrystallization kinetics, grain sizes, and textures during multipass hot rolling.* Metall. Mater. Trans. A, 1996. **27A**: p. 4133-4144.

50. Sellars, C.M. and J.A. Whiteman, *Recrystallization and grain growth in hot rolling.* Metal Sciene, 1979. **13**: p. 187-194.

51. Chopard, B. and M. Droz, *Cellular automata modeling of physical systems.* 1998, Cambridge ; New York: Cambridge University Press. 326.

52. Hesselbarth, H.W. and I.R. Gobel, *Simulation of recrystallization texture by cellular automata.* Acta Metall. Mater., 1991. **39**(9): p. 2135-2143.

53. Gutierrez, I., F. Castro, J.J. Urcola, and M. Fuentes, *Recrystallized grain size of commercial-purity aluminum after hot torsion within steady-state regime.* Materials Science and Technology, 1990. **6**(9): p. 819-828.

54. Wells, M.A., *Mathematical modelling of the microstructure and texture changes during hot tandem rolling of AA5182 and AA5052 aluminum alloys, Ph. D Thesis.* 1995, University of British Columbia: Vancouver, Canada.

55. Dauda, T.A. and A.J. McLaren. in *Modelling of Metal Rolling Processes 3.* 1999. London: IoM Communications Ltd.

56. McLaren, A.J. and C.M. Sellars. *Strip Cast., Hot Cold Work. Stainless Steels, Proc. Int. Symp.* 1993. Montreal, Canada: CIM.

57. Brand, A.J., S. Kalz, and R. Kopp, *Microstructural simulation in hot rolling of aluminum alloys.* Computational Materials Science, 1996. **7**(1&2): p. 242-246.

58. Mirza, M.S., C.M. Sellars, K. Karhousen, and P. Evans, *Multipass rolling of aluminum alloys: finite element simulations and microstructural evoltion.* Mater. Sci. and Tech., 2001. **17**: p. 874-879.

59. Wells, M.A., D.M. Maijer, S. Jupp, G. Lockhart, and M.R. van der Winden, *Mathematical model of deformation and microstructural evolution during hot rolling of aluminum alloy 5083.* Mater. Sci. Technol., 2003. **19**(4): p. 467-476.

60. Nes, E., *Modelling of work hardening and stress saturation in FCC metals.* Prog. Mater. Sci., 1998. **41**(3): p. 129-193.

61. Nix, W.D., J.C. Gibeling, and D.A. Hughes, *Time dependent deformation of metals.* Metall. Mater. Trans. A, 1985. **16**(12): p. 2215-2226.

62. Zhu, Q. and C.M. Sellars. in *Modelling of metal rolling processes*. 1996: The institute of materials.

63. Baxter, G.J., T. Furu, Q. Zhu, J.A. Whiteman, and C.M. Sellars, *The influence of transient deformation conditions on recrystallization during themomechanical processing of aluminum alloy Al-1% Mg.* Acta Mater., 1999. **47**(8): p. 2367-2376.

64. Sellars, C.M. in *THEMEC '97, International Conference on Thermomechanical Processing of Steels and Other Materials* . 1997. Wollongong, Australia.

65. Duan, X. and T. Sheppard, *Simulation of substructural strengthening in hot flat rolling.* J. Mat. Proc. Tech., 2002. **125-126**: p. 179-187.

66. Castro-Fernandez, F.R., C.M. Sellars, and J.A. Whiteman, *Changes of Flow Stress and Microstructure During Hot Deformation of Al--1Mg--1Mn.* Mater. Sci. and Tech., 1990. **6**(5): p. 453-460.

67. Vatne, H.E., R. Shahani, and E. Nes, *Deformation of cube oriented grains and formation of recrystallized cube grains in a hot deformed commercial AlMgMn aluminum alloy.* Acta Mater., 1996. **44**: p. 4447-4462.

68. McShane, H.B., C.P. Lee, and T. Sheppard, *Structure, anisotropy, and properties of hot rolled AA5083 alloy.* Mater. Sci. and Tech., 1990. **6**: p. 428-440.

69. Sheppard, T. and X.J. Duan, *Modelling of static recrystallisation by the combination of empirical models with finite element method.* J. Mater. Sci, 2003. **38**: p. 1747-1754.

70. Duan, X.J. and T. Sheppard, *Computation of substructural strengthening by the integration of metallurgical models into the finite element code.* Comput. Mater. Sci., 2003. **27**(3): p. 250-258.

71. Ahmed, H., M.A. Wells, D.M. Maijer, B.J. Howes, and M.R. van der Winden, *Modelling of microstructure evolution during hot rolling of AA5083 using an*

internal state variable approach integrated into an FE model. Mater. Sci. Eng., A, 2005. **390**(1-2): p. 278-290.

72. Laasraoui, A. and J.J. Jonas, *Prediction of Steel Flow Stresses at High Temperatures and Strain Rates.* Metall. Mater. Trans. A, 1991. **22A**(7): p. 1545-1558.

73. Vatne, H.E., T. Furu, R. Orsund, and E. Nes, Mater. Sci. Technol., 1996. **12**: p. 201-210.

74. Timothy, S.P., H.L. Yiu, J.M. Fine, and R.A. Ricks, *Simulation of single pass of hot rolling deformation of aluminum alloy by plane strain compression.* Mater. Sci. Technol., 1991. **7**(3): p. 255-261.

75. van der Winden, M.R., H.E. Vatne, and C.M. Sellars. *Modelling the texture evolution during break-down rolling of AA3104 with special attention to the effect of the distribution of second phase particles.* in *Hot deformation of aluminum alloys II.* 1998. Rosemont, Illinois: The minerals, metals, and materials society.

76. Marthinsen, K., S. Abtahi, K. Sjolstad, B. Holmedal, E. Nes, A. Johansen, J.A. Saeter, T. Furu, O. Engler, Z.J. Lok, J. Talamantes-Silva, C. Allen, and C. Liu, *Modelling the evolution of microstructure and mechanical properties during processing of AA3103.* Aluminium, 2004. **80**(6): p. 729-738.

CHAPTER 3

SCOPE AND OBJECTIVES

3.1 Objectives of Research Program

The primary objective of the present study is:

- To improve the scientific understanding of recrystallization behavior during hot rolling of aluminum alloys and predict the fraction recrystallized and final grain size in rolled products employing mathematical modeling techniques.
- To apply the model to understand and optimize the recrystallization behavior in industrial multi-pass hot rolling scenarios.

To achieve this objective, the following research tasks have been identified:

- Development of a mathematical model using the commercial FE code ABAQUS to predict the thermal and deformation history experienced by the material during single and multi-pass hot rolling.
- Development and use of an internal state variable microstructure model in conjunction with the thermo-mechanical FE model of the rolling process to predict the evolution of the deformed microstructure, in terms of state variables and their evolution during rolling and in the inter-pass region.
- Validation of the both the deformation and microstructure model using experimental data obtained from an industrial-scale pilot rolling facility under a wide range of industrially relevant hot rolling schedules.
- Application of the verified model to understand the recrystallization behavior through the thickness of the AA5083 sheet between passes and after rolling is complete and thereafter provide enhanced understanding of industrial hot rolling.

Although several models that relate processing history, and microstructure evolution have been developed and validated to date (as mentioned in Chapter 2), the uniqueness of this proposal lies in:

- Modelling multi-pass hot rolling for AA5083 where different recrystallization levels may occur between rolling passes and the correct accumulation of the

material stored energy throughout each stage of the rolling process using a state variable approach.

- The integration of the FE thermo-mechanical model results into a microstructure model for an AA5083 aluminum alloy during multi-pass hot rolling to provide a detailed description of microstructure changes during deformation. This was done by using predicted incremental values of strain, strain rate and temperature that develop during rolling.
- Extensive validation of both the thermo-mechanical and the microstructure model based on experimental measurements conducted using an industrial rolling mill under various rolling conditions to ensure the applicability of the model under different rolling scenarios.
- Applications of the verified model to investigate the effect of strain partitioning during multi-pass hot rolling on the material stored energy as well as to generate industrially relevant operational curves that can be used to understand the evolution in material stored energy during multi-pass hot rolling and thus optimize the rolling process.

3.2 Scope of the Research Program

The overall goal of this research program was to develop fundamental knowledge to understand the microstructure evolution of AA5083 aluminum sheet during single and multi-pass hot rolling processes. The complex interaction between deformation temperature, strain and strain rate determines the material stored energy and subsequent recrystallization kinetics. A key aspect of this work is the way in which the stored energy is accumulated and quantified in the material in situations where no or only partial recrystallization occurs in the inter-pass region. In addition, there is a need to validate the microstructure predictions against industrial data using a wide range of industrially relevant rolling conditions. Critical to simulating industrially relevant conditions is that the deformation conditions are transient and the thermal history varies throughout the roll bite. In addition, the chilling effect of the work roll causes a large thermal gradient throughout the strip. The research program focused primarily on modelling the microstructure evolution which is achieved by developing a process model capable of describing the deformation conditions and the microstructure evolution for hot rolling cases.

3.2.1 Model Development

A fundamentally-based 2-D model was developed to predict the distribution of strain, strain rate and temperature through the thickness of the strip for an AA5083 aluminum alloy using the commercial finite element (FE) software package, ABAQUS. The development of the thermo-mechanical model entailed the implementation of appropriate boundary conditions to simulate hot rolling process. Additional heat transfer boundary conditions were employed in the inter-pass region to simulate the strip-air cooling during multi-pass rolling cases.

A physically-based microstructure model using internal state variables microstructure model has been developed in conjunction with the FE simulation of the rolling process to predict the evolution of the material stored energy and subsequent recrystallization after deformation is complete. A challenging aspect in modelling microstructure evolution during multi-pass rolling for AA5083, is that recrystallization is often not complete between hot rolling passes and hence the accumulation of stored energy in situations where various recrystallization levels occur through the strip thickness between rolling passes must be correctly accounted for. The principle of additivity was employed to account for the continuous cooling conditions that occurred in the inter-pass region and after rolling was complete. A law of mixtures was used to determine the initial entry value to the next rolling pass of the strain, dislocation density, average subgrain size and average misorientation angle between the subgrains.

3.2.2 Model Validation

To obtain industrial data suitable for model validation, an experimental program was undertaken using Corus' single-stand reversible rolling facility located in IJmuiden, the Netherlands on 200mm x 400mm x 9mm samples of AA5083 aluminum alloy instrumented with thermocouples both at the centerline and the surface. A voltage signal corresponding to the applied rolling load was recorded simultaneously. A series of eleven samples were rolled using different multi-pass rolling conditions to vary the driving pressure for recrystallization and the resulting microstructure. The recorded temperature data at the center and the surface of the strip and the measured voltage corresponding to the rolling load were used to validate the

thermo-mechanical FE model. The inter-pass boundary conditions were validated by comparing the model predicted temperature against measured data acquired from the thermocouple. Once the rolling experiments were completed, the strip was sectioned and the final microstructure through the thickness of the strip was characterized in terms of both the fraction recrystallized and the recrystallized grain size. These measurements were used to validate the microstructure model predictions.

Figure 3.1 shows an overview of the research work that was carried out in this research project.

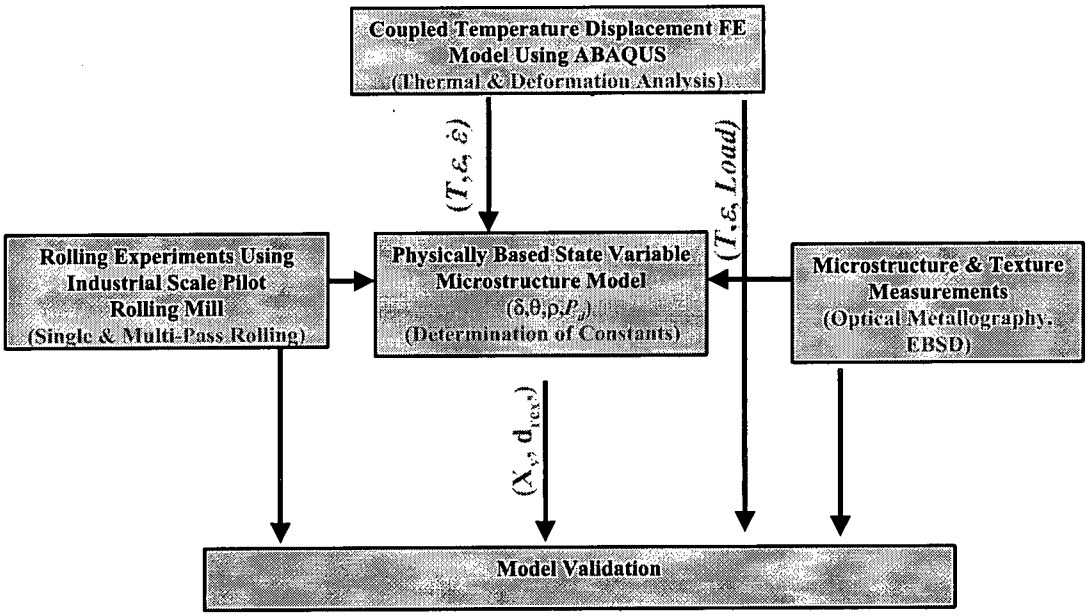

Figure 3.1 – Overview of modelling and experimental work carried out in this research program

CHAPTER 4

Rolling Experimental Program

4.1 Introduction

A series of hot rolling experiments were conducted using Corus' multi-mill rolling facility, located in IJmuiden, the Netherlands, to validate both the thermo-mechanical and microstructure models of hot rolling. During a previous study conducted, a series of six single-pass hot rolling experiments were conducted to validate the deformation model for single-pass rolling cases[1]. During the course of this doctoral research project, multi-pass hot rolling experiments were conducted to further validate the deformation and the microstructure model for multi-pass hot rolling cases.

The main objective of the experimental work was to validate the correct method to describe the accumulation of stored energy in the material during hot rolling and determine how the ensuing microstructure evolution was influenced. One of the main considerations when designing the experimental test matrix was to ensure that the rolling schedule chosen was industrially relevant. The experiments consisted of rolling samples of AA5083 aluminum alloy under a variety of temperatures, strains, strain rates, holding times between passes and holding times after second-pass rolling. The following section summarizes the details of the single pass hot rolling experiments conducted previously. The rest of the chapter focus on the experimental work conducted in this research work namely: the microstructure validation of single-pass rolled samples and the multi-pass hot rolling experiments.

4.2 Single-Pass Rolling Experiments

4.2.1 Previously Conducted Experimental Work

During a previous study conducted utilizing Corus multi-mill research facility located in IJmuiden, the Netherlands, an experimental program was undertaken where a series of six single-pass rolling experiments were conducted to validate the model

predicted thermo-mechanical history [2]. Table 4.1 provides details of the rolling conditions used for each of the tests in the study.

Table 4.1 – Matrix of single stand rolling experiments runs[2]

Sample No.	ε	Average $\dot{\varepsilon}$ (s^{-1})	T_{entry} (°C)	T_{hold} (°C)	Time prior to quench (s)
1	0.29	22.9	460	447	3
2	0.52	14.5	448	424	15
3	0.28	11.8	397	382	8
4	0.27	22.3	390	396	3
5	0.27	22.3	320	325	3
6	0.26	11.5	315	314	4

During the previous study, the experiments consisted of rolling instrumented samples of AA5083 aluminum alloy under different temperature, strain and strain rate conditions and then quenching the samples within 3-15 seconds after rolling was complete[2]. The experimental measurements were used to verify model predicted temperature and strain during single-pass rolling.

4.2.2 Microstructure Characterization of Single-Pass Rolled Samples (performed as part of this doctoral research work)

The first step of this doctoral research project was to characterize the microstructure evolution in the previously rolled samples for use to construct and validate a microstructure model for single-pass rolling cases. Specifically, optical microscopy and Electron Back Scatter Diffraction (EBSD) were used to determine the fraction recrystallized and recrystallized grain size on the single-pass rolled samples.

The initial microstructure of the single-pass hot rolled material contains elongated grains. Using quantitative image analysis and employing linear intercept method based on ASTM E112-96 standard, the grain size was determined to be 70.0 μm which did not vary significantly from the center to the surface. The average length of the grains was 77.2μm and the average height was 19.8μm.

The samples were sectioned and mounted to expose the microstructure through the thickness of the material in the rolling direction. The mounted samples were polished and anodized to reveal the final microstructure. Image analysis of the specimens was employed to quantify the percent recrystallization in each sample at three through-thickness locations from the center to the surface. The volume fraction of the recrystallized grains was determined according to the ASTM E562-89 standard point counting technique at each location in the sample. For each location, measurements were repeated to ensure accuracy whereby a minimum of 24 fields were analyzed.

A heat treatment was carried out at 500°C for 40 minutes to ensure that the sample was fully recrystallized through the strip thickness to facilitate recrystallized grain size measurements using line intercept technique. Full recrystallization was difficult to confirm considering the grains' relatively elongated nature after the heat treatment procedure. As a result, microhardness measurements using a load of 100g were carried out for both the as rolled and heat treated samples. As can be seen in **Figure 4.1**, a significant softening effect was measured and indicates that recrystallization has occurred.

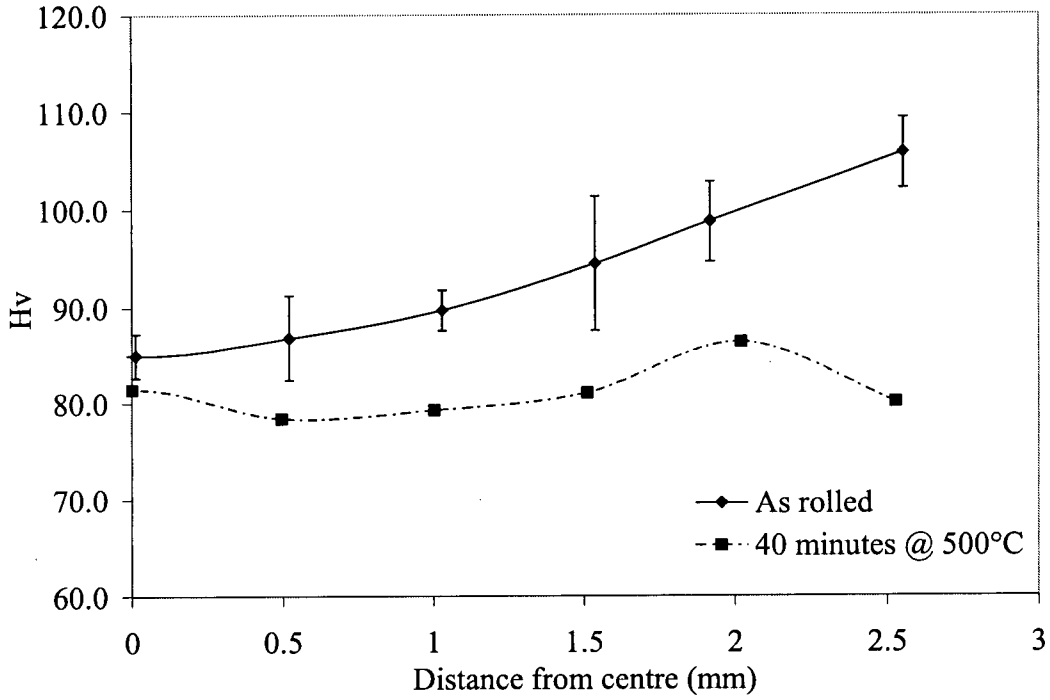

Figure 4.1 – Hardness profile for single-pass rolled sample no. 2 comparing the as-rolled sample to the heat-treated samples for different time increments.

Electron Backscattered Diffraction Pattern (EBSD) images based on crystallographic orientation were utilized to confirm recrystallization and measure the average recrystallized grain size to compare with the optically measured recrystallized grain size for sample no. 2. The selected EBSD scan area was 0.26 mm^2 with a step size of 3 μm. Average grain size measurements using the EBSD data were performed using a linear intercept technique at three locations through the thickness of each sample, namely: center, quarter-thickness, and surface. A comparison between the grain shapes and sizes measured via the EBSD and the optical micrographs is shown in **Figure 4.2** for sample no. 2 at the center and the surface of the strip.

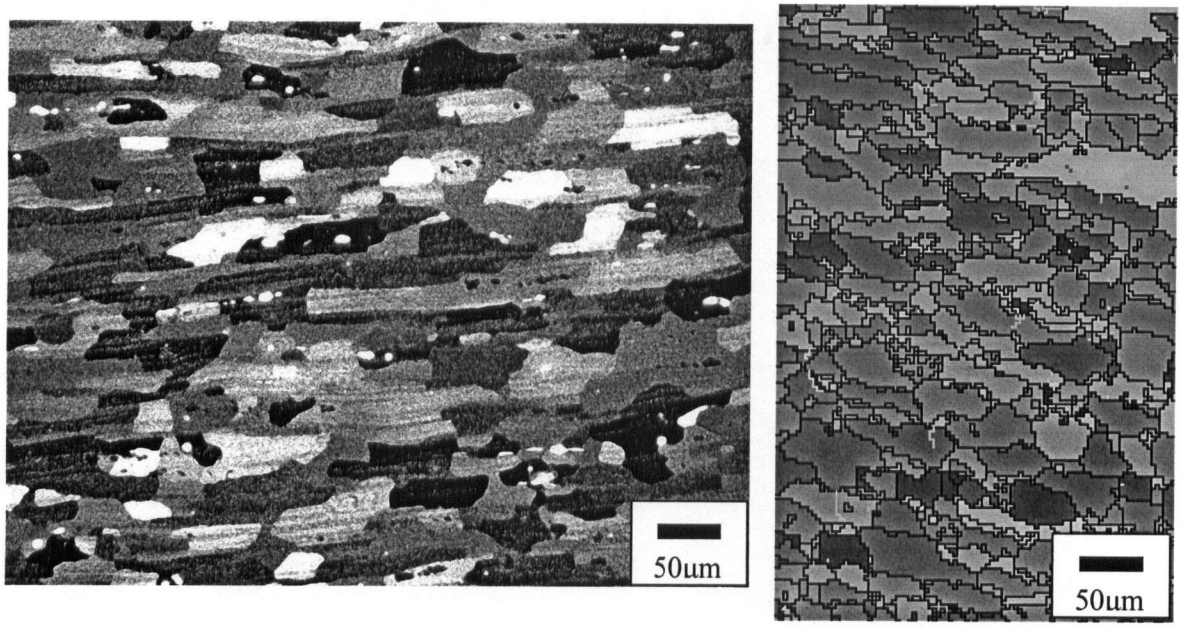

a) Optical micrograph vs. EBSD map at the strip center

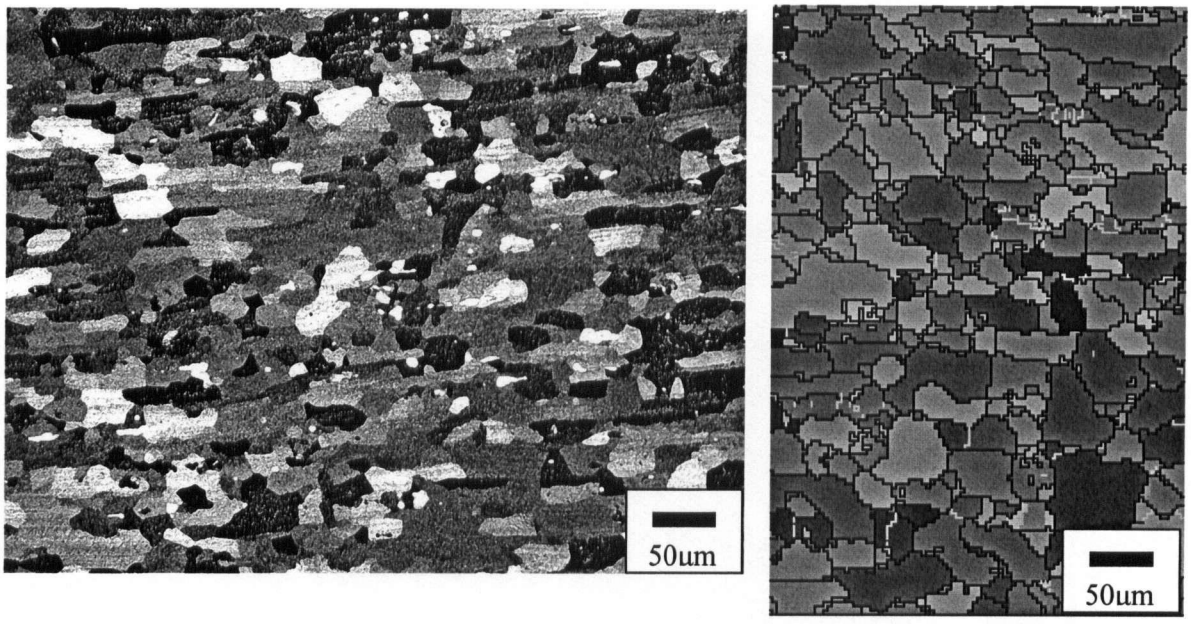

b) Optical micrograph vs. EBSD map at the strip surface

Figure 4.2 – Optical micrograph vs. EBSD map for single-pass rolled sample no. 2 at (a) the strip center, and (b) the strip surface after heat treatment. Note: EBSD maps show sub-grain boundaries in cyan colored lines (assuming a misorientation angle less than or equal to 3°) and grain boundaries outlined in black (assuming a misorientation angle less than or equal to 15°).

As shown in Figure 4.2, the EBSD map shows very little grain sub-structure indicating strain free grains and that complete recrystallization has occurred.

The measured fraction recrystallized and recrystallized grain size data was used to determine the appropriate constants for use in the microstructure model and also served as a validation of the proposed microstructure model for single-pass rolling cases as will be shown in Chapter 6.

Once the single-pass rolling model was validated, the author conducted multi-pass rolling experiments using Corus' multi mill rolling facility during the course of this doctoral research project. A detailed description of the multi-pass hot rolling experiments conducted during the course of the doctoral research project is detailed in the following section.

4.3 Multi-Pass Hot Rolling Industrial Plant Trials (Carried out as part of this doctoral research work)

4.3.1 Sample Description

The experimental work, conducted during the course of this doctoral research work, was carried out on aluminum alloy AA5083 (Al – 4.5% Mg) supplied by Corus in slab gauge form (after break down rolling for testing). The material was DC cast to sheet ingots 500 mm thick that were subsequently breakdown rolled to 20 mm which was further rolled to 9.6mm. Due to variation in the measured initial thickness between different plates, the material was further rolled to 9 mm thickness to ensure uniform starting thickness of the material. To promote a homogeneous starting microstructure, the material was heat treated for 2 hours at 450°C. The chemical composition for the AA5083 used in this research is shown in Table 4.2. The initial microstructure of the starting material at the centerline and the surface of the strip is shown in **Figure 4.3**.

Table 4.2 – Chemical composition of AA5083 (wt %)

Mg (%)	Mn (%)	Si (%)	Fe (%)	Cr (%)	Zn (%)	Al (%)
4.45	0.64	0.27	0.22	0.09	0.12	Remainder

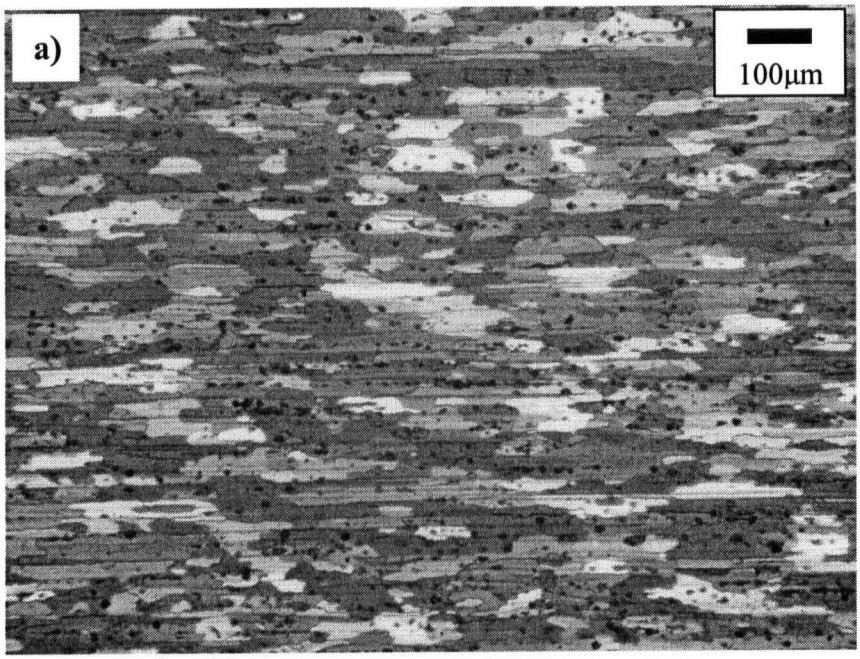

a) Optical micrograph at the strip centerline

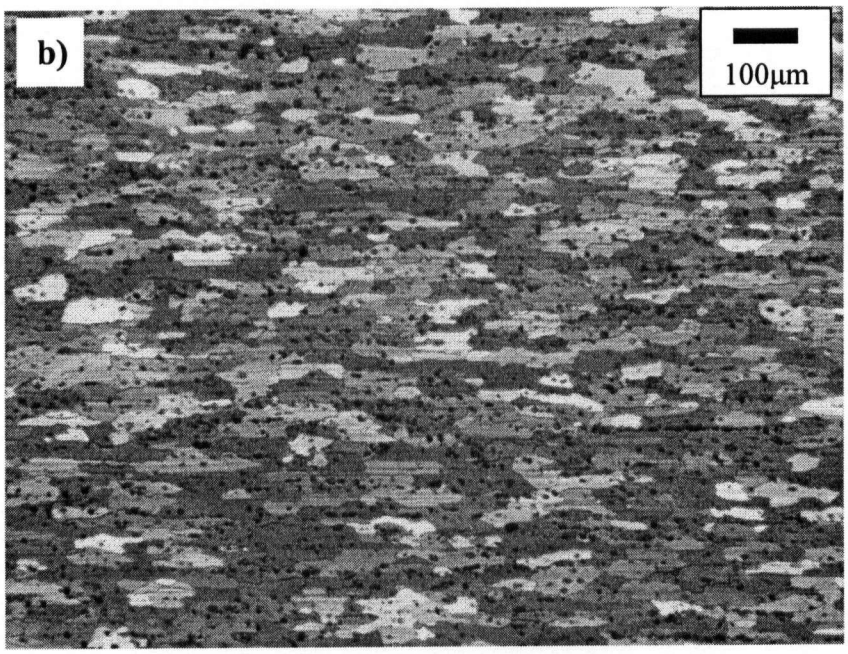

b) Optical micrograph at the strip surface

Figure 4.3- Starting sample microstructure at: (a) Centerline, (b) Surface of the strip

As can be seen from **Figure 4.3**, the initial microstructure shows elongated grains with slight variation from the center to the surface of the strip. Complete recrystallization in the heat treated samples was confirmed using the Electron Back Scatter Diffraction (EBSD) system to evaluate grain sub-structure. The EBSD maps show very little substructure indicating strain free grains and that complete recrystallization had occurred. The elongated nature of the grains may be due to the presence of disperosoids which inhibits growth in certain directions resulting in recrystallized elongated grains. Using image analysis and employing the line intercept technique, the average grain size using was determined to be ~35 μm which did not vary significantly through the strip thickness with a standard deviation of 2.3 μm and an average aspect ratio of 1.66.

4.3.2 Sample Instrumentation

All the samples were instrumented with four Type E intrinsic thermocouples for centerline and surface temperature measurements. The details of the sample geometry and setup for sample instrumentation are shown in **Figure 4.4**. The nominal sample dimensions are 400mm long x 200mm wide x 9mm thick with the long side parallel to the rolling direction.

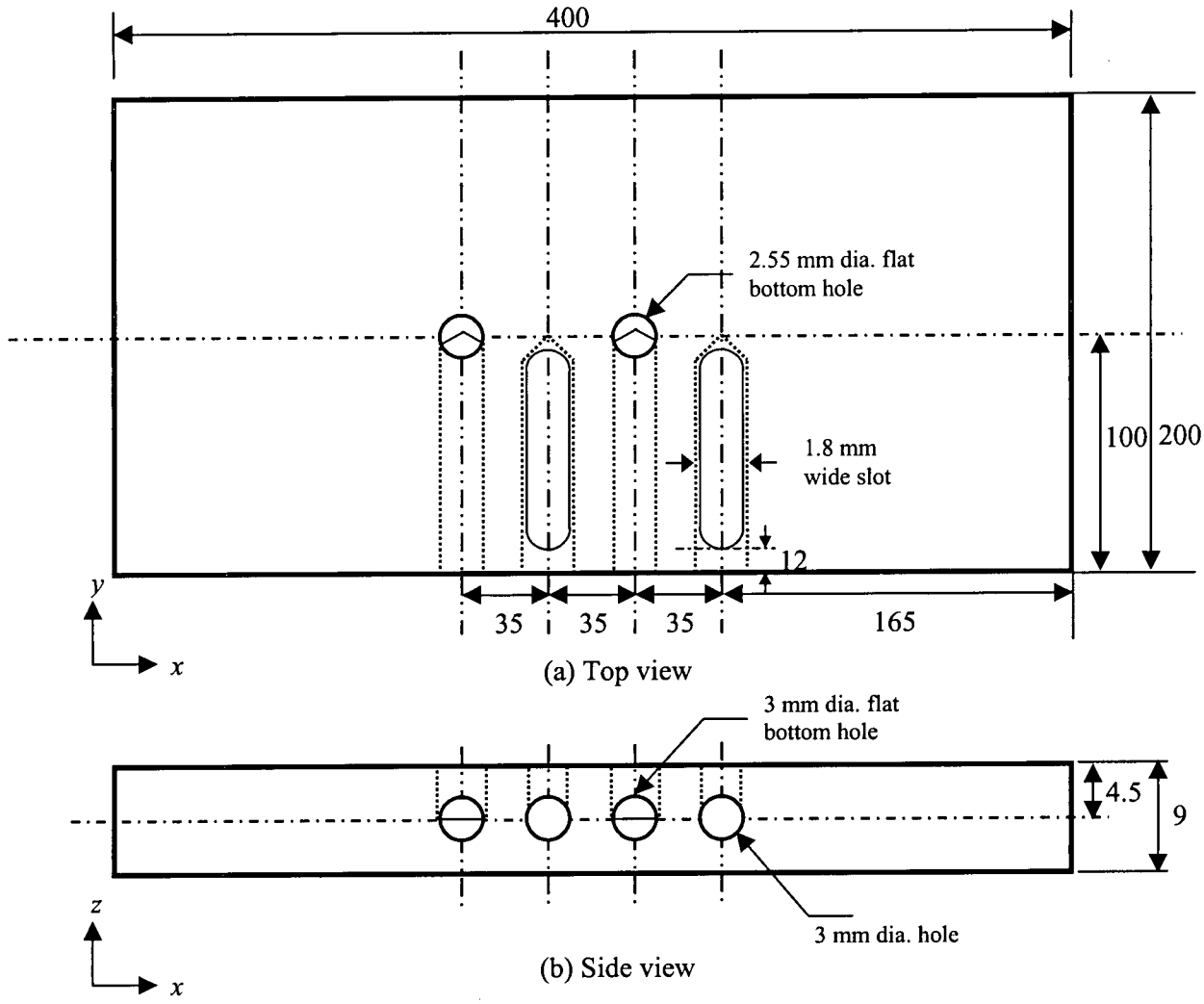

Figure 4.4 – A schematic diagram showing the (a) top and (b) side views of the geometry for the rolled samples. Note: Units are in mm (not to scale)

Figure 4.4 shows a schematic drawing of the sample indicating the location of the two-centerline thermocouples and two-surface ones. For each centerline thermocouple, a 2.55 mm diameter flat bottom hole was drilled from the sample top surface to the sample centerline to accurately position the thermocouples as shown in **Figure 4.4a**. For the surface thermocouples, a 1.6 mm wide x 4.5mm deep groove was machined from the mid-width of the sample to within 12 mm from the sample outside edge as shown in **Figure 4.4a**. Four 3 mm access holes for metal clad thermocouples wires were drilled into the side of each sample to the mid-width of the sample (**Figure 4.4b).** For the centerline thermocouples, the access holes were drilled

just long enough so as to intersect the top-drilled flat bottom holes and to provide a short ledge on which the thermocouple junction was made (**Figure 4.4a**). The 12 mm of material left along the edge of the sample ensured that the surface thermocouples would remain clamped in position following the first pass.

In an effort to reduce the scatter in the recorded temperature and improve the quality of the recorded data, in comparison to the single-pass rolled samples, commercially available metal-sheathed, Type-E intrinsic thermocouple wire was used to instrument the samples for multi-pass rolled samples. This wire consisted of a single pair of thermo-element wire measuring 0.25 mm in diameter, magnesium oxide insulation and Inconel 600 sheathing measuring 1.57 mm in diameter. Typically the length of the thermocouple wire used was 4.5 m. The thermocouples were connected to a data acquisition board using shielded thermocouple-grade extension wire supplied with a ground wire. The length of an extension wire measured 15 m. The drain wire was connected to the Inconel sheath of the thermocouple wire in order to maintain an electrical ground from the thermocouple tip to the data acquisition board. The data acquisition computer was electrically floated, and a single ground wire connected the data acquisition board to the rolling mill. A schematic drawing of the thermocouple placement details is shown in **Figure 4.5**. A picture of a rolling sample that further illustrates the instrumentation details is shown in **Figure 4.6**.

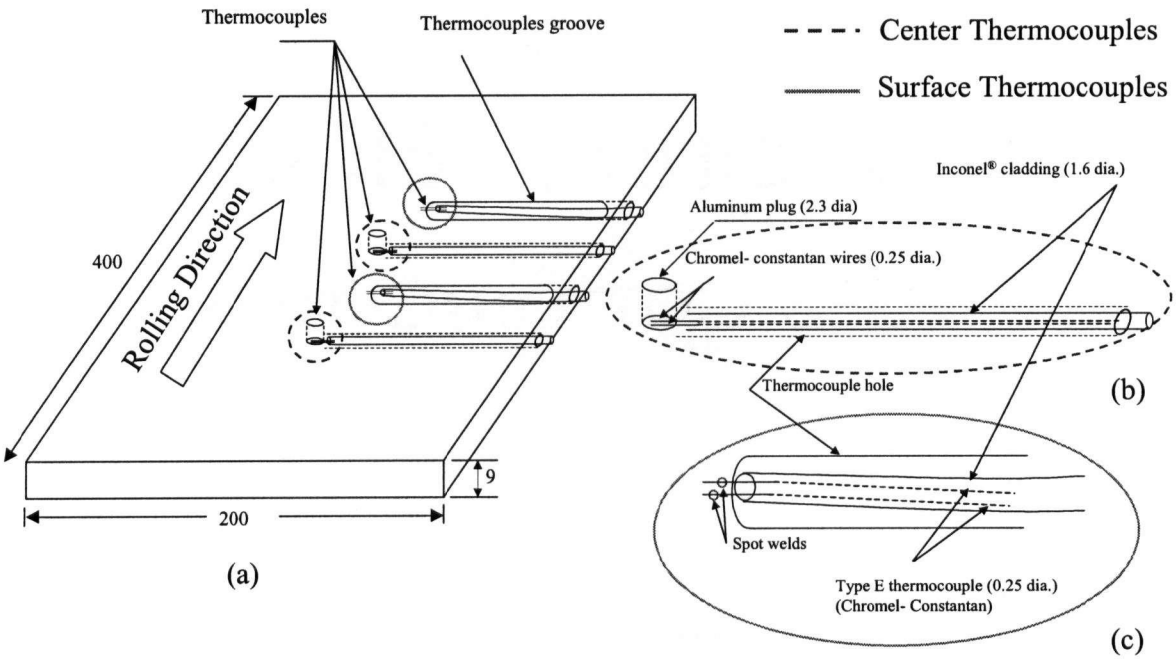

Figure 4.5 – A schematic diagram of thermocouple placement details showing: (a) sample geometry, (b) Centerline thermocouples, (c) Surface thermocouples. Note: Units are in mm (not to scale)

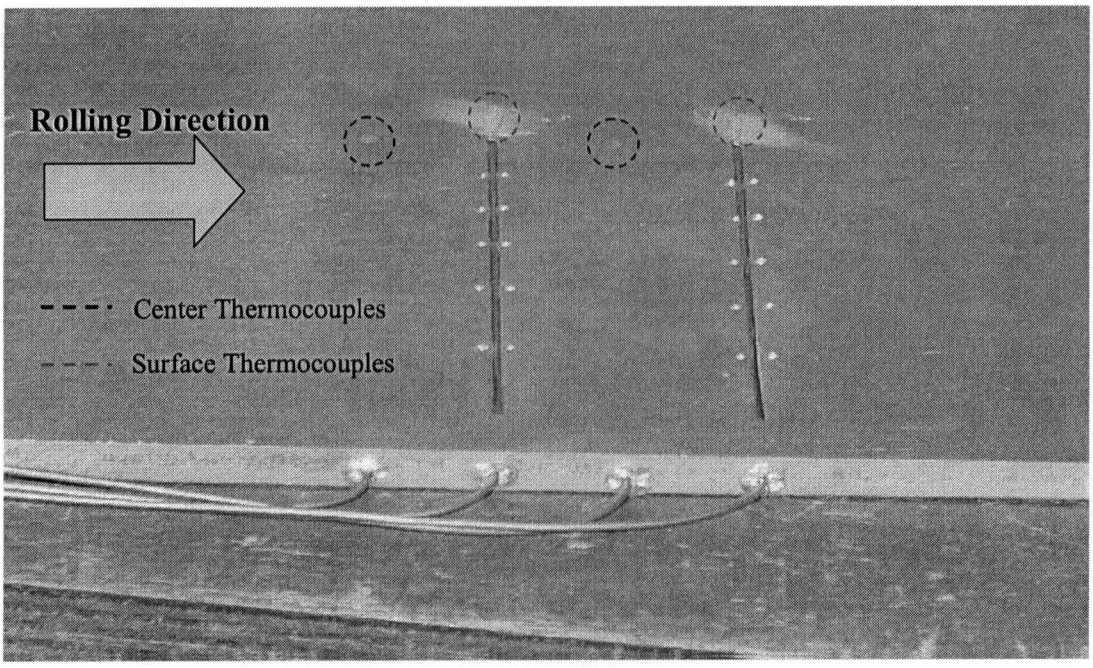

Figure 4.6 – A picture of an instrumented sample illustrating both centerline and surface thermocouple instrumentation details

As shown in **Figure 4.5**, the Chromel-Constantan thermocouple wires were positioned and held in place at the center of the sample using cylindrical plugs of aluminum, made of AA5182 to form an intrinsic thermocouple junction. On the sample surface, exposed Chromel-Constantan wires were placed approximately 0.5 mm apart and were spot-welded to the sample surface to establish another intrinsic junction. Intrinsic thermocouple use the sample material to complete the circuit which decreases the response time of the thermocouple compared to an extrinsic thermocouple[3]. The transient response of the Type E intrinsic thermocouple used during the rolling experiments was calculated based on Henning and Parker model[4, 5]. It was found that ~ 0.4 ms is necessary for the thermocouple to reach 95% of the steady state e.m.f. which is lower than the used temperature data acquisition frequency in this experimental work which ranged between ~ 470- 650 Hz (i.e., a data point is collected every ~ 1.5-2 ms). Thus, it was concluded that the thermocouple response times is reasonable and hence Type E intrinsic thermocouple wires can be used to record thermal profiles during rolling.

The sample surface was center punched close to the surface thermocouple slots to maintain the position of the thermocouple wires as shown in **Figure 4.6**. Four thermocouples were installed in each sample (two centerline thermocouples and two surfaces ones). Redundant centerline and surface thermocouples were installed to ensure that at least one signal was recorded at each of the two locations. This was necessary due to the delicate nature of the thermocouples wires which may result in wire breakage especially during sample handling.

A Panasonic notebook computer, Instrunet 100 signal conditioning amplifier and Instrunet 230 PCMCIA controller card system was used for data acquisition. The voltage range for the thermocouples was ± 80mv, and ± 5 v for the load signals. A voltage divider was used to half the recorded signals from the multi-mill during rolling. An integration time in the order of 0.0005 s was employed to minimize the noise and smooth collected data. The frequency of temperature acquisition during the rolling trials depended primarily on the number of recorded signals. Most of the samples had four thermocouples installed and the recording frequency was approximately 462 Hz. A higher data collection frequency was employed for one of

the rolled samples where three thermocouple signals (rather than four) were recorded at 612 Hz.

4.3.3 Rolling Load Measurement

Two voltage signals from the rolling mill operation panel that correspond to the applied load at each of the rolls were recorded during rolling. The voltage signals were collected at 10 Hz using the same data acquisition system used to collect the temperature data. The two voltage signals were recorded and subsequently added to determine the total measured voltage which was converted to the corresponding rolling load using a calibration factor. A calibration curve was constructed to devise a relationship between rolling loads and recorded voltage. To construct the calibration curve, a known rolling load, based on the mill control station data, was applied and the corresponding measured voltage was recorded. The procedure was repeated at different rolling loads to produce the calibration curve as shown in **Figure 4.7**. The work roll velocity was determined by multiplying the RPM of the work roll during the experiment (measured with a tachometer located on the drive shaft) by the work roll diameter.

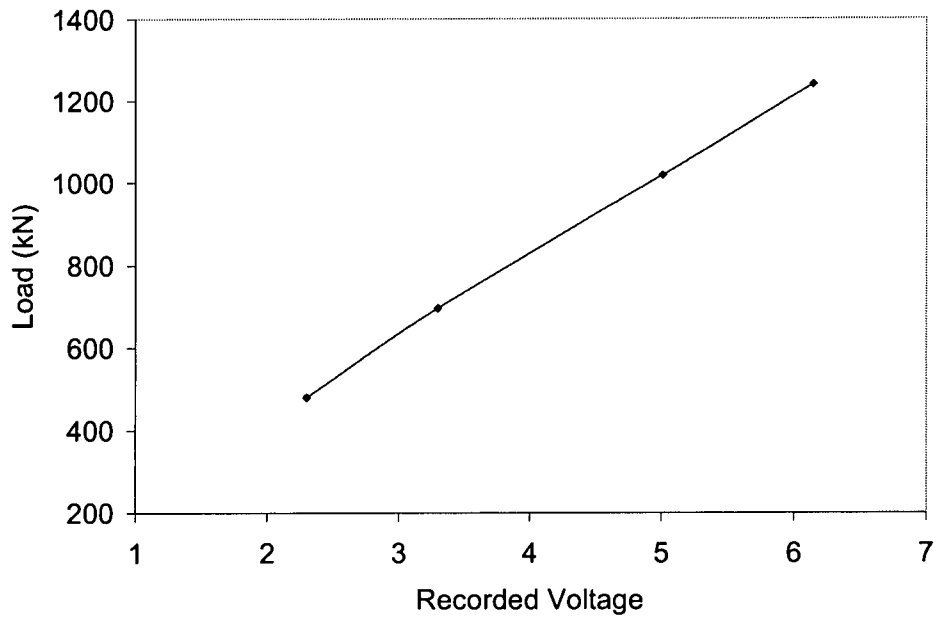

Figure 4.7 – A calibration curve which shows the corresponding load for each measured voltage.

4.3.4 Rolling Experiments

A series of eleven two-pass hot rolling experiments was conducted to validate both the thermomechanical and the microstructure model. The main objective of the experimental work was to determine a suitable method to describe how energy accumulates in the material as a result of deformation in cases where different levels of recrystallization have occurred prior to the second-pass. The experiments were performed by rolling instrumented samples of AA5083 aluminum specimens under a variety of temperatures, strains, strain rates and holding times both in the inter-pass region and after rolling was complete before quenching the sample. The actual temperature, strain rate and total strain achieved during each test were evaluated from the measured data and used in the data analysis. A summary of the experimental test matrix is shown in Table 4.3.

Table 4.3-Rolling conditions for multi-pass hot rolling trials using Corus' rolling mill.

Sample	Pass number	Entry temp (°C)	Mean strain rate (s^{-1})	Strain	Hold time (s)	Z (s^{-1})
1	1	450	~5.8	0.30	20	$1.75x10^{11}$
	2	380	~13.6	0.30	5	$5.47x10^{12}$
2	1	430	~5.8	0.30	20	$3.49x10^{11}$
	2	359	~13.6	0.30	25	$1.33x10^{13}$
3*	**1**	**445**	**~5.8**	**0.30**	**20**	$2.08x10^{11}$
	2	**370**	**~13.6**	**0.30**	**15**	$8.28x10^{12}$
4	1	445	~5.8	0.30	7	$2.08x10^{11}$
	2	386	~13.6	0.30	15	$4.29x10^{12}$
5	1	440	~5.8	0.30	35	$2.46x10^{11}$
	2	363	~13.6	0.30	15	$1.12x10^{13}$
6	1	405	~5.8	0.30	20	$8.70x11^{11}$
	2	344	~13.6	0.30	15	$2.60x10^{13}$
7	1	480	~5.8	0.30	20	$6.71x10^{10}$
	2	412	~13.6	0.30	15	$1.57x10^{12}$
8	1	440	~5.8	0.24	20	$2.46x10^{11}$
	2	389	~13.6	0.30	15	$3.80x10^{12}$
9	1	440	~5.8	0.36	20	$2.46x10^{11}$
	2	377	~13.6	0.30	15	$6.18x10^{12}$
10	1	445	~4.7	0.30	20	$1.68x10^{11}$
	2	365	~13.6	0.30	15	$1.02x10^{13}$
11	1	440	~7	0.30	20	$2.97x10^{11}$
	2	382	~13.6	0.30	15	$5.04x10^{12}$

*** Baseline sample**

The experimental test matrix was designed to validate the model under a wide variety of industrially relevant rolling conditions. Though most of the inter-pass times in Table 4.3 are not typical for tandem rolling cases, the chosen conditions and inter-pass times were deemed to be suitable to validate the proposed deformation and microstructure rolling model under different process parameters. Moreover, it is believed that the microstructure results obtained based on the conditions described in Table 4.3 can be extended to understand microstructure evolution during breakdown rolling cases where the inter-pass times will be closer to the ones used in these experiments.

The experimental test matrix was also designed to examine the effect of the following parameters:

1) The effect of changing the holding time after second pass rolling on the material stored energy and subsequent fraction recrystallized (samples no. 1,2,3).
2) The effect of changing the hold time in the inter-pass region on the resulting microstructure after second-pass deformation (samples no. 3,4,5).
3) The effect of initial temperature on the fraction recrystallized after second-pass hot rolling (samples no. 3,6,7).
4) The effect of changing the reduction schedule (strain) during first-pass rolling on the resulting fraction recrystallized after second-pass deformation (samples no. 3,8,9).
5) The effect of changing the strain rate (rolling speed) during first-pass rolling on the resulting fraction recrystallized after second-pass rolling (samples no. 3,10,11)

The Corus' multi-mill is designed as a research tool aimed at simulating industrial rolling process conditions with two basic configurations for hot rolling and cold rolling. The hot rolling configuration is used for breakdown rolling, plate rolling and finish rolling of aluminum. This setup includes:

(i) A pre-heating furnace used to heat the sample to the required temperature,
(ii) Pre- heated work rolls with a diameter of 400 mm. The work rolls are made of steel with an internal oil circulation system to maintain the desired roll temperature.
(iii) A 50m rolling table[6].

Though the Corus pilot scale research mill is an experimental facility, it can used to simulate industrial hot rolling processes effectively. Specifically, the multi mill facility work roll diameter of 400 mm, a speed range between 0.1-20 m/s and a maximum roll force of 1800 kN[6], closely simulates the actual work roll diameter and operation conditions in industrial setting. The only differences between the pilot

scale work roll and the ones used in actual aluminum production is the width of the work roll. A layout of the experimental setup using Corus' multi-mill is shown in **Figure 4.8**.

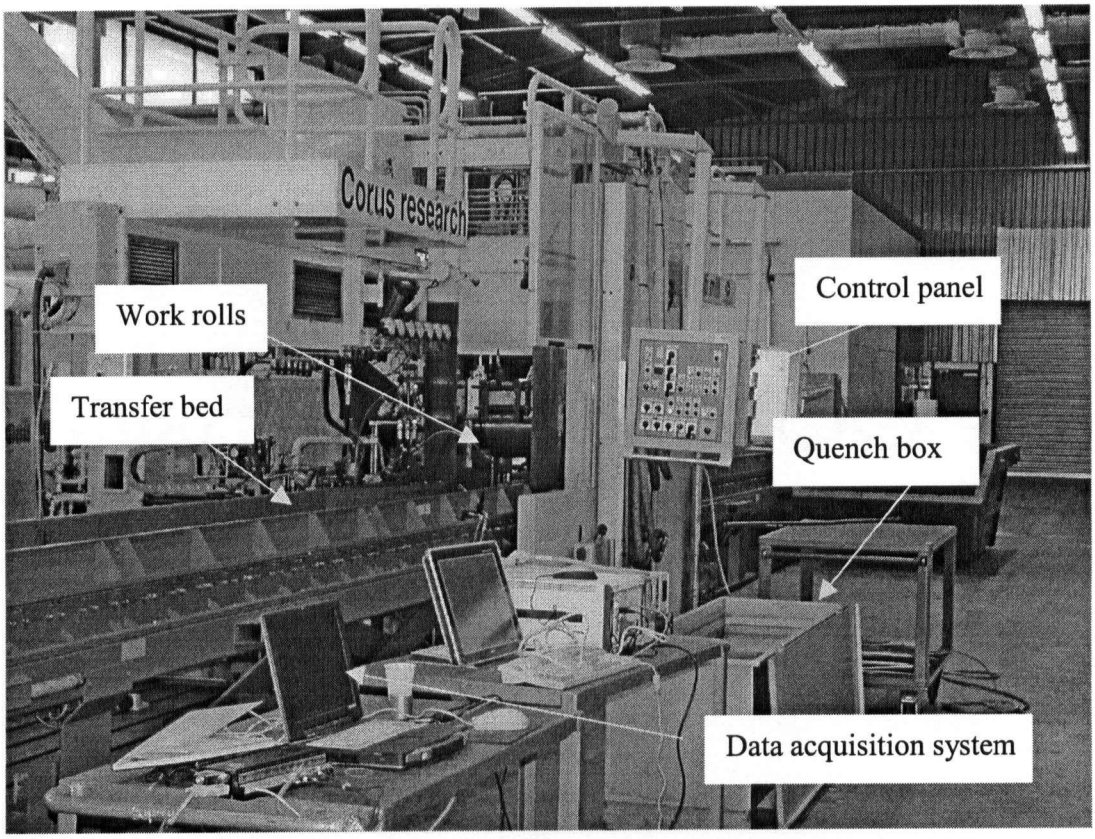

Figure 4.8 – Experimental setup (Corus multi-mill).

During the experiments, the work rolls were preheated to ~90°C using circulating oil. The preheating furnace was set to 460°C. The furnace was capable of heating the samples to the required temperatures in approximately 40-50 minutes. The sample was then transferred from the furnace to the work rolls using the transfer bed. The data acquisition system was located near the work rolls as shown in **Figure 4.8**. The quench tank was located ~1.5 meters from the roll bite exit. At the time of the plant trial, the automatic oil emulsion lubrication system was not operating. As a result, the oil emulsion lubricant was manually applied before each run.

The rolling trials were initiated by heating the sample in the preheating furnace (not shown in **Figure 4.8)** to the required temperature. Samples were usually held in the furnace for a period of time that varied between one to two hours before rolling. The samples were removed from the furnace and manually transferred to the roll bite entrance. The samples were then manually fed into the roll bite ensuring that the thermocouples leads were held clear. Following first-pass rolling, the samples were held for the required holding time and the rolling direction was reversed. The samples were manually fed into the roll bite for second-pass rolling. Following second-pass rolling in the reverse direction, the samples were held for the required period of time followed by water quenching in the quench tank. Following the water quench, the data acquisition was stopped.

It should be noted that the only means to attain multi-pass rolling during the industrial rolling trials was to reverse the rolling mill direction upon completion of the first pass rolling to facilitate sample handling and ensure that the thermocouple wires remain out of the roll bite. Thus, the inter-pass times shown in Table 4.3 during multi-pass hot rolling does not reflect typical inter-pass times during industrial tandem rolling. However, these trials can be used to verify the microstructure model predictions running under the same rolling conditions. Moreover, the author believes that the model predicted microstructure kinetics during multi-pass rolling can be applied to account for a typical tandem rolling inter-pass times which will be further discussed in Chapter 7.

4.3.5 Microstructure Characterization

4.3.5.1 Fraction recrystallized characterization

After the rolling trials were complete, the samples were sectioned and mounted in an acrylic resin. The surface of interest; i.e., the through thickness of the strip in the rolling direction (RD-ND plane) was subsequently polished to a 1 μm finish. The samples were anodized using Barker's reagent to examine the microstructure optically. To reveal the microstructure, the sample was examined under polarized light. Table 4.4 lists the anodizing procedure used to reveal the microstructure.

Table 4.4- Anodizing conditions used for AA5083 aluminum alloy.

Material	Anodizing solution	Anodizing Conditions
AA5083	Baker's reagent: 200ml distilled water + 6ml HBF_4 (48 wt% solution)	Electrolyte: pure Al as a cathode and the AA5083 sample as anode. 30V dc for 1.5-2 minutes.

Image analysis of the samples was employed to quantify the fraction recrystallized in each sample at three through thickness locations, namely the centerline, quarter-thickness and sub-surface locations on the strip. The volume fraction of recrystallized grains was determined according to the ASTM E562-89 standard point counting method. In this method, a grid with a number of equally spaced points was placed over the micrograph. The number of points falling within recrystallized grains was counted and averaged for the selected number of fields. The average number of counted points expressed as a percentage of the total number of points is assumed to be an unbiased statistical estimation of the volume percent of recrystallized grains. The grains were characterized based on their aspects ratios. Grains were considered equiaxed when they had a maximum aspect ratio of ~1.1. Grains with a higher aspect ratio were considered to be elongated. For every sample, five micrographs were taken at each strip location at different areas and a minimum of 25 fields were measured (5 fields/micrograph). The variation of the measurements at each location was used to determine the 95% Confidence Index (CI) and thus determine the standard deviation in the measured fraction recrystallized.

4.3.5.2 Recrystallized grain size characterization

In order to be able to measure the recrystallized grain size utilizing the linear intercept technique, it was necessary to attain a complete recrystallization of the sample. Thus, a section from each sample was heat treated at 400°C for 60 minutes followed by air-cooling. The average recrystallized grain size was measured using a linear intercept method based on ASTM E112-96 standard at two different locations through the thickness, namely the centerline and subsurface of the strip using the Clemex Vision^{TM} professional edition image analysis software. At each location through the thickness of the strip, five micrographs were taken along the rolling direction with a total of at least 500 recrystallized grains being analyzed per

micrograph using image analysis. The variation in the measured recrystallized grain size at each of these locations was used to calculate the standard deviation in the measured recrystallized grain size.

The recrystallized grain size was also measured at the center of the strip for one of the samples (sample no. 3) according to ASTM E112-88 standard employing Jeffries' method to confirm the validity of the results obtained using line intercept method. A minimum of 500 grains was counted during the analysis.

4.4 Experimental Results

In the following section, the measured data for the multi-pass hot rolling experiments conducted during the course of this research project are presented. Specifically, the measured thermal profile during the two-pass rolling cases, the measured rolling load, the measured volume fraction of recrystallized grains and the measured recrystallized grain size are presented. The data will thereafter be utilized to validate the proposed model predictions which will be further discussed in Chapter 6.

4.4.1 Sample Thickness After Two-Pass Rolling

The final thickness of the samples was measured using a digital thickness meter. Five measurements of the thickness were taken at different locations on the sample and used to calculate an average value that was considered the final thickness of the material. The final measured thickness of the rolled samples is summarized in Table 4.5.

Table 4.5 – Final measured sample thickness after two-pass rolling.

Sample Number	Initial thickness (mm)	Final thickness (mm)	Total strain
1	9	5.02	0.58
2	9	5.00	0.58
3	9	4.95	0.60
4	9	5.56	0.48
5	9	4.99	0.58
6	9	5.01	0.58
7	9	4.89	0.61
8	9	5.18	0.55
9	9	4.77	0.64
10	9	4.84	0.62
11	9	4.89	0.61

4.4.2 Temperature Measurement Through-Thickness of the Strip

The rolling environment is electrically noisy, primarily due to the presence of motors driving the work rolls. This electrical noise leads to a relatively noisy thermocouple signal which in turn results in a relatively large scatter in recorded temperature data. The resulting noisy thermocouple signals were smoothed using 3-point, 5-point and 10-point moving averages for all the samples. An example of the raw thermocouple data for sample no. 3 during first-pass rolling is compared to the smoothed data for the 3-point and 5-point moving average cases in **Figure 4.9**.

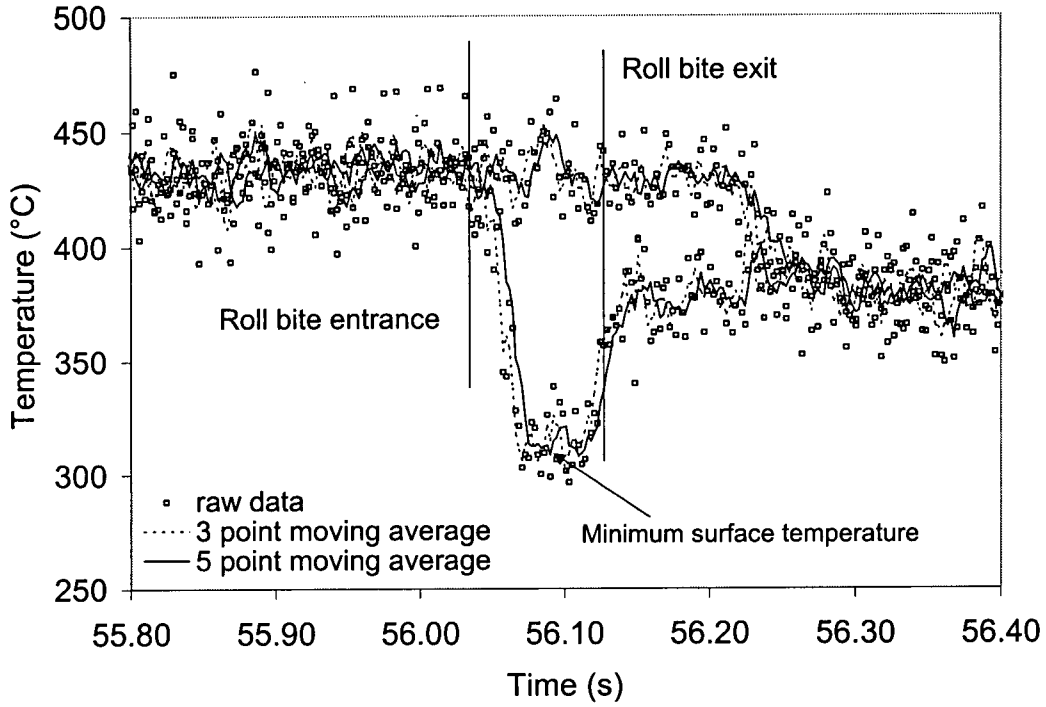

Figure 4.9 - Raw temperature data versus filtered data during first-pass rolling, Sample no. 3

Figure 4.9 shows that applying the 5-point moving average method reduces the noise in the measured temperature to ~5°C at the surface and ~8°C at the centerline of the strip while maintaining the trends of the original data. Although a 10-point moving average reduces the noise considerably further, it changes the recorded temperature trends significantly. Thus, a 5-point moving average was considered satisfactory and applied to reduce the recorded noise for the eleven rolled samples.

Figure 4.10a and **b** show the temperature changes that occur during first-pass hot rolling and second-pass hot rolling, respectively for sample no. 8. Referring to these figures, typical centerline temperature profiles are for both first-pass and second-pass rolling. Though a slight increase in temperature was expected at the strip centerline during rolling due to the heat released during plastic deformation, it could not be clearly determined as can be seen in **Figure 4.10a** and **b** due to the relative scatter and noise in recorded temperature data. The temperature drops at the surface due to the interface heat transfer between the relatively cold roll and the hot strip.

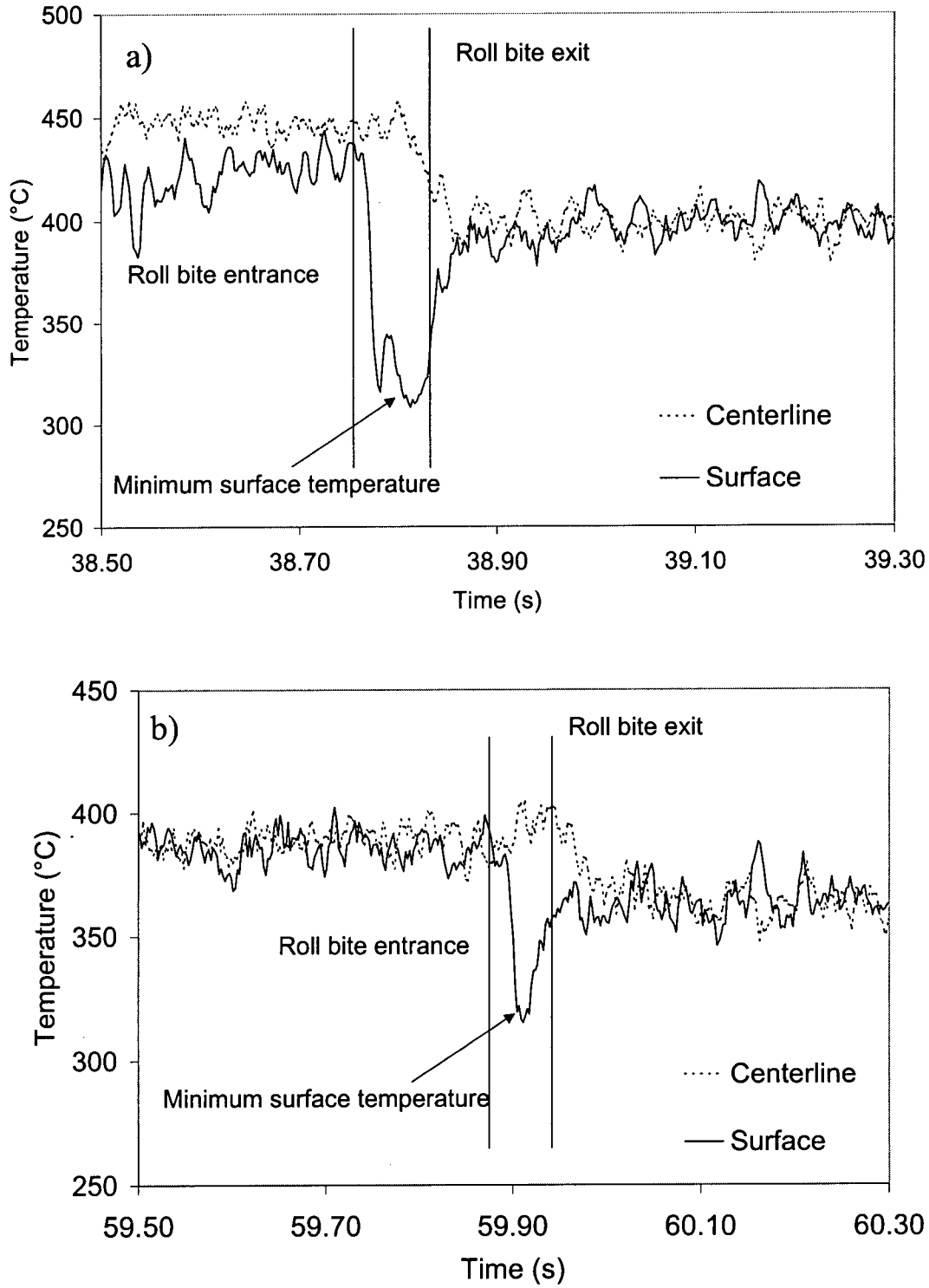

Figure 4.10 – Measured temperatures during (a) first-pass hot rolling, (b) second-pass hot rolling for sample no. 8.

Although Type-E thermocouple wires were used to reduce the scatter in the recorded data, the recorded data, shown in **Figure 4.9** and **4.10**, shows scatter due to the noise in the recorded electrical signals during rolling. **Figure 4.10** indicates that there may be a slight increase in the centerline temperature during deformation as the metal is being rolled. Unfortunately, the recorded data exhibits a relatively large scatter and the peak could not be determined clearly. The surface temperature changed rapidly during rolling due to the chilling effect of the work rolls at the interface roll-strip interface. The temperature rises again after deformation is completed to an equilibrated temperature. This is due to the fact that heat from central region conducts towards the surface[7]. The temperatures distribution equilibrates within ~ 0.1-0.2 seconds after exiting the roll bite.

4.4.3 Measured Rolling Loads

Two Voltage signals that correspond to the applied rolling load at each of the rolls were recorded during rolling. The rolling load was calculated by adding the collected two voltage signals and multiplying them by a calibration factor determined based on the data shown in **Figure 4.7** to convert them to rolling load. Load measurement was carried out during first-pass and second-pass rolling for the eleven rolled samples. The rolling load measurements indicate that the recorded rolling load was uniformly distributed during rolling. **Figure 4.11** shows the experimentally measured rolling load during first-pass rolling for sample no. 9.

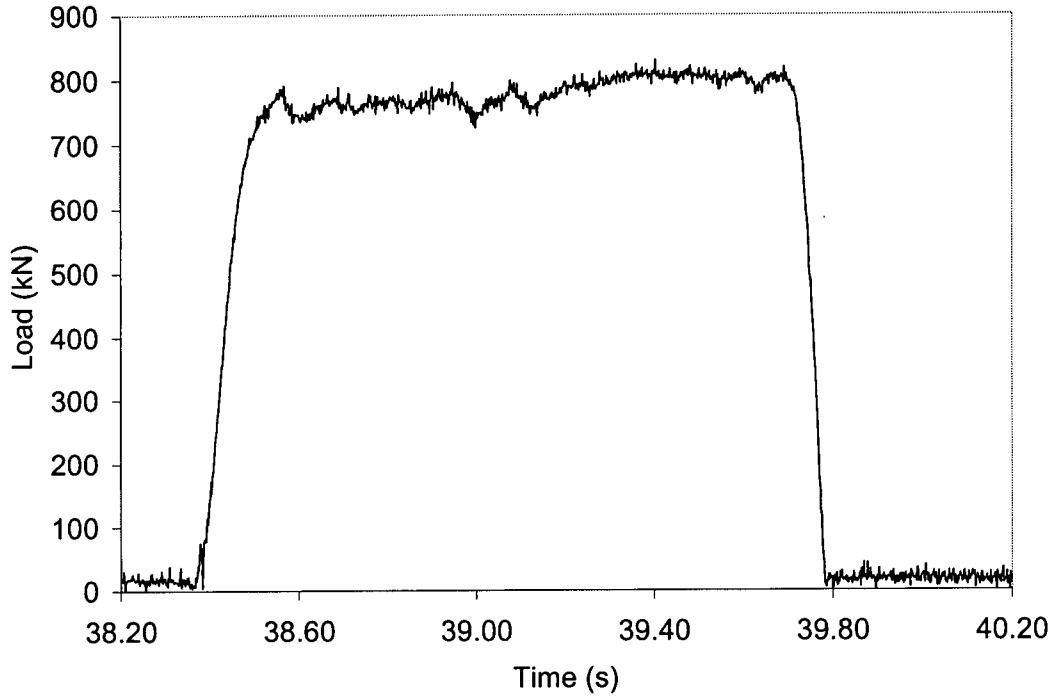

Figure 4.11 – Experimentally measured rolling load profile during first-pass rolling of sample no.9.

It can be seen from **Figure 4.11** that the measured rolling load shows a uniform distribution during rolling. The "uniform" part of the recorded rolling load was averaged over the rolling time to determine an average value of the rolling load during each pass; i.e., the experimentally measured rolling loads are the average measured rolling load during rolling of the entire sample. A summary of the experimentally measured rolling loads is shown in Table 4.6.

Table 4.6 - Summary of experimentally measured average rolling load.

Sample Number	First pass average rolling load (kN)	Second pass average rolling load (kN)
1	723	927
2	721	968
3	721	927
4	721	762
5	744	1030
6	783	1030
7	663	855
8	608	923
9	797	902
10	886	1022
11	711	923

4.4.4 Microstructure Characterization

4.4.4.1 Characterization of through-thickness fraction recrystallized

For each of the eleven rolled samples, the final microstructure through the thickness of the strip was examined to determine the volume fraction of recrystallized grains as discussed earlier. The final microstructure for sample no. 5 at the centerline and sub-surface is shown in **Figure 4.12**.

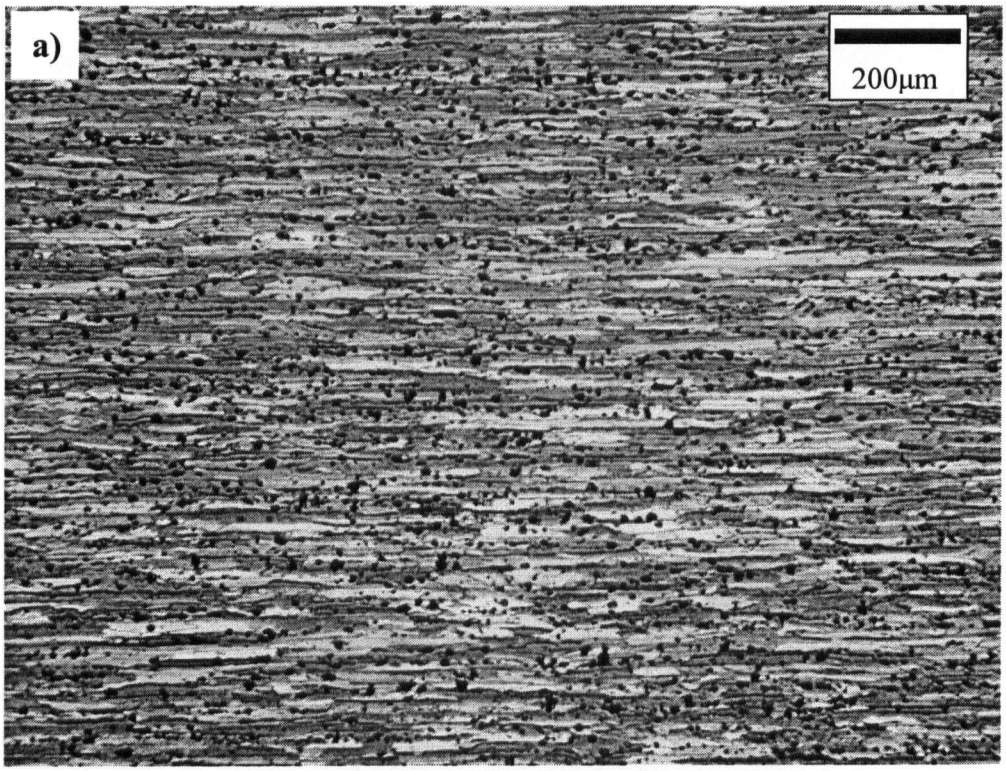

a) Microstructure after two-pass hot rolling at the strip centerline

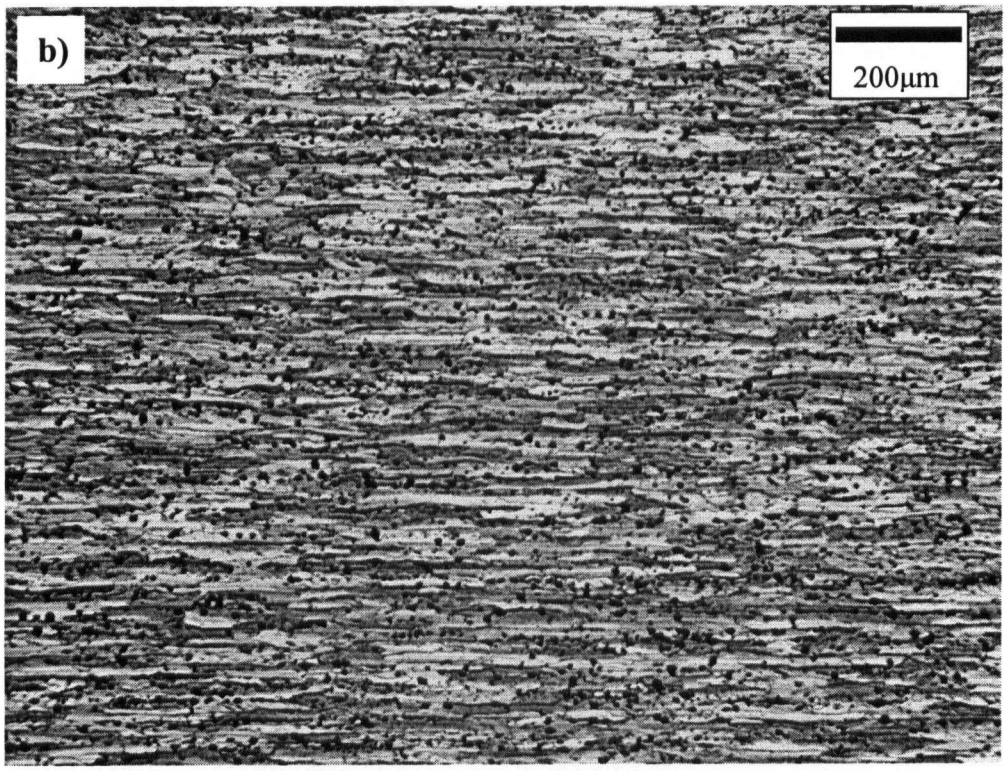

b) Microstructure after two-pass hot rolling at the strip subsurface location

Figure 4.12 – Final microstructure of sample no.5 after two-pass hot rolling at (a) Centerline and (b) subsurface locations on the strip

Figure 4.12 shows that very little recrystallization occurred in this sample after two-pass hot rolling. This observation was consistent for the eleven- rolled samples where the maximum attained recrystallization level was below 20%. A summary of the measured fraction recrystallized (X_v) through the thickness of the strip is shown in Table 4.7.

Table 4.7- Summary of measured volume fraction of recrystallized grains

Sample Number	Location		
	Center	Quarter-thickness	Sub-surface
	Percentage fraction recrystallized (standard deviation)		
1	3.8 (1.83)	5.2 (1.96)	8.1 (3.17)
2	9.1 (3.31)	10.4 (3.32)	12.5 (2.98)
3	6.7 (2.87)	8.0 (2.13)	8.6 (3.05)
4	8.5 (1.83)	9.2 (2.22)	9.6 (1.79)
5	3.6 (1.50)	4.9 (1.07)	6.5 (1.95)
6	4.0 (1.43)	4.3 (1.22)	5.1 (1.27)
7	12.2 (3.52)	12.7 (3.27)	15.3 (1.68)
8	3.7 (1.53)	4.5 (2.04)	6.0 (1.72)
9	5.9 (1.94)	6.8 (3.30)	7.6 (1.67)
10	6.2 (2.27)	7.7 (2.75)	8.3 (1.92)
11	6.2 (1.26)	7.8 (2.52)	8.5 (2.50)

The test matrix was designed based on preliminary model predictions to obtain a significant variation in the fraction recrystallized under different hot rolling conditions. This would allow for validation of the model predictions against a wide range of microstructures. Unfortunately, analysis of the experimental data showed that the fraction recrystallized for all of the samples was low, less than 20%.

4.4.4.2 Characterization of recrystallized grain size

For each of the eleven rolled samples, a heat treatment was applied to ensure full recrystallization through the thickness of the strip in order to be able to determine the recrystallized grain size using the linear intercept technique as discussed

previously. The final microstructure after employing the heat treatment procedure for sample no.5 at the centerline and sub-surface is shown in **Figure 4.13**.

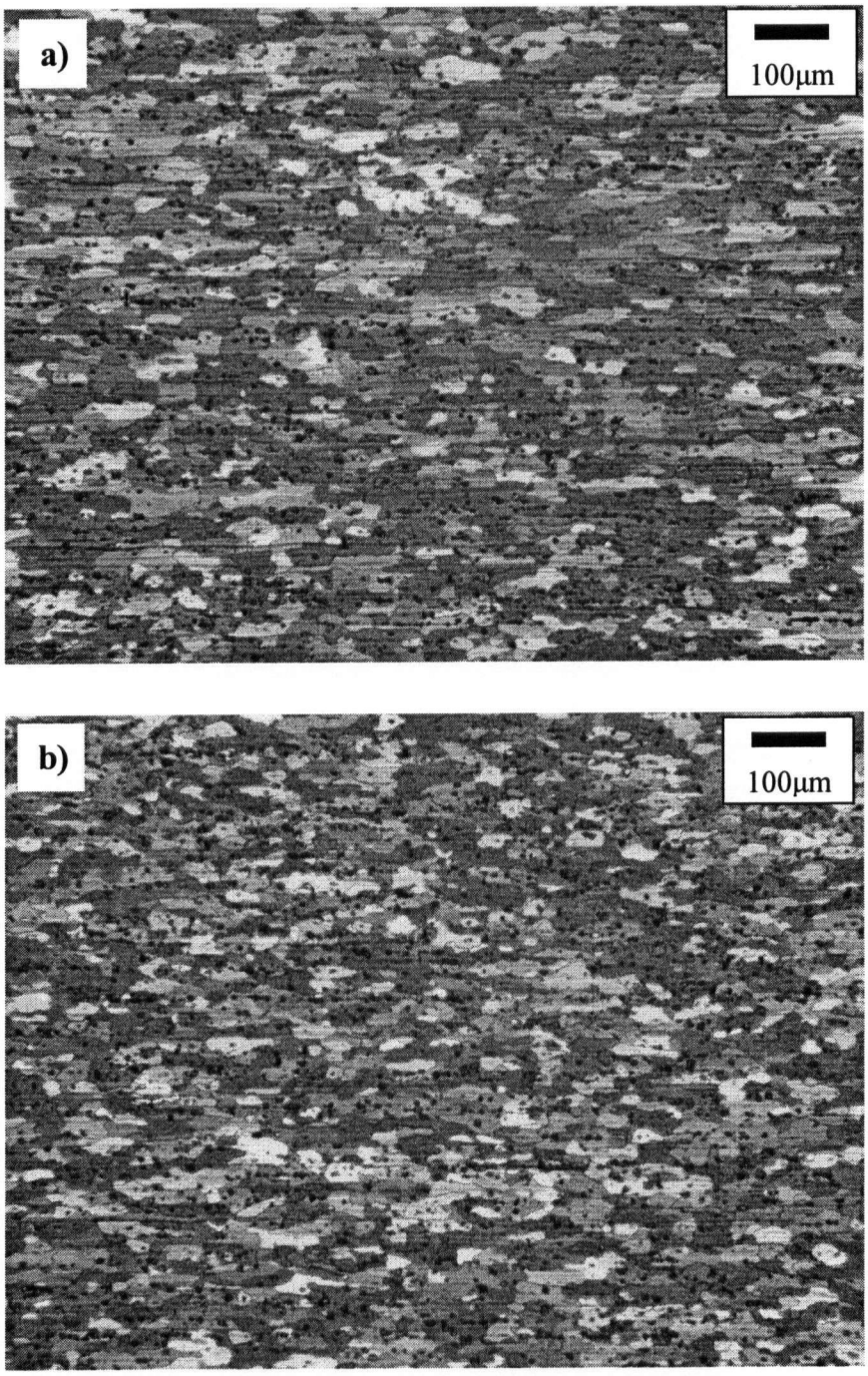

Figure 4.13 – Recrystallized microstructure for sample no. 5 at (a) Centerline and (b) subsurface locations on the strip

The previous figure shows that there is a minor difference between the centerline and the sub-surface recrystallized grain size. The recrystallized structure shows relatively elongated grains both at the centerline and the subsurface of the strip. A summary of the measured recrystallized grain size both at the centerline and subsurface locations in the strip is shown in Table 4.8.

Table 4.8 - Summary of measured recrystallized grain size.

Sample Number	Location	Recrystallized grain size (μm)	Average aspect ratio	Standard deviation
1	Center	31.7	1.62	2.1
	Sub-surface	28.8	1.65	2.5
2	Center	28.5	1.62	2.2
	Sub-surface	27	1.59	1.8
3	Center	30.1	1.64	2.5
	Sub-surface	29	1.63	1.3
4	Center	30.2	1.64	2.7
	Sub-surface	29	1.60	2.2
5	Center	29.3	1.62	3
	Sub-surface	25.9	1.59	2
6	Center	29.4	1.74	3
	Sub-surface	29.7	1.58	1.7
7	Center	32.2	1.62	2
	Sub-surface	29.5	1.60	1.6
8	Center	32.2	1.65	1.5
	Sub-surface	27.9	1.60	1.9
9	Center	28.1	1.64	2.8
	Sub-surface	25.8	1.59	2.1
10	Center	30.5	1.63	1.1
	Sub-surface	27.9	1.57	0.9
11	Center	31.6	1.65	2.3
	Sub-surface	28.3	1.60	1.7

The optical measurements through the thickness of the strip show a trend of slightly decreasing recrystallized grain size from the centerline to the subsurface of the strip for all the samples. This trend can be attributed to the different deformation conditions that occur near the surface of the strip as compared to the center. Specifically, it is a function of higher strains.

The measurements also indicate that the measured values of the recrystallized grain size after two-pass rolling did not change significantly compared to the starting material grain size. Specifically, the measured grain size has changed from 35 μm for the start material to ~30 μm after two-pass rolling for sample no. 3, the baseline sample.

4.5 Summary

The plant trial conducted at Corus' multi-mill rolling facility on AA5083 aluminum alloy was very successful. An extensive experimental program was undertaken using a series of eleven multi-pass rolled samples under different rolling conditions including: holding time after two-pass rolling, inter-pass holding time, changes in initial temperature, reduction schedule and rolling velocities during first-pass rolling. The thermocouples located at the centerline and surface of the strip were used to capture the thermal profile during multi-pass rolling. Rolling loads were successfully measured during both the first-pass and the second-pass rolling. Microstructure characterization was carried out through the thickness of the strip in terms of both the fraction recrystallized and the recrystallized grain size for the eleven-rolled samples. Hence, the industrial plant trials provided a broad range of industrially relevant multi-pass rolling conditions to understand the accumulation of the material stored energy and provide a sound basis for the model development and validation.

References

1. Wells, M.A., D.M. Maijer, S. Jupp, G. Lockhart, and M.R. van der Winden, *Mathematical model of deformation and microstructural evolution during hot rolling of aluminum alloy 5083.* Mater. Sci. Technol., 2003. **19**(4): p. 467-476.

2. Jupp, S., *Mathematical modelling of the microstructural evolution during the hot rolling of AA5083 aluminum alloys, M. Sc. thesis.* 2001, University of British Columbia: Vancouver, Canada.

3. McGee, T., D., *Principles and methods of temperature measurements.* 1988: John Wiley & Sons, Inc. 581.

4. Henning, C.D. and R. Parker, *Transient response of an intrinsic thermocouple.* Trans. asme, J. Heat Trasfer, 1967: p. 146-154.

5. Maglic, K.D. and B.S. Marsicanin, *Factors affecting the accuracy of transient response of intrinsic thermocouples in thermal diffusivity measurement.* High Temperatures- High Pressures, 1973. **5**: p. 105-110.

6. Corus Research Development and Technology, *Introduction to the research mill of Corus Reserach Development and Technology.* 2000: IJmuiden, Netherlands.

7. Timothy, S.P., H.L. Yiu, J.M. Fine, and R.A. Ricks, *Simulation of single pass of hot rolling deformation of aluminum alloy by plane strain compression.* Mater. Sci. Technol., 1991. 7(3): p. 255-261.

CHAPTER 5

MODEL DEVELOPMENT

5.1 Introduction

In line with the goals of the research project, a thermo-mechanical mathematical model capable of simulating the deformation that occurs during multi-pass hot rolling of aluminum alloys was developed to predict the temperature, strain, and strain rate through the thickness of the strip during deformation. Hot rolling simulation is a fully coupled problem that is highly non-linear due to the interaction between temperature, strain and strain rate during deformation. Based on the reviews of the current modelling activities[1-4], it is clear that the finite element (FE) technique provides a convenient procedure to mathematically model the development of the temperature and strain distributions which occurs during the rolling process.

The thermo-mechanical model employed in this study was used to predict the evolution of temperature, strain and strain rate in the strip throughout the rolling process and to simulate inter-pass cooling for multi-pass rolling schedules. The thermo-mechanical model results were then integrated into a microstructure model to simulate through thickness microstructure evolution in terms of dislocation density, average subgrain size and average misorientation angle between subgrains and thus determine the material stored energy during deformation and subsequent recrystallization kinetics. The general modelling approach that was employed to simulate the hot rolling process incorporating both the thermo-mechanical and microstructure model is shown in **Figure 5.1**. This chapter provides an overview of the FE thermo-mechanical model and the internal state variable microstructure model that were adapted to simulate the industrial hot rolling process.

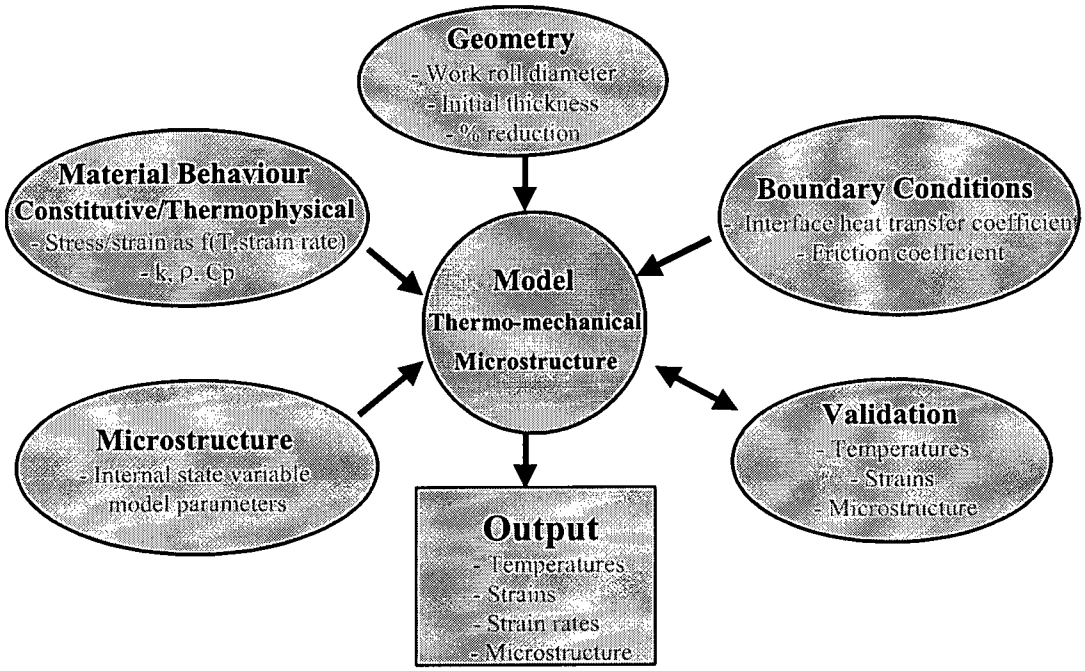

Figure 5.1- A schematic diagram of the mathematical model overview

5.2 Finite Element Thermo-Mechanical Model

In this research work, the rolling model was developed to simulate hot rolling for aluminum alloy AA5083 to predict the temperature, strain and strain rate evolution through the thickness of the strip. The commercial FE software, ABAQUS was employed to solve this problem. The reader is referred to the text by Zienkiewicz and Taylor[5] for a complete explanation of the finite element solution procedure. Discussion in the following section includes an overview of the finite element (FE) concepts relevant to the formulation of the deformation and thermal model and an overview of the FE model. A detailed description of the FE method will not be presented because these algorithms were not developed during the course of this research program.

In the following section, a description of the general mathematical formulation of the problem and the development of the FE thermo-mechanical model will be presented.

5.2.1 FEM Background

The generalized concept of FE analysis is to obtain an approximate solution, $\hat{\phi}(x,y)$, for a problem, represented by $A(\phi)=0$, within the discretized domain Ω[5] with boundary conditions, represented by $B(\phi)=0$, on the boundary Γ, employing a set of differential equations that are developed for sub domain region Ω^e, which is shown in **Figure 5.2**.

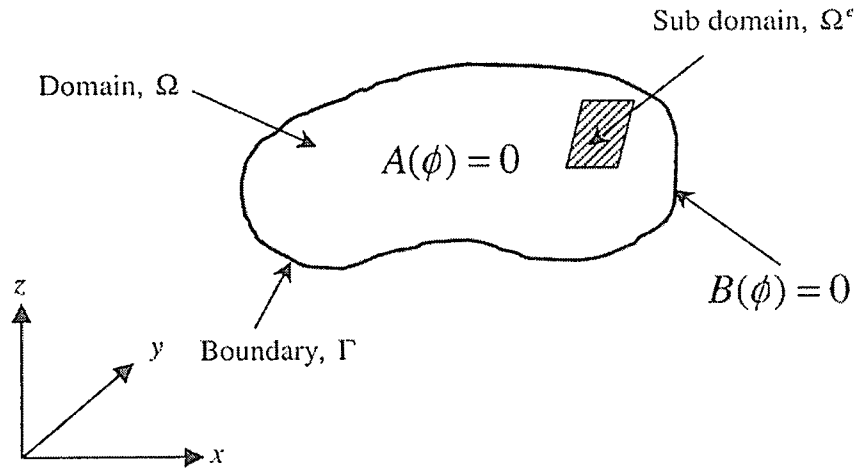

Figure 5.2 – Schematic of the problem domain as they apply to FE method[5].

These FE equations can be derived using the variation principle or method of weighted residual where they can be utilized to solve a wide variety of engineering problems dealing with deformation or heat transfer, respectively. In deformation analysis, the desired solution is usually displacement and loads while it is the temperature throughout the domain in heat transfer problems.

5.2.2 Finite Element Interpolation

One of main components of the FE formulation are the interpolation functions which are implemented to approximate the exact solution, $\phi(x,y)$, to approximate solution, $\hat{\phi}(x,y)$ to satisfy the governing partial differential equations with in the

solution discretized domain Ω. The approximate solution can be calculated according to the following equation:

$$\hat{\phi} = \sum_{i=1}^{n} N_i(x,y)\phi_i \tag{5.1}$$

Where N_i are the nodal interpolation functions, n is the number of nodes per element and ϕ_i are the value of the solution at the node. In standard FE formulation, the interpolation functions, also named shape functions, can be linear, quadratic or higher order polynomials chosen based on the number of nodes per element.

Interpolation functions are also used to map elements from arbitrary shape in global coordinate space (x,y) to regular shape in local coordinate system (ζ,η) as illustrated in **Figure 5.3**. Elements are named "isoparametric" when the same shape function is used for both coordinate transformation and solution function. In this research work, 4- node quadrilateral isoparametric elements were employed for the 2D rolling model.

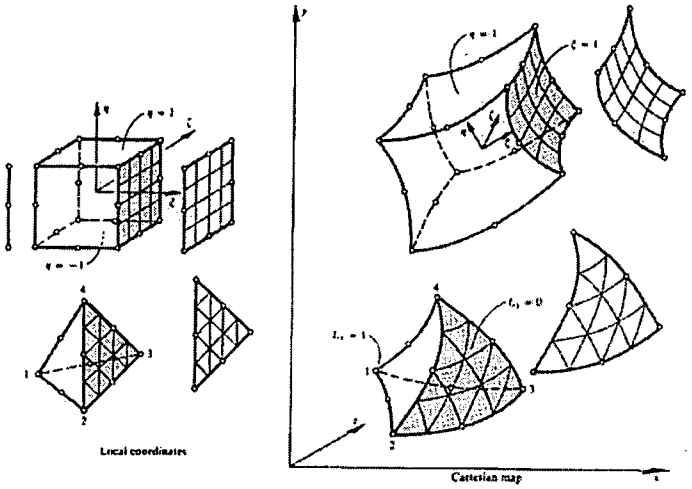

Figure 5.3 – Mapping of different element types from the global coordinate system to the local coordinate system[5].

5.2.3 Mathematical Formulation of the FE Thermo-Mechanical Model

5.2.3.1 FE formulation of the deformation model in ABAQUS

A 2D rolling model was developed to simulate strip deformation during hot rolling of AA5083. During deformation, ABAQUS provides the integral statement needed for the rolling problem formulation in terms of a finite element approximation via the principle of virtual work. The principle of virtual work states that "if the displacements corresponding to the exact solution to the problem, with the stresses satisfying the equations of equilibrium, is perturbed by adding arbitrary virtual displacements, then the work done by the external forces along these virtual displacements equals the work done by the stresses along the corresponding virtual strains", or[6, 7]:

$$\delta W = \delta W_{ext} + \delta W_{\text{int}} = 0 \tag{5.2}$$

where δW_{int} is the change in the internal virtual work and δW_{ext} is the change in the external virtual work.

Based on the principle of virtual work, the following variational equation is used by ABAQUS[8] to model the deformation process during hot rolling:

$$\delta\Phi = \int_V \sigma\bar{\dot{\varepsilon}} dV - \int_S t^T \delta u \cdot dS - \int_V f^T \delta u \cdot dV \tag{5.3}$$

where V and S are the volume and surface area of the work piece, respectively, σ is the effective stress, $\bar{\dot{\varepsilon}}$ is the effective strain rate, u is the nodal displacement, t is the traction force per unit of current area and f is the body force at any point within the volume under consideration per unit of current volume.

Equation 5.3 is the basic equation for finite element discretization. Once the solution of the displacement field that satisfy the basic equation is obtained, then the corresponding stress can be calculated. Equation 5.3 can be expressed in terms of nodal point displacements (u) and their variation (δu), and a set of algebric equations (stiffness equations) as follows:

$$\frac{\delta\Phi}{\partial u_i} = \sum_j \left(\frac{\delta\Phi}{\partial u_i}\right)_j = 0 \tag{5.4}$$

Linearization of this equation is achieved by Taylor expansion near an assumed point $u=u_0$ (initial guess) as shown in the following equation:

$$\left[\frac{\partial\Phi}{\partial u_i}\right]_{u=u_0} + \left[\frac{\partial^2\Phi}{\partial u_i \partial u_j}\right]_{u=u_0} \Delta u_j = 0 \tag{5.5}$$

Equation 5.6 can be written in matrix form as shown in Equation 5.6.

$$[K]\{\Delta u\} = \{f\} \tag{5.6}$$

where $[K]$ is the stiffness matrix, $\{\Delta u\}$ is the displacement term and $\{f\}$ is the residue of the nodal points.

5.2.3.2 FE formulation of the thermal model in ABAQUS

Since the material is rolled at high temperatures, a thermal analysis must also be included and coupled with the deformation analysis. The thermal analysis involves solving the transient heat transfer problem which describes the variation in temperature with time through the thickness of the strip during rolling. During the rolling process, the temperature distribution in the strip and the work roll can be calculated using the governing partial differential equation shown in Equation 5.7:

$$\frac{\partial}{\partial x}\left(k_x(T)\frac{\partial T}{\partial x}\right) + \frac{\partial}{\partial y}\left(k_y(T)\frac{\partial T}{\partial y}\right) + \dot{Q} - \rho c_p(T)\frac{\partial T}{\partial t} = 0 \tag{5.7}$$

where ρ is the density, c_p (T) is the temperature dependent specific heat, k (T) is the temperature dependent thermal conductivity with the subscripts x and y representing its components in both directions, x is the distance along the length of the strip, y is the distance through the thickness of the strip which is indicated in **Figure 5.4** and $\dot{Q}$ is a heat generation term representing the heat released due to plastic work. The heat generation term, $\dot{Q}$, is calculated using Equation 5.8

$$\dot{Q} = \eta \bar{\sigma} \bar{\dot{\varepsilon}} \tag{5.8}$$

where $\bar{\sigma}$ is the effective flow stress, $\bar{\dot{\varepsilon}}$ is the effective strain rate and η is the efficiency of conversion of deformation energy to heat; the latter is assumed to be 0.95 for aluminum alloys[2, 9].

In order to find the spatial and temporal distribution of temperature, $T(x, y, t)$, Equation 5.8 can be solved by employing a finite element discretization of the spatial derivatives, as explained earlier. To derive the elemental equations from Equation 5.7, the Galerkin method is invoked[5] as shown in the following equation:

$$\int_{\Omega^e} \left[\frac{\partial}{\partial x}\left(k_x \frac{\partial T}{\partial x} \right) + \frac{\partial}{\partial y}\left(k_y \frac{\partial T}{\partial y} \right) + \dot{Q} - \rho c_p \frac{\partial T}{\partial t} \right] N_i d\Omega = 0 \tag{5.9}$$

After certain mathematical manipulations, the resulting mathematical equations reduce to:

$$\left[C^e\right]\left\{\frac{dT^e}{dt}\right\} + \left[\left[K_c^e\right] + \left[K_h^e\right]\right]\left\{T^e\right\} = \left\{R_Q^e\right\} + \left\{R_q^e\right\} + \left\{R_h^e\right\} \tag{5.10}$$

Or in a general form:

$$\left[C^e\right]\left\{\dot{T}^e\right\} + \left[K^e\right]\left\{T\right\} = \left\{R^e\right\} \tag{5.11}$$

where $\left[C^e\right]$ is the elemental heat capacitance matrix and $\left[K^e\right]$ is the elemental heat conduction matrix, the vector $\left\{R^e\right\}$ is the heat flux (load) vector arising from internal heat generation, specified surface heating and surface convection, $\left\{\dot{T}^e\right\}$ is the vector of temperature change with time and $\left\{T\right\}$ is the temperature vector.

The transient response of the nonlinear system of equations resulting from the assembly of the system of elemental equations, Equation 5.11, is calculated using a step by step recurrence technique where temperatures are stored by ABAQUS at the nodal positions in a solution increment and then interpolated to the integration point locations before solving the elemental differential equations.

For a fully coupled temperature-displacement analysis, ABAQUS solves a system of coupled equations represented by Equation 5.12[8].

$$\begin{bmatrix} K_{uu} & K_{uT} \\ K_{Tu} & K_{TT} \end{bmatrix} \begin{Bmatrix} \Delta u \\ \Delta T \end{Bmatrix} = \begin{Bmatrix} R_u \\ R_T \end{Bmatrix} \tag{5.12}$$

where ΔT and Δu are the respective corrections to the incremental temperature and displacement, K_{ij} are the sub-matrices of the fully coupled stiffness matrices and R_T and R_u are the thermal and mechanical residual vectors, respectively. These thermal and mechanical systems of equations are solved simultaneously using the Newton's method.

5.2.4 Numerical Integration

In order to assemble the matrix of elemental differential equations describing the global problem in **Figure 5.2**, numerical integration is needed on elemental basis. The numerical integration of the variational equation used by ABAQUS[8] to model the deformation process and temperature distribution, Equations 5.3 and 5.9 respectively, was carried out using Gauss quadrature method. This method is particularly well suited to FE analysis because it requires the least number of function evaluations. In a 2D domain, the Gauss quadrature integration of a function $f(\zeta,\eta)$ can be described by the following equation:

$$\int_{-1}^{1}\int_{-1}^{1} f(\zeta,\eta)d\zeta d\eta = \sum_{j=1}^{m}\sum_{i=1}^{m} W_i W_j f(\zeta_i,\eta_j) \tag{5.13}$$

where W_i, W_j are weighting coefficients at locations i, j respectively and m is the number of integration, Gauss, points within an element in each direction. Employing this integration formulation, the 2D quadrilateral elements utilized in this study are defined with 2x2 integration points. The integration points provide one of the means by which spatially dependent variables can be calculated in the FE models. For example, the temperatures and strains in a deformation problem are solved at the nodes but can be interpolated at the integration points.

5.2.5 Sources of Nonlinearity in the FE Analysis

Most engineering problems encountered have some form of non-linearity; i.e., the relationship between the applied loads and the response of the system is not constant. Sources of non-linearity may arise due to changes in material properties and boundary conditions during the analysis. During hot rolling, the temperature dependence of the thermo-physical properties (heat capacitance, thermal conductivity) and the interaction between thermal and strain fields are major sources of nonlinearity.

5.2.6 ABAQUS Solution Procedure of Transient Nonlinear Problem

ABAQUS is a good platform for solving deformation and heat transfer problems due to its highly developed nonlinear solution procedures and a well-documented method for extending the program's capabilities via user written subroutines. The software is particularly well suited to solving the rolling problem because its nonlinear solution capabilities are highly developed and robust.

ABAQUS uses a modified Newton-Raphson numerical technique to solve the non-linear FE equations. The technique is an incremental solution algorithm that employs a series of step wise approximations to approach the solution and may require several iterations to determine an acceptable solution for a given time increment[8, 10]. An acceptable result is reached when the incremental change in the calculated solution becomes small relative to a certain tolerance value[8]. Thus, time step selection is an important issue and ABAQUS has addressed this through the implementation of an adaptive time step algorithm. When setting up the problem, the user supplies a maximum and a minimum time step and a tolrance for the maximum solution change within a time increment. Based on the solution change tolerance and rate of convergence of the solution, ABAQUS adapts the time step to ensure solution accuracy while maintaining the largest possible time step. It often takes ABAQUS several iterations to determine an acceptable solution for a given time increment.

5.2.7 Model Geometry and FE Mesh

In the rolling model, two main components were considered, namely the work roll and the strip. Employing symmetry along the centerline, only the top half of the strip is considered in the model. Previous models showed that the thermal effect in the work roll does not extend beyond 5mm thickness[11]. The work roll geometry is limited to a 90° section with a thickness of 5 mm, and diameter of 400 mm. An image showing the geometry of the sheet and work roll is shown in **Figure 5.4**.

To model hot rolling of AA5083 aluminum alloy, the work roll geometry was modeled with 5 elements in the radial direction and 90 elements in the circumferential direction resulting in 450 elements in total. The initial geometry of the strip is 24 cm long while the initial thickness of the strip was 9.6 mm to simulate single-pass rolling experiments conducted previously and 9 mm to simulate the multi-pass rolling experiments that were carried out in this thesis research work. The strip geometry was modeled with 75 elements in the longitudinal direction, and 4 elements in the through-thickness direction with a bias ratio of approximately 3 resulting in 300 elements in total. A sensitivity analysis was employed to determine the effect of changing the mesh density on the model results which will be discussed later in this chapter. A gradient in the mesh density through the thickness of the strip was employed to accurately describe the large gradient in solution variables (temperatures, strains, and strain rates) during rolling with a finer mesh density closer to the strip surface. The length of the modeled strip was set to 24 cm which was found to be a suitable length to achieve steady state conditions in the strip[12].

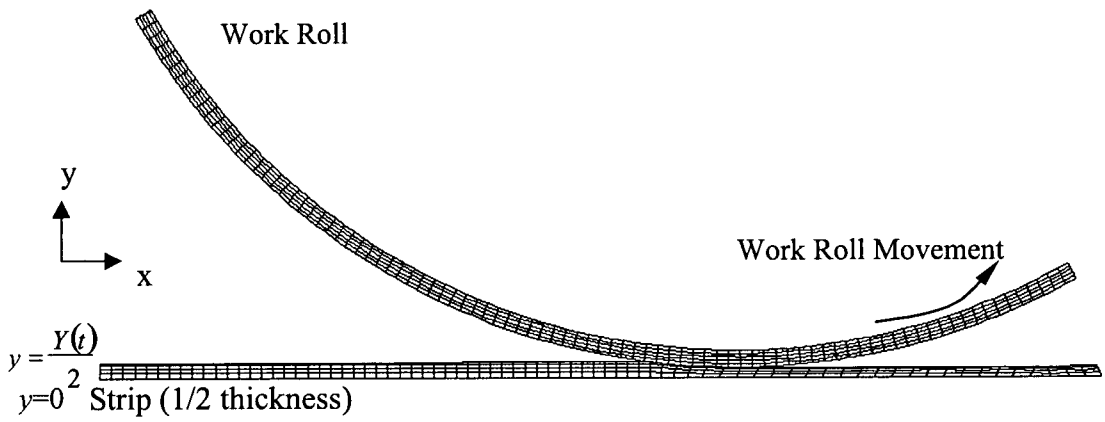

Figure 5.4 – A picture showing the geometry of the hot rolling model developed using ABAQUS.

In both the strip and work roll, the type of elements used in the ABAQUS simulations was 4 node bilinear plane strain elements. The use of plane strain elements is based on the assumption that deformation can be neglected in the *z*-directions which is a reasonable assumption at the strip centerline.

5.2.8 Model Boundary Conditions

5.2.8.1 Thermal boundary conditions

Thermal boundary conditions are needed to describe the heat transfer conditions at the strip centerline, at 5mm from the surface of the work roll and at the contact interface between the strip and work roll.

Referring to **Figure 5.4**, the boundary conditions in the model are defined as:

1) At the centerline of the strip, symmetry is assumed:

$$-k_{strip} \cdot \frac{\partial T}{\partial \hat{n}} = 0 \quad @\ t>0;\ y=0 \tag{5.14}$$

where k_{strip} is the strip thermal conductivity and $\hat{n}$ is the outward facing normal on the surface of interest.

2) At a radius 5mm from the work roll surface; i.e. at the inside radius of the work roll, an adiabatic condition is assumed:

$$-k_{roll} \cdot \frac{\partial T}{\partial \hat{n}} = 0 \quad @\ t>0,\ r = r_{5mm} \tag{5.15}$$

where k_{roll} is the work roll thermal conductivity. The thickness of the work roll was sufficient to avoid only increase in the temperature along the roll inner radius and confirm the validity of this boundary condition.

3) At the contact interface between the strip and the work roll, an interfacial heat transfer coefficient is assumed:

$$k_{strip} \cdot \frac{\partial T}{\partial \hat{n}} = -k_{roll} \cdot \frac{\partial T}{\partial \hat{n}} = h \cdot \left(T_{strip} - T_{roll}\right) \quad @\ t>0;\ y = \frac{Y(t)}{2} \text{ or } r = r_o \tag{5.16}$$

where h (in W m^{-2} ˚C^{-1}) is the interface heat transfer coefficient, Y is the thickness of the strip and q is the heat flux.

The literature survey shows that the interface heat transfer coefficient is related to the interface pressure during rolling[12-14]. For AA5083, in the model, the interface heat transfer coefficient was taken to be a function of pressure using the following relationship[12, 13]:

$$h = 11.394 \cdot P + 137.53 \tag{5.17}$$

where P (in Kg mm^{-2})is the interface pressure

In order to model the temperature change in the strip in the inter-pass region, the following boundary condition was assumed:

$$-k\frac{\partial T}{\partial \hat{n}} = h_{\text{int}}(T - T_{\infty}) + \varepsilon\sigma(T^4 - T_{\infty}^4) \tag{5.18}$$

where k is the strip thermal conductivity, T_{∞} is the far field or surrounding temperature equal to 35°C, h_{int} is the convection heat transfer coefficient which was assumed to be 4.5 Wm^{-2} °C^{-1}[15], σ is the Stefan-Boltzmann constant and ε is the emissivity which is assumed to be equal to 0.09[15]. This relation was employed both in the inter-pass region and after the second pass rolling was completed before quenching.

5.2.8.2 Mechanical boundary conditions

Boundary conditions describing the mechanical interactions of the strip and the roll are needed to complete the physical description of the process. Symmetry in the strip was maintained through a boundary condition of zero displacement in the through-thickness direction at the strip centerline. A displacement boundary condition was also employed to prevent the strip movement in the y-direction. A contact boundary condition was imposed along the strip/roll interface. A literature survey of friction models employed for hot rolling did not show a significant benefit of one

interface friction model over the others[2, 3, 16, 17]. Interfacial friction for the contact area was modeled using Coulomb friction, where the frictional force is proportional to the normal force as shown in Equation 5.19:

$$\tau_{crit} = \mu \cdot P \tag{5.19}$$

where τ_{crit} is the critical shear stress, and μ is the coefficient of friction. A baseline coefficient of friction of 0.3 was used in the model which is a typical value for lubricated hot rolling conditions[4]. The friction algorithm within ABAQUS offers several different options to describe static and dynamics friction conditions. For this study, static friction has been assumed without transition to or from dynamic friction conditions.

The roll gap and rolling speed are defined by applying a displacement and rotational velocity to a node representing the center of the roll. The displacement and rotation experienced by the center node are translated to the nodes along the inner radius of the roll via multi-point constraints.

5.2.9 Material Properties

The steel work roll was defined as an elastic material with a Young's modulus of 200 GPa. The thermophysical properties of the steel work roll are shown in Table 5.1[2, 12].

Table 5.1 – Thermophysical properties used for the steel work roll[2].

Heat Capacity ($J\ kg^{-1}\ K^{-1}$)	Thermal Conductivity ($W\ m^{-1}\ K^{-1}$)	Density ($kg\ m^{-3}$)
460	14	7876

The strip is assumed to behave as an elastic-viscoplastic material with a temperature independent elastic modulus of 70 GPa. The large differences in elastic moduli between the work roll and the strip causes the work roll to behave as a virtually rigid material. The range of temperatures and strain rates experienced by the

material during the rolling process is large, hence it is necessary to define the strip's plastic behavior as a function of both temperature and strain rate.

5.2.9.1 Material constitutive behavior

Several constitutive equations have been reported in literature to model the material behavior during hot rolling of an AA5083 aluminum alloy[18]. For example, the Norton-Hoff[19] relation, which includes two material related constants, has been applied to determine the flow stress in the material during rolling as a function of equivalent strain, strain rate, strain rate sensitivity, strain hardening exponent and as an exponential function of temperature [18]. Another equation adopted in literature was introduced by Hensel *et al.*[20], which include five material related constants, which calculates the flow stress in the material during rolling as a function of strain rate and as an exponential function of equivalent strain and temperature. Of these equations, Duan *et al.*[18] concluded that for small deformations, the choice of the hyperbolic sine functions tend to under predict the rolling load while it is judged to be suitable for relatively large deformation conditions. Hence, a hyperbolic sine equation, shown in Equation 5.20, which relates the steady state flow stress of the material to the strain rate and temperature under which it is deformed was implemented in this research work to model material behavior during rolling [2, 21]:

$$\dot{\varepsilon} = A(sinh(\alpha\sigma_{ss}))^m \left(\frac{-Q_{def}}{RT_{def}}\right) \tag{5.20}$$

where A, α and m are material constants and σ_{ss} is the steady-state flow stress, Q_{def} is the activation energy for deformation, R is the universal gas constant. The constitutive equation for AA5083 aluminum alloys was employed based on Chen *et al*[2] data. The coefficients of the hyperbolic sine equation for AA5083 deformation are summarized in Table 5.2[2].

Table 5.2 - Summary of hyperbolic sine constants for AA5083.

Material	A	α (MPa^{-1})	M	Q_{def} ($kJ\ mol^{-1}$)
AA5083	$2.87x10^8$	0.04	2.26	162.5

In order to assess the chosen constants in the hyperbolic equation for AA5083 aluminum alloy, a study was conducted in Corus research facility for an AA5083 aluminum alloy where the flow stress was measured under a deformation temperature that varies from 340- 550°C and strain conditions which vary from 0.01-24 during plane strain compressions tests[12]. A comparison between the measured and the calculated flow stress using both the constants illustrated in Table 5.2 as well as the reported constants in literature by Duan and Sheppard (A=1.02x10^{10}, α=0.014, m=3.65, Q_{def}=145.1 kJ mol^{-1}[18] is shown in **Figure 5.5.**

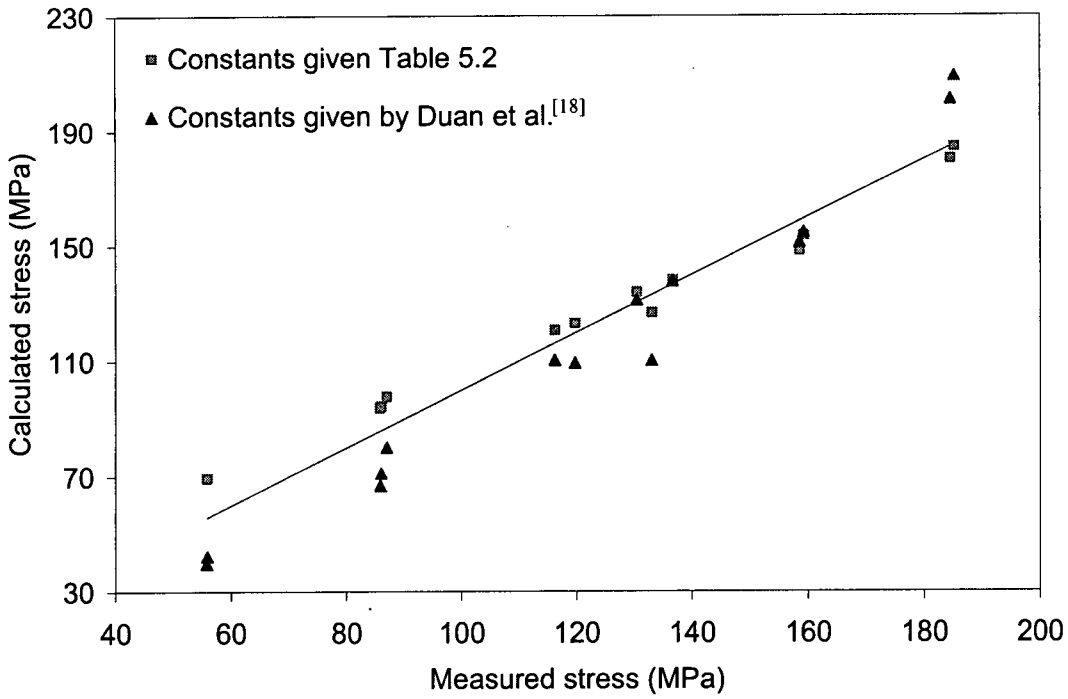

Figure 5.5 – A comparison between the experimentally measured and calculated flow stress using hyperbolic sine equation for an AA5083 aluminum alloy[12].

As can be seen in **Figure 5.5**, a better agreement between the experimental measurements and the calculated flow stress for AA5083 aluminum alloy was achieved using the constants given in Table 5.2 and thus were used to model the material behavior.

In order to implement the material behaviour in the model, data tables of flow stress at specified strain rates and temperatures were generated and input to ABAQUS. For each temperature and strain rate within the model, the flow stress at each integration point is calculated based on a linear interpolation between the tabular data points.

The thermophysical properties for AA5083 are shown in Table 5.3[2]. The density of the strip was assumed to be constant at 2660 kg m^{-3}[2].

Table 5.3 – Thermophysical properties used for AA5083[2].

Temperature (°C)	Heat Capacity (J kg^{-1} K^{-1})	Thermal Conductivity (W m^{-1} K^{-1})
14	930.0	143.4
280	990.0	167.1
306	1010.0	170.2
410	1050.0	174.1
505	1160.0	185.4

5.2.10 Rolling Load Analysis

The rolling loads in this research work were based on the reaction force at the central node of the work roll. Since the idealized model assumes a roll width of 1 m while the actual roll width used in Corus to carry out the experiments was only 350 mm, it was necessary to convert the model predicted rolling load. This was achieved by adjusting the predicted reaction forces at the center node of the work roll from the idealized model simulation, which assumed a roll width of 1 m, to the actual roll width of 350 mm. In other words, the predicted reaction forces at the roll center node was multiplied by a factor of 350/1000 representing the differences between the actuall roll width and the model assumed one. Finally, since the rolling load during experimental measurements were recorded at the end of the work roll, it was necessary to divide the model predicted results by two to determine the point load at each roll end where the measurements were taken.

5.2.11 Calculation of Zener Hollomon Parameter During Rolling

During the rolling process, Dauda *et al.* suggested that the average Z during rolling can be calculated by averaging the history of Z on the basis of time or

strain[22]. In this research work, the average Z for each node during rolling was calculated using the average strain rate and temperature at the element integration points for each time increment during rolling. This averaging methodology was proposed by Sheppard *et al.* and can be summarized in the following relation[3, 23]:

$$\overline{Z} = \frac{\sum_{i=1}^{N} Z_i \Delta t_i}{t} \tag{5.21}$$

where Δt_i is the time increment of the ith increment, Z_i is the Zener-Hollomon parameter of the ith increment, t is the total deformation time and N is the number of increment. It was found by studies conducted by Sheppard *et al.*[23] and Duan *et al*[3]. that good agreement between experimental measurements and model predictions can be achieved by using the average Z values, thus a time average of Z values is implemented in this research.

In order to calculate the average strain rate and deformation temperature during rolling for each time increment, a FORTRAN based user-defined subroutine, named *uvarm.f** was used in ABAQUS where the Z values were calculated for each time increment during rolling and stored as user defined field variables.

5.2.12 Rolling Process Model Steps in ABAQUS

Several loading steps are implemented to simulate the rolling process. The initial starting position of the work roll is above the strip but not in touch with the strip; i.e., there is a small clearance. During the first step, the work roll is lowered to obtain the desired reduction, pinching the head of the strip against the centerline. In the second step, the work roll rotates at the desired radial velocity. The strip is drawn into the roll bite due to the surface interaction between the work roll and the strip. The second step is completed when the work roll has rotated far enough for the entire strip to exit the roll bite. During the second step, a user-defined subroutine, named *uvarm.f** was used in ABAQUS to calculate the average deformation temperature and strain rate during rolling. During the third step, the inter-pass region is simulated by applying inter-pass cooling to the strip for a certain time corresponding to the inter-pass time.

* uvarm.f is a user subroutine provided by ABAQUS which can be accessed by a user to define and calculate output quantities that are functions of any of the available integration point quantities within the FE model.

During the fourth step, the work roll is further lowered, pinching the head of the strip against the centerline, based on the second-pass reduction. This is followed by rolling the strip in the reverse direction where the roll velocity is doubled during the fifth step to simulate second-pass hot rolling. In the final step, the strip is held for a certain to simulate second-pass hot rolling. In the final step, the strip is held for a certain period of time to simulate strip cooling after second-pass rolling prior to quenching.

5.2.13 Finite Element Model Parameters Analysis

An analysis was carried out to quantify the influence of changing the mesh density on the predicted temperature profile through the thickness of the strip at the roll bite exit. Further analysis was carried out to quantify the influence of changing the value of the efficiency of conversion of deformation energy to heat on the predicted centerline temperature and thus justify the selected value in the model. The results of this analysis are presented in the following section.

5.2.13.1 Effect of changing the mesh density on the predicted FE model results

Two aspects of mesh density were considered, namely the length and the through thickness of the strip and longitudinally. An analysis was conducted to investigate the effect of changing the number of elements through the thickness of the strip on the model predictions is shown in **Figure 5.6**. An analysis was carried out previously to determine the effect of changing the longitudinal mesh density on the predicted temperature is shown below in **Figure 5.7**[12]. In addition, an analysis was conducted to investigate the effect of changing the number of elements through the thickness of the strip on the predicted strains at the surface of the strip is shown in **Figure 5.8**.

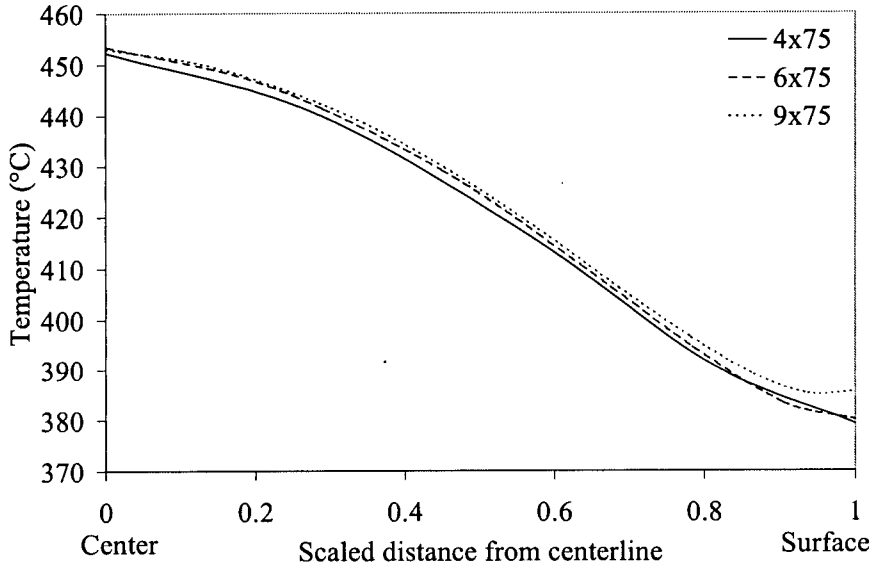

Figure 5.6 - Effect of changing the mesh density through the thickness of the strip on the model predicted temperature at the roll bite exit (T_{entry} = 448°C, $\bar{\dot{\varepsilon}}$ = 14.5 s^{-1}, ε = 0.52).

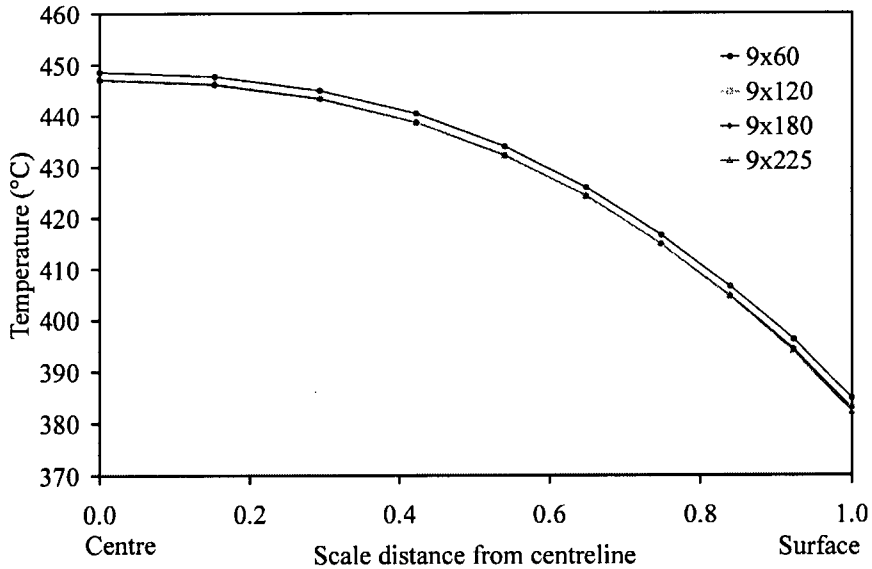

Figure 5.7- Effect of changing the mesh density in the longitudinal direction on the model predicted temperature at the roll bite exit (T_{entry} = 448°C, $\bar{\dot{\varepsilon}}$ = 14.5 s^{-1}, ε = 0.52)[12].

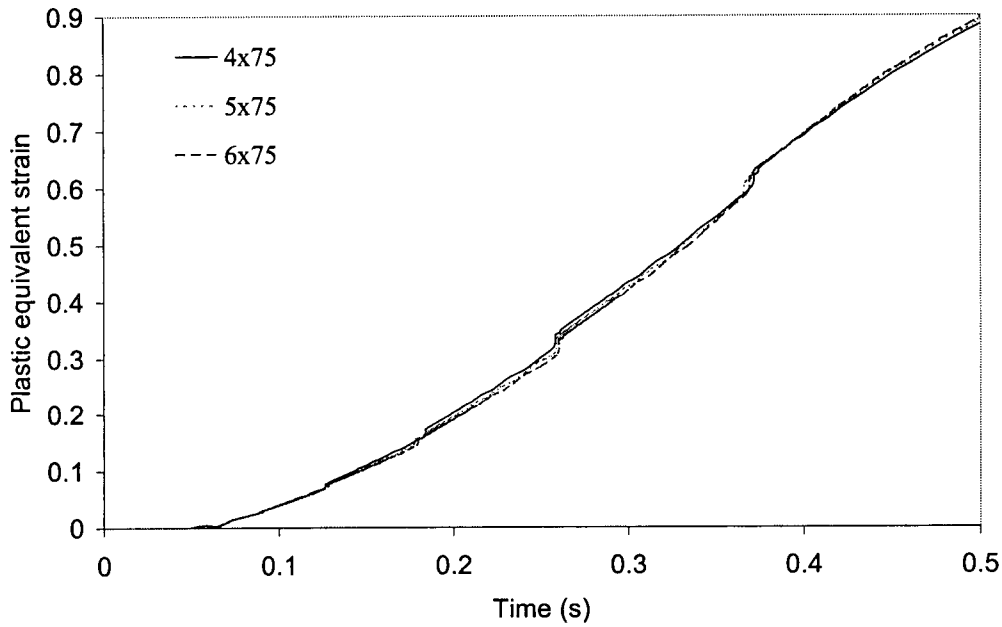

Figure 5.8- Effect of changing the mesh density through the thickness of the strip on the model predicted strain at the surface of the strip during rolling (T_{entry} = 448°C, $\bar{\dot{\varepsilon}}$ = 14.5 s^{-1}, ε = 0.52).

Figure 5.6 and **5.7** show that increasing the number of elements both longitudinally (from 60 to 225) or through the thickness of the strip (from 4 to 9) do not have a significant effect on the predicted temperatures. **Figure 5.8** shows that increasing the number of elements through the thickness of the strip (from 4 to 6) does not have a significant effect on the predicted von Mises plastic equivalent strain during rolling at the surface of the strip. Therefore, it was concluded that a sufficient mesh density to achieve optimum solution is 75 elements in the longitudinal direction and 4 elements in the through thickness direction with an aspect ratio of approximately 3 resulting in 300 elements in total.

5.2.13.2 Effect of changing the efficient of conversion of deformation energy to heat on the predicted FE model results

In this study, the efficiency of conversion of deformation energy to heat is assumed to be 95% for aluminum alloys. Most of the literature values are within the range of 90-95% indicating that 90-95% of the work done during deformation is dissipated as heat[2, 9]. A sensitivity analysis was carried out where the value of the

baseline conversion efficiency used in this study (95%) was altered by ± 5%. The predicted temperatures at the strip centerline were compared as shown in **Figure 5.9**. The predicted centerline temperatures are relatively insensitive to changes in the conversion efficiency which indicates that the selected value of 95% for the conversion efficiency is suitable for this modelling work.

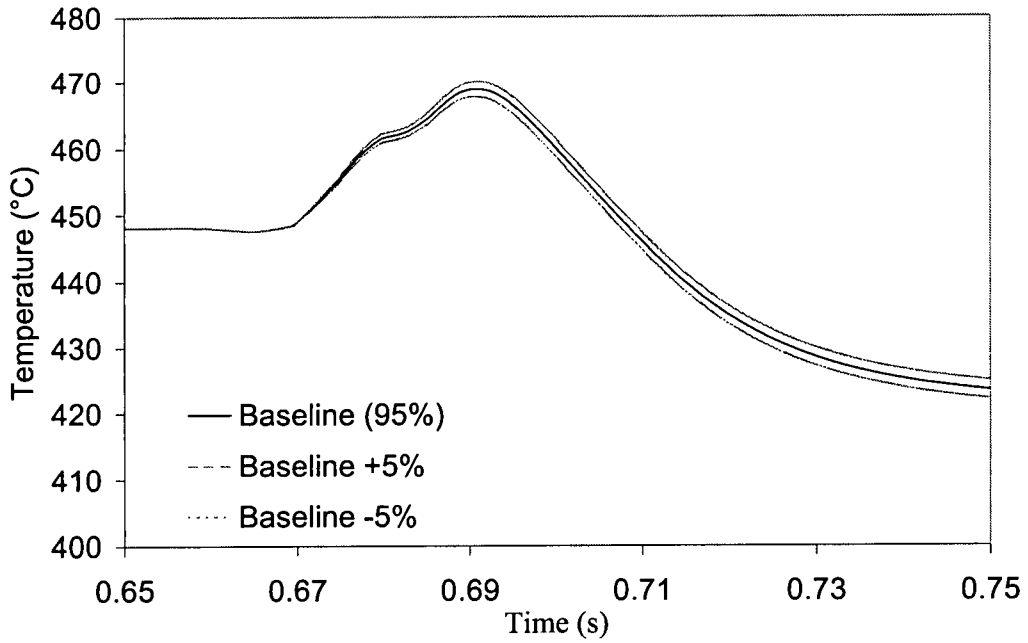

Figure 5.9 - Effect of altering the inelastic heat fraction on the predicted temperature at the strip centerline (T_{entry} = 448°C, $\bar{\dot{\varepsilon}}$ = 14.5 s^{-1}, ε = 0.52).

5.3 Internal State Variable Microstructure Model

The microstructure model adapts the internal state variable approach[24] described by Sellars *et al.*, where microstructure evolution processes, such as recrystallization, are related to the stored energy that develops in the material during deformation. The internal state variables include average dislocation density, average subgrain size and average misorientation angle between subgrains during rolling as well as the density of nucleation sites available for recrystallization in the material after deformation is complete. Each of these variables is related to the processing parameters employed during hot rolling, such as deformation temperature, strain and strain rate. The evolution of these variables can, in general, be expressed with a set of

coupled, first order differential equations which are integrated over the temperature-deformation history of the rolling process to predict the stored energy in the material after the deformation is complete. Using this philosophy, the final microstructure throughout the sheet can be predicted.

The dislocation substructure is one of the key parameters in the microstructure that determines the stored energy during hot deformation and hence the subsequent recrystallization behavior. In the hot rolling process there are mainly two competing effects namely the dynamic recovery during rolling and subsequent static recrystallization in the inter-pass region and after rolling is complete. During deformation processes, the stored energy of the material can be lowered by dislocation movement, which leads to annihilation of dislocations. This usually happens during deformation where dislocations of opposite signs can annihilate each other when they move towards each other via glide and climb mechanisms. This causes dynamic recovery during deformation[10]. Static recrystallization occurs when a hot deformed material is subsequently annealed, where the lower stored energy due to dynamic recovery can affect recrystallization kinetics[10]. During hot rolling these two mechanisms are competing in the sense that as dynamic recovery occurs, it reduces the stored energy in the material, which in turn reduces the driving pressure for subsequent static recrystallization.

The dislocation substructure can be described using three internal state variables, which include[24]:

1) internal dislocation density,
2) average subgrain size,
3) average misorientation across subgrain boundaries.

Research has shown that in aluminum alloys, these variables evolve during hot deformation and typically reach a steady state value after a critical strain value is reached[3, 25]. As deformation proceeds, the dislocation density and the misorientation angle between the subgrains increase whereas the subgrain size decreases until steady state is reached. Beyond the critical strain, the substructure and, hence the flow stress of the material during deformation, remains constant.

The evolution of the subgrain size (δ), the random dislocation density (ρ_r) and the misorientation between the subgrains (θ), expressed in differential form in Equations 5.22-5.24, is based on the classical theory of work hardening and dynamic recovery as described by Sellars *et al.*[24, 25]:

$$d\rho_r = d\rho_r^+ + d\rho_r^- = (C_1\rho_r^{1/2} - C_2\frac{\sigma_f}{Z}\rho_r)d\varepsilon \tag{5.22}$$

$$d\theta = \frac{1}{\varepsilon_\theta}(\theta_{ss} - \theta)d\varepsilon \tag{5.23}$$

$$d\delta = \frac{\delta}{\varepsilon_\delta \delta_{ss}}(\delta_{ss} - \delta)d\varepsilon \tag{5.24}$$

In Equation 5.22, $d\rho_r^+$ is the dislocation generation term and $d\rho_r^-$ is the dislocation annihilation, which represent the dynamic recovery term, during hot rolling, ρ_r is the random dislocation density, C_1 and C_2 are material based constants, Z is the average Zener-Hollomon parameter for the deformation which incorporates both the deformation temperature and the strain rate $\left(Z = \dot{\varepsilon}\, exp\left(\frac{Q_{def}}{RT_{def}}\right)\right)$[26], Q_{def} is the activation energy for deformation and σ_f is the frictional stress. Equation 5.22 can be used to describe the evolution of random internal dislocation density as a function of incremental strain during rolling. In Equations 5.23 and 5.24, the evolution of the average misorientation angle between subgrains, θ, and subgrain size, δ, are influenced by the characteristic strains; ε_θ and ε_δ, respectively. These strains are related to the Z parameter as $\varepsilon_\delta \propto Z^{3/4}$, $\varepsilon_\theta \propto Z^{1/4}$. In these equations, $d\varepsilon$ is the incremental strain imposed during rolling, δ_{ss} and θ_{ss} are the steady state subgrain size and steady state misorientation angle, respectively.

Based on the observations that subgrain structure is in the form of microbands oriented at ~ 35° to the rolling plane with low misorientation subgrain boundaries within them, Baxter *et al.* concluded that the higher misorientation angle boundaries in the band are geometrically necessary boundaries to accommodate lattice curvature[27]. Thus, the internal dislocation density can be estimated by evaluating two

terms namely, the random, or statistical, dislocation density (ρ_r), and the geometrically necessary dislocation density (ρ_g). Random dislocations are produced due to homogenous strains [11]. When the material does not deform homogenously; i.e., when there is a strain gradient where some parts of the material deform more than others due to differences in microstructure, dislocations are stored in this material to accommodate the strain gradient, and allow compatible deformation of the entire material without the creation of internal voids. These types of dislocations are termed "geometrically necessary dislocations". This accommodation of deformation is done via changing the lattice curvature which is a result of constraining the neighboring grains[14].

The density of the geometrically necessary dislocations can be estimated using Equation 5.24 which relates the density of the geometrically necessary dislocations to the lattice radius of curvature and the deformation parameters, namely: the average subgrain size, and the average misorientation angle between subgrains.

$$\frac{1}{R_g} = \rho_g b + \frac{\theta}{\delta} \tag{5.25}$$

where $\frac{1}{R_g}$ is the local lattice curvature and b is the Burgers vector. The local lattice curvature and Burgers vectors were assumed to be constant[27]. The evolution of geometrically necessary dislocations during rolling were calculated based on the evolution of the average subgrain size and average misorientation angle between subgrains at each strain increment during rolling as shown in Equations 5.23 and 5.24. The development of curvature is further illustrated in **Figure 5.10**.

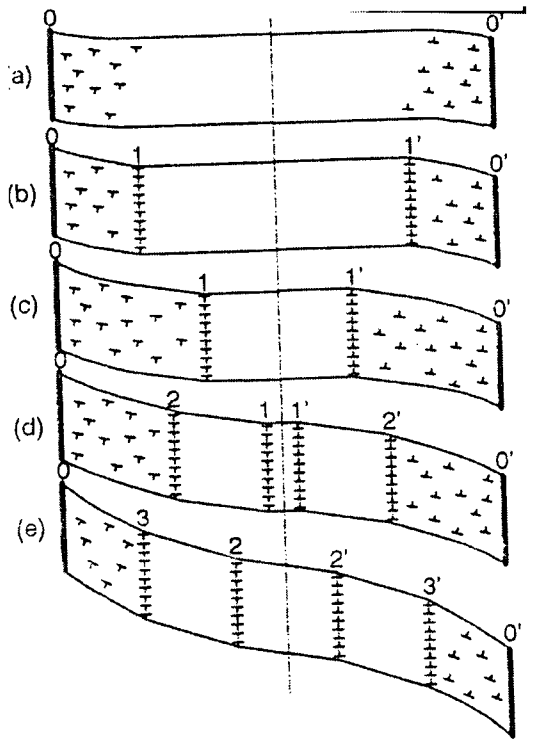

Figure 5.10 – Schematic diagram of lattice curvature development[14].

Figure 5.10 shows the local excess dislocation density with the same Burgers vector within subgrains termed "geometrically necessary dislocations" and their relation to lattice curvature. Due to local variations in dislocation interaction, the dislocation glide velocity will exhibit variations. Hence slower moving dislocations will be caught up by the faster moving ones resulting in tilt boundary formation (1 1') as shown in (b) resulting in lattice curvature. Then, the applied stress causes the boundary to migrate, where they finally annihilate each other, and new dislocation boundaries (2 2') are formed causing a new tilt boundary, and curvature as shown in **Figure 5.10c** and **d**. Finally, the process continues as the strain increases where (2 2') migrate towards each other, and a new dislocation boundary (3 3') is formed as shown in **Figure 5.10e**[14].

Assuming transient deformation conditions, the total internal dislocation density can be evaluated based on the evolution of ρ_r (random dislocation density) and ρ_g (the geometrically necessary dislocation density) as shown below in Equation 5.26:

$$\rho_i = \rho_r + \rho_g \tag{5.26}$$

5.3.1 Modelling Static Recrystallization Behavior During Single-Pass Rolling

Within the internal state variable model, the nucleation density (N_v) is defined based on the grain boundary area per unit volume, S_v, and the subgrain size, δ, as shown in Equation 5.27. The model considers nucleation to occur exclusively at grain boundaries. Although nucleation can occur at other locations such as particles, other research has shown that the majority of the nucleation in these alloys occurs at grain boundaries, especially under high temperature deformation conditions[25].

$$N_v = \left(\frac{C_3}{\delta^2}\right) S_v(\varepsilon) \tag{5.27}$$

where C_3 is a material constant that accounts for the probability of finding a subgrain with a size larger than the critical size required to provide a nucleation site for recrystallization as well as geometric parameters.

Assuming rolling is a plane strain operation, S_v can be estimated according to Equation 5.28[3]:

$$S_v = \left(\frac{2}{d_o}\right)[\exp(\varepsilon) + \exp(-\varepsilon) + 1] \tag{5.28}$$

where d_o (in μm) is the initial grain size assuming uniform equiaxed structure.

Metallographic examination of the starting material used in this research revealed that the recrystallized microstructure consisted mainly of elongated grains with an average aspect ratio of 2:1. Thus, Equation 5.28 was modified to account for the elongated nature of the grains, assuming that the steady state recrystallized microstructure consists of rectangular shaped grains, as shown in Equation 5.29:

$$S_V = 2\left[\frac{\exp(-\varepsilon)}{d_2} + \frac{\exp(\varepsilon)}{d_1} + 1\right] \tag{5.29}$$

where d_2 is the grain width in the x-direction and d_1 is the grain length in the y-direction. This relation can be derived from simple geometry as shown in ***Appendix A***.

The stored energy in the material due to the deformation can then be estimated based on Equation 5.30[3, 25]:

$$P_D = \frac{Gb^2}{10}\left[\rho_i\left(1-\ln\left(10b\rho_i^{1/2}\right)\right)+\frac{2\theta}{b\delta}\left(1+\ln\left(\frac{\theta_c}{\theta}\right)\right)\right] \tag{5.30}$$

where G is the shear modulus, b is the Burgers vector, ρ_i is the internal dislocation density governed by Equation 5.22, θ is the misorientation angle governed by Equation 5.23, and θ_c is the critical misorientation of a high angle boundary (~10°).

The time to achieve 50% recrystallization can then be calculated based on the stored energy, P_D, and the density of recrystallization nuclei, N_v, as shown in Equation 5.31[25]:

$$t_{0.5} = \frac{C_4}{P_D N_v^{1/3}} \tag{5.31}$$

The final fraction recrystallized can then be estimated using an Avrami-type equation as described previously and shown below in Equation 5.32:

$$X_v = 1-\exp\left(-0.693\left(t/t_{0.5}\right)^n\right) \tag{5.32}$$

The recrystallized grain size can be estimated using Equation 5.33[25, 28]:

$$d_{rex} = D(N_v)^{-1/3} \tag{5.33}$$

where D is a constant.

In this work, the majority of the constants in the physically-based model used to model hot rolling process were taken from the literature for an AA5083 aluminum alloy. The material based constants C_3 and C_4 were determined based on the measured single-pass rolling microstructure data in this research. The physically-based model constant values and initial assumed values of the total dislocation density (ρ_o), average subgrain size (δ_o) and average misorientation angle (θ_o) for the initial microstructure before deformation are shown in Table 5.4. The JMAK exponent was assumed to be equal to 2 based on the literature reported values for AA5083[3]. This assumption can be justified based on the fact that grain growth during recrystallization may be constrained by the sample geometry or other internal microstructure constraints that limit the grain growth to two-dimensions which in turn results in a lower JMAK exponent[26]. The microstructure model sensitivity to the change in the JMAK exponent from 2 to 3 is further discussed in Chapter 7.

Table 5.4 – Parameters used in the physically-based microstructure model[3].

Parameter	Value
C_1	83.916 $m^2 N^{-1}s^{-1}$
C_2	$1.75x10^6$ N $m^{-1}s^{-1}$
C_3	0.0018
C_4	$7.82x10^{13}$ Ns m^{-5}
n	2
b	$2.86x10^{-10}$ m
G	$2.05x10^{10}$ Pa
$1/R_g$	$5x10^4$ m^{-1}
σ_f	$25x10^6$ Pa
Q_{def}	145.1 kJ/mole
ρ_o	$1x10^{11}$ m^{-2}
δ_o	$1x10^{-6}$ m
θ_o	0°
θ_{ss}	2.8°
ε_θ	$5x10^{-5}Z^{-1/4}$
ε_δ	$9x10^{10}Z^{-1}$
Q_{rex}	183 kJ/mole
D	2.347

5.3.2 Multi-Pass Hot Rolling Modelling Aspects

The commercial hot rolling process is a continuous non-isothermal process. For example, there is continuous cooling by convection/radiation of the strip between rolling passes. In order to apply isothermal recrystallisation equations to this non-isothermal process, a principle of additivity was employed both in the inter-pass region and after rolling was complete to account for the non-isothermal cooling of the strip as a function of time in the inter-pass region. Under these conditions, the application of a temperature compensated time parameter, W, is employed as shown in Equations 5.34 – 5.36 to predict the fraction recrystallized, X_v based on the thermal history experienced by the material[29]:

$$X_V = 1 - \exp\left(-0.693 \cdot \left(\frac{W}{W_{0.5}}\right)^n\right) \tag{5.34}$$

$$W = \sum_i \partial t_i \cdot \exp\left(\frac{-Q_{rex}}{RT_i}\right) \tag{5.35}$$

$$W_{0.5} = t_{0.5} x \exp\left(\frac{-Q_{rex}}{RT_a}\right) \tag{5.36}$$

T_a is the temperature the strip equilibrates to after exiting the roll pass, t_i is the time interval during which the slab has a temperature of T_i and Q_{rex} is the activation energy for recrystallization. This methodology was employed at different through-thickness locations of the strip which correspond to different integration points in the FE model to account for non-isothermal cooling conditions through the thickness of the strip.

One of the main challenges in extending the model to multi-pass rolling cases lies in being able to track the changes in the internal state variables in the inter-pass region during multi-pass rolling based on the fraction recrystallized between passes. In this microstructure model, a law of mixtures was employed to account for microstructure changes due to static recrystallization in the inter-pass region. A law of mixtures was used to determine the initial entry values to the second pass rolling of the strains, dislocation density, average subgrain size and average misorientation angle between the subgrains at different locations through the thickness of the strip based on the fraction recrystallized between passes[29]. These relations are illustrated in Equations 5.37-5.40:

$$\varepsilon_2^{eff} = X_1 \varepsilon_{rex} + (1 - X_1)\varepsilon_1 \tag{5.37}$$

$$\rho_2^{eff} = X_1 \rho_{rex} + (1 - X_1)\rho_1 \tag{5.38}$$

$$\delta_2^{eff} = X_1 \delta_{rex} + (1 - X_1)\delta_1 \tag{5.39}$$

$$\theta_2^{eff} = X_1 \theta_{rex} + (1 - X_1)\theta_1 \tag{5.40}$$

where the numbers 1 and 2 represent the 1st and 2nd pass, respectively. Recrystallized grains were assumed to exhibit the following characteristics: ε_{rex} equal to 0, ρ_{rex} equal to 1x 10^{11} m^{-2}, δ_{rex} equal to 1x10^{-6} m and θ_{rex} equal to 0°. These values were taken to coincide with the original values used prior to first pass deformation.

Similarly, a law of mixtures was applied to estimate the initial entry values of the average grain size to second pass rolling. In order to account for the elongated nature of the starting material, an initial structure that was approximated as a rectangular shape was assumed. After first pass rolling was complete, the material is held for a certain period of time corresponding to the inter-pass time where some of the grains remain in the deformed condition and the rest are recrystallized before entering the second-pass during rolling. This concept is further illustrated in **Figure 5.11**.

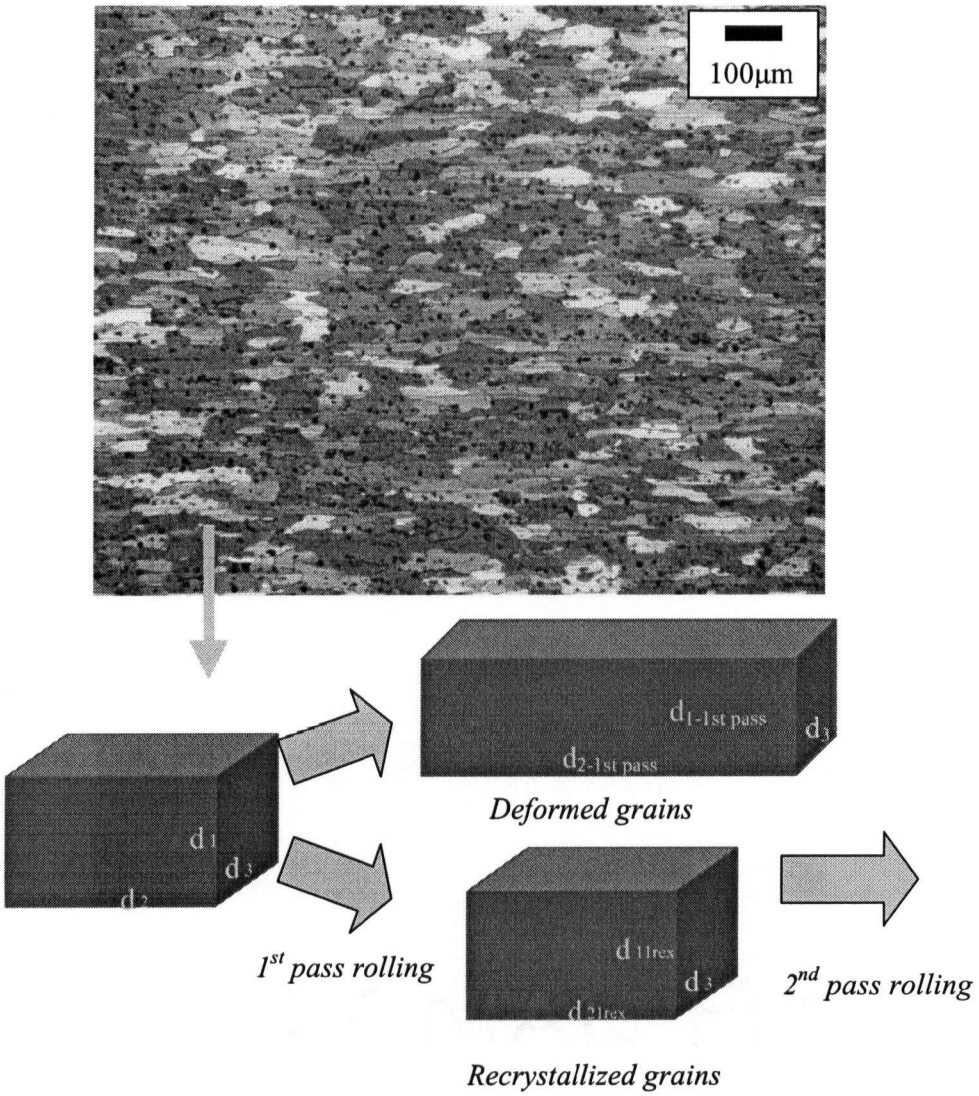

Figure 5.11 – A schematic illustration of the material composite structure that consist of deformed grains and recrystallized ones before second-pass rolling

The initial value of the grain size before second pass rolling was calculated based on a law of mixtures which accounts for the composite grain structure that consists of a mixture of deformed and recrystallized grains as shown in Equations 5.41- 5.42:

$$d_{2-2ndpass} = X_v d_{21rex} + (1 - X_v) d_{2-1st\ pass} \tag{5.41}$$

$$d_{1-2ndpass} = X_v d_{11rex} + (1 - X_v) d_{1-1st\ pass} \tag{5.42}$$

where $d_{1-1st\ pass}$ & $d_{2-1st\ pass}$ are calculated based on the strain that the parent grain exhibits during first pass rolling and d_{rex} is the model predicted recrystallized grain size in the inter-pass region, d_2 is the grain width in the x-direction and d_1 is the grain length in the y-direction as shown in **Figure 5.11**.

5.3.3 Integrating ABAQUS FE modelling results to the microstructure model

An ABAQUS user defined subroutine was employed to extract the values of temperature and strain rate during rolling and through the thickness of the strip at each time increment as discussed previously in section 5.2.12. The microstructure model was "weakly coupled" to the thermo-mechanical model where the deformation parameters, along with the von Mises plastic equivalent strain were extracted and used offline in a spreadsheet as inputs to calculate the microstructure evolution during the rolling process

In the microstructure model, the incremental strain and Zener Holloman parameter (Z), estimated based on the temperature and strain rate, at the integration points through the strip thickness were used as inputs. The change in dislocation density, average subgrain size and average misorientation angle were calculated during rolling as a function of incremental strain change based on Equations 5.21-5.23. The grain boundary area per unit volume was calculated as a function of total applied strain during deformation based on Equation 5.28. At the roll bite exit, the

total driving pressure, nucleation density and subsequently $t_{0.5}$ and recrystallized grain size (d_{rex}) were estimated based on the calculated state variable exit values.

In the inter-pass region, the principle of additivity was employed where the predicted thermal profile in the inter-pass region was used to calculate the final W at different through-thickness locations in the strip. The fraction recrystallized was estimated based on Equation 5.33. The law of mixtures, Equations 5.36-5.41, were employed based on the predicted fraction recrystallized in the inter-pass region to determine the average microstructure state variable entry values to the second pass rolling. It should be noted that the law of mixtures was applied at different locations, corresponding to the material integration points in the FE model, through the thickness of the strip. Thus, the model was able to account for the variation in the microstructure through the strip-thickness at different locations. A similar procedure was used for second pass rolling.

5.4 Summary

A model simulating hot rolling of AA5083 aluminum alloy to predict the thermo-mechanical deformation and microstructure evolution during both single-pass and multi-pass hot rolling has been presented. The 2-D coupled temperature-displacement finite element (FE) thermo-mechanical model has been described with details of the geometry, FE mesh and boundary conditions. The FE boundary conditions include both thermal boundary conditions at the strip centerline, the roll center and the roll-strip interface and mechanical boundary conditions including friction behavior at the roll-strip contact interface.

A physically-based internal state variable microstructure model was employed to understand and predict the material stored energy and subsequent recrystallization kinetics during both single-pass and multi-pass hot rolling through the strip thickness. The challenge of capturing and tracking the accumulation of stored energy during multi-pass rolling and the non-isothermal cooling in the inter-pass region was addressed by employing the principle of additivity and rule of mixtures to different model variables to account for microstructure changes in the inter-pass region. The

application and validation of this model for various single-pass and multi-pass hot rolled AA5083 will be discussed in the next chapter.

References

1. Mirza, M.S., C.M. Sellars, K. Karhousen, and P. Evans, *Multipass rolling of aluminum alloys: finite element simulations and microstructural evoltion.* Mater. Sci. and Tech., 2001. **17**: p. 874-879.

2. Chen, B.K., P.F. Thomson, and S.K. Choi, *Computer Modelling of microstructure during hot flat rolling of aluminium.* Mater. Sci. Technol., 1992. **8**(1): p. 72-77.

3. Duan, X.J. and T. Sheppard, *Influence of forming parameters on static recrystallization behaviour during hot rolling aluminium alloy 5083.* Modell. Simul. Mater. Sci. Eng., 2002(10): p. 363-380.

4. Wells, M.A., *Mathematical modelling of the microstructure and texture changes during hot tandem rolling of AA5182 and AA5052 aluminum alloys, Ph. D Thesis*. 1995, University of British Columbia: Vancouver, Canada.

5. Zienkiewicz, O.C. and R.L. Taylor, *The finite element method, 4th edition.* 1994: McGraw-Hill book company.

6. Bathe, K.J., *Finite element procedure*. 2002, New Delhi: Prentice Hall of India.

7. Huebner, K.H., D.L. Dewhirst, D.E. Smith, and T.G. Byrom, *The finite element Method for engineers*. 2001, NewYork: John Wiley & Sons, INC. 720.

8. *ABAQUS theory manual, Version 6.2*. 1997.

9. Timothy, S.P., H.L. Yiu, J.M. Fine, and R.A. Ricks, *Simulation of single pass of hot rolling deformation of aluminum alloy by plane strain compression.* Mater. Sci. Technol., 1991. **7**(3): p. 255-261.

10. Sengupta, J., *Mathematical modelling of the evolution of thermal field during start-up phase of the direct chill casting process for AA5182 sheet ingots, Ph.D. thesis*. 2002, The University of British Columbia: Vancouver, Canada.

11. Wells, M.A., D.J. Lloyd, I.V. Samarasekera, J.K. Brimacombe, and E.B. Hawbolt, *Modeling the microstructural changes during hot tandem rolling of AA5XXX aluminum alloys. Part III.* Metall. Mater. Trans. B, 1998. **29B**: p. 709-720.

12. Jupp, S., *Mathematical modelling of the microstructural evolution during the hot rolling of AA5083 aluminum alloys, M. Sc. thesis*. 2001, University of British Columbia: Vancouver, Canada.

13. Hlady, C.O., *Master's Thesis*, in *Metals and Materials Engineering*. 1994, University of British Columbia: Vancouver.

14. Devadas, C., I.V. Samarasekera, and E.B. Hawbolt, *The thermal and metallurgical state of steel strip during hot rolling: Part I. Characterisation of the heat transfer coefficient.* Metall. Mater. Trans. A, 1991. **22A**: p. 307-319.

15. Holman, J.P., *Heat Transfer*. 1997: McGraw Hill.

16. Beynon, J.H. and C.M. Sellars, *Modelling microstructure and its effects during multipass hot rolling.* ISIJ International, 1992. **32**: p. 359-367.

17. Lenard, J.G. and Z. Malinowski, *Measurement of friction during the warm rolling of aluminum.* J. Mat. Proc. Tech., 1993. **39**: p. 357-371.

18. Duan, X. and T. Sheppard, *The influence of the constitutive equation on the simulation of a hot rolling process.* J. Mat. Sci., 2004. **150**: p. 100-106.

19. Hoff, N.J., Q. Appl. Mech., 1954. **49**(2): p. 49.

20. Hensel, A., T. Rehtanz, and G. Ochlstoter, *forming technological parameters of selected hot forming methods.* Neue Hutte., 1984. **29**(1): p. 1-6.

21. Sellars, C.M., *Modelling microstructural development during hot rolling.* Mater. Sci. Technol., 1990. **6**: p. 1072-1081.

22. Dauda, T.A. and A.J. McLaren. in *Modelling of Metal Rolling Processes 3*. 1999. London: IoM Communications Ltd.

23. Sheppard, T. and X.J. Duan, *Modelling of static recrystallisation by the combination of empirical models with finite element method.* J. Mater. Sci, 2003. **38**: p. 1747-1754.

24. Sellars, C.M. and Q. Zhu. *Microstructural evolution during hot deformation of aluminum-magnesium alloys*. in *Hot Deformation of Aluminum Alloys II*. 1998. Rosemont, USA: TMS.

25. Sellars, C.M. and Q. Zhu, *Microstructureal modelling of aluminum alloys during themomechanical processing.* Mater. Sci. Eng., A, 2000. **280**: p. 1-7.

26. Humphreys, F.J. and M. Hatherly, *Recrystallization and related annealing phenomena*. 1996, NewYork: Pergamon Press. 363.

27. Baxter, G.J., T. Furu, Q. Zhu, J.A. Whiteman, and C.M. Sellars, *The influence of transient deformation conditions on recrystallization during themomechanical processing of aluminum alloy Al-1% Mg.* Acta Mater., 1999. **47**(8): p. 2367-2376.

28. Vatne, H.E., R. Shahani, and E. Nes, *Deformation of cube oriented grains and formation of recrystallized cube grains in a hot deformed commercial AlMgMn aluminum alloy.* Acta Mater., 1996. **44**: p. 4447-4462.

29. Ahmed, H., M.A. Wells, D.M. Maijer, and M.R. van der Winden. *Modeling of microstructure evolution during multi-pass rolling for AA5083 using a physically based approach integrating FE model predictions.* in *Proceedings of 9th International Conference on Aluminium Alloys (ICAA9).* 2004. Brisbane, Australia.

CHAPTER 6

MODEL RESULTS AND DISCUSSION

6.1 Introduction

The various thermo-mechanical and microstructure changes during multi-pass hot rolling were analyzed with the 2-D thermo-mechanical finite element (FE) and internal-state-variable microstructure models described in the previous chapter. Multi-pass hot rolling experimental results obtained in the course of this research program were utilized to validate the thermo-mechanical model in terms of temperature change during rolling at the centerline and surface of the strip as well as the rolling loads.

Validation of the physically-based microstructure model consisted of determining the appropriate model constants to be used for AA5083 aluminum alloy for single-pass hot rolling cases. This was achieved by comparing the model predictions of the fraction recrystallized and the recrystallized grain size at locations through the thickness of the sheet to the experimental measurements that were obtained using the metallographic techniques described in Chapter 4.

Further analysis was carried out during the course of this doctoral research using multi-pass hot rolled material to validate the microstructure model under different strain, strain rate, temperature and holding time conditions. Validation of the physically-based microstructure model for the multi-pass hot rolling cases was achieved by comparing the predictions of the fraction recrystallized and the recrystallized grain size at different locations through the thickness of the strip to the experimental measurements.

6.2 Single-Pass Hot Rolling Model Validation

In a previous study conducted at the University of British Columbia (UBC), the thermo-mechanical model was validated against the experimentally measured temperatures, strains and rolling loads for single pass rolled samples[1]. During this

study, model validation for single-pass rolled samples were carried out for the thermo-mechanical model developed within ABAQUS by comparing the predicted temperatures, strains and rolling loads during single-pass hot rolling cases to experimental measurements.

The conclusions of this previous study conducted on single-pass hot rolled samples include the following[1]:

(i) A comparison between the predicted and experimentally measured temperatures shows that the temperature predictions match the measurements reasonably well at the centerline and the surface of the strip for single-pass rolled cases,

(ii) A comparison between the measured and the predicted von Mises equivalent strain through the thickness of the strip during single pass rolling show that the measurements match the model predictions reasonably well with a minor deviation of ~ 7% exhibited by the predictions close to the surface.

(iii) A comparison between the predicted and measured loads indicated that there is less than a ~6% difference. Thus it was concluded that this minor discrepancy between the predicted and measured rolling load indicates that the friction coefficient of 0.3 is suitable and adequately represents the friction conditions between the work roll and the strip.

The reader is referred to Wells *et al.* for further details regarding the single-pass hot rolling deformation model validation[2].

6.3 Application of Physically Based Model to Predict Microstructure Evolution During Single-Pass Hot Rolling

The internal state variable model was originally developed and applied on Al-1%Mg aluminum alloys[3, 4]. Thus, in order to apply the model to AA5083 aluminum alloy (Al-5%Mg), some of the model constants needed to be determined based on experimental data. Initially, model constants were published for an AA5083 by Duan *et al.*[5] based on previously reported experimental data in the literature by Timothy *et al.*[6]. No rolling experiments was carried out in the study conducted by Duan *et al.*[5] to further verify their selected constants.

One of the first tasks in this doctoral work focused on tuning the physically based microstructure model for each of the six single-pass hot rolled samples where by the predicted fraction recrystallized and recrystallized grain sizes were compared to the experimental measurements under a wide variety of deformation conditions to determine the appropriate model constants that can be utilized to model microstructure evolution during rolling. Some of the original constant values reported in the literature by Duan *et al.* [5] were altered to reduce the difference between the predicted and experimentally measured fraction recrystallized and recrystallized grain size for the single-pass rolled samples. Specifically, C_3 in Equation 5.27 (used to calculate the nucleation density) was altered from the original literature value of 0.004[5, 7] to 0.0018 and C_4 in Equation 5.31 (used to calculated $t_{0.5}$) was altered from $7.0x10^{13}$[5, 7] to $7.82x10^{13}$. A comparison between the conatants, namely C_1 and C_2 in Equation *5.22* (used to calculate dislocation density), C_3 in Equation 5.27 (used to calculate the nucleation density) and C_4 in Equation 5.31 (used to calculated $t_{0.5}$), published for AA5083[5] and the adopted constants in the physically based model in this research is shown in Table 6.1. A comparison showing the effect of altering the physically based constants on the model predicted fraction recrystallized through the thickness of the strip for single-pass rolled sample no. 2 is shown in **Figure 6.1**.

Table 6.1 – A comparison between published constants in literature and the ones obtained using single-pass hot rolled experiments.

Parameter	Value (AA5083) published data[5]	Value (AA5083) Current reserach
C_1	83.916 $m^2 N^{-1}s^{-1}$	83.916 $m^2 N^{-1}s^{-1}$
C_2	$1.75x10^6$ N $m^{-1}s^{-1}$	$1.75x10^6$ N $m^{-1}s^{-1}$
C_3	0.004	0.0018
C_4	$7.00x10^{13}$ Ns m^{-5}	$7.82x10^{13}$ Ns m^{-5}

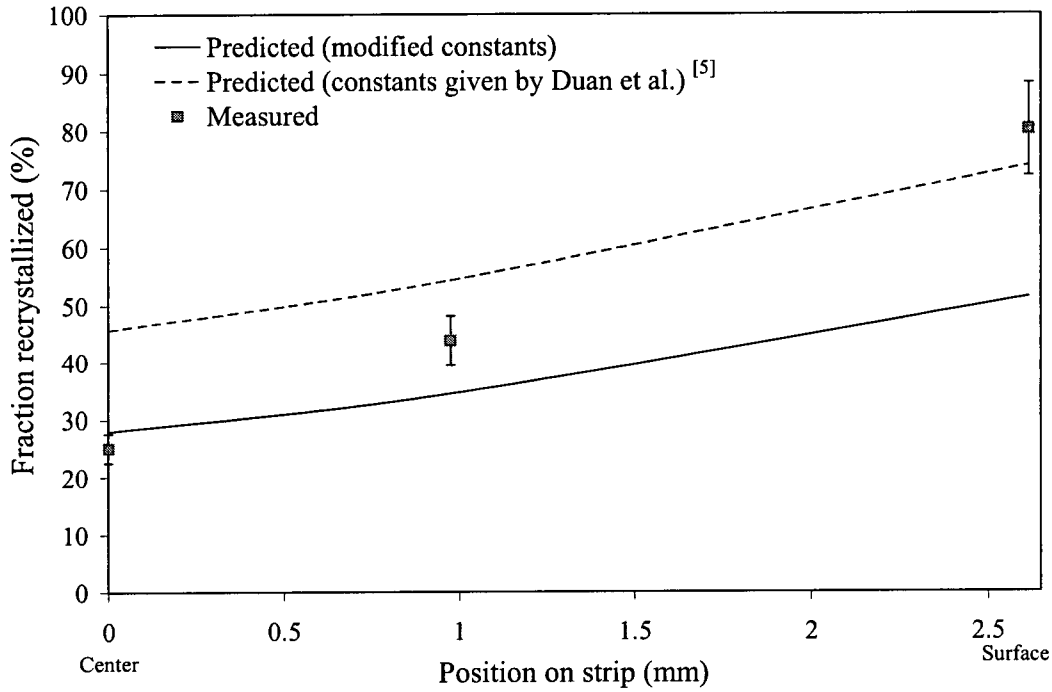

Figure 6.1 – Effect of altering the internal state variable model constants based on single-pass rolling experiments on the predicted fraction recrystallized through thickness of strip for sample no. 2.

It can be seen from **Figure 6.1** that the model predictions are sensitive to changes in the model constants which will be further discussed in Chapter 7. The model sensitivity to the constants used indicate that careful experimental measurements need to be made to identify some of the model parameters accurately under a range of deformation conditions. During this research project, the constants were accurately determined for AA5083 aluminum alloy based on single-pass rolling experiments. For each of the six single-pass rolled samples, the predictions of the through thickness distribution of the fraction recrystallized and the recrystallized grain size against experimental measurements shows that they match each other reasonably well with an overall trend of increasing fraction recrystallized and decreasing recrystallized grain size from the center to the surface of the strip. A comparison between the measured and predicted fraction recrystallized for samples nos. 2 and 4 is shown in **Figure 6.2**. The two samples selected represent: (i) deformation with a low *Z*-parameter and large strain, sample no. 2 and (ii) deformation with a high *Z*-parameter and small strain, sample no. 4.

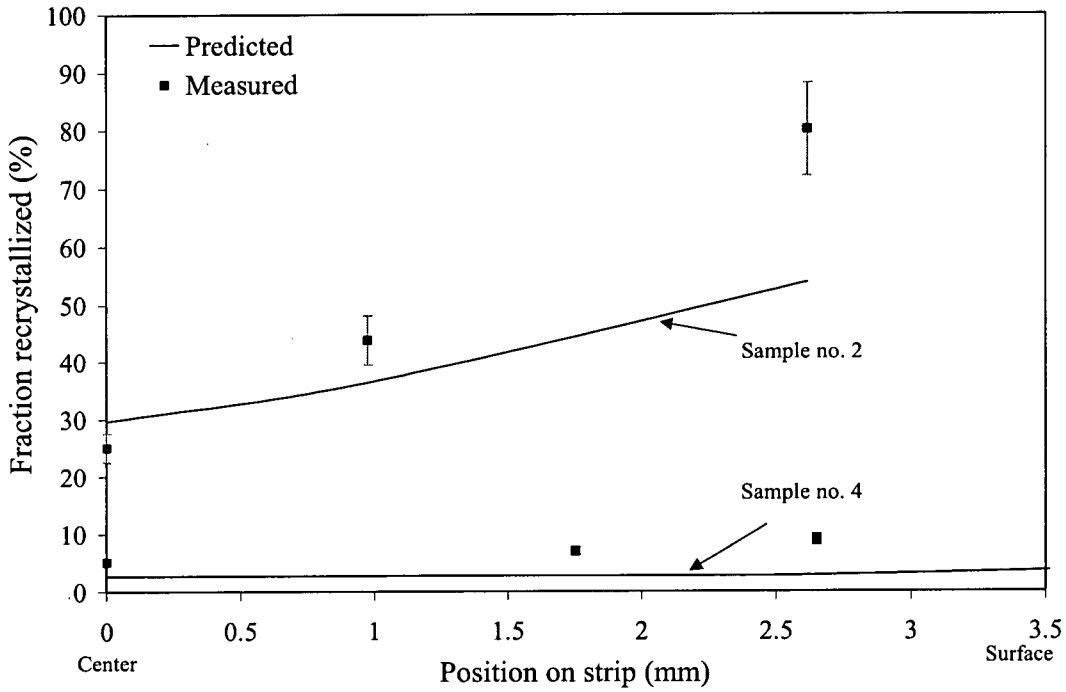

Figure 6.2 – Comparison of the internal state variable model predictions of fraction recrystallized through thickness of strip with experimental measurements for single-pass rolled samples no. 2 and 4.

As can be seen in **Figure 6.2**, for sample no. 2, a significant amount of recrystallization has occurred, whereas for sample no. 4, very little recrystallization has occurred. Although sample no. 4 has a higher level of stored energy as compared to sample no. 2, due to lower entry temperature, it did not exhibit as much recrystallization after quenching because sample no. 2 was held for a much longer period of time before being quenched as compared to sample no. 4 (i.e., 15 seconds versus 3 seconds) as illustrated in Table 4.1. The predictions were in reasonable agreement with the measured values for sample no. 4 at the centerline, while the model under predicted the fraction recrystallized by a difference of ~ 6% close to the surface of the strip. The model under predicted the fraction recrystallized for sample no. 2 close to the surface of the strip and was in reasonable agreement with the measurements difference close to the strip centerline. The difference close to the surface of the strip was ~25%. Although the predictions showed deviations from the

measurements close to the surface of the strip, the model correctly predicted the overall trend in terms of fraction recrystallized. In addition, the predictions of microstructure evolution for the wide range of hot deformation conditions studied were reasonable.

To further validate the microstructure model, a comparison between the predicted average recrystallized grain size and the measurements was conducted. A comparison between the optical and EBSD measured grain size with the model predictions for sample no. 2 is shown in **Figure 6.3** and a comparison of the predicted recrystallized grain size and the optical measurements for samples no. 4 is shown in **Figure 6.4**.

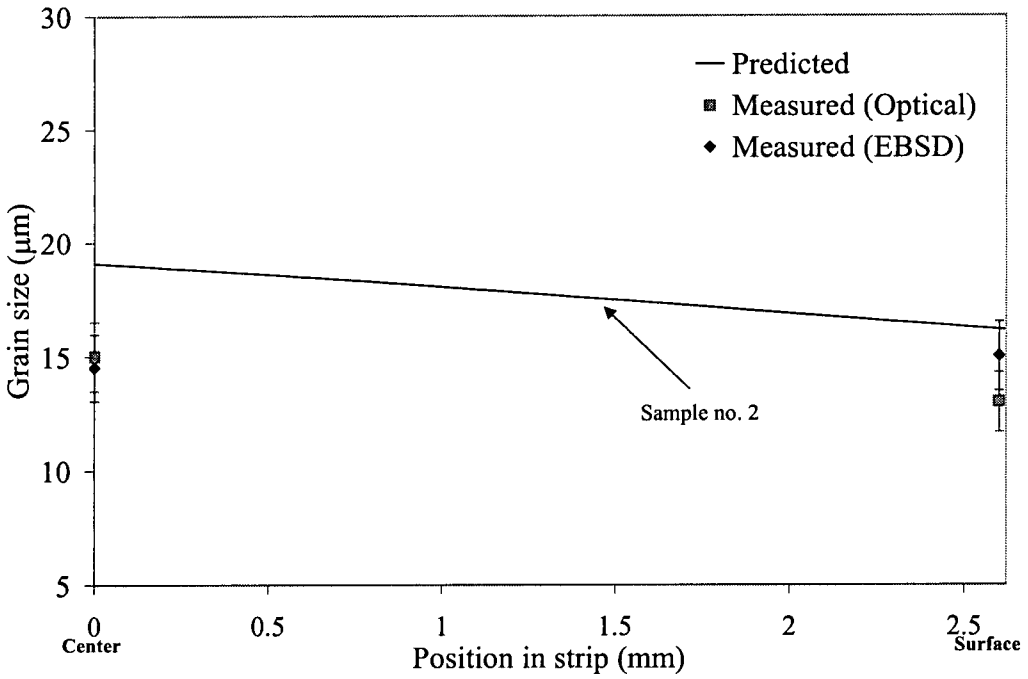

Figure 6.3 – Comparison of the internal state variable model predictions of recrystallized grain size through thickness of strip against experimental measurements using image analysis and EBSD for single-pass rolled sample no. 2 (T_{entry} = 448°C, $\bar{\dot{\varepsilon}}$ = 14.5 s^{-1}, ε = 0.52).

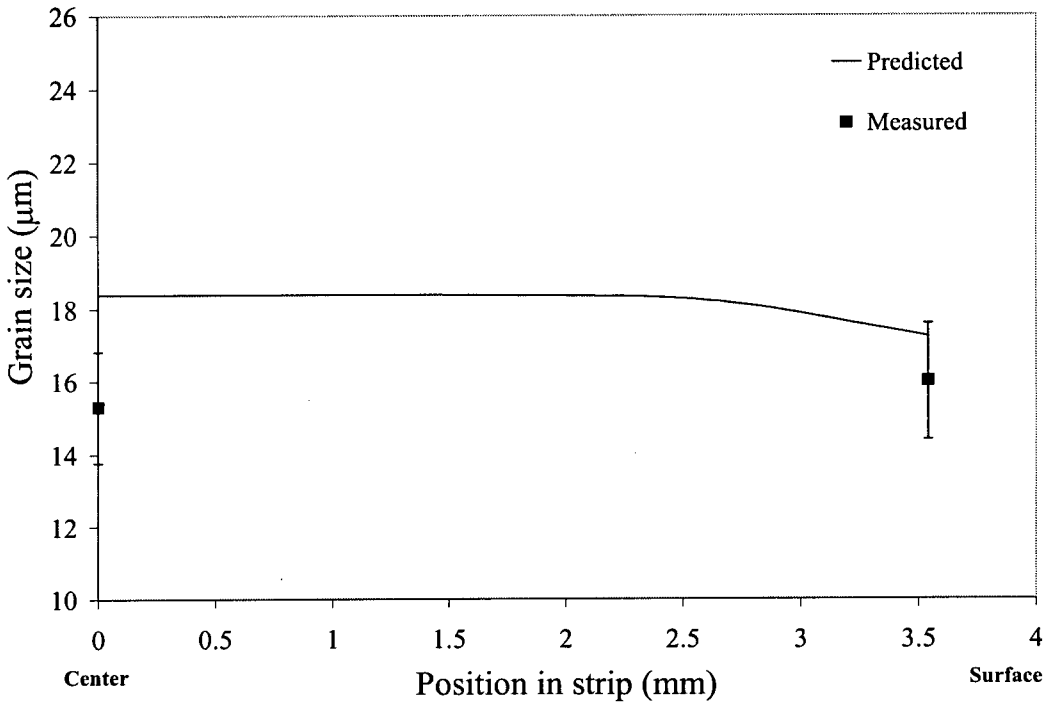

Figure 6.4 – Comparison of the internal state variable predicted recrystallized grain size through the thickness of the strip with experimental measurements for single-pass rolled sample no. 4 (T_{entry} = 460°C, $\bar{\dot{\varepsilon}}$ = 22.9 s^{-1}, ε = 0.29).

As shown in these figures, the model predicted recrystallized grain size matches the measurements reasonably well. The model overpredicted the recrystallized grain size by ~3 μm for both sample no. 2 and 4 at the strip centerline while the predictions fall within the measurmenet error at the surface of the strip. The model predictions show a trend of decreasing recrystallized grain size from the center to the surface of the strip in both **Figures 6.3** and **6.4**. The optical measurements through the strip thickness indicated a decreasing recrystallized grain size for sample no.2 , shown in **Figure 6.3**, and a near constant measured recrystallized grain size for sample no.4 shown in **Figure 6.4**.

In view of the differences between the predicted and measured thermal history for single-pass rolled cases, the impact of this temperature difference on the predicted microstructure was assessed. For all the 6 single-pass rolled samples, the measured thermal history at the center of the strip was used as input to the microstructure model. The microstructure predictions using the thermal history were then compared

to the experimental measurements. This comparison indicated that there was not any significant improvement in the microstructure model predictions. The most drastic change was observed in sample no. 2 where the fraction recrystallized dropped by ~5% and the recrystallized grain size increased by ~2% at the strip centerline.

Considering the experimental variation and sources of error leading to a relatively wide scatter in the measured temperature data, the results indicate that the mathematical model developed simulates the industrial hot rolling process reasonably well in terms of the temperature which occur during the rolling operation. The predicted fraction recrystallized matched the measurements relatively well at the strip centerline and showed a deviation from the measurements close to the surface of the strip. The predicted recrystallized grain size showed a minor deviation compared to the measurements. The overall model predicted fraction recrystallized and recrystallized grain size trend was correct. In addition, considering the strong sensitivity of the microstructure model predictions to the constants the predictions of microstructure evolution for a wide range of hot deformation conditioned studied was reasonable.

The next step was to extend the predictive capability of the model to multi-pass hot rolling cases where the modified values of the constants will be incorporated into the microstructure model and the model's ability to predict both the fraction recrystallized and the recrystallized grain size for the eleven two-pass rolled samples will be assessed. The internal state variable model application to multi-pass hot rolling cases is detailed in the following section of this chapter.

6.4 Model Results and Discussion for Multi-Pass Hot Rolling Cases

Once the model analysis and validation for the single-pass hot rolling cases was completed, the model was extended to multi-pass hot rolling. An approach was proposed and implemented to quantify the accumulation of the material stored energy in cases where no or only partial recrystallization occurs in the inter-pass region through the thickness of the strip. The thermo-mechanical model developed using ABAQUS was extended to account for changes that occur in the inter-pass region and

validated by comparing the model predictions of temperatures and rolling loads against experimentally measured data for the eleven multi-pass rolled samples produced under different conditions, as shown in Table 4.3. Validation of the physically-based microstructure model for multi-pass rolling was achieved by comparing the predictions of the fraction recrystallized and the recrystallized grain size through the thickness of the strip to the experimental measurements. The following sections discuss the model application and validation work for multi-pass hot rolling.

6.4.1 Temperature Validation for Multi-Pass Hot Rolling Cases

Temperature validation was carried out at the centerline and surface of the strip. The locations of the thermocouples are illustrated in **Figures 4.4** and **4.5** in Chapter 4. All of the temperature measurements at the centerline and the surface of the eleven multi-pass sample show reasonable agreement when compared to the model predictions during both first-pass and second-pass hot rolling. **Figures 6.5** and **6.6** show typical temperature comparisons at the strip centerline and surface during first-pass rolling and second-pass rolling, respectively for sample no. 4.

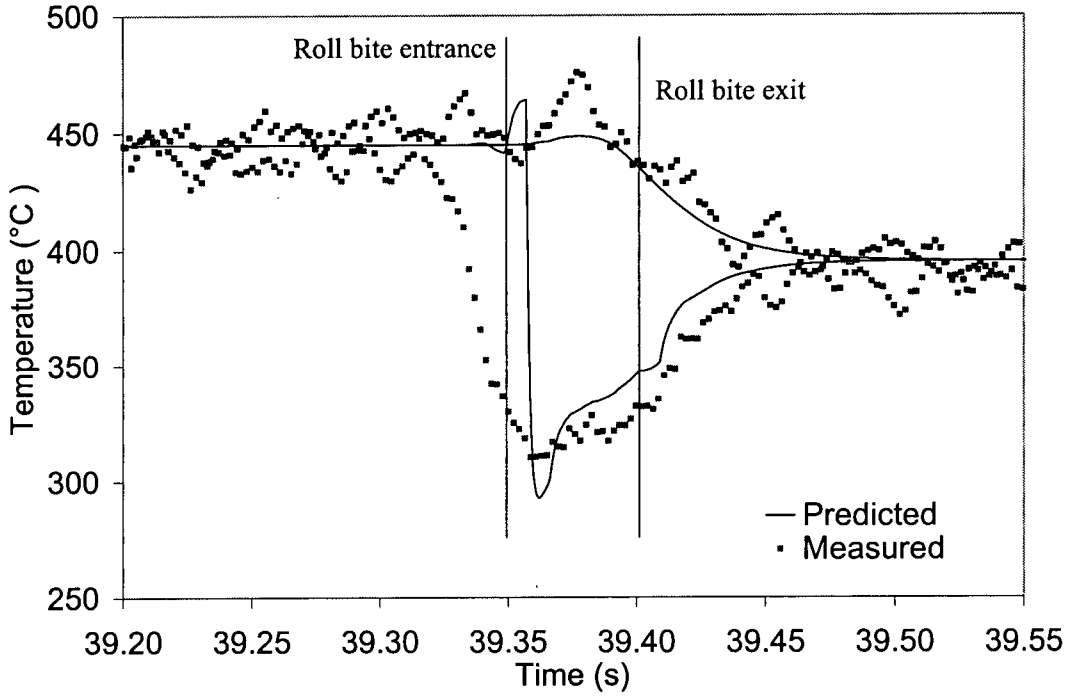

Figure 6.5 – Comparison of predicted centerline and surface temperatures during first-pass rolling against experimental measurements for sample no. 4.

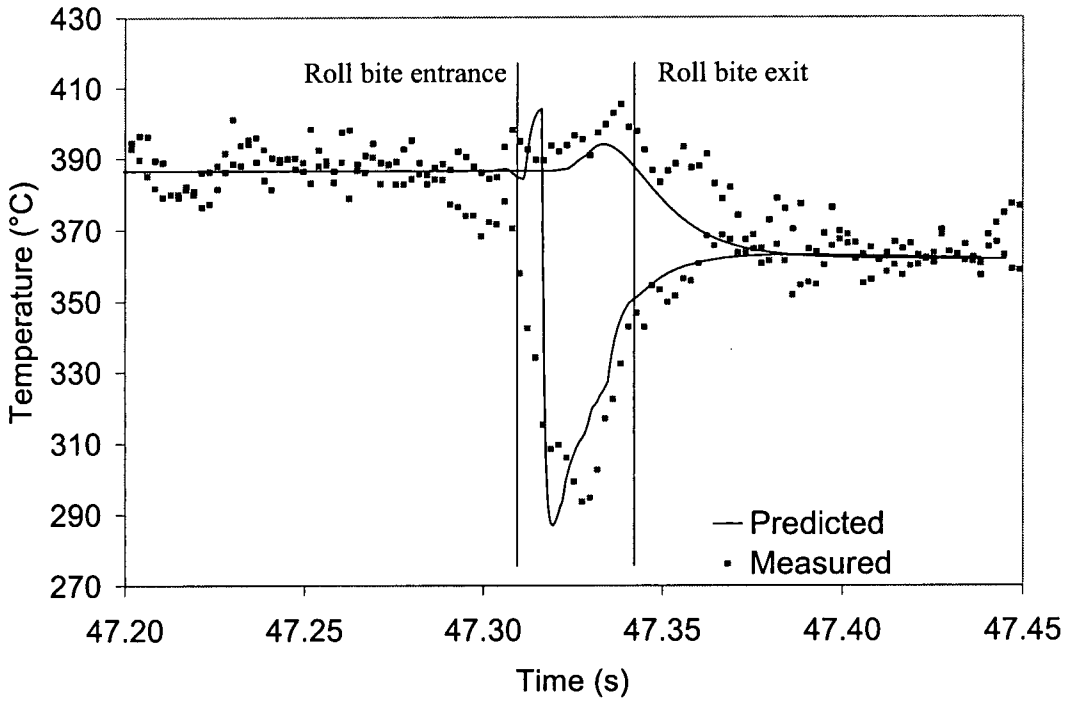

Figure 6.6 – Comparison of predicted centerline and surface temperatures during second-pass rolling against experimental measurements for sample no. 4.

As can be seen in **Figure 6.5** and **6.6**, the centerline temperature increases to a maximum value during deformation as the metal is being rolled due to the heat released as a result of plastic deformation. The rate of heat generation resulting from plastic deformation at the strip centerline exceeds the rate of conduction towards the surface. The cooling effect from the surface eventually dominates and the temperatures at the strip centerline drops just prior to exiting the roll bite. The surface temperatures predicted for each pass show a small temperature increase prior to being in contact with the roll bite. Timothy *et al.*[6] observed the same phenomena and suggested that the small initial maximum temperature indicates that deformation occurs prior to contact of the strip with the work roll. The temperature drops rapidly during rolling due to the chilling effect of the rolls at the strip surface. The temperature rises again after deformation is completed to an equilibrated temperature value. This may be due to the fact that the heat generated in the central region soon flows towards the surface[6]. The temperature distribution stabilizes within ~ 0.1-0.2 seconds after exiting the roll bite.

In order to analyze the accuracy of the measured temperature increase at the centerline, a comparison between the measured temperature increase and the calculated temperature increase that would result if the material were deformed adiabatically under equivalent conditions was carried out. Assuming that 95% of plastic work per unit volume is dissipated as heat[8], then the adiabatic change in temperature can be estimated based on the following equation[6]:

$$\Delta T_{adiabatic} \leq \frac{0.95\sigma_{ss}\bar{\varepsilon}}{\rho C_p} \qquad (6.1)$$

where σ_{ss} is the steady state flow stress, $\bar{\varepsilon}$ is the plastic equivalent strain, ρ is the material density and C_p is the material specific heat that is estimated based on the material initial temperature before rolling (~460°C) in this case. Assuming that σ_{ss} is equal to 110 MPa, ρ is equal to 2660 kg/m^3 and C_p is equal to 1120 J/kg K[6], and substituting a strain of ~0.24 and ~0.30 which correspond to the strain applied to sample no. 8 during first-pass and second-pass rolling, respectively, $\Delta T_{adiabatic}$ can be estimated. The calculated $\Delta T_{adiabatic} \leq$ 8.3 K and 11 K for the first-pass and second-pass rolling respectively is found to be more than the measured ΔT at the center of the

strip which is about ~6 K during first-pass rolling and ~5 K during second-pass rolling. Since this is not an adiabatic process, this indicates that the measured temperature increases at the center of the strip during rolling are reasonable.

The temperature drop in the inter-pass region was calculated employing the boundary conditions described in Chapter 5 and assuming an ambient temperature of 35°C based on the measured ambient temperature while conducting the rolling trials. A comparison between the measured and predicted temperature profile for sample no. 4 is shown in **Figure 6.7**. The relatively good fit between the measured and predicted temperature profiles in the inter-pass region indicates the suitability of the heat transfer boundary conditions employed in the inter-pass region.

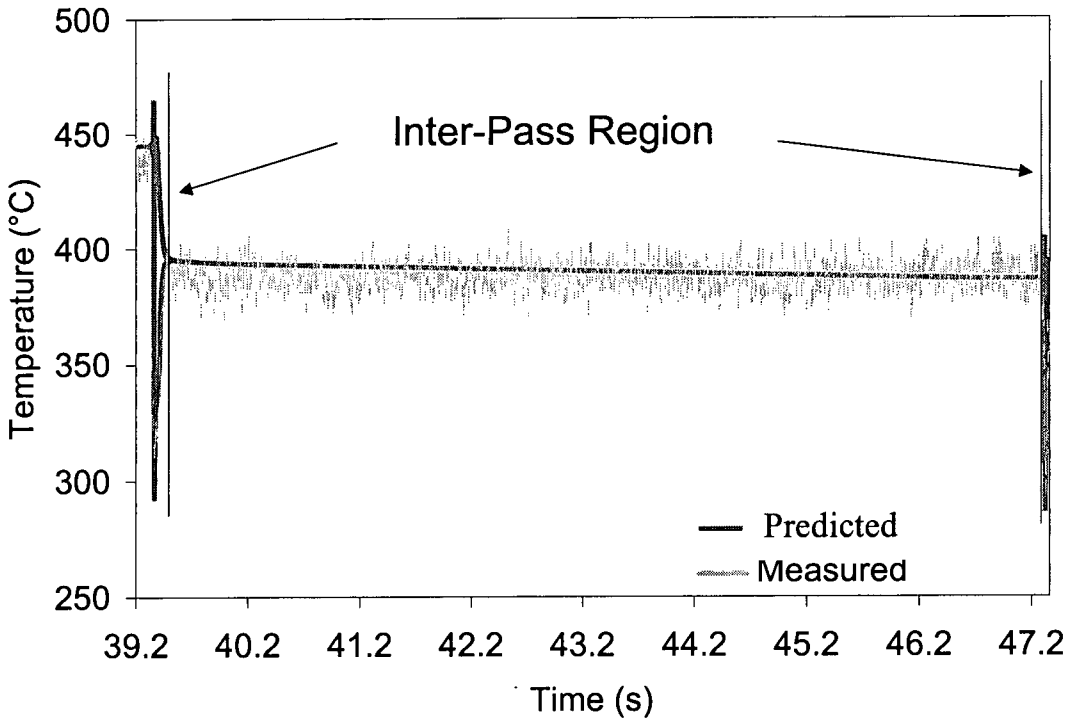

Figure 6.7 – Comparison of model predicted inter-pass temperature against experimental measurements for sample no. 4.

Referring to **Figures 6.5** and **6.6** for sample no. 4, the maximum temperature predictions at the centerline are within 2% and 6.5% of the measured maximum during first and second pass rolling, respectively. The maximum predicted surface temperature deviates from the measurement by ~ 6% during first-pass rolling and

almost exactly matches the measured profile during second-pass rolling. The differences between model predictions and the measurements could be due to the applied thermal boundary conditions in the model at the interface between the work roll and the strip which may be extracting too much heat. This in turn may affect the heat generation rate due to plastic work at the strip centerline which result in lower predicted temperature. Another reason for the discrepancy between the experimental measurements and the predictions at the surface of the strip may be attributed to the inability to acquire temperature data fast enough to experimentally show the true minimum temperature reached during rolling.

One of the main factors contributing to the discrepancy between the model predictions and the measurements is related to large scatter in the acquired data during rolling. This scatter in the measured data could be attributed to the nature of the rolling environment which may result in noisy electrical-based measurements resulting in a scatter in the measured temperature. Though several attempts were made to reduce the noise in the measurements by using type-E thermocouples during the multi-pass rolling trials and increasing the data collection frequency to 473Hz to increase the number of collected data points during rolling, the collected data was still relatively noisy due to the nature of the rolling environment. Considering the variation in temperature that is possible within the experimental data due to the noisy rolling environment, the model predictions match the experimental measurements reasonably well through the roll bite during first-pass and second-pass rolling and in the inter-pass region. A comprehensive temperature validation for the multi-pass rolled samples can be found in ***Appendix B***.

6.4.2 Rolling Load Validation for Multi-Pass Hot Rolling

One of the main challenges in rolling modeling is to describe the required contact between the strip and the work roll. Severals approaches were reported in literature to attain the contact between the roll and the strip including an initial push of the work piece into the roll gap by a punch[5]. The punch continues to push the work piece into the roll gap till an enough frictional force is achieved to pull the strip into the rok roll where the punch separates from the workpiece[5]. In this research, during the first step of the rolling simulation, the work roll is above, but not in contact with

the strip. The work roll is then lowered to obtain the desired strip reduction, pinching the head of the strip against the centerline. This step, completed in 0.5 s in simulation time, was necessary to ensure that the roll is in firm contact with the strip at the desired reduction level before the actual rolling of the strip. Thereafter, the second step of the rolling simulation consists of rotating the work roll at the desired radial velocity as explained earlier in Chapter 5. A typical model predicted rolling load profile during these two-steps is shown in **Figure 6.8**.

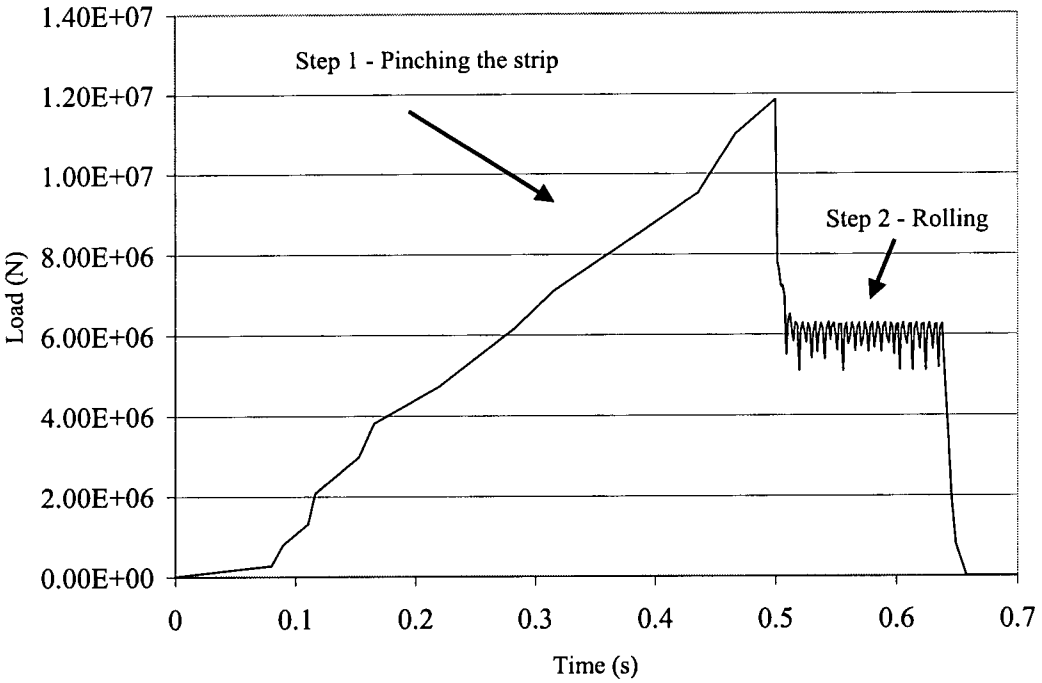

Figure 6.8 – Model Predicted reactionary force at the central node of the work roll during rolling (T_{entry} = 390°C, $\bar{\dot{\varepsilon}}$ = 22.3 s^{-1}, ε = 0.27)[2].

As shown in **Figure 6. 8**, the predicted roll load at the central node of the roll continues to increase during the first step of the simulation where the work roll pinches the strip because the contact area between the work roll and the strip continues to increase during the pinching process. The rolling load thereafter drops and remains relatively uniform during rolling as expected.

The predicted rolling load for each multi-pass rolled sample was determined by extracting the reaction forces at the center node of the work roll from the FE model

and converting this value to a comparable load that was measured during the plant trials. The "uniform" part of the predicted rolling load was averaged over the rolling time to determine an average value of the model predicted rolling load during each pass. The average value of the model predicted rolling load is compared to the experimentally measured average rolling load, described in Chapter 4. A comparison between the predicted and the measured rolling load for sample no. 4 is shown in **Figure 6.9**. A further comparison between the predicted and the measured rolling loads for the eleven multi- pass rolled sample conditions, illustrated in Table 4.3, can be found in ***Appendix C***.

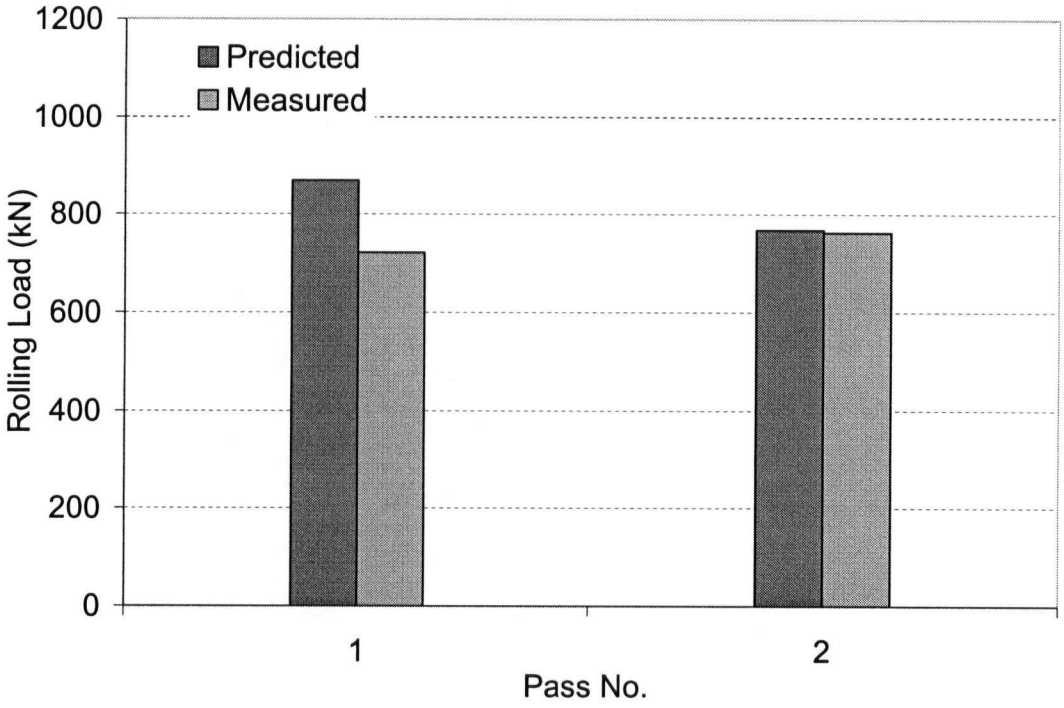

Figure 6.9 – Comparison of predicted rolling loads during rolling to experimental measurements for sample no. 4.

The model was able to predict the average rolling load during multi-pass rolling reasonably well. A comparison between the predicted and measured load in **Figure 6.9** shows a difference of ~ 14% during first pass rolling and less than ~ 1% during second pass rolling. In general, the average difference between the predicted rolling loads and the measurements for the eleven rolled samples was about ~ 15% during first pass rolling and ~ 10% during second pass rolling. The discrepancy

between the measured and the predicted rolling load could be attributed to the choice of constitutive behavior, friction conditions, and predicted temperatures. The discrepancy between the measured and predicted rolling loads for multi-pass rolled samples are consistent with the fact that the model slightly under predicts the temperatures both at the centerline and the surface of the strip, leading to higher flow stresses which in turn increases the predicted rolling loads. The discrepancy may be attributed to the fact that the flow stress was calculated based on a hyperbolic sine equation without accounting for the effect of change in dislocation density during rolling on the predicted flow stress, thus the effect of dynamic recovery during rolling were not considered.

6.4.3 Microstructure Validation for Multi-Pass Hot Rolling

6.4.3.1 Through-thickness fraction recrystallized validation

For each of the eleven multi-pass hot rolled samples, the predicted fraction recrystallized and recrystallized grain sizes were compared to the experimental measurements. In general, the predicted fraction recrystallized matches the measurements reasonably well for all of the samples. **Figure 6.10** shows a comparison between measured and predicted fraction recrystallized for the multi-pass rolled sample nos. 1 and 7 for conditions illustrated in Table 4.3. **Figure 6.10** shows that a noticeable amount of recrystallization has occurred for sample no. 7 whereas very little recrystallization has occurred in sample no. 1. A further comparison between the predicted fraction recrystallized and the experimental measurements for other multi-pass rolled samples can be found in ***Appendix D***.

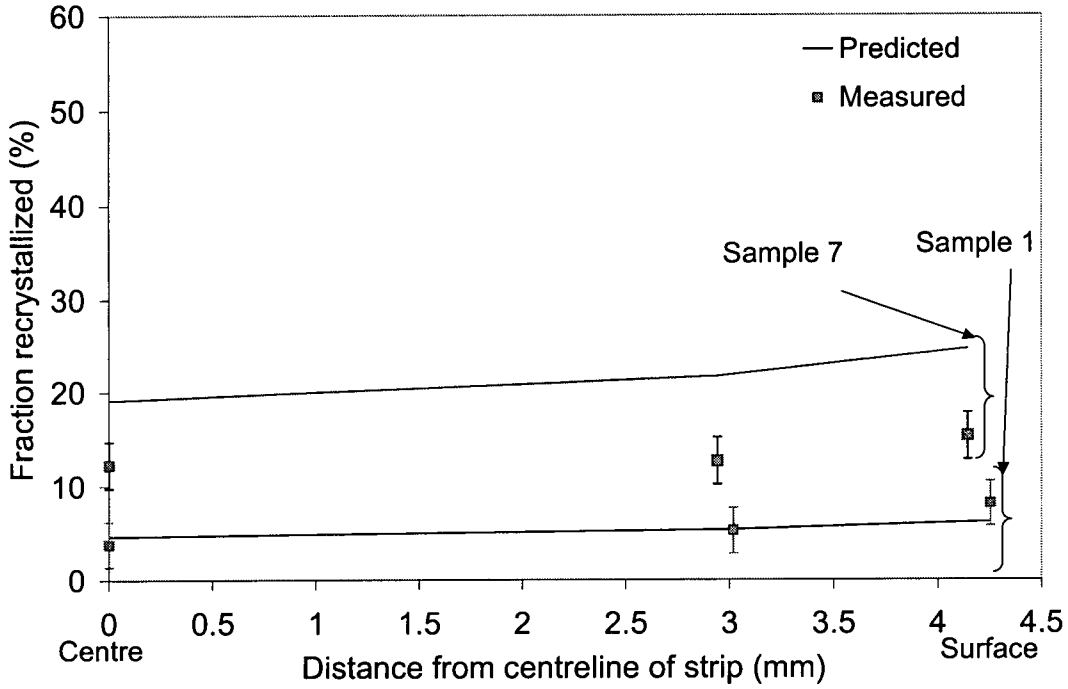

Figure 6.10 – Comparison of the internal state variable model predictions of fraction recrystallized through the thickness of the strip with experimental measurements for multi-pass rolled samples no. 1 and 7.

Figure 6.10 shows that the variation in recrystallized fraction through the strip thickness was not significant. This may be attributed to the relatively small initial sample thickness, 9mm, which was further reduced during rolling to 4-5 mm. In order to assess the effect of altering the initial thickness on the variation of the predicted fraction recrystallized through the strip thickness, an initial thickness of 20 mm was assumed and a two-pass rolling schedule was applied with a strain value of 0.3 per pass and initial entry temperature of 445°C. The predicted fraction recrystallized through the thickness of the strip is shown in **Figure 6.11**.

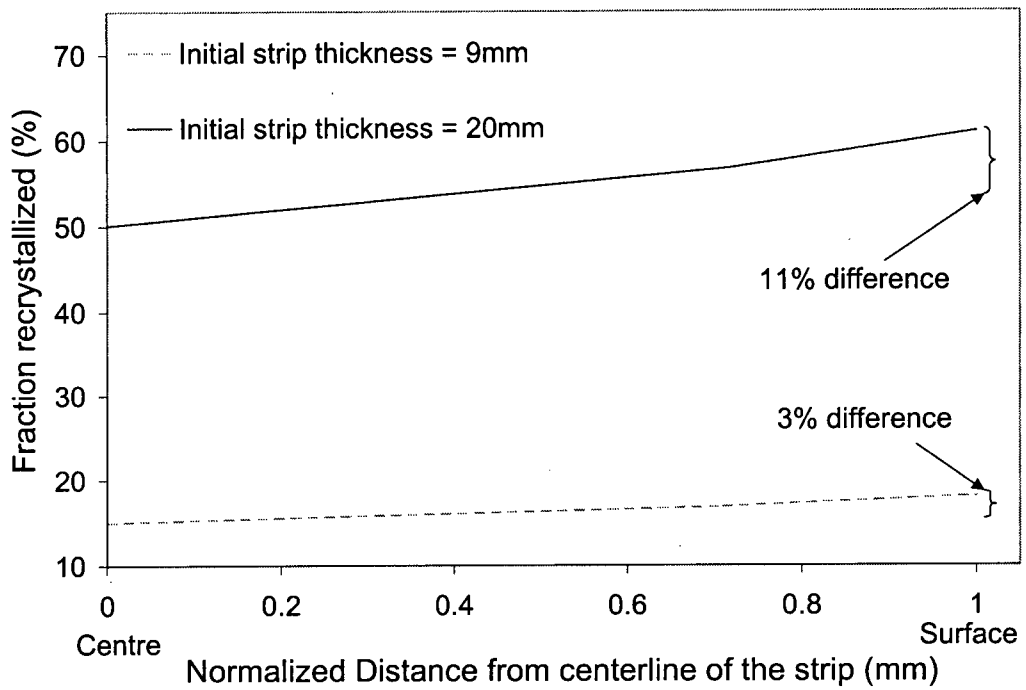

Figure 6.11 –Internal state variable model predictions through the thickness of the strip assuming an initial strip thickness of 20 mm

As can be seen from **Figure 6.11**, the simulation results indicate that the fraction recrystallized varies from 50% at the strip centerline to 61% at the subsurface location when the initial strip thickness increases from 9 to 20mm. Thus, it can be concluded that a relatively large variation in the predicted fraction recrystallized through the strip thickness can be achieved by increasing the original thickness of the strip.

6.4.3.1.1 Through-thickness fraction recrystallized validation at higher fraction recrystallized

The experimental measurements of fraction recrystallized indicate a low level of fraction recrystallized for the eleven multi-pass rolled samples through the strip thickness which varied from 3.8% to 15.3%. Although a reasonable agreement between the predicted and measured fraction recrystallized was achieved, lab-based experiments were conducted for samples no.3, 7 and 9 which involved heat treatment of the samples to achieve higher levels of recrystallization so that the application of

model predictions at higher level of recrystallization can be assessed. The three samples selected represent: (i) deformation with a low Z- value, referring to sample no. 7, (ii) deformation with a high Z- value, referring to sample no.9, where Z is the temperature compensated strain rate of the form $Z = \dot{\varepsilon}\exp\left(\frac{Q_{def}}{RT_{def}}\right)$ and Q_{def} is assumed to be equal to 145.1kJ/mol, and (iii) baseline sample, referring to sample no.3.

All the isothermal heat treatments were carried out at the University of British Columbia (UBC) using a salt bath (60% potassium nitrate and 40% sodium nitrite) furnace. The salt bath temperature was controlled with an Omega CN9000A auto tune temperature controller. The temperature of the salt bath was checked using a type-K thermocouple before sample immersion.

The thermal history that the material experienced during heat treatment was recorded using the following procedure: Thermocouple wires were spot-welded to the sample surfaces and then the samples were immersed in a salt bath set at 350°C. Time-temperature data was collected in real time using a data acquisition system connected to the thermocouples. The holding time ranged from 27-38 seconds. All holding times were measured using a stopwatch from the first immersion in the salt bath and included the time to reach the required temperature. Upon completion of the heat-treatment, samples were quenched in water. A typical heating cycle for one of the samples (sample no.9) in the salt bath is shown in **Figure 6.12**.

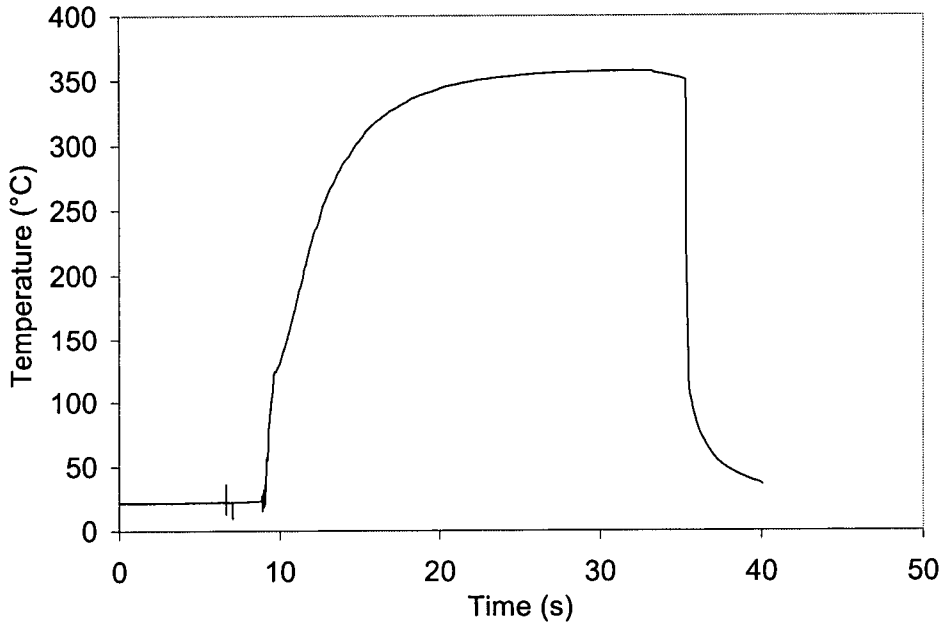

Figure 6.12 – A typical salt bath heating cycle (sample no. 9).

Upon completion of the heat-treatment, samples were mounted, polished and anodized using Barker's reagent. Measurements were carried out to determine the fraction recrystallized at the center of the strip according to the ASTM E562-89 standard point counting method.

The thermal history experienced during the heat treatment was integrated into the model including both the heat up time and the time till quenching utilizing the additivity principle, Equation. 5.35 –5.36 in Chapter 5, where T_a in Equation 5.36 was taken as the recorded sample stabilized temperature. The modified calculations of W and $W_{0.5}$ after incorporating the thermal profile were employed to predict the fraction recrystallized. The predicted fraction recrystallzied is compared to the measurements for the heat-treated samples at the strip centerline in **Figure 6.13**.

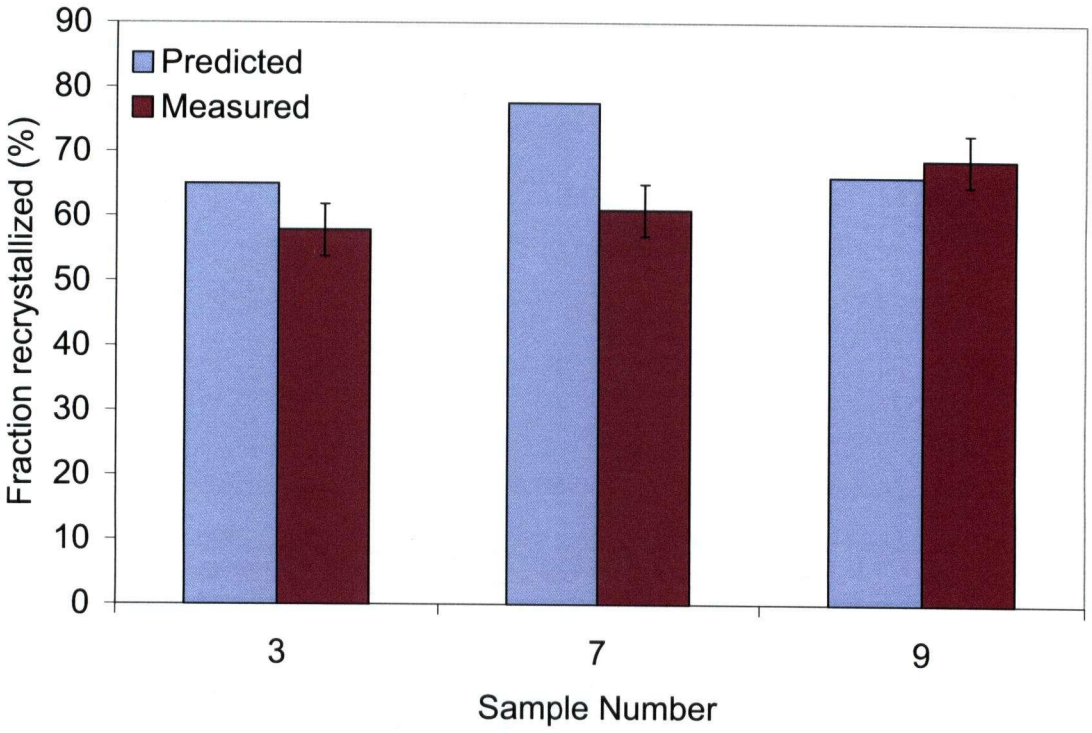

Figure 6.13 – Comparison of the internal state variable model predictions of fraction recrystallized at the centerline of the strip with experimental measurements for the heat-treated samples.

Figure 6.13 shows that the model predictions are in reasonable agreement with the measured values of the fraction recrystallized at different recrystallization levels which indicate that the model was able to properly capture the microstructure evolution for the annealed samples for different total times. The reasonable match between the predicted and the experimentally measured fraction recrystallized at both low and high recrystallization levels shows the capability of the microstructure model to track the accumulation of stored energy during multi-pass rolling and thus predict the resulting microstructure. This capability indicates the merit of the suggested approach and assumptions stated in the course of the microstructure model development and explained in Chapter 5, section 5.3.

6.4.3.2 Through-thickness recrystallized grain size validation

A comparison between the predicted recrystallized grain size and optical measurements for sample no. 5 is shown in **Figure 6.14**. A further comparison between the predicted recrystallized grain size and the experimental measurements for other multi-pass rolled samples can be found in ***Appendix D***.

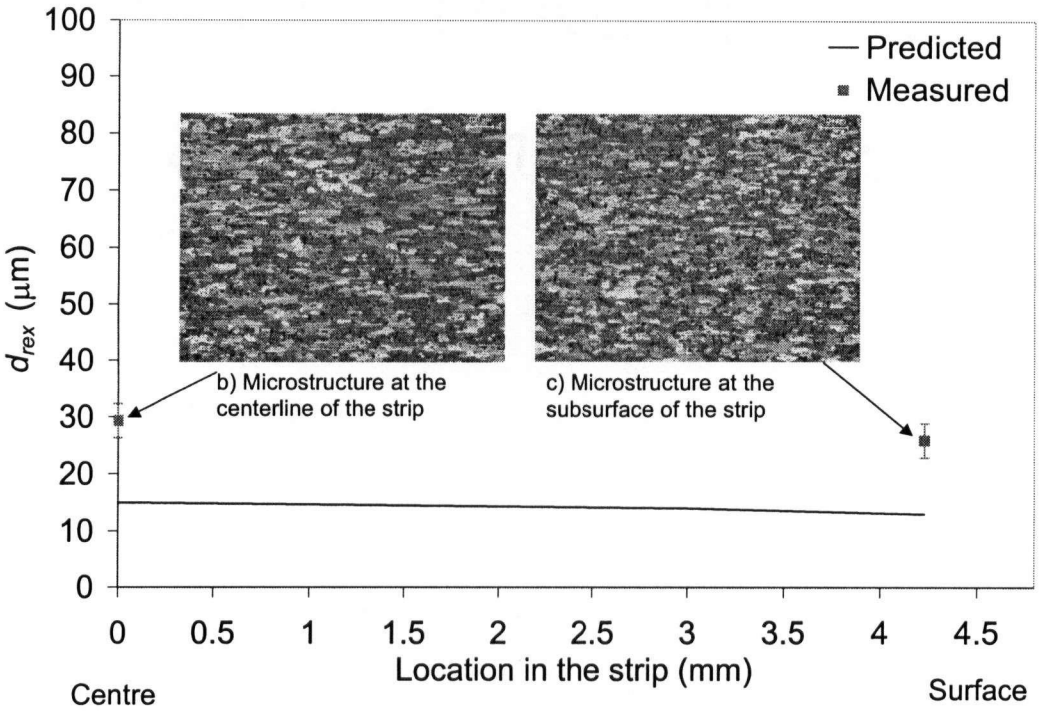

Figure 6.14 - Comparison of internal state variable model predictions of recrystallized grain size through the thickness of the strip with experimental measurements using image analysis for sample no. 5.

As can be seen in **Figure 6.14**, the model was able to account for the differences in grain size through the strip thickness where a smaller grain size was predicted closer to strip surface and a coarser one at the strip centerline. However, the predictions show a constant deviation from the nominal experimental measurements of ~ 11 μm corresponding to ~ 30% difference for the eleven multi-pass hot rolled samples. It was also noted that the measured recrystallized grain size after two pass rolling did not change significantly compared to the starting material grain size. Specifically, the measured grain size has changed from 35 μm for the start material to

30.1 and 29 μm at the center and the sub-surface of the strip respectively after two-pass rolling for sample no.3 (the baseline sample). This may be attributed to the presence of dispersoids or second phase particles in the material which may have precipitated in the matrix during both homogenization and hot rolling. This may affect the recrystallized grains shape and growth rate. The predictions of dispersoids effect are beyond the scope of this research project. It is unclear why the model was not able to more accurately predict the recrystallized grain size in this material. A part of the discrepancy can also be attributed to error in the recrystallized grain size measurements, which is typically ~10 %.

6.5 Summary

This chapter detailed the thermo-mechanical and microstructure model validation for single-pass and multi-pass hot rolling cases under a wide variety of industrially relevant deformation conditions. The validation work indicated that the predicted temperature and rolling load fits the experimental measurements relatively well which indicates the merit of the proposed boundary conditions. The internal state variable model was successfully implemented for an AA5083 aluminum alloy where the model constants were determined based on single-pass rolled samples and thereafter employed to multi-pass hot rolled samples. The model prediction match the experiments reasonably well in terms of fraction recrystallized through the strip thickness while the predicted recrystallized grain size deviates from the experimental measurements by ~ 11 μm.

Several conclusions can be drawn in regards to the new aspects of this research work. First, the proposed multi-pass hot rolling model for AA5083 was able to capture the correct accumulation of the material stored energy throughout each stage of the rolling process and extend the internal state variable approach to multi-pass hot rolling which has not been reported previously. Moreover, the extensive validation of both the thermo-mechanical and the microstructure model based on experimental measurements conducted using an industrial rolling mill that closely mimics industrial rolling conditions to ensure the applicability of the model under different rolling scenarios indicates the merit of the proposed modelling approaches in

this research work. To the author's knowledge, such extensive validation under wide variety of industrially relevant rolling conditions has not been previously performed.

References

1. Jupp, S., *Mathematical modelling of the microstructural evolution during the hot rolling of AA5083 aluminum alloys, M. Sc. thesis*. 2001, University of British Columbia: Vancouver, Canada.

2. Wells, M.A., D.M. Maijer, S. Jupp, G. Lockhart, and M.R. van der Winden, *Mathematical model of deformation and microstructural evolution during hot rolling of aluminum alloy 5083.* Mater. Sci. Technol., 2003. **19**(4): p. 467-476.

3. Shercliff, H.R. and A.M. Lovatt, *Modelling of microstructure evolution in hot deformation.* Philos. Trans. R. Soc. London, Ser. A, 1999. **357**: p. 1621-1643.

4. Furu, T., H.R. Shercliff, G.J. Baxter, and C.M. Sellars, *The influence of transient strain-rate deformation conditions on the deformed microstructure of aluminum alloy Al-1% Mg.* Acta Mater., 1999. **47**: p. 2377-2389.

5. Duan, X.J. and T. Sheppard, *Influence of forming parameters on static recrystallization behaviour during hot rolling aluminium alloy 5083.* Modell. Simul. Mater. Sci. Eng., 2002(10): p. 363-380.

6. Timothy, S.P., H.L. Yiu, J.M. Fine, and R.A. Ricks, *Simulation of single pass of hot rolling deformation of aluminum alloy by plane strain compression.* Mater. Sci. Technol., 1991. **7**(3): p. 255-261.

7. Ahmed, H., M.A. Wells, D.M. Maijer, B.J. Howes, and M.R. van der Winden, *Modelling of microstructure evolution during hot rolling of AA5083 using an internal state variable approach integrated into an FE model.* Mater. Sci. Eng., A, 2005. **390**(1-2): p. 278-290.

8. Chen, B.K., P.F. Thomson, and S.K. Choi, *Computer Modelling of microstructure during hot flat rolling of aluminium.* Mater. Sci. Technol., 1992. **8**(1): p. 72-77.

CHAPTER 7

MODEL APPLICATION

7.1 Introduction

The validated microstructure model was initially used to examine the effect of changing the model constants on the predicted microstructure evolution for single-pass hot rolling cases at the strip centerline. A further sensitivity analysis was carried out utilizing multi-pass rolling model results to investigate the effect of changing the rolling process parameters on the material stored energy and resulting fraction recrystallized at the strip centerline. The model was employed to further examine the effect of strain partitioning during multi-pass hot rolling while maintaining a constant total strain. The model was utilized to generate industrially relevant operational curves to predict the material stored energy and subsequent recrystallization under different rolling conditions.

7.2 Model Sensitivity Analysis

7.2.1 Sensitivity Analysis of the Finite Element Thermo-Mechanical Model

In the following section, a sensitivity analysis to quantify the influence of changing: the interface heat transfer coefficient, and the interface friction coefficient on the predicted thermo-mechanical results are presented.

7.2.1.1 Effect of changing the interface heat transfer coefficient on the FE model predicted temperature and strain profile

The effect of the interface heat transfer coefficient on the predicted temperature and through-thickness strain was examined by altering the interface heat transfer coefficient values, calculated using Equation 5.17, by ±15%. The results were compared to the experimentally measured temperature and strain for the simulated condition for single-pass rolled sample no. 2. The effect of changing the interface heat

transfer coefficient on the predicted temperatures and through thickness strains is shown in **Figure 7.1**[1].

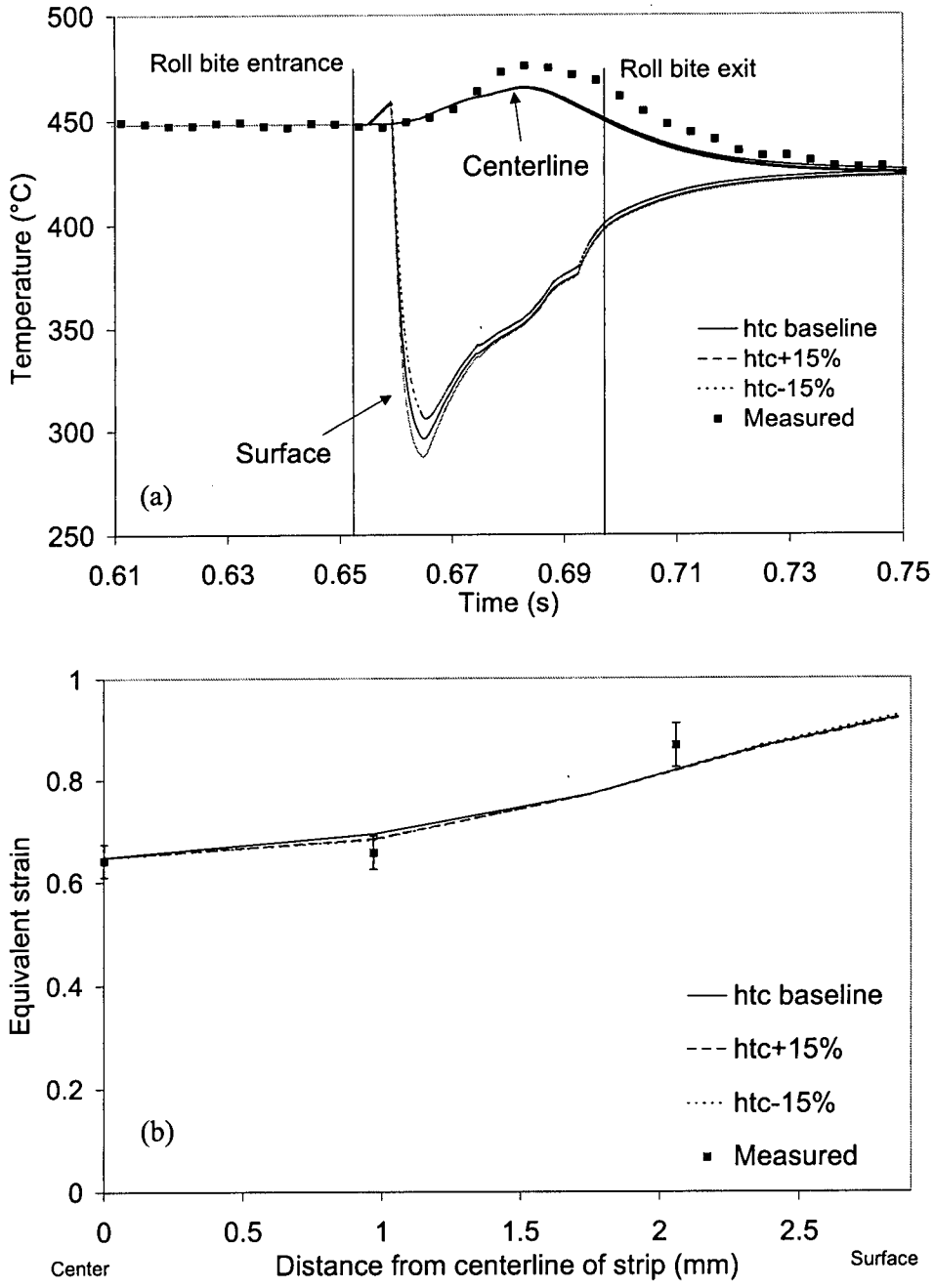

Figure 7.1 – Effect of change in interface heat transfer coefficient on the predicted (a) temperature, (b) strain through the strip thickness[1].

As shown in **Figure 7.1a**, changing the heat transfer coefficient by ± 15% does not cause a significant change in the predicted centerline temperature but does cause a minor change in the temperature at the surface of the strip; the higher the interface heat transfer coefficient, the lower the temperature at the surface of the strip during rolling. Also, changing the heat transfer coefficient by ± 15% does not cause any noticeable change in the temperature that the strip equilibrates too after exiting the roll bite. **Figure 7.1b** indicates that changing the interface heat transfer coefficient has little effect on the predicted equivalent strain through the thickness of the strip.

7.2.1.2 Effect of changing the interface friction coefficient on the FE model predicted temperature and strain profile

In this modelling work, a friction coefficient of 0.3 is considered to be representative of the friction coefficient in a rolling mill based on data found by Chen *et al.*[2] A sensitivity analysis was carried out to investigate the effect of altering the interface friction coefficient on the predicted temperature and strain profiles through the thickness of the strip as shown in **Figure 7.2**. During this analysis the friction coefficient was altered by ±15% from the base line value of 0.3. A comparison to the experimental measurements for single-pass hot rolled case no. 2 was carried out [1].

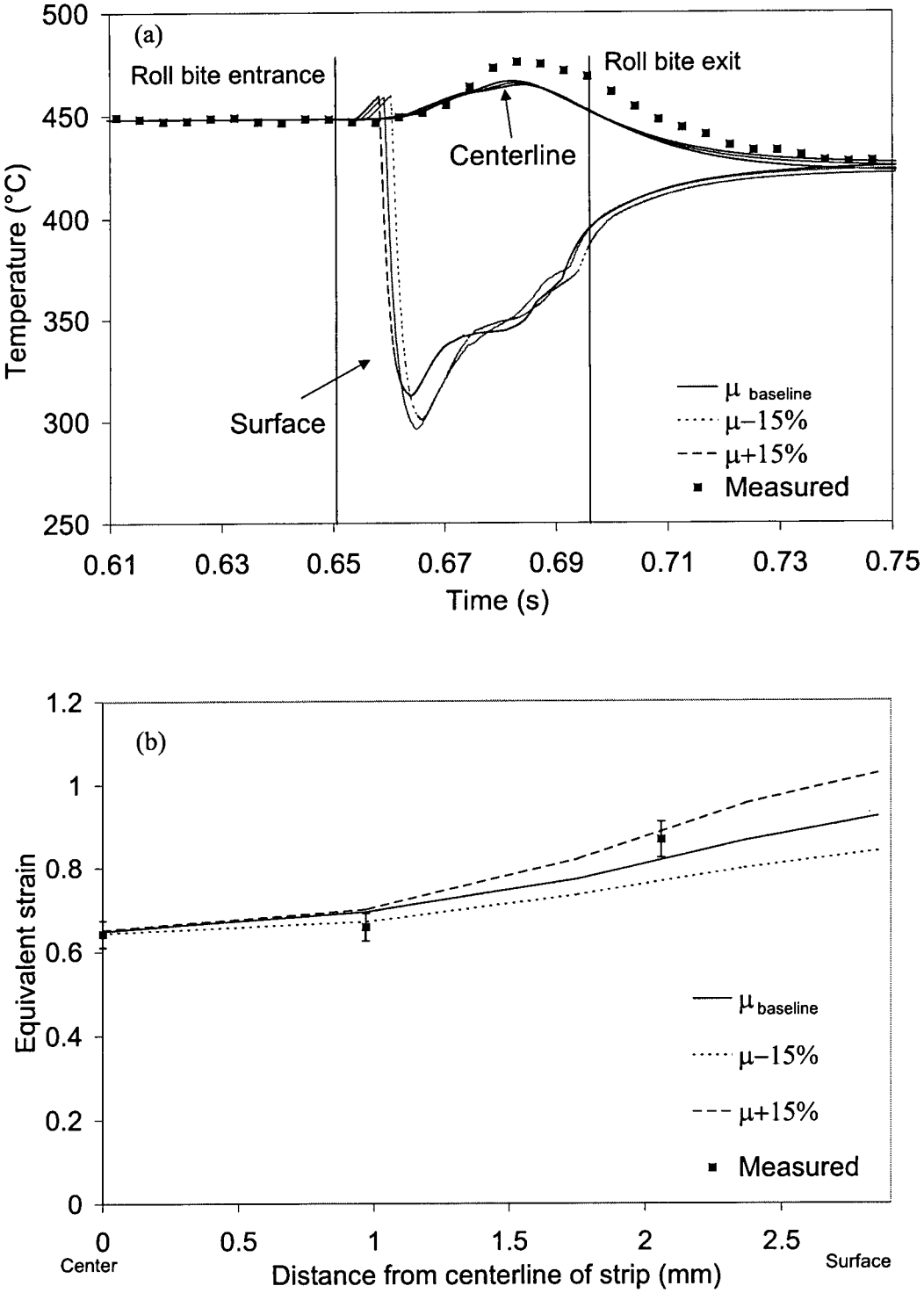

Figure 7.2 – Effect of change in interface friction coefficient on the predicted (a) temperature, (b) strain through the strip thickness[1].

Figure 7.2a shows that changing the coefficient of friction results in a change in the strip surface temperature but very little effect being predicted at the center of the strip. The effect of the coefficient of friction is most evident at the surface of the strip, as changing the friction coefficient leads to a change in the shear stresses at the surface that can influence the temperature[1]. **Figure 7.2b** shows that the predicted strains have a strong dependency on the friction coefficient, especially close to the surface, where the strain values vary from 0.84 to 1 depending on the coefficient of friction used.

7.2.1.3 Effect of changing the interface heat transfer and interface friction coefficient on model predicted rolling load

The variation in rolling load due to ± 15% changes in the interfacial heat transfer coefficient and friction coefficient is illustrated in **Figure 7.3**[1]. The measurement values are based on single-pass hot rolled sample no.2.

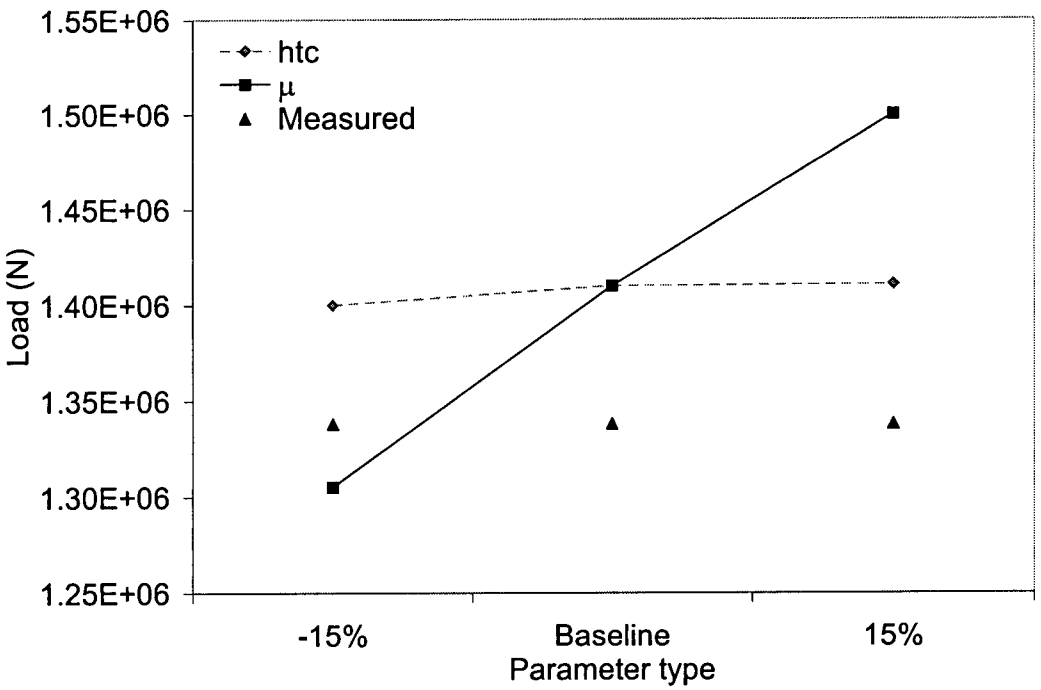

Figure 7.3- Effect of changing the interface heat transfer coefficient and friction coefficient on predicted rolling load[1].

The results shown in **Figure 7.3** indicate that changing the heat transfer coefficient by ±15% has only a minor effect on the predicted rolling load. However, changing the friction coefficient has a much stronger influence on the rolling load with the larger predicted rolling load values at higher friction coefficients[1]. Although a better fit between the measured and predicted rolling load was achieved when the friction coefficient was reduced by 15%, a baseline value of 0.3 was chosen based on the strain and thermal profile comparisons and the reported literature values[2].

7.2.2 Sensitivity Analysis of the Microstructure Model

In view of the slight differences between the model predictions and the measurements, a sensitivity analysis was carried out to investigate the effect of changing some of the constants used in the microstructure model on the predicted fraction recrystallized. The validated multi-pass rolling model was utilized to carry out a sensitivity analysis for multi-pass hot rolling cases to examine the effect of changing various rolling parameters and holding times on predicted fraction recrystallized at the strip centerline after two-pass hot rolling, assuming a sets of rolling conditions that yield a relatively high fraction recrystallized and another one that result in relatively lower fraction recrystallized. Finally, the sensitivity of predictions at relatively high fraction recrystallized were compared to experimental measurements. The following section summarizes the sensitivity analysis findings.

7.2.2.1 Sensitivity Analysis of the Model Constants

A sensitivity analysis has been conducted to investigate the effects of altering some of the parameters used in the microstructure model on the predicted fraction recrystallized. The rolling conditions relevant to single-pass rolled sample no. 2, as illustrated in Table 4.1, were chosen for the sensitivity analysis since these conditions produced the highest amount of recrystallization examined. For the sensitivity analysis, the following model constants were considered: C_1, C_2 in Equation 5.22, C_3 in Equation 5.27, and C_4 in Equation 5.31. These constants were altered by ± 20%. Additionally, the effects of changing θ_c from 10° to 15° in Equation. 5.30, and the

Avrami exponent, n, from 2 to 3 in Equation 5.32 were considered. The results are summarized in Tables 7.1 and 7.2.

Table 7.1 – Summary of sensitivity analysis of the microstructure model constants on the predicted fraction recrystallized (Xv) (as percentage difference from baseline value) for sample no. 2.

Position in strip from centre (mm)	Constants							
	C_1		C_2		C_3		C_4	
	- 20%	+ 20%	- 20%	+ 20%	- 20%	+ 20%	- 20%	+ 20%
0 (centre)	0	0	0	0	-12.2	10.9	36.1	-27.6
0.98 (1/4 thickness)	0	0	0	0	-11.7	10.4	39.4	-26.8
2.62 (surface)	0	0	0	0	-10.7	8.4	12.1	-24.5

Table 7.2 - Summary of sensitivity analysis of altering Avrami exponent and critical misorientation angle on X_v (as percentage difference from baseline value) for sample no. 2.

Position in strip from centre (mm)	Constants	
	n= 3	$\theta_c = 15°$
0 (centre)	25	22.5
0.98 (1/4 thickness)	22.1	19.0
2.62 (surface)	4.3	17.0

Tables 7.1 and 7.2 indicate that the model predictions of fraction recrystallized are relatively sensitive to C_3 and extremely sensitive to C_4, with predictions changing by ~10-39%. The model predictions appear to be insensitive to the C_1 and C_2 constants that are used to calculate the random dislocation density. The model predictions are also sensitive to changes in the Avrami exponent, as well as the critical misorientation angle.

In addition to evaluating the effects of the microstructure model constants on the fraction recrystallized, their effects on the predicted recrystallized grain size at the strip centerline were also analyzed. It was found that the predicted recrystallized grain size is not sensitive to changes in the constants C_1, C_2, and C_4. The predicted recrystallized grain size is sensitive to changes in constant C_3, which is used to calculate the nucleation density, with predictions changing by ~ 6%.

The sensitivity of the microstructure predictions to the modelling constants indicates that careful experimental measurements need to be made to identify these parameters accurately under a range of deformation conditions in order to be able to use the microstructure model to simulate industrial deformation conditions.

7.2.2.2 Sensitivity Analysis of Microstructure Evolution During Multi-Pass Rolling to Changes in the Rolling Process Parameters

A further sensitivity analysis was carried out to investigate the effect of changing different rolling parameters during multi-pass hot rolling, namely: (i) holding time after second pass rolling, (ii) inter-pass holding time, (iii) strip entry temperature, (iv) first-pass rolling strain and (iv) first-pass rolling strain rate on the predicted fraction recrystallized at the strip centerline after second pass rolling is complete. The verified microstructure model was employed to further study the sensitivity of fraction recrystallized at the strip centerline. The sensitivity analysis was carried out utilizing two different sets of conditions which yield low fraction recrystallized and high fraction recrystallized after second pass rolling, respectively. In order to obtain low fraction recrystallized, the model runs that were used to mimic the experimental conditions were used to conduct the sensitivity analysis. The simulation conditions used to examine the sensitivity analysis at low fraction recrystallized are illustrated in Table 4.3. A baseline modelling case was run with an entry temperature of 445°C, a total strain of 0.6, a first pass strain rate of 5.8 s^{-1} which is doubled during second pass rolling, an inter-pass time of 20 s and a hold time of 15 s after second pass rolling which results in 15% fraction recrystallized at the strip centerline. The model predicted fraction recrystallized was always below 20%. A summary of the model predicted sensitivity analysis at relatively low fraction recrystallized is shown on Table 7.3.

Table 7.3 – Summary of model predicted sensitivity analysis of fraction recrystallized to changes in different rolling parameters at the strip centerline for conditions that yield low fraction recrystallized (as percentage difference from the baseline prediction).

Response	Deformation Condition Modelling Results									
	$t_{after\ 2nd\ pass}$		$t_{inter\text{-}pass}$		T_{entry}		$\varepsilon_{1st\ pass}$		$\dot{\varepsilon}_{1st\ pass}$	
	+67%	-67%	+67%	-67%	+10%	-10%	+20%	-20%	+20%	-20%
X_v ($_{Model\ low\ Xv}$)	24	-69	-25	27.5	27	---	12	-8.7	1.2	-1.3

The verified microstructure model was also employed to further study the sensitivity of fraction recrystallized at the strip centerline where the rolling conditions were altered to obtain a higher fraction recrystallized at the strip centerline. A baseline modelling case was run with an entry temperature of 460°C, a total strain of 0.6, a first pass strain rate of 10 s^{-1} which is doubled during second pass rolling, an inter-pass time of 10 s and a hold time of 30 s after second pass rolling which results in 35% fraction recrystallized at the strip centerline. In order to examine the effect of changing the rolling parameters on the predicted fraction recrystallized after second pass rolling, each of them was altered in the model by a percentage that corresponds to the original experimental percentage change. The sensitivity analysis results of recrystallized fraction at the strip centerline are summarized in Table 7.4.

Table 7.4 – Summary of model predicted fraction recrystallized sensitivity analysis for conditions that yield high fraction recrystallized at the strip centerline (as percentage difference from the baseline prediction).

Response	Deformation Condition Modelling Results									
	$t_{after\ 2nd\ pass}$		$t_{inter\text{-}pass}$		T_{entry}		$\varepsilon_{1st\ pass}$		$\dot{\varepsilon}_{1st\ pass}$	
	+67%	-67%	+67%	-67%	+10%	-10%	+20%	-20%	+20%	-20%
X_v ($_{Model\ high\ Xv}$)	27.6	-52.1	-6.3	11.6	-54.4	22	10.5	-10.3	1	4.8

The sensitivity of fraction recrystallized to changing the hold time after second-pass rolling at both low and high fraction recrystallized conditions indicate that the fraction recrystallized increases at the strip centerline as the holding time after second pass increases and vice versa. This trend is expected because increasing the holding time after second-pass rolling at a relatively higher temperature would allow future nucleation and growth to take place leading to higher fraction recrystallized.

Table 7.3 and 7.4 show that as the holding time between passes increases, fraction recrystallized decreases at the strip centerline. This general trend is expected since increasing the inter-pass time would allow further recrystallization to take place in the inter-pass region which reduces the overall material stored energy and subsequently reduces the fraction recrystallized after second-pass rolling. It is noted that a relatively higher sensitivity to change in the inter-pass time is noticed at the set of conditions that yield relatively lower fraction recrystallized. This larger sensitivity could be attributed to the fact that any small change at a relatively low level of fraction recrystallized can lead to a relatively higher sensitivity. The model predicted level of recrystallization for the two rolled samples that were used to assess the effect of changing the inter-pass hold time on strip centerline recrystallized fraction ranged between 11.3% for the low inter-pass time case and 19.1% for the high inter-pass time case.

The sensitivity analysis summary also indicates that increasing or decreasing the strain rate during first-pass rolling does not cause any significant changes in fraction recrystallized after second-pass rolling is complete at both low fraction recrystallized and high fraction recrystallized conditions.

In general, there are two competing mechanisms that are affected by change in the entry temperature. On one hand, dynamic recovery increases with increasing entry temperature; thus thermally activated processes such as dislocation climb will increase leading to lower driving pressure for static recrystallization. On the other hand, static recrystallization increases, via nucleation and growth, as the entry temperature increases. In order to further understand the modelling results shown in Tables 7.3 and 7.4. The model predicted driving pressure after second-pass hot rolling

at low and high fraction recrystallized cases for the baseline conditions and for the cases where the entry temperature increases by 10% is shown in **Figure 7.4**

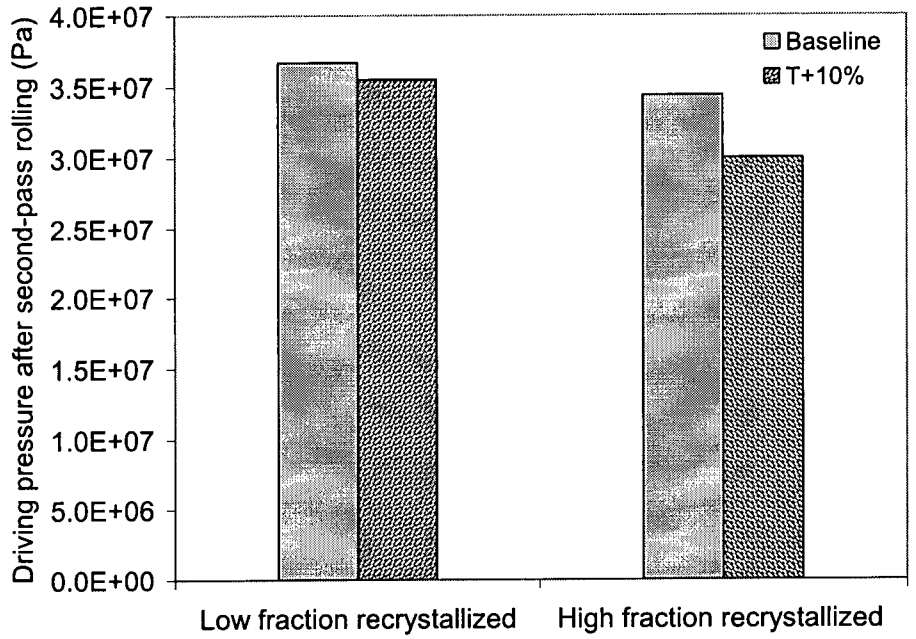

Figure 7.4 – Effect of changing the entry temperature on the predicted driving pressure for recrystallization after second-pass rolling.

Figure 7.4 shows that as the entry temperature increases by 10% from the baseline values, the predicted driving pressure after second pass rolling decreases at the strip centerline for both the low and high fraction recrystallized cases. This indicates that recovery may play a major role in lowering the available driving pressure for recrystallization. This can be attributed to lower dislocation density and vice versa.

The results in Table 7.4 for the high fraction recrystallized cases agree with the trends shown in the above figure indicating a decrease in the model fraction recrystallized as the entry temperature increases. However, this trend cannot be seen in Table 7.3 for the lower fraction recrystallized cases which show a 27% increases from the baseline corresponding increase in the fraction recrystallized from 15% at the baseline to 19% for the higher temperature case. The reason behind this discrepancy for the two cases can be examined by considering the percentage

difference in the driving pressure between the baseline condition and the higher entry temperature condition at low and high fraction cases as well as examining the stabilized temperature after the second-pass rolling is complete. **Figure 7.4** shows a percentage difference between the baseline case and the higher temperature case of ~3% at low fraction recrystallized which increases to ~13% at higher fraction recrystallized. It was also noted that the stabilized temperature after second-pass rolling for the baseline sample for low fraction recrystallized, 353°C, case was relatively lower than higher temperature sample, 374°C which in turn increases the subsequent recrystallization kinetics. The minor difference in driving pressure and higher stabilized temperature for the higher entry temperature case might offset the trend i.e., leading to higher fraction recrystallized as the temperature increases, which explains the trend in Table 7.3.

As illustrated in Table 7.3 and 7.4, increasing the first pass strain results in a relatively high fraction recrystallized and vice versa at both low fraction recrystallized and high fraction recrystallized levels. This trend can be attributed to the fact that increasing the first-pass strain leads to an increase in the material driving pressure, especially when short inter-pass hold time is considered, which contributes to the final fraction recrystallized. The model sensitivity results indicate a slight sensitivity of the predicted fraction recrystallized at the strip centerline to changes in the strain experienced during first-pass rolling.

7.3 Multi-Pass Rolling Model Application

7.3.1 Effect of Strain Partitioning During Rolling on the Material Stored Energy and Subsequent Recrystallization Kinetics

An analysis has been conducted to investigate the effect of strain partitioning during multi-pass hot rolling on the material stored energy. The analysis was done by altering the strain applied in the first-pass rolling as compared to the second-pass rolling strain while keeping the total strain constant. The material stored energy was quantified in terms of the driving pressure after second-pass hot rolling and the subsequent time required to achieve 50% recrystallization ($t_{0.5}$). The verified internal state variable model was employed to carry out this study considering rolling

scenarios at both high Z-value (low deformation temperature) and low Z-value (high deformation temperature) conditions. In order to investigate high Z-value conditions, the deformation temperature was assumed to be 410°C and the first-pass strain rate was assumed to be 10 s^{-1} which was doubled during second-pass rolling. Low Z-value employed at a deformation temperature of 470 °C and a strain rate of 3 s^{-1} which was doubled during second pass rolling. Four separate cases, shown in Table 7.5, were run for each Z-condition.

Table 7.5 - Rolling conditions employed to investigate the effect of strain partitioning on model predicted material stored energy*

Case Number	$\varepsilon_{1stpass}$	$\varepsilon_{2nd\ pass}$	ε_{total}	Inter-Pass Hold time (s)
1	0.50	0.10	0.60	20
2	0.35	0.25	0.60	20
3	0.20	0.40	0.60	20
4	0.10	0.50	0.60	20

* Initial strip thickness is 9mm

The results of the analysis showing the driving pressure and subsequent time to achieve 50% recrystallization ($t_{0.5}$) as a function of first pass strain are shown in **Figure 7.5** and **7.6**, respectively.

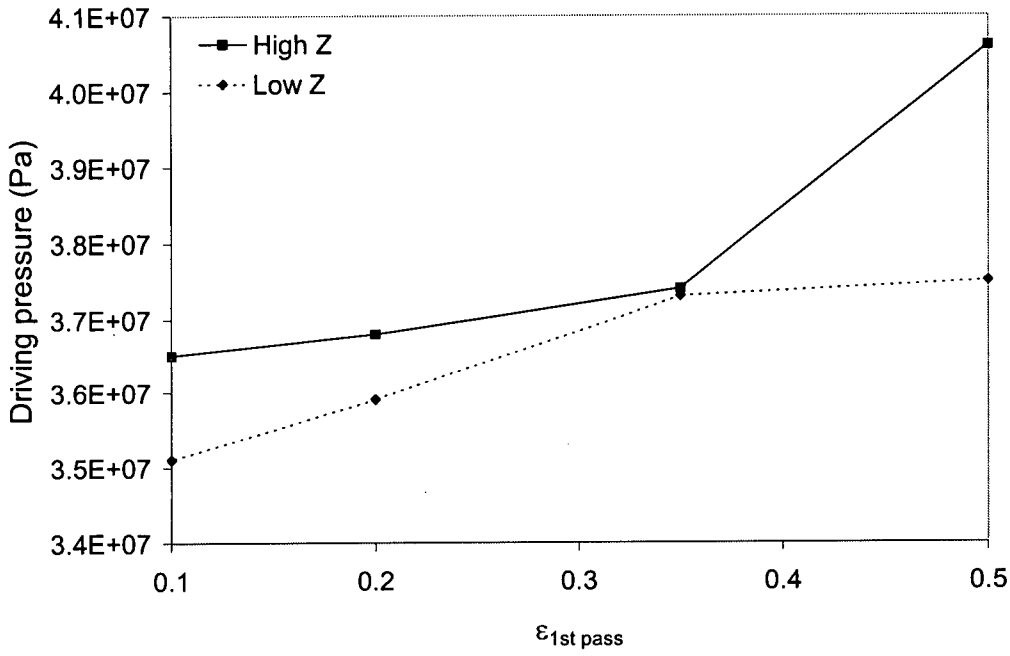

Figure 7.5 – Effect of changing the deformation schedule during rolling on the predicted driving pressure after second pass rolling

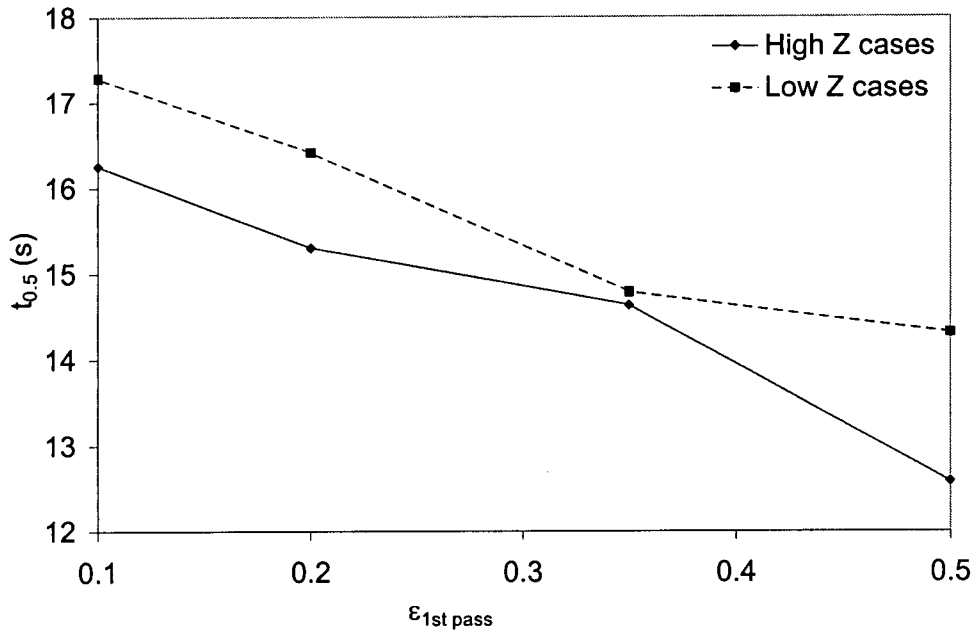

Figure 7.6 – Effect of changing the deformation schedule during rolling on the predicted time to achieve 50% recrystallization after second pass rolling

Figures 7.5 and **7.6** show that as the first-pass rolling strain increases, in comparison to second-pass rolling strain, the material stored energy increases, thus the time needed to achieve 50% recrystallization decreases for both the low Z and high Z cases. As shown in **Figures 7.5** and **7.6**, as the amount of strain imparted during first-pass rolling increase, the stored energy in the material after second-pass rolling increases and thus the time required to achieve 50% recrystallization decreases. This trend is evident under both high and low Z conditions.

In order to evaluate the reasons for this effect further, the thermal history of the material under different strain histories was evaluated for low Z cases as shown in **Figure 7.7**.

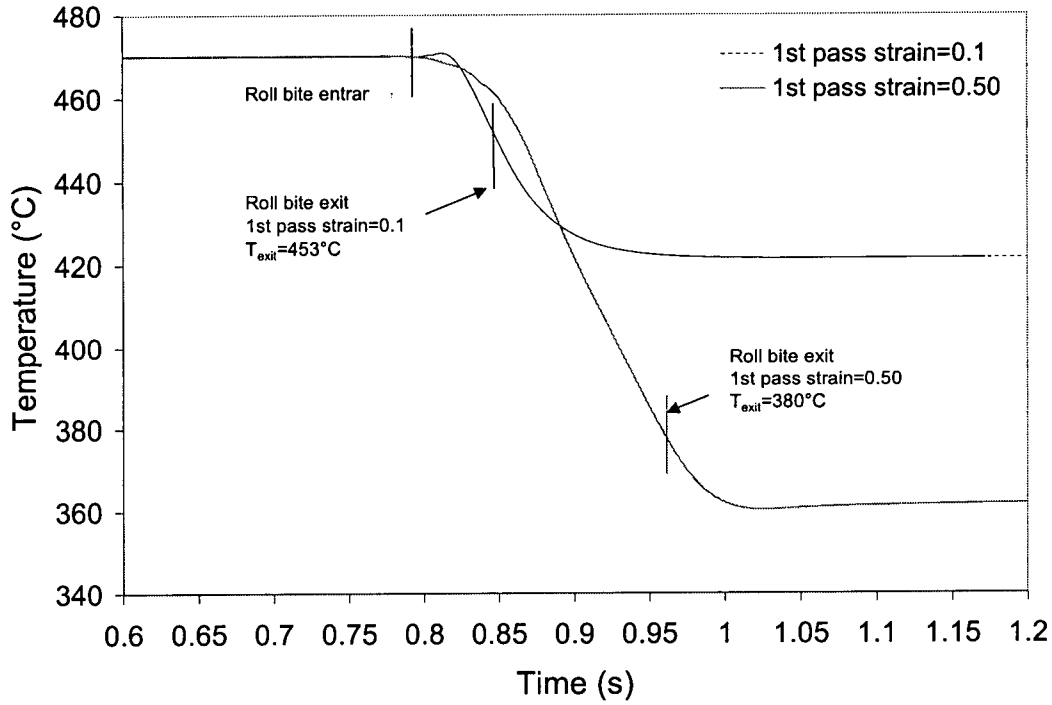

(a) Thermal profile for low Z cases at the centerline of the strip

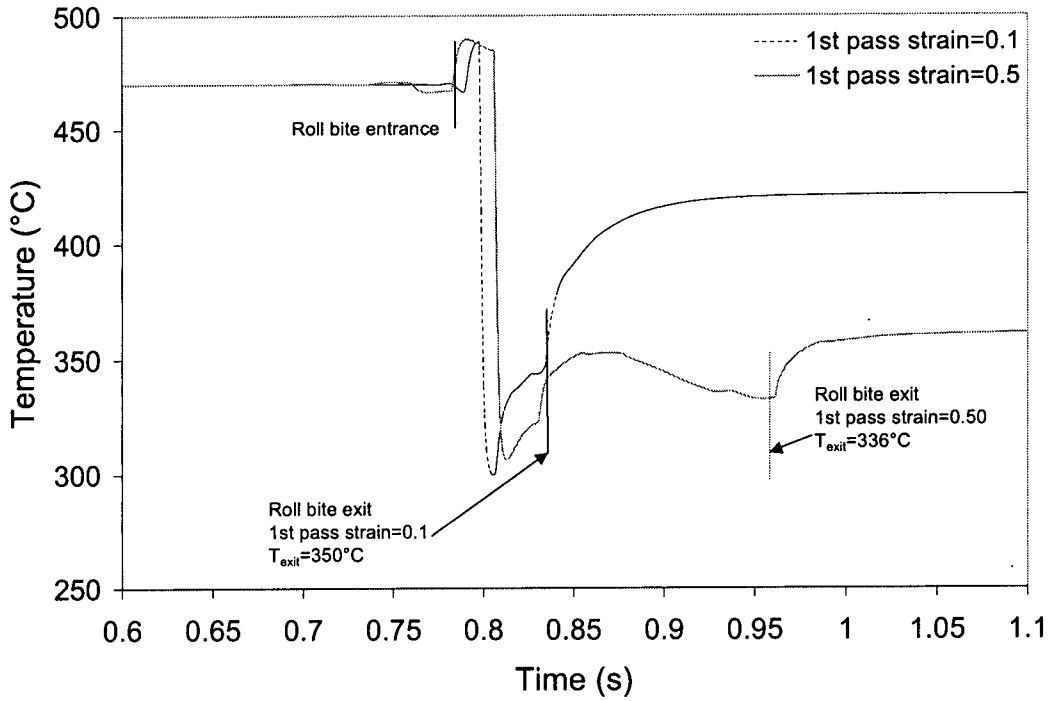

(b) Thermal profile for low Z cases at the surface of the strip

Figure 7.7 – thermal profile for low Z case no. 1 and 4 during first pass rolling at (a) the centerline of the strip, (b) surface of the strip

It can be seen in **Figure 7.7** that as the first pass strain increases from 0.1 to 0.5, the exit temperature after first pass rolling decreases. This can be attributed to the fact that the speed of the roll was altered to maintain a constant strain rate at different strains which in turn resulted in a longer contact time between the relatively cold work roll and the strip for material reduced to a higher strain. Specifically, the model results show that the work roll was in contact with the strip for 0.05 s during first pass rolling for case 1 at a strain of 0.1 compared to 0.17s for case 4 where the first pass strain is 0.5. Based on the results in **Figure 7.7**, the material stored energy after first pass rolling will increase as the first pass strain increases which can be attributed to the lower exit temperature at higher first pass strain levels. This agrees with the sensitivity analysis summary in Tables 7.3 and 7.4.

A small peak, which is mainly attributed to heat of deformation at the strip centerline, was noticed for a first pass strain equal to 0.1 which was not noted for the case where the first pass strain was equal to 0.5 as shown in **Figure 7.7a**. A further analysis showed that the thermal profile at the strip centerline is expanded over a prolonged period of time for the first pass strain case of 0.5 due to the fact that the "relatively cold" work roll remains in contact with the strip for a longer period of time which explains the fact that no sharp peak was noted for case 4 where the first pass strain is 0.5.

A further analysis was carried out where different strain conditions were employed to mimic the thermal profile obtained for the cases studied in Table 7.4. It was noted that the predicted driving pressure values after two pass rolling at different strain conditions and similar thermal profile match relatively well. This observation suggests that the effect of first pass strain on the material driving pressure shown in **Figures 7.5** and **7.6** is primarily due to the thermal effect and is mainly attributed to the fact that the exit temperature after first pass rolling decreases as the strain increases due to the longer contact time between the work roll and the strip which increases the material stored energy.

These conclusions can be used to further understand industrial hot rolling processes for aluminum alloys. For example, based on the findings in this section, a higher fraction recrystallized in industry can be achieved by increasing first pass

strain while maintaining a constant strain rate. Also, the previously mentioned rational indicates that as the roll diameter increases while maintaining a fixed strain and strain rate conditions, the contact time between the work roll and the strip increases resulting in lower temperature at the roll bite exit which in turn increases the material stored energy and results in higher fraction recrystallized. Thus, an industrially relevant conclusion can be made indicating that a larger roll diameter can lead to a higher fraction recrystallized at the strip-centerline after two-pass hot rolling at a fixed strain and strain rate conditions.

7.3.2 Industrial Operational Curves

7.3.2.1 Effect of changing the inter-pass holding time on predicted fraction recrystallized after two pass hot rolling at different Z's

The model was further employed to generate industrially relevant operational curves that can be used to understand the evolution in material stored energy during multi-pass hot rolling and thus optimize the rolling process. This was done by using the model under a range of deformation conditions and inter-pass times typical of industrial hot rolling. Though the inter-pass times assumed in the generation of this operational curve apply primarily to steckel rolling mill, the results can of these curves can be utilized to calculate the driving pressure and subsequent fraction recrystallized for tandem rolling cases where the inter-pass times are shorter.

Two-pass rolling conditions were used to generate this curve whereby the total strain, assumed to be 0.6, was divided equally between passes. The first-pass strain rate was assumed to be 10 s^{-1} which was doubled during second pass rolling. The analysis was carried out by altering the inter-pass time from 1 second, which is considered to simulate inter-pass times during tandem rolling where the fraction recrystallized between passes was less than 2%, to 120 seconds which can be used for process optimization in steckel mill rolling. The investigation was carried out for a range of deformation temperatures namely 526, 506, 486, 466, and 414°C. In order to calculate the fraction recrystallized after second pass rolling, a holding time of 30 s was assumed after second-pass rolling is complete. It should be noted that isothermal conditions were assumed both at the inter-pass region and after rolling is complete. A

typical thermal profile during two-pass hot rolling employed to conduct this investigation is shown in **Figure 7.8**.

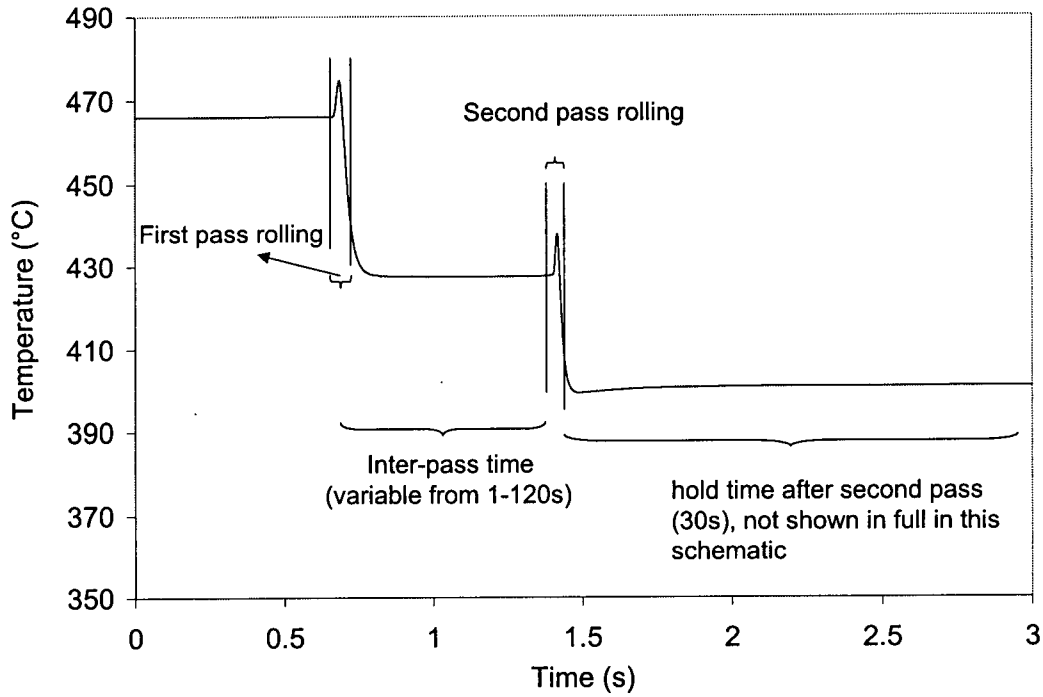

Figure 7.8 – A typical thermal profile employed during the course of the simulations used to construct the operational curves as a function of inter-pass times

A selected portion of the generated operational curve showing the relationship between the deformation conditions, represented in terms of Zener Hollomon parameter, based on the sample entry temperature prior to first pass rolling and average strain rate during first pass rolling, and the driving pressure and the fraction recrystallized at different inter-pass times after two-pass hot rolling at the strip centerline is shown in **Figures 7.9** and **7.10**, respectively.

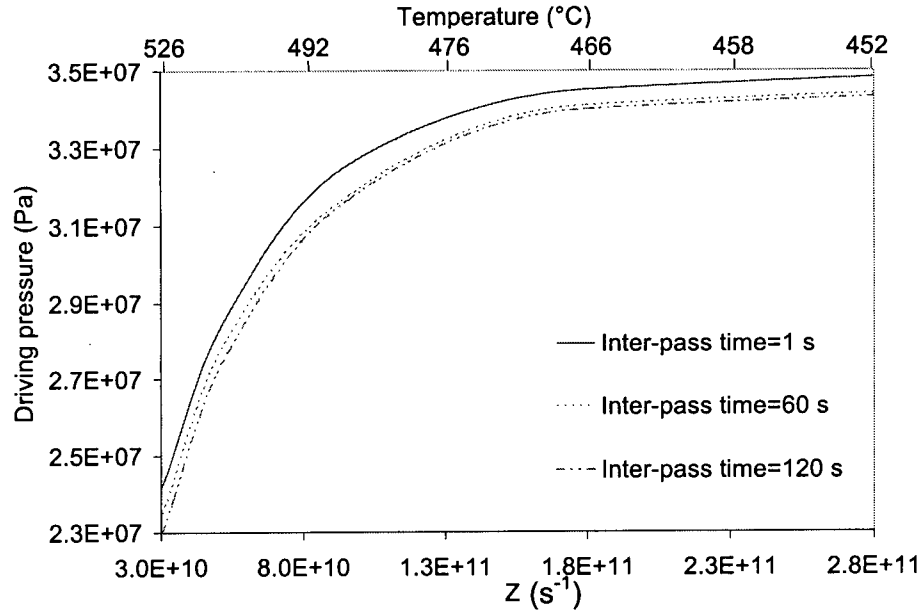

Figure 7.9 – Operational curve showing the relationship between the driving pressure and Z at different inter-pass times after second pass rolling at the center (t_i=9mm, $V_{roll\text{-}1stpass}$=0.83 m s^{-1}, $V_{roll\text{-}2nd\ pass}$=1.44 m s^{-1}, $\varepsilon_{1stpass} = \varepsilon_{2ndpass}$ =0.30, $\dot{\varepsilon}_{1stpass}$ =10s^{-1}, $\dot{\varepsilon}_{2ndpass}$ =20s^{-1}).

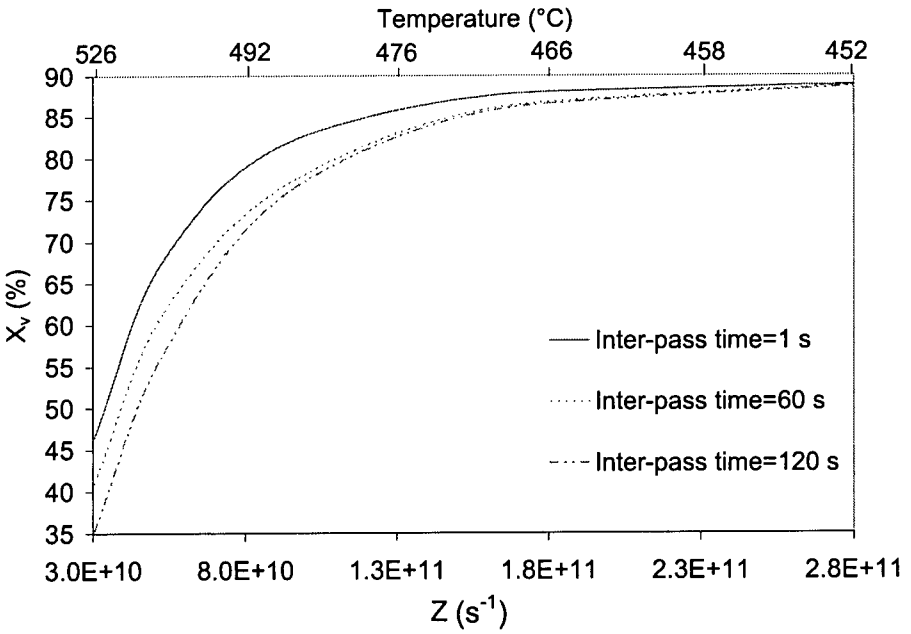

Figure 7.10 – Operational curve showing the relationship between the fraction recrystallized and Z at different inter-pass times after second pass rolling at the center (t_i=9mm, $V_{roll\text{-}1stpass}$=0.83 m s^{-1}, $V_{roll\text{-}2nd\ pass}$=1.44 m s^{-1}, $\varepsilon_{1stpass} = \varepsilon_{2ndpass}$ =0.30, $\dot{\varepsilon}_{1stpass}$ =10s^{-1}, $\dot{\varepsilon}_{2ndpass}$ =20s^{-1}).

The operational curves presented in **Figure 7.9** and **7.10** can be used in industrial practice to understand the evolution in the material driving pressure at different Z conditions and inter-pass hold times. For example, at a Z equal to 3.05 $x10^{10}$, which correspond to an entry temperature of 526°C, a strain rate of 10 s^{-1} and an inter-pass hold time of 1 s, the driving pressure after second pass rolling is equal to $2.4x10^{7}$ which results in a fraction recrystallized of 46.5% assuming 30 s holding time after second pass rolling. In comparison, at a Z equal to 1.8 $x10^{11}$, which corresponds to an entry temperature of 466°C, a strain rate of 10 s^{-1} at the same inter-pass hold time of 1 s, the driving pressure after second pass rolling is equal to $3.45x10^{7}$ which results in a fraction recrystallized of 88% assuming 30 s holding time after second pass rolling.

Other industrially relevant conclusions can be drawn based on the previous operational curves. It can be seen in **Figure 7.9** and **7.10** that the predicted driving pressure and subsequent fraction recrystallized is not sensitive to changes in the inter-pass time at high Z-values. Specifically, It can be seen that very little change in the predicted driving pressure and subsequent fraction recrystallized can be observed beyond a Z value of ~ $1.8x10^{11}$ which correspond to deformation temperature of 466°C. Thus, the optimum conditions to run the mill to achieve higher fraction recrystallized at the strip centerline after two-pass hot rolling is to reduce the entry temperature to 466°C and the inter-pass time. Conversely, a lower fraction recrystallized can be achieved by increasing the entry temperature to 526°C, corresponding to Z equal to $3.05x10^{10}$, and increasing the inter-pass time to be in the range of 90-120 s.

The data presented in **Figure 7.9** and **7.10** can be utilized to construct an operational curve to determine the holding time required after second pass hot rolling to achieve full recrystallization at the centerline of the strip at different inter-pass times and entry temperatures as shown in **Figure 7.11**.

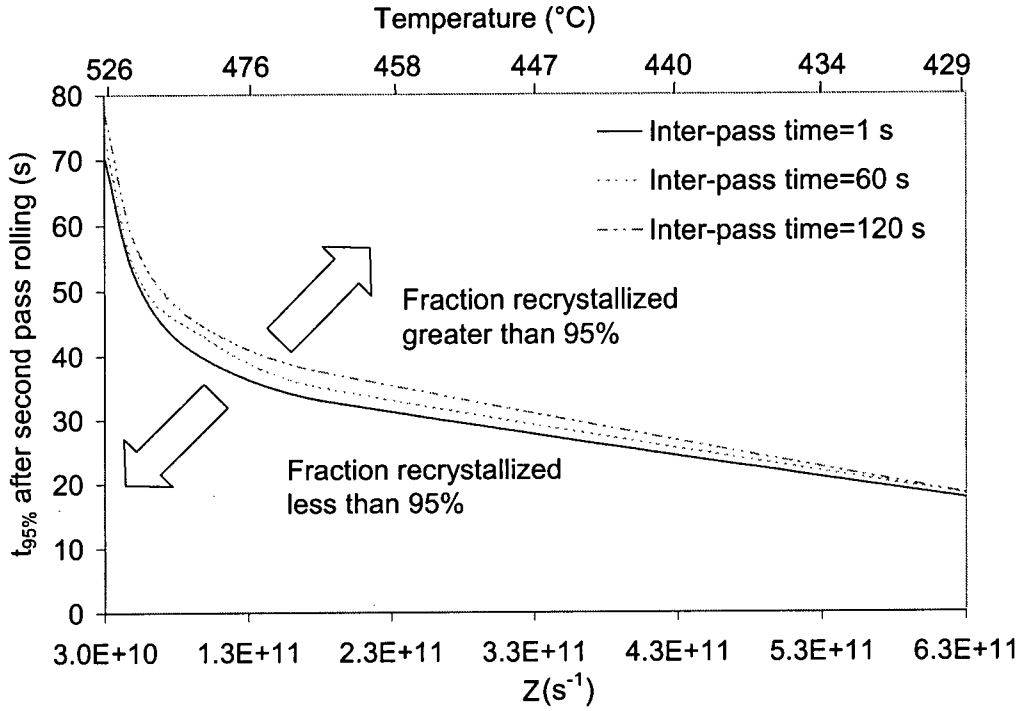

Figure 7.11 – Operational curve showing the holding time required after second pass rolling to achieve a fraction recrystallized of 95% at the strip centerline at different Z and inter-pass times (t_i=9mm,$V_{roll\text{-}1stpass}$=0.83 ms^{-1}, $V_{roll\text{-}2ndpass}$=1.44 ms^{-1}, $\varepsilon_{1stpass}$=0.30, $\varepsilon_{2ndpass}$=0.30, $\dot{\varepsilon}_{1stpass}$=10$s^{-1}$, $\dot{\varepsilon}_{2ndpass}$=20$s^{-1}$).

The data presented in **Figure 7.11** assumes that full recrystallization in the material is achieved if more than 95% of the material is recrystallized. **Figure 7.11** can be utilized to determine the holding time after second pass rolling to achieve full recrystallization in the material under different rolling conditions and at different entry temperatures and inter-pass times.

7.3.2.2 Effect of changing the total strain on predicted fraction recrystallized after two pass hot rolling at different Z's

The model was employed to generate an operational curve relating the material driving pressure and thus subsequent fraction recrystallized after two-pass hot rolling to the rolling deformation conditions at different total strains. Two-pass rolling conditions were used to generate this curve whereby the total strain conditions

of 0.2, 0.4, 0.6 and 0.8 divided equally between passes were examined. The first-pass strain rate was assumed to be 10 s^{-1} which was doubled during second-pass rolling. A constant inter-pass holding time of 90s was assumed. The investigation was carried out at different deformation temperatures namely 526, 506, 486, 466, and 414°C. Fraction recrystallized after second pass rolling was calculated assuming a holding time of 30 s after second-pass rolling is complete. It should be noted that isothermal conditions were assumed both at the inter-pass region and after rolling is complete. A selected portion of the generated operational curve showing the relationship between the deformation conditions, represented in terms of Zener Hollomon parameter, and the driving pressure and the fraction recrystallized at different total strains during two-pass hot rolling at the strip centerline is shown in **Figures 7.12** and **7.13**, respectively.

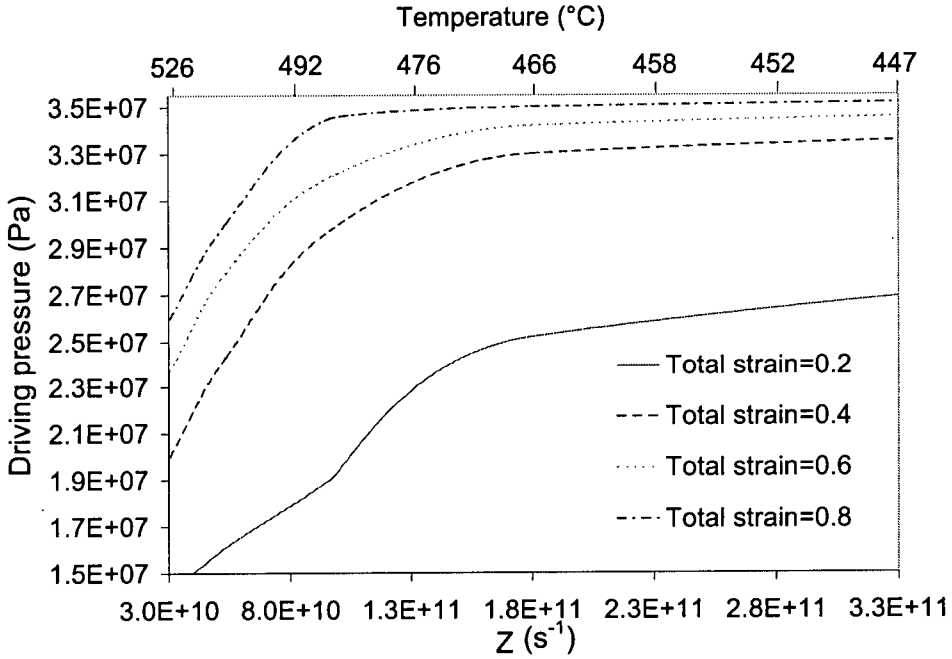

Figure 7.12 – Operational curve showing the relationship between the driving pressure and Z at different total strain conditions after second pass rolling at the center, (t_i=9mm, $\dot{\varepsilon}_{1stpass}$=10$s^{-1}$, $\dot{\varepsilon}_{2ndpass}$=20$s^{-1}$).

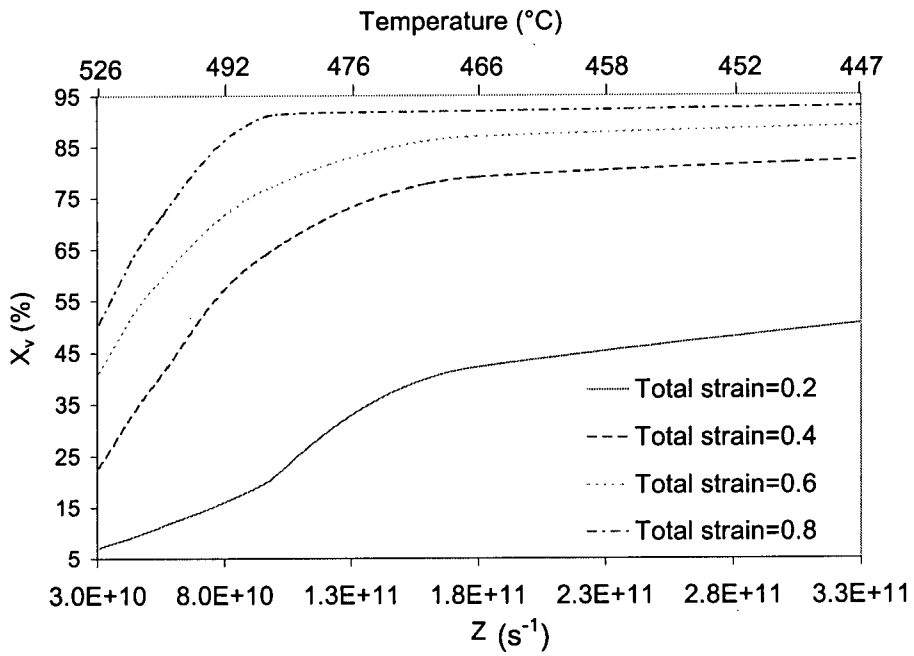

Figure 7.13 – Operational curve showing the relationship between the fraction recrystallized and Z at different total strain conditions after second pass rolling at the center (t_i=9mm, $\dot{\varepsilon}_{1stpass}$=10$s^{-1}$, $\dot{\varepsilon}_{2ndpass}$=20$s^{-1}$).

Several conclusions can be drawn from the operational curves presented in **Figures 7.12** and **7.13**. It can be seen that as Z increases, the values of the driving pressure and subsequent recrystallization kinetics increase for different total strain levels. Also, the driving pressure and subsequent recrystallization increases with increasing total strain at the strip centerline. It can also be seen that as the total strain increases, the Z value at which the saturation driving pressure is reached decreases which may be attributed to the fact that the driving pressure increases with increasing total strain at the strip centerline.

The operational curves presented in **Figure 7.12** and **7.13** can also be used in industrial practice to control the material driving pressure at different total strains and Z conditions. For example, at a Z equal to 3.05 $x10^{10}$, which correspond to an entry temperature of 526°C and a total strain of 0.2, the driving pressure after second pass rolling is equal to $1.4x10^{7}$ would result in a fraction recrystallized of 7% assuming 30 s holding time after second pass rolling. When a total strain of 0.8 is assumed at the same Z, the driving pressure increases to $2.6x10^{7}$ resulting in a fraction recrystallized of 50.5%. In comparison, at a Z equal to 1.8 $x10^{11}$, which correspond to an entry temperature of 466°C at a total strain of 0.2, the driving pressure after second pass rolling is equal to $2.52x10^{7}$ which results in a fraction recrystallized of 42%. The predicted fraction recrystallized increases to 92% corresponding to a driving pressure of $3.5x10^{7}$ at a total strain of 0.8. This simple comparison is an example of the application of these curves to industrial hot rolling to optimize the process and control microstructure evolution.

Other industrially relevant conclusions can be drawn based on the previous operational curves. It can be seen in **Figure 7.12** and **7.13** that the driving pressure value, and corresponding fraction recrystallized, saturates at lower Z value as the total strain increases. Specifically, It can be seen that very little change in the predicted driving pressure and subsequent fraction recrystallized can be observed beyond a Z value of ~ $8x10^{10}$ which correspond to deformation temperature of 492°C at a total strain level of 0.8. In comparison, at a total strain level of 0.6, the predicted driving pressure and subsequent fraction recrystallized values is saturated beyond a Z value of ~ $1.8x10^{11}$ which correspond to deformation temperature of 466°C. Thus, the

optimum conditions to run the mill to achieve higher driving pressure and fraction recrystallized at the strip centerline after two-pass hot rolling is to increase the total strain to 0.8 and increase the entry temperature to ~490°C. Alternatively, a higher driving pressure can also be achieved at a lower strain level of 0.6 at relatively lower deformation temperature of ~466°C.

Based on the sensitivity analysis findings, strain partitioning effect and operational curves results shown in **Figures 7.5-7.6, 7.9-7.13**, various industrial strategies can be recommended to achieve higher fraction recrystallized after second-pass hot rolling at the strip centerline. One option is to run the rolling mill at a total strain level of 0.8 where the first pass strain should be equal to 0.6 and the second pass strain should be equal to 0.2 assuming an inter-pass hold time of 90 s and a strain rate of $10s^{-1}$ during first pass rolling which is doubled during the second pass. The entry temperature should be lower than 492°C at these deformation conditions since the driving pressure saturates below this value, **Figure 7.12**, which lead to higher driving pressure and faster subsequent recrystallization kinetics. Another possible strategy is to run the mill at a total strain level of 0.4 where the first pass strain is equal to 0.3 and the second pass strain equal to 0.1 assuming an inter-pass hold time of 90 s and a strain rate of $10s^{-1}$ during first pass rolling which is doubled during the second pass. The entry temperature should be lower than 466°C at these deformation conditions since the driving pressure saturates below this value. It should be noted that higher fraction recrystallized after two-pass hot rolling can be achieved if it is industrially possible to decrease the inter-pass hold time from the assumed 90 s to 60 s. It should also be noted that increasing the roll diameter would also result in higher fraction recrystallized. These proposed strategies and conclusions show that the model can be utilized as a powerful tool to optimize and control the resulting microstructure.

References

1. Ahmed, H., M.A. Wells, D.M. Maijer, and M.R. van der Winden. *A sensitivity analysis of the work-roll strip interface parameters used during modelling of hot rolling for AA5083.* in *Hot Deformation of Aluminum Alloys III.* 2003. San Diego, USA: TMS.

2. Chen, B.K., P.F. Thomson, and S.K. Choi, *Computer Modelling of microstructure during hot flat rolling of aluminium.* Mater. Sci. Technol., 1992. **8**(1): p. 72-77.

CHAPTER 8

SUMMARY AND CONCLUSIONS

The control of the deformation and microstructure evolution during hot rolling of aluminum alloy is critical in order to be able to control the final sheet properties. Several complexities are associated with microstructure evolution especially during multi-pass hot rolling. To start with, the microstructure evolution is determined by complex interactions between the deformation history the material experiences during rolling in terms of deformation temperature, strain and strain rate, and the material changes that occur during rolling. Multi-pass hot rolling constitutes another challenge because the through-thickness changes that occur in the inter-pass region can change the material stored energy and subsequent recrystallization kinetics. Specifically, the way in which the stored energy is accumulated in a situation where various levels of recrystallization occur through the strip thickness needs to be understood to follow microstructure evolution.

The complexity of the interaction between deformation and microstructure evolution during multi-pass rolling requires further understanding of the rolling process parameters on microstructure evolution to achieve the desired microstructure in terms of through-thickness fraction recrystallized and recrystallized grain size. A common practice to understand and predict microstructure evolution during multi-pass hot rolling was to model the process employing a purely empirical approach based on the available experimental data. This does not provide enough explanation of the physics of the recrystallization process. Recently, a number of computer based FE models were implemented to predict rolling deformation conditions and a physically-based microstructure approach was suggested to understand microstructure evolution during single-pass rolling with the intent of employing these models to serve as a tool to understand and predict thermo-mechanical and microstructure evolution during hot rolling. It is of prime importance that these models are able to capture all the complexity of the industrial rolling process if they are to be utilized as useful tools. Based on the literature review, the models developed to date have several shortcomings, which are: (i) no attempt has been made to account for changes in different material variables such as dislocation density, average subgrain size and

average misorientation angles between subgrains at different locations through the strip thickness to account for changes in the driving pressure in the inter-pass region, (ii) the integration of an FE thermo-mechanical model results into an internal state variable microstructure model to track the changes in thermo-mechanical process parameters namely: strain, strain rate, temperature and link them to microstructure evolution and driving pressure for recrystallization has not been attempted previously for multi-pass hot rolling cases, (iii) most of the relationships that describe microstructure evolution have used laboratory measurements to validate the thermo-mechanical and the microstructure models. Very few attempts were made to utilize an industrial-scale rolling facility that captures the complexity of the industrial rolling to validate the rolling models.

In order to obtain industrially relevant data to verify the rolling model, both single-pass and multi-pass hot rolling industrial trials were performed using Corus' multi-mill industrial rolling facility in IJmuiden, the Netherlands. Rolling process parameters such as hold time, entry temperature, strain and strain rate were varied to obtain industrially relevant data at different rolling conditions that could be used to validate the rolling model. Temperature data was recorded using thermocouples at the strip centerline and surface. Rolling loads were also recorded to verify the thermo-mechanical model. Metallographic analysis was carried out at different strip locations to measure the through thickness fraction recrystallized and recrystallized grain size which was employed to verify the microstructure model and understand the sensitivity of the model predictions to changes in the rolling process parameters.

A comprehensive mathematical model was developed utilizing the commercial finite element package ABAQUS to predict through-thickness temperature, rolling load, strain and microstructure evolution during both single-pass and multi-pass hot rolling. An internal state variable microstructure approach that accounts for changes in the material: average subgrain size, average misorientation angle between subgrains and total dislocation density was utilized to calculate the material stored energy and subsequent recrystallization as a function of deformation conditions. The application of the model to simulate industrial hot rolling of AA5083 and predict recrystallization kinetics for both single-pass and multi-pass hot rolling has been achieved. The model accounts for change in microstructure evolution in the inter-pass region through the

thickness of the strip. A new approach to capture and track the accumulation of stored energy during multi-pass hot rolling and predict the resulting microstructure during the non-isothermal cooling in the inter-pass region and after rolling was applied which is unique to this research program. The overall model development and validation process especially for multi-pass hot rolling represents a significant improvement over existing models.

The six single-pass and eleven multi-pass hot rolled samples were examined and used to verify the model developed during the course of this research program. The model validation process involved "fine tuning" the microstructure model constants based on single-pass rolling data. The resulting model was utilized to predict microstructure during multi-pass rolling cases. Traditionally, thermo-mechanical and microstructure models predictions were validated using plane strain compression data that mimic certain rolling conditions. To the author's knowledge, the extensive validation process for both the thermo-mechanical and microstructure model utilizing pilot-scale mill data under such a variety of industrially relevant multi-pass hot rolling conditions has not been reported in the published literature to date.

A comparison between the model predictions to the experimentally measured data lead to the following conclusions:

- The mathematical thermo-mechanical finite element model using ABAQUS was able to simulate both the single-pass and the multi-pass hot rolling processes reasonably well in terms of temperature change during first-pass and second-pass hot rolling and in the inter-pass region as well as rolling load. This capability indicates the suitability of the selected friction boundary conditions and shows the merit of the selected heat transfer boundary conditions at the interface between the work roll and the strip and in the inter-pass region.
- The microstructure model constants were fine-tuned based on single-pass hot rolling data and utilized to predict microstructure evolution for multi-pass hot rolled samples. The microstructure model was able to predict the fraction recrystallized and the recrystallized grain size through the thickness of the strip for single-pass rolled samples where the model predictions match the measurements

reasonably well. The model was also able to predict the fraction recrystallized for multi-pass hot rolled samples through the strip thickness under different rolling conditions and different levels of recrystallization reasonably well which indicates the validity of the proposed approach to account for the changes that occur in the inter-pass region. The model predicted a decreasing recrystallized grain size trend for all samples from the centerline to the subsurface locations of the strip. The predicted recrystallized grain size has an almost constant deviation from the experimental measurements by ~11μm. Experimental measurements show that the recrystallized grain size after two-pass hot rolling did not exhibit any significant changes compared to the start material grain size while the model predicted a smaller recrystallized grain size after two pass rolling.

- Additional sensitivity analysis was carried out which shows the model sensitivity to changes in the model constants that describe nucleation density and time required to achieve 50% recrystallization. Although the internal state variable microstructure model gives insight into the physics of the process during hot rolling, it still includes modelling constants which need to be determined based on experimental data.
- The model was employed to investigate the effect of changing rolling process parameters during multi-pass hot rolling on predicted fraction recrystallized at the strip centerline after rolling is complete. It was found that changing the hold time between passes and after rolling is complete before quenching as well as changing the entry temperature affect fraction recrystallized at the strip centerline considerably. The study indicates that strain has a minor effect on fraction recrystallized at the strip centerline after multi-pass hot rolling is complete while strain rate effect is almost negligible.
- The verified model was utilized to investigate the effect of strain partitioning during multi-pass hot rolling on the material stored energy where it was found that as the first-pass rolling strain increases, in comparison to second-pass rolling strain, the material stored energy increases, thus the time needed to achieve 50% recrystallization decreases.
- The model was further employed to generate industrially relevant operational curves that can be used to understand the evolution in material stored energy during multi-pass hot rolling and thus optimize the rolling process. A different set

of simulation conditions were used to generate an operational curve relating the material driving pressure and thus subsequent fraction recrystallized after two-pass hot rolling to the rolling deformation conditions at different inter-pass hold times and total strains.

Thus, the model has proven to be a powerful tool that can be used to further optimize and control the resulting microstructure. This would serve as a powerful industrial tool to achieve the desired properties.

8.1 Recommendations For Future Work

The conclusions drawn from this research project was based on the predictions of the FE thermo-mechanical model and the state variable microstructure model. Though, the model serves as a powerful tool that gives an insight and provide scientific understanding to the physics of the microstructure evolution during multi-pass hot rolling process, several improvements can be incorporated in the model to make it more robust and to decrease the model current limitations which include:

- Extending the model prediction to three-pass and four-pass rolling scenarios.
- The model does not account for static recovery which may play a role in the final predicted microstructure. If a static recovery model is incorporated into the current model, further insight and understanding of the process could be achieved.
- If a relationship can be incorporated into the model that estimates flow stress based on change in dislocation density, it may decrease the discrepancy between the model predicted and experimentally measured rolling load and provide further understanding of flow stress evolution during rolling as a function of dislocation density.
- The effect of particle size and distribution on recovery and recrystallization kinetics and the final grain size has not been incorporated into this model and would provide much insight if it could be integrated.
- Incorporating a sub-model to predict recrystallized crystallographic texture for both single and multi-pass rolling would improve the model capabilities significantly.
- If a relationship can be reached to account for change in microstructure evolution based on changes in the alloy composition for similar aluminum alloy systems, the model robustness can be improved significantly. Considerable experimentation is needed to devise such a relationship.

If these changes were incorporated, a robust general model that can account for process changes would be generated which would serve as a state-of-art tool that will play a crucial role towards engineering microstructure evolution and ultimately control sheet properties during hot rolling.

Appendix A

DERIVATION OF GRAIN BOUNDARY AREA PER UNIT VOLUME RELATIONSHIP

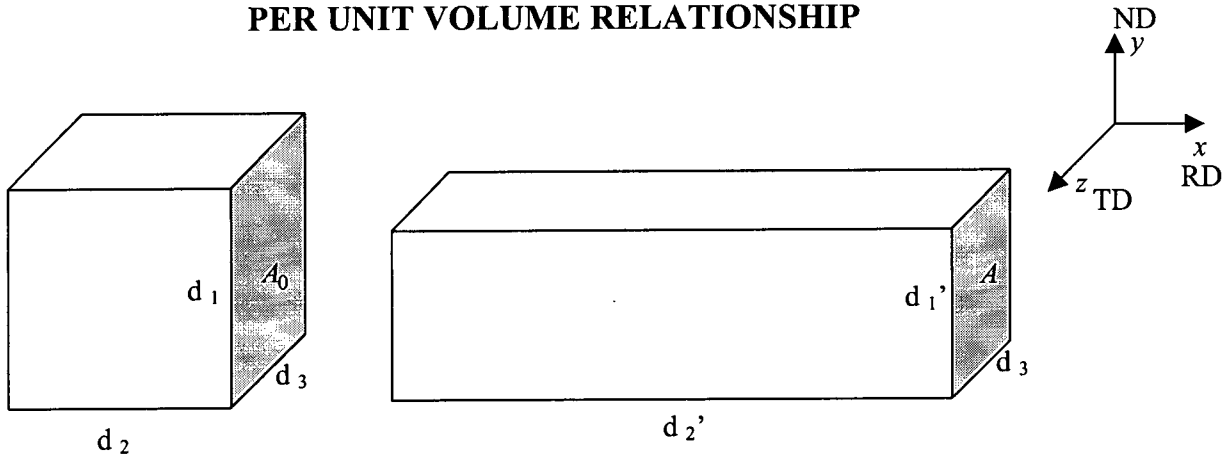

$$r = \frac{A_0 - A}{A_0} = 1 - \frac{A}{A_0}$$

$$\frac{A_0}{A} = \frac{1}{1-r}$$

$$\varepsilon = \ln\left(\frac{A_0}{A}\right) = \ln\left(\frac{1}{1-r}\right) \quad \ldots(1)$$

$$\frac{1}{1-r} = \exp(\varepsilon)$$

$$r = \frac{A_0 - A}{A_0} = \frac{d_3 d_1 - d_3 d_1'}{d_3 d_1} = 1 - \frac{d_1}{d_1'}$$

$$d_1' = d_1(1-r) \ldots(2)$$

$$\varepsilon_{zz} = 0\,,\ \varepsilon_{yy} = \ln\left(\frac{d_1'}{d_1}\right),\ \varepsilon_{xx} = \ln\left(\frac{d_2'}{d_2}\right)$$

$$\varepsilon_{xx} + \varepsilon_{yy} + \varepsilon_{zz} = 0$$

$$\varepsilon_{yy} = -\varepsilon_{xx}$$

$$\ln\left(\frac{d_1'}{d_1}\right) = -\ln\left(\frac{d_2'}{d_2}\right)$$

$$\frac{d_1'}{d_1} = \frac{d_2}{d_2'}$$

$$d_2' = \frac{d_1 d_2}{d_1'} = \frac{d_1 d_2}{d_1(1-r)} \quad \text{"From (2)"}$$

$$d_2' = \frac{d_2}{(1-r)} \ldots(3)$$

$$S_A = 2d_3 d_1' + 2d_1' d_2' + 2d_3 d_2'$$

$$= 2d_3 d_1(1-r) + 2d_1(1-r)\frac{d_2}{(1-r)} + \frac{2d_2 d_3}{(1-r)} \quad \text{"From (2) \& (3)"}$$

$$= 2d_3 d_1 \exp(-\varepsilon) + 2d_1 d_2 \exp(\varepsilon)\exp(-\varepsilon) + 2d_2 d_3 \exp(\varepsilon) \quad \text{"From (1)"}$$

Unit volume $(v) = d_1 d_2 d_3$

Then by dividing (S_A) by unit volume

$$S_V = \frac{2\cancel{d_3}\cancel{d_1}}{\cancel{d_1} d_2 \cancel{d_3}}\exp(-\varepsilon) + \frac{2\cancel{d_1}\cancel{d_2}}{\cancel{d_1}\cancel{d_2} d_3} + \frac{2\cancel{d_2}\cancel{d_3}}{d_1\cancel{d_2}\cancel{d_3}}\exp(\varepsilon)$$

$$= \frac{2}{d_2}\exp(-\varepsilon) + \frac{2}{d_3} + \frac{2}{d_1}\exp(\varepsilon)$$

Assuming d_3 is equal to the unit depth

$$S_V = 2\left[\frac{\exp(-\varepsilon)}{d_2} + \frac{\exp(\varepsilon)}{d_1} + 1\right] \ldots(4)$$

Appendix B

TEMPERATURE VALIDATION

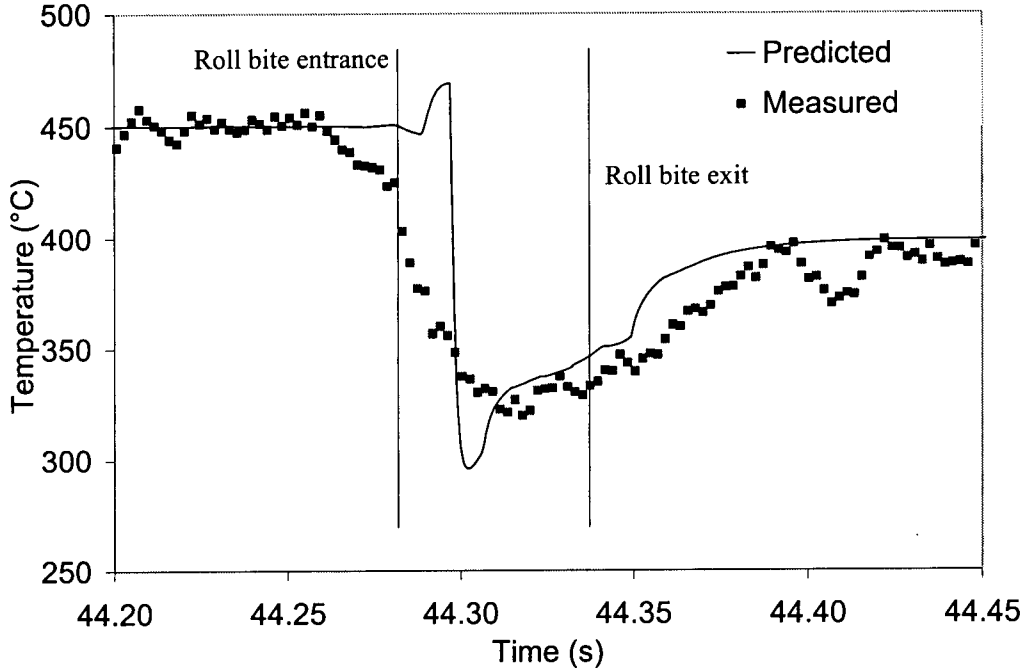

Figure B1.1 – Comparison of model predicted surface temperature during the first pass rolling to experimental measurements for sample no. 1.

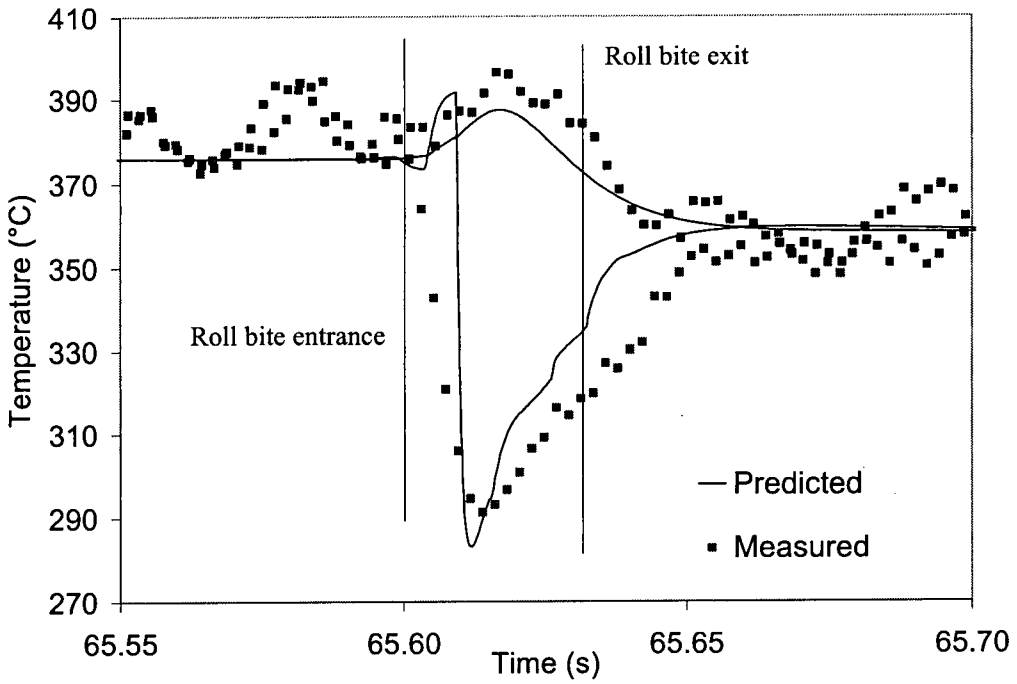

Figure B1.2 – Comparison of model predicted centerline and surface temperatures during the second pass rolling to experimental measurements for sample no. 1.

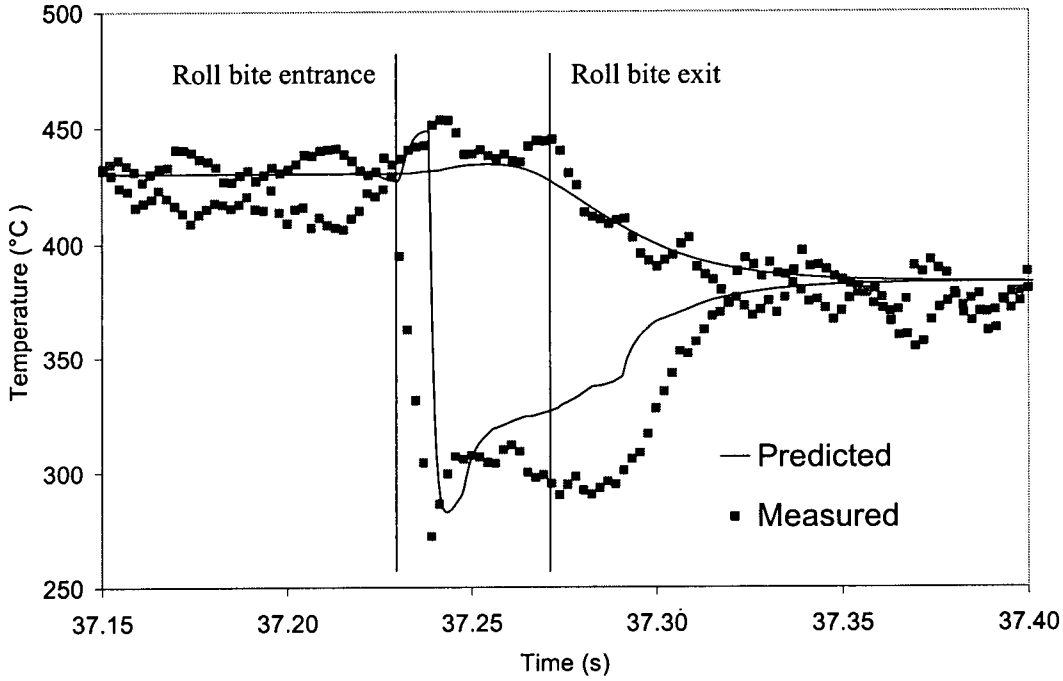

Figure B2.1 – Comparison of model predicted centerline and surface temperatures during the first pass rolling to experimental measurements for sample no. 2.

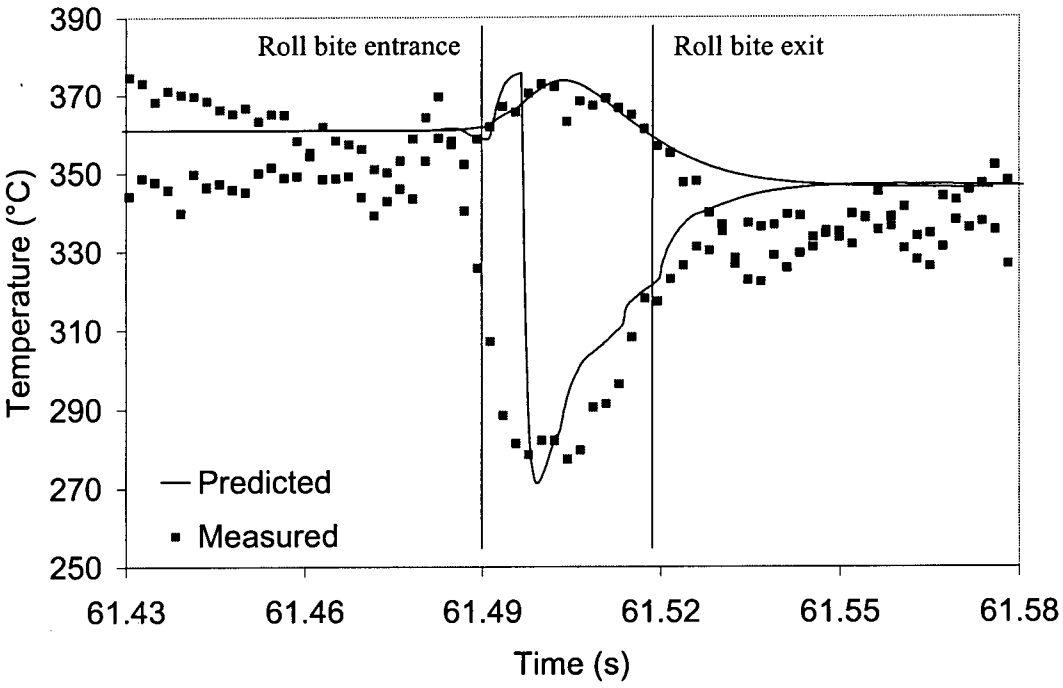

Figure B2.2 – Comparison of model predicted centerline and surface temperatures during the second pass rolling to experimental measurements for sample no. 2.

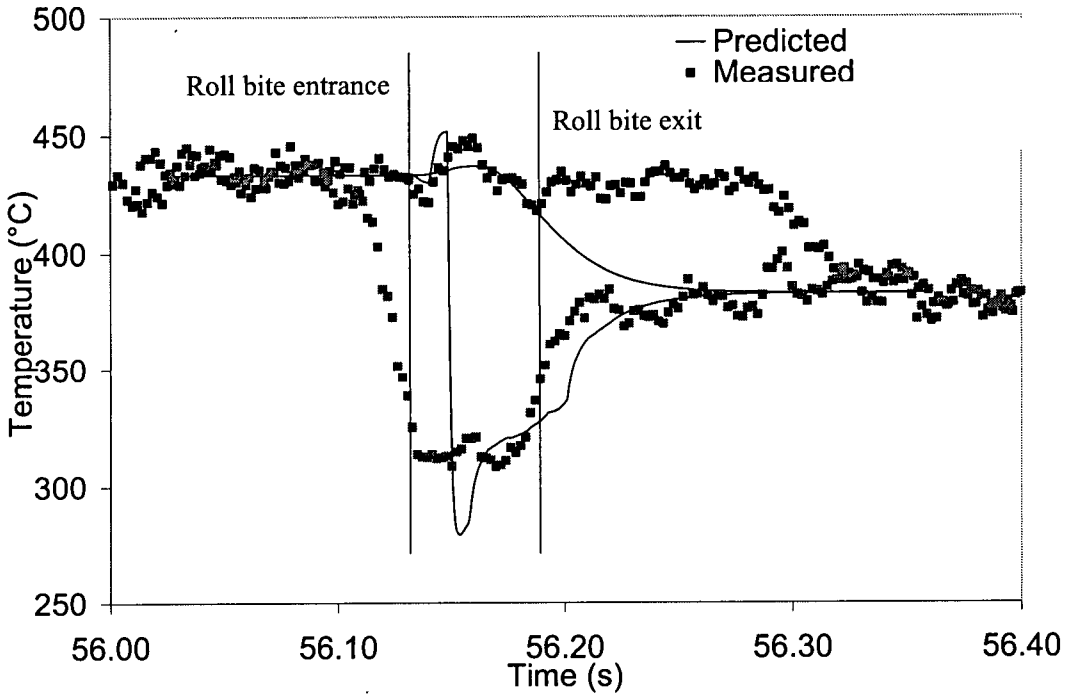

Figure B3.1 – Comparison of model predicted centerline and surface temperatures during the first pass rolling to experimental measurements for sample no. 3.

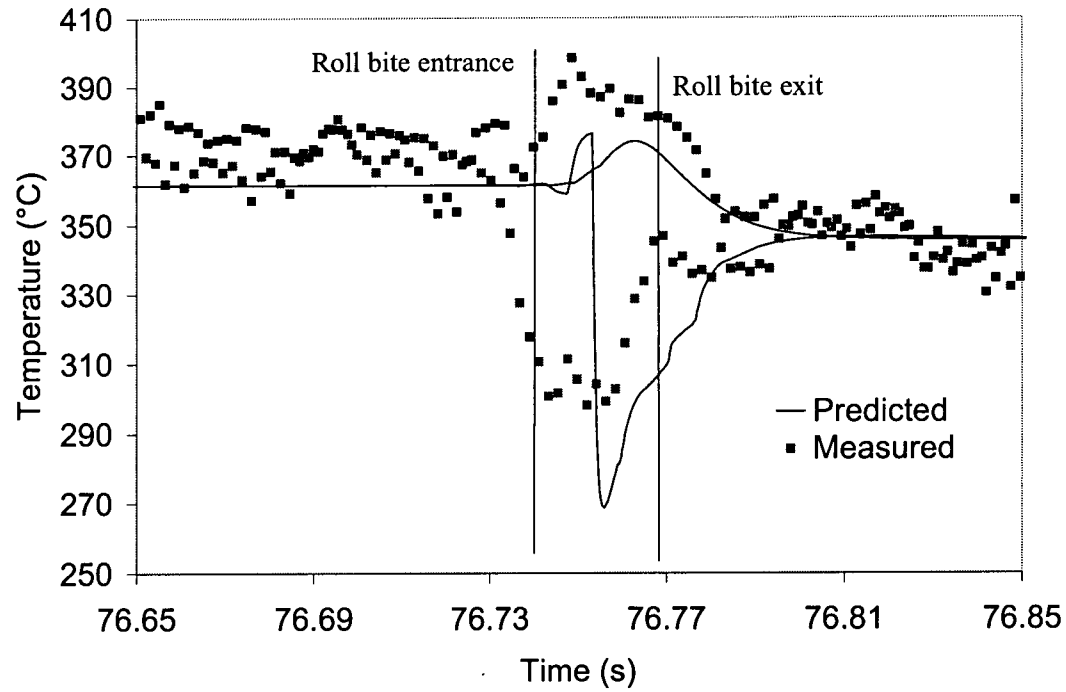

Figure B3.2 – Comparison of model predicted centerline and surface temperatures during the second pass rolling to experimental measurements for sample no. 3.

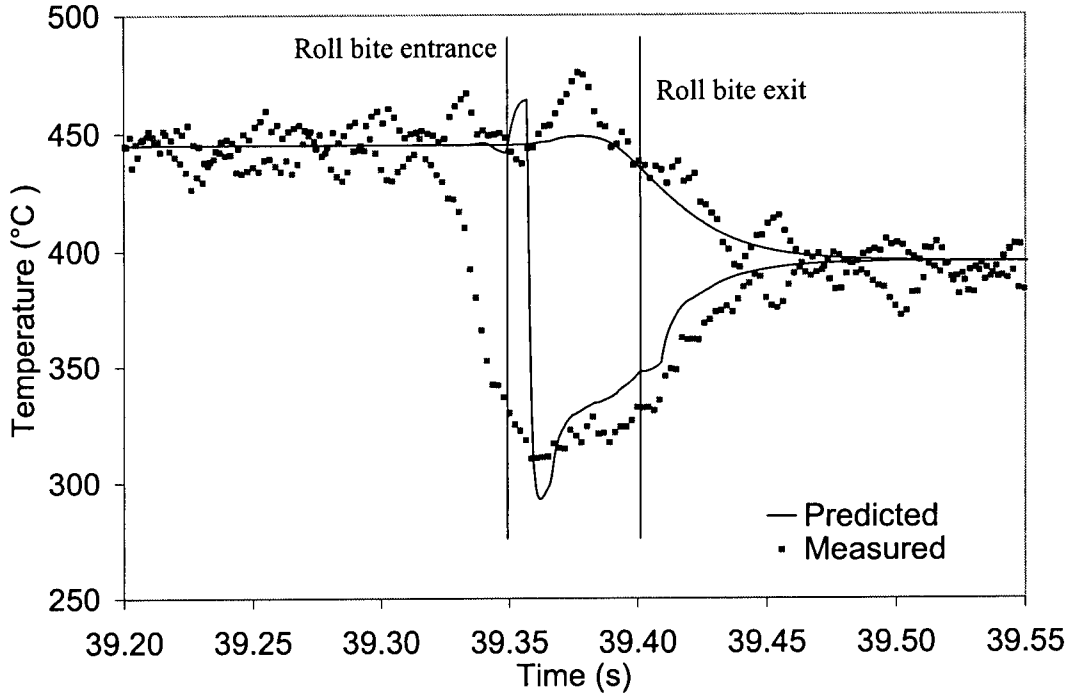

Figure B4.1 – Comparison of model predicted centerline and surface temperatures during the first pass rolling to experimental measurements for sample no. 4.

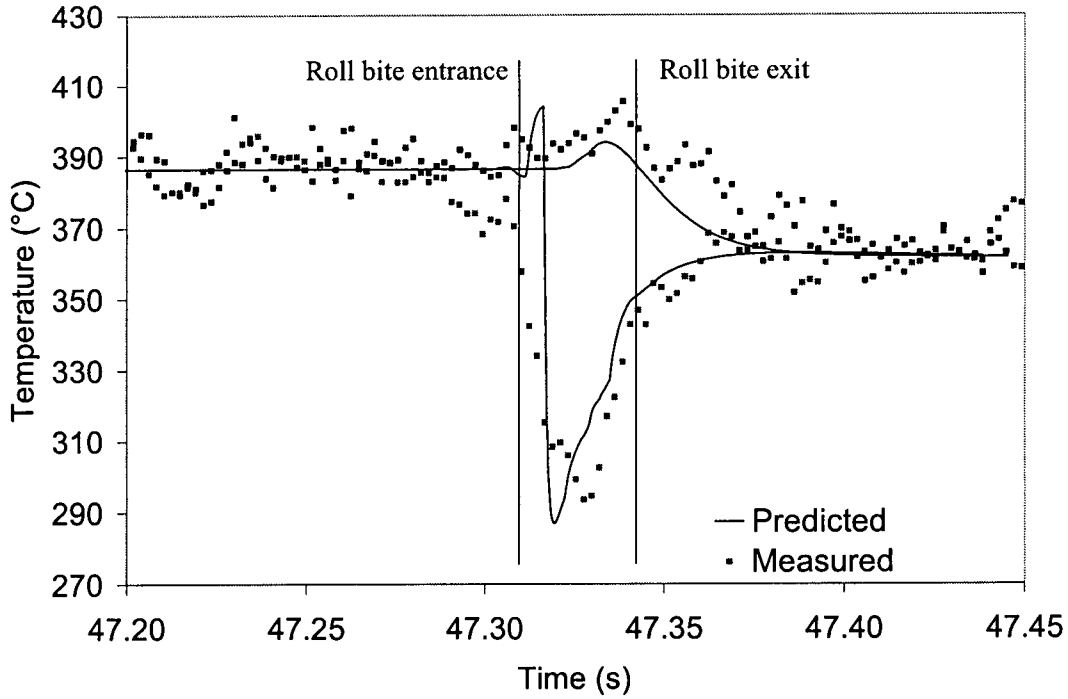

Figure B4.2 – Comparison of model predicted centerline and surface temperatures during the second pass rolling to experimental measurements for sample no. 4.

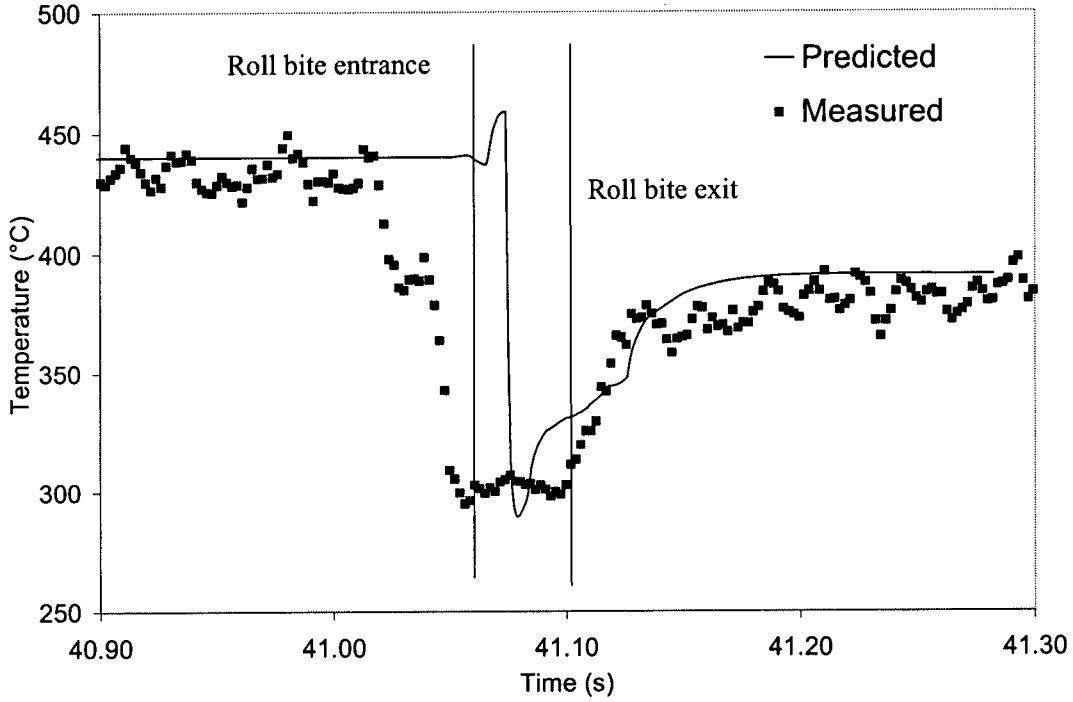

Figure B5.1 – Comparison of model predicted surface temperature during the first pass rolling to experimental measurements for sample no.5.

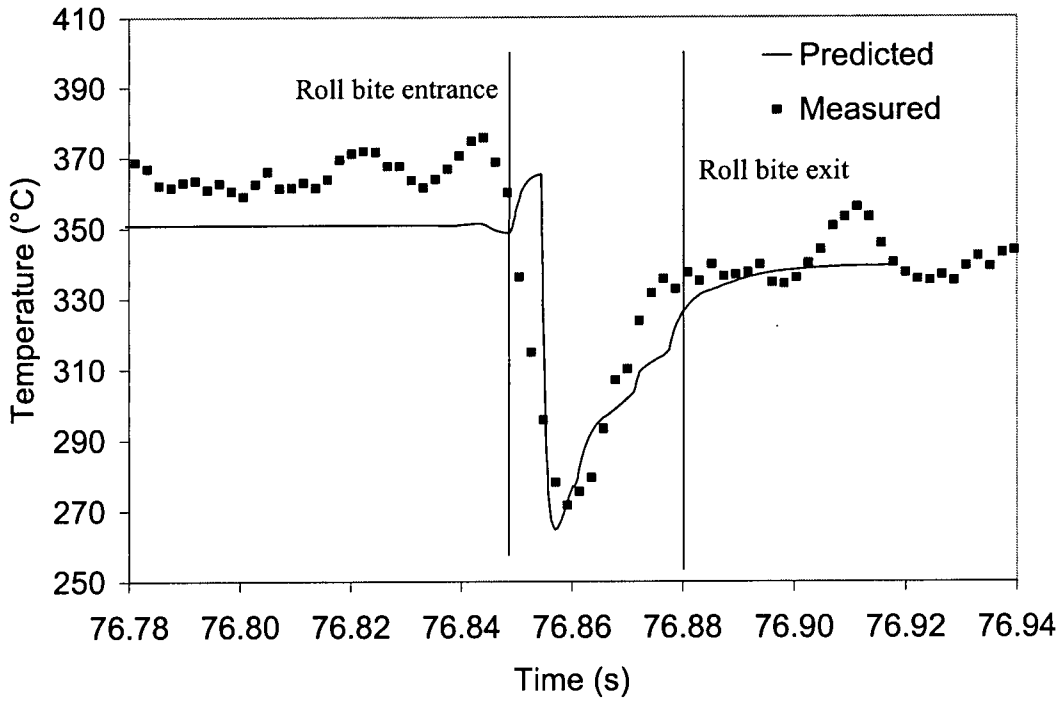

Figure B5.2 – Comparison of model predicted surface temperature during the second pass rolling to experimental measurements for sample no.5.

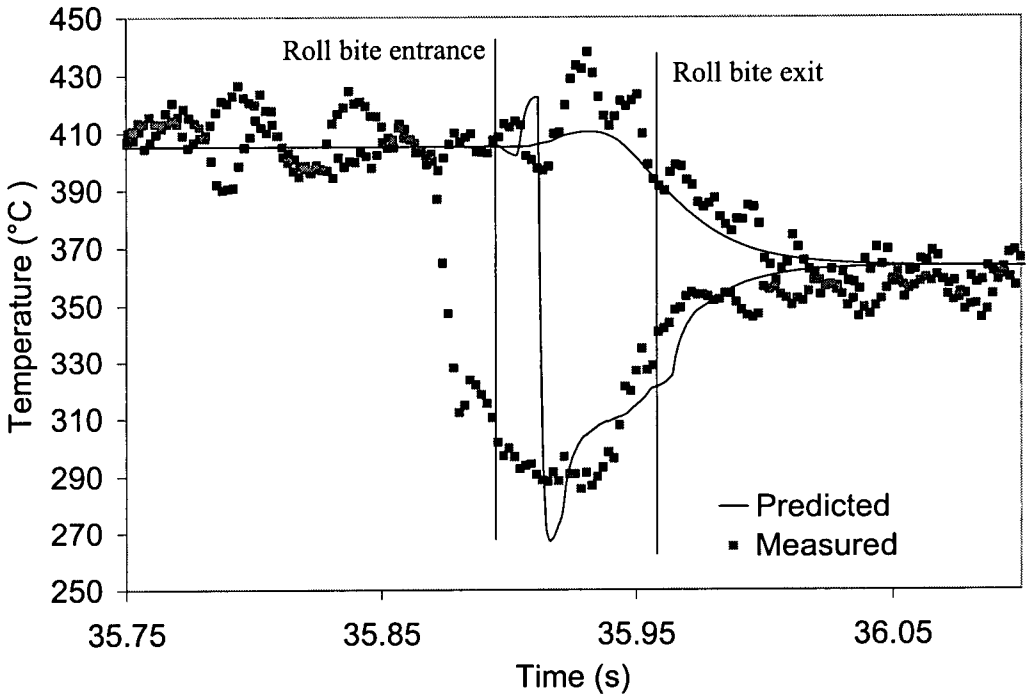

Figure B6.1 – Comparison of model predicted centerline and surface temperatures during the first pass rolling to experimental measurements for sample no.6.

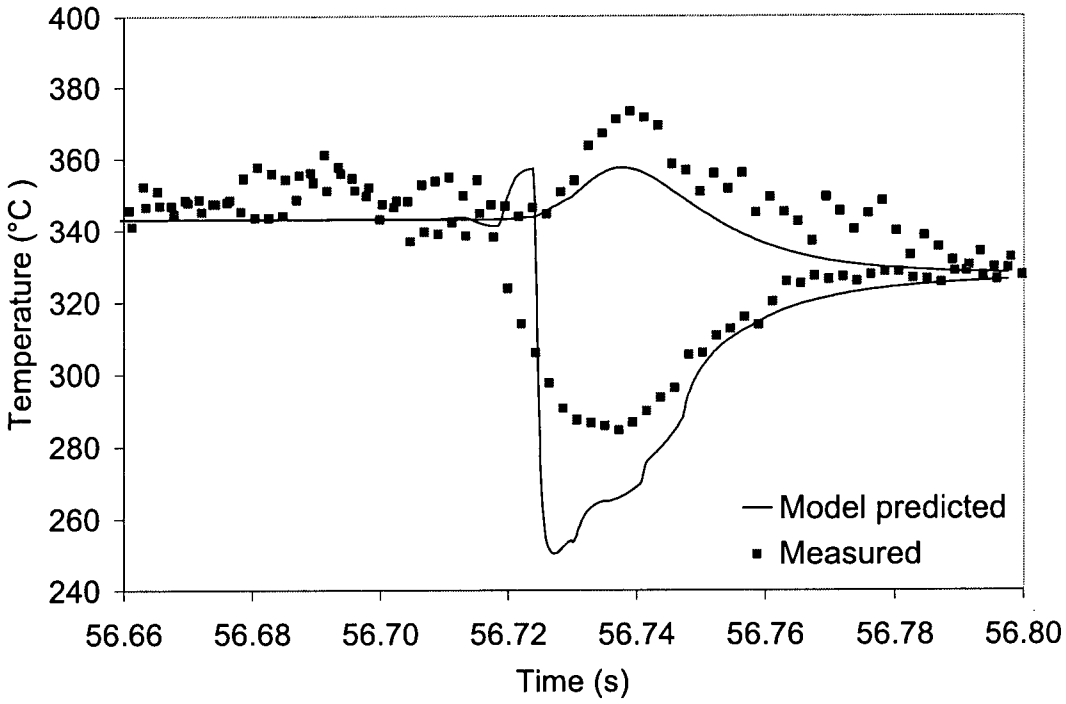

Figure B6.2 – Comparison of model predicted centerline and surface temperatures during the second pass rolling to experimental measurements for sample no. 6.

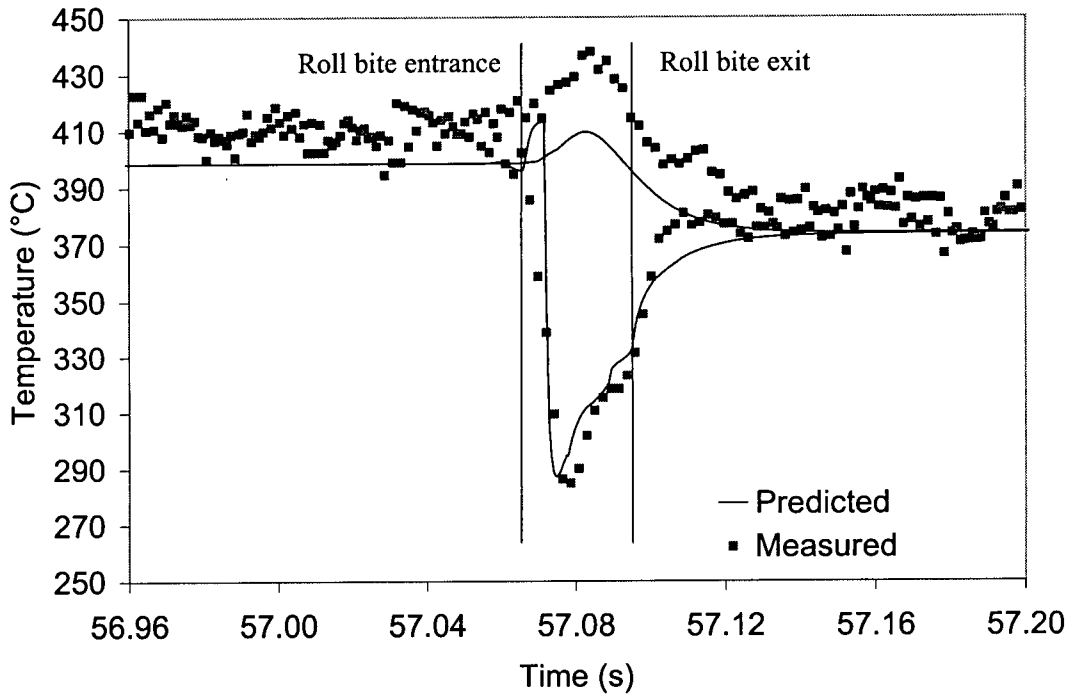

Figure B7.2 – Comparison of model predicted centerline and surface temperatures during the second pass rolling to experimental measurements for sample no. 7.

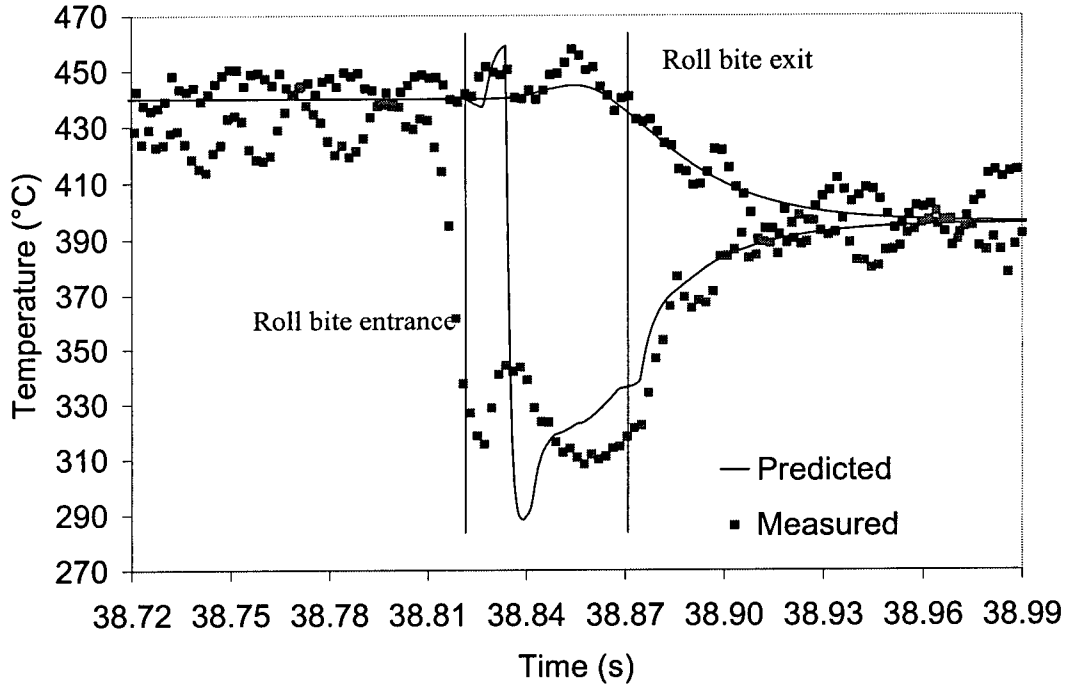

Figure B8.1 – Comparison of model predicted centerline and surface temperatures during the first pass rolling to experimental measurements for sample no.8.

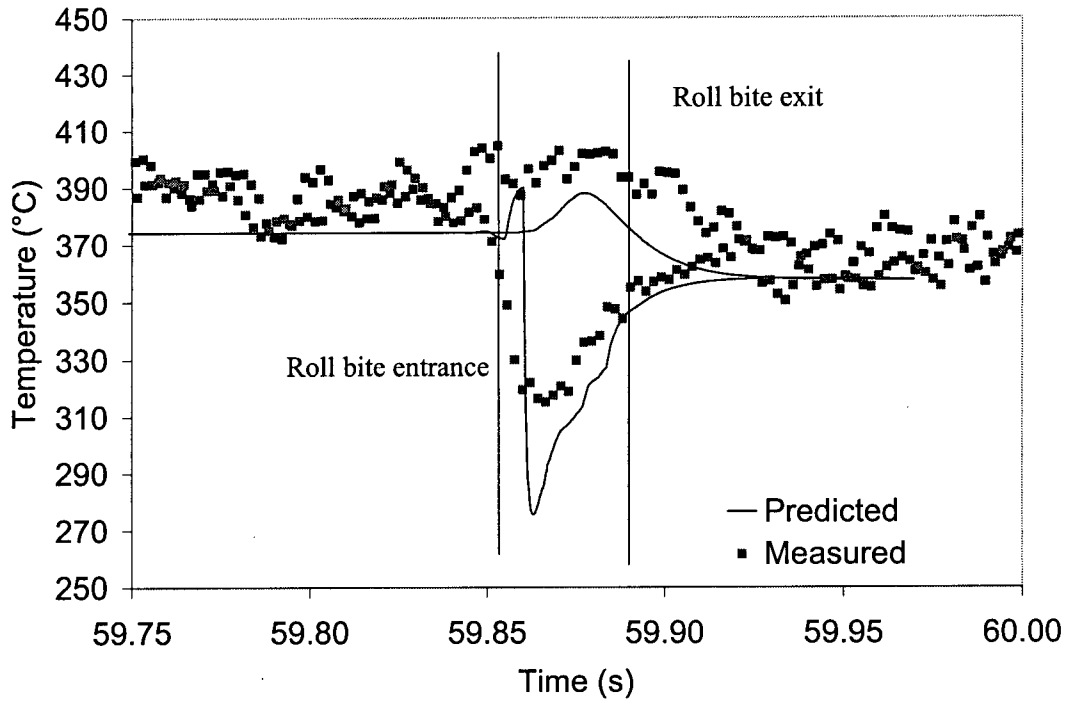

Figure B8.2 – Comparison of model predicted centerline and surface temperatures during the second pass rolling to experimental measurements for sample no. 8.

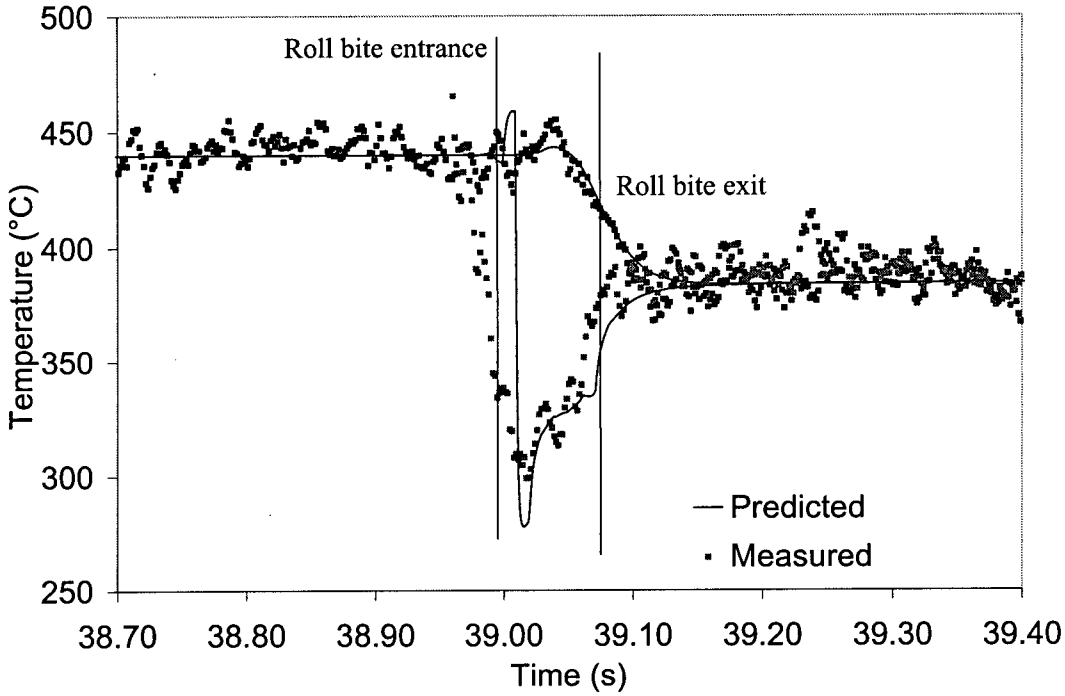

Figure B9.1 – Comparison of model predicted centerline and surface temperatures during the first pass rolling to experimental measurements for sample no.9.

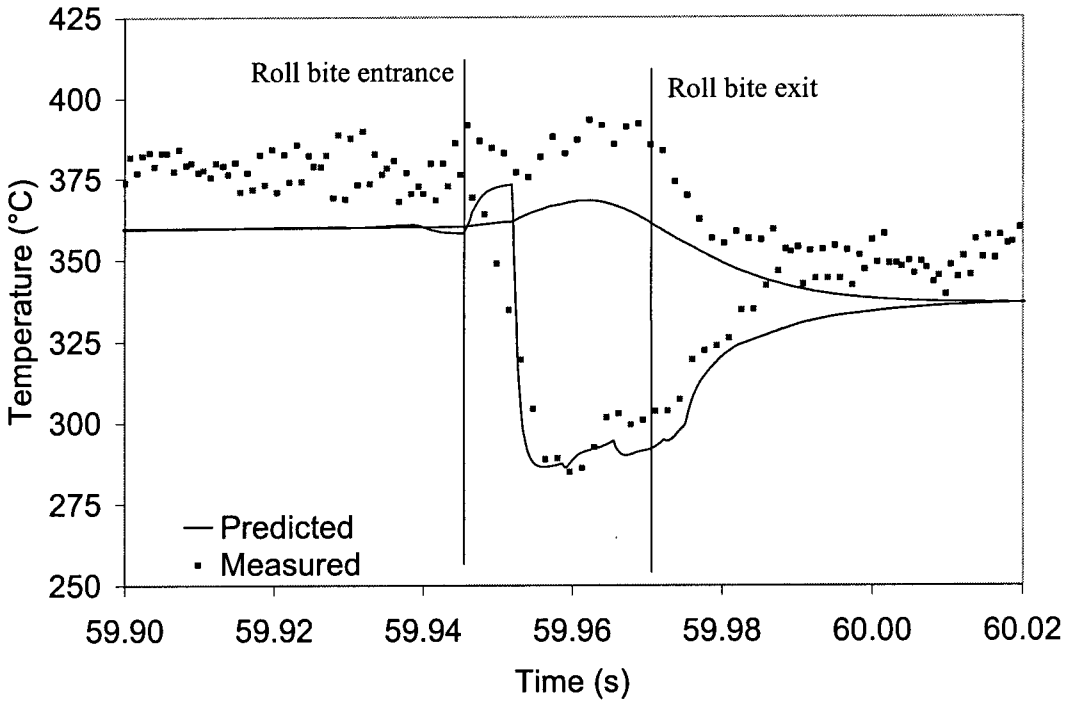

Figure B9.2 – Comparison of model predicted centerline and surface temperatures during the second pass rolling to experimental measurements for sample no.9.

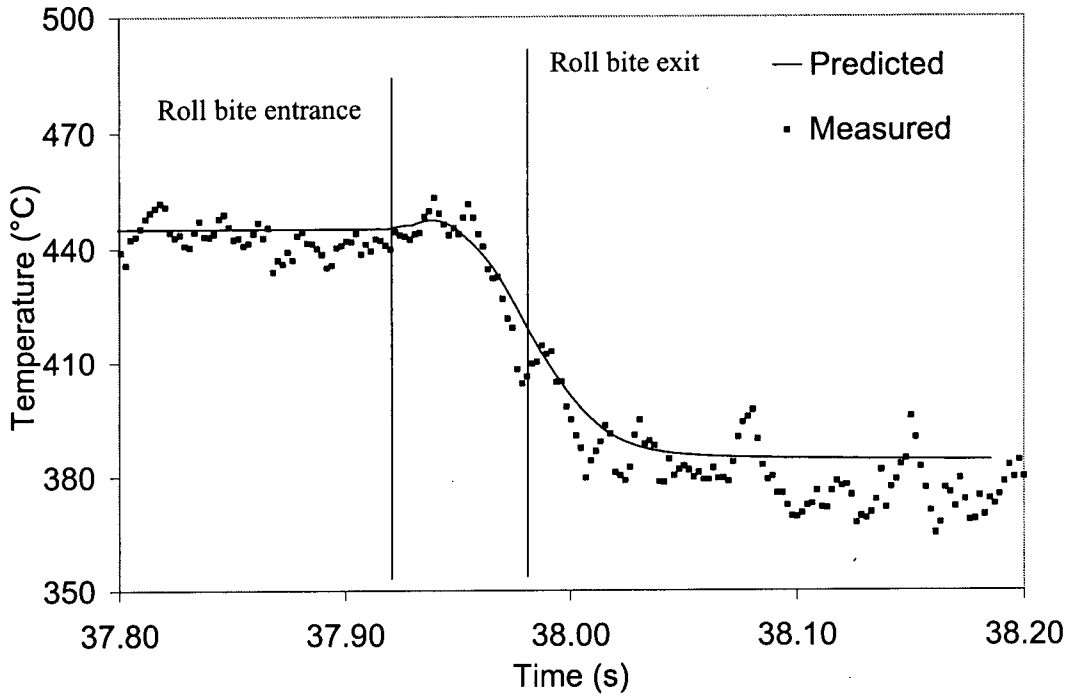

Figure B10.1 – Comparison of model predicted centerline temperature during the first pass rolling to experimental measurements for sample no.10.

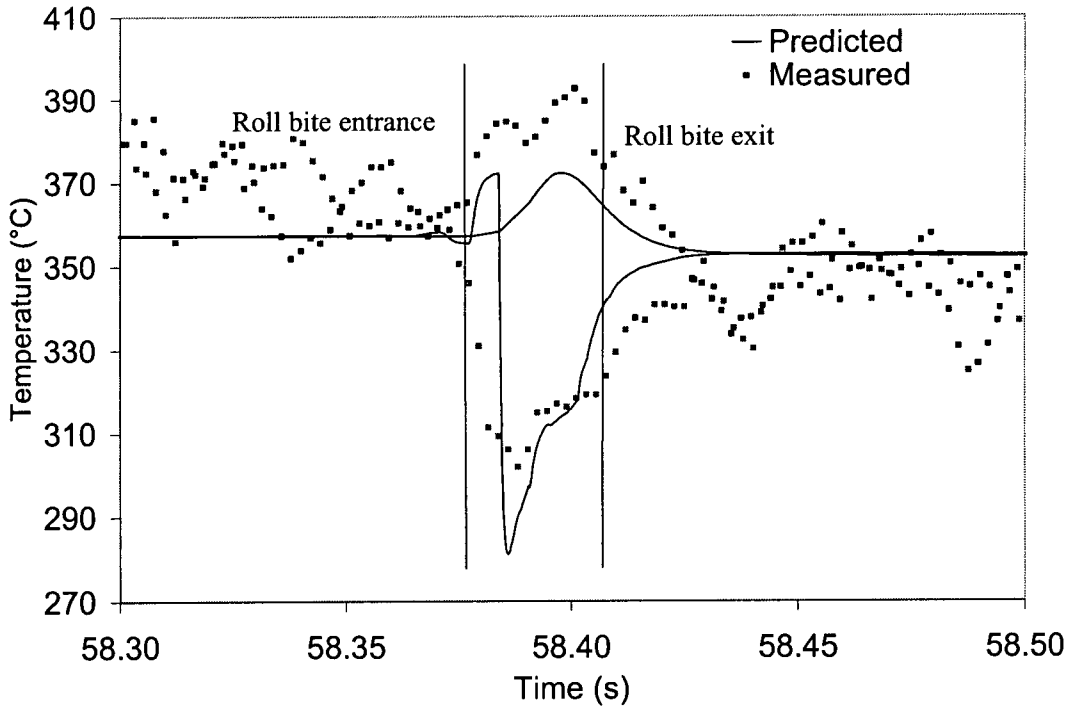

Figure B10.2 – Comparison of model predicted centerline and surface temperatures during the second pass rolling to experimental measurements for sample no.10.

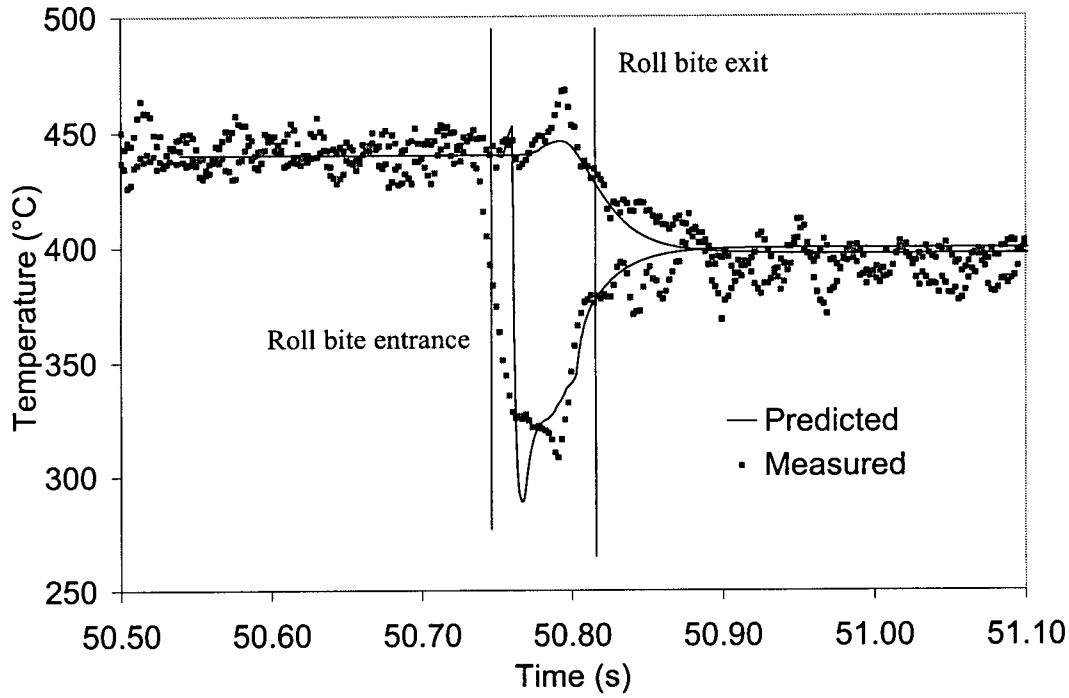

Figure B11.1 – Comparison of model predicted centerline and surface temperatures during the first pass rolling to experimental measurements for sample no.11.

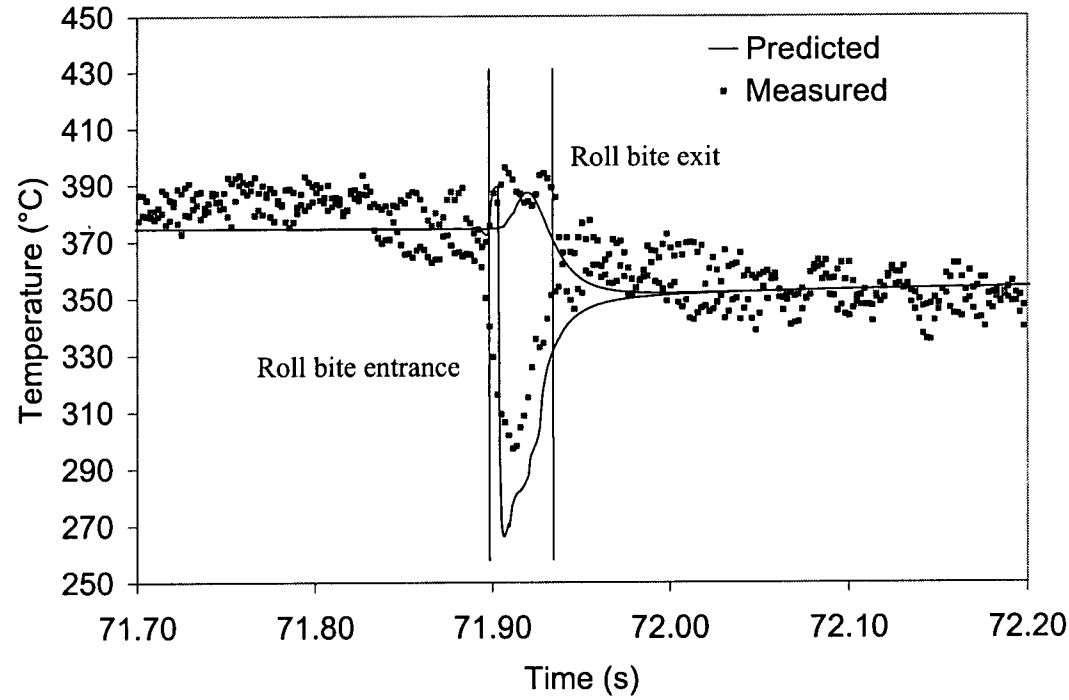

Figure B11.2 – Comparison of model predicted centerline and surface temperatures during the second pass rolling to experimental measurements for sample no.11.

Appendix C

ROLLING LOAD VALIDATION

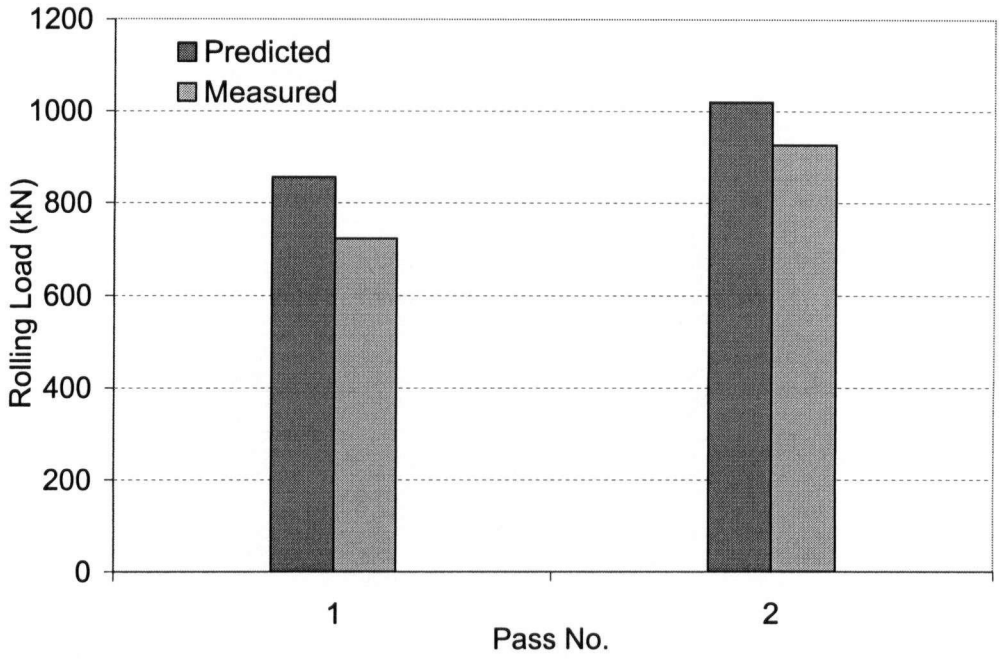

Figure C1.1 – Comparison of model predicted loads during rolling to experimental measurements for sample no. 1.

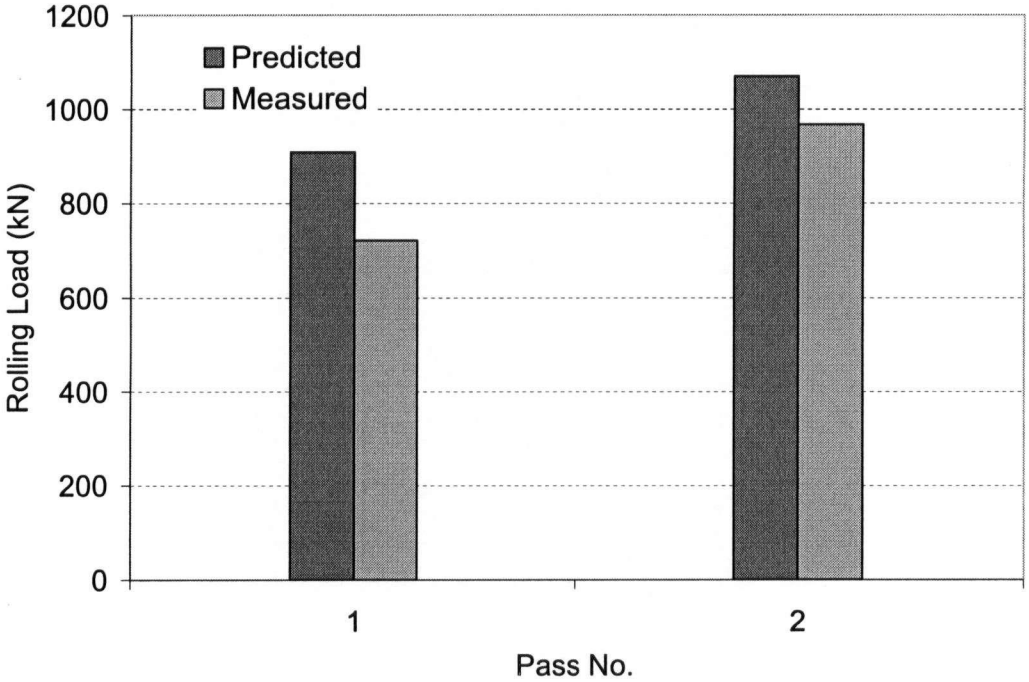

Figure C2.1 – Comparison of model predicted loads during rolling to experimental measurements for sample no. 2.

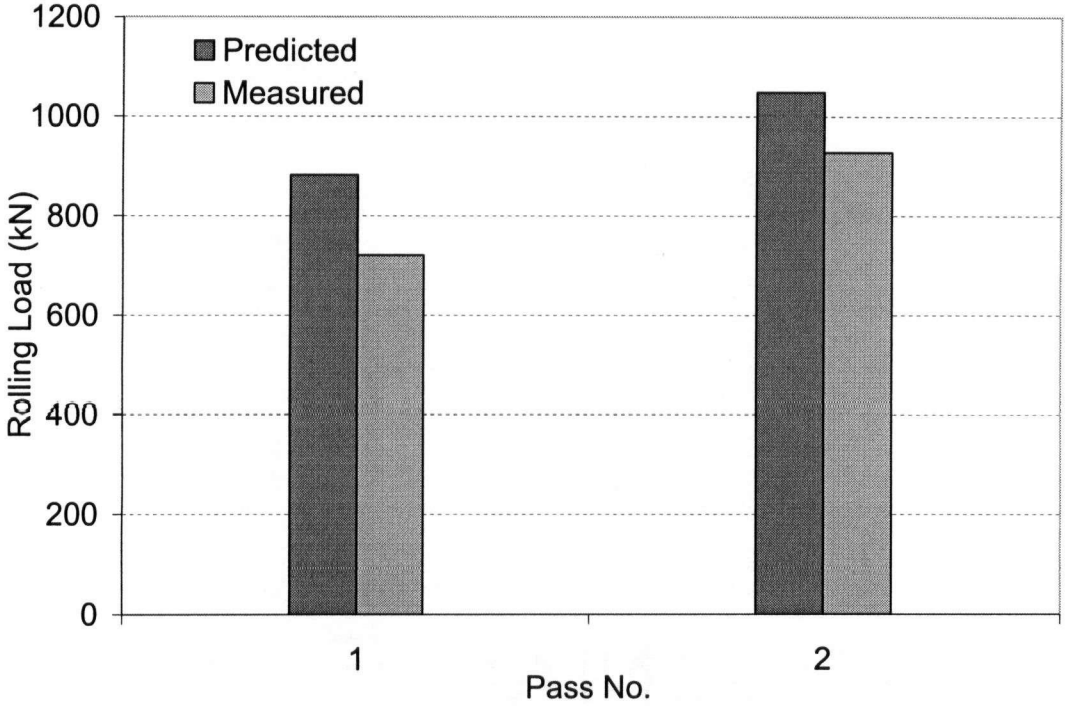

Figure C3.1 – Comparison of model predicted loads during rolling to experimental measurements for sample no. 3.

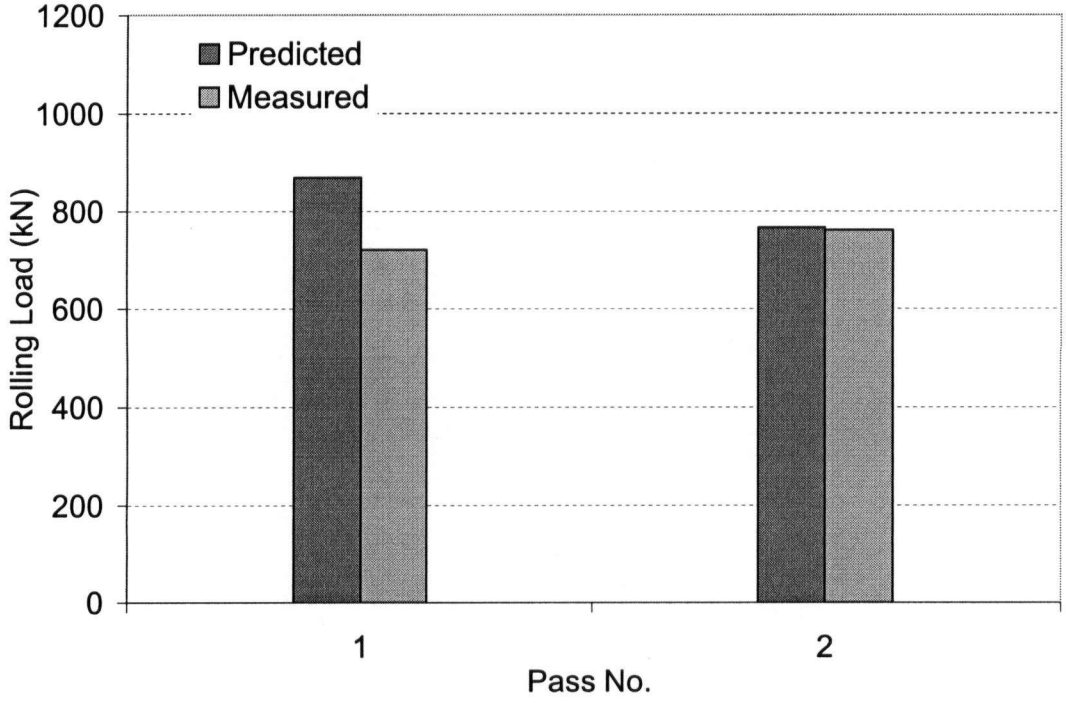

Figure C4.1 – Comparison of model predicted loads during rolling to experimental measurements for sample no. 4.

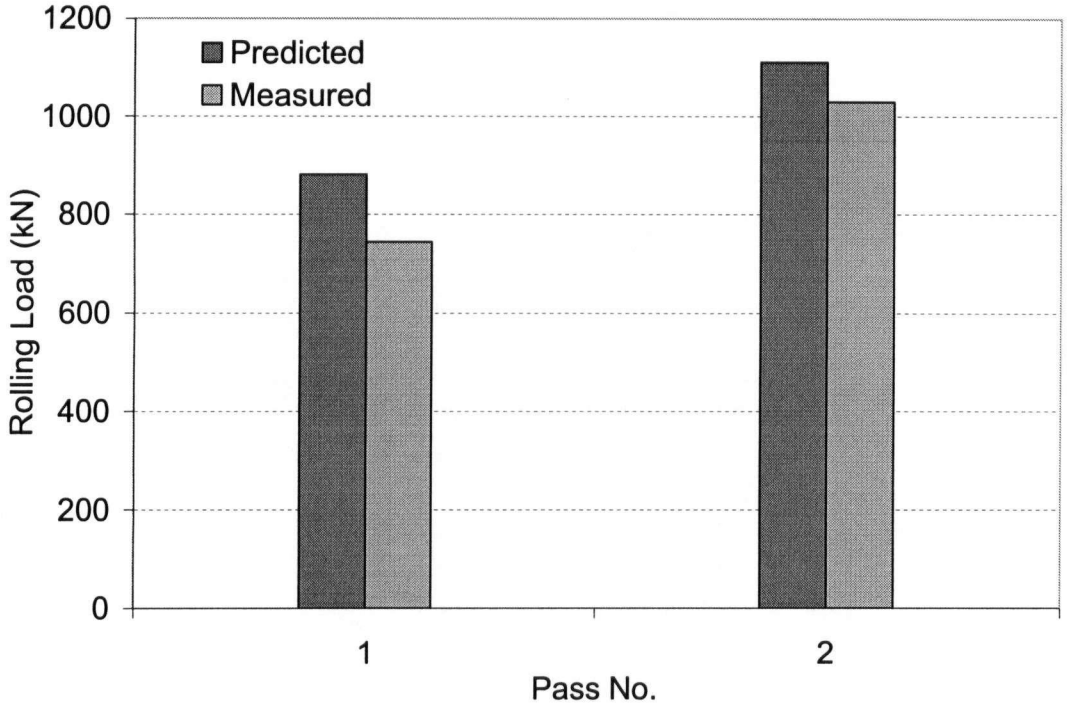

Figure C5.1 – Comparison of model predicted loads during rolling to experimental measurements for sample no. 5.

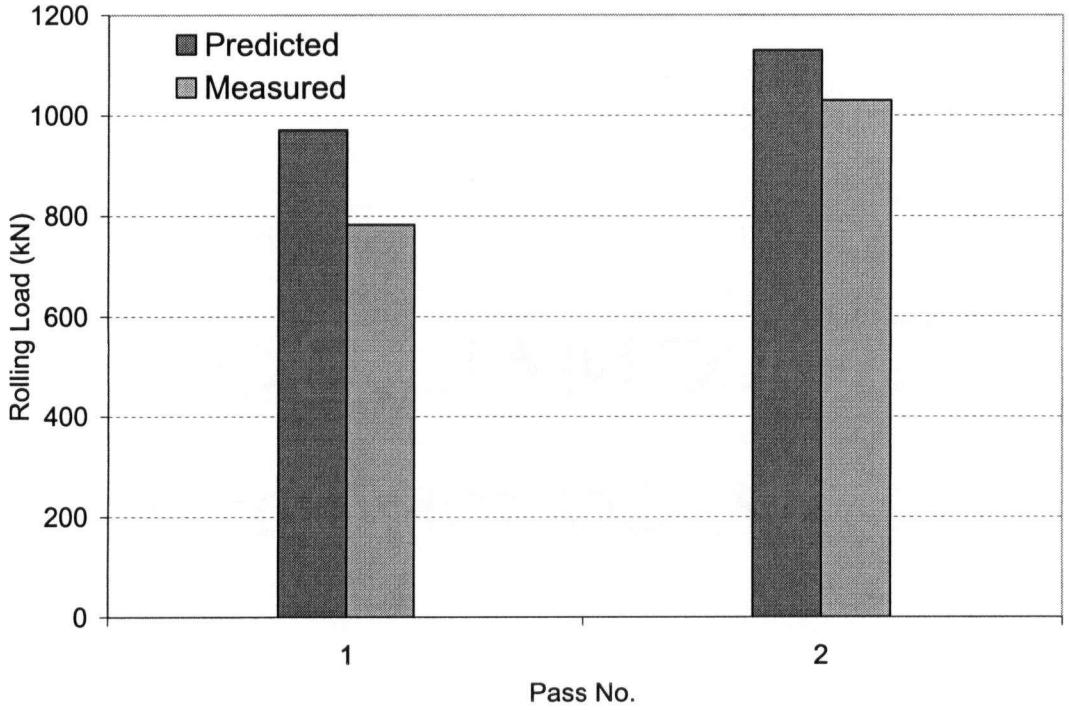

Figure C6.1 – Comparison of model predicted loads during rolling to experimental measurements for sample no. 6.

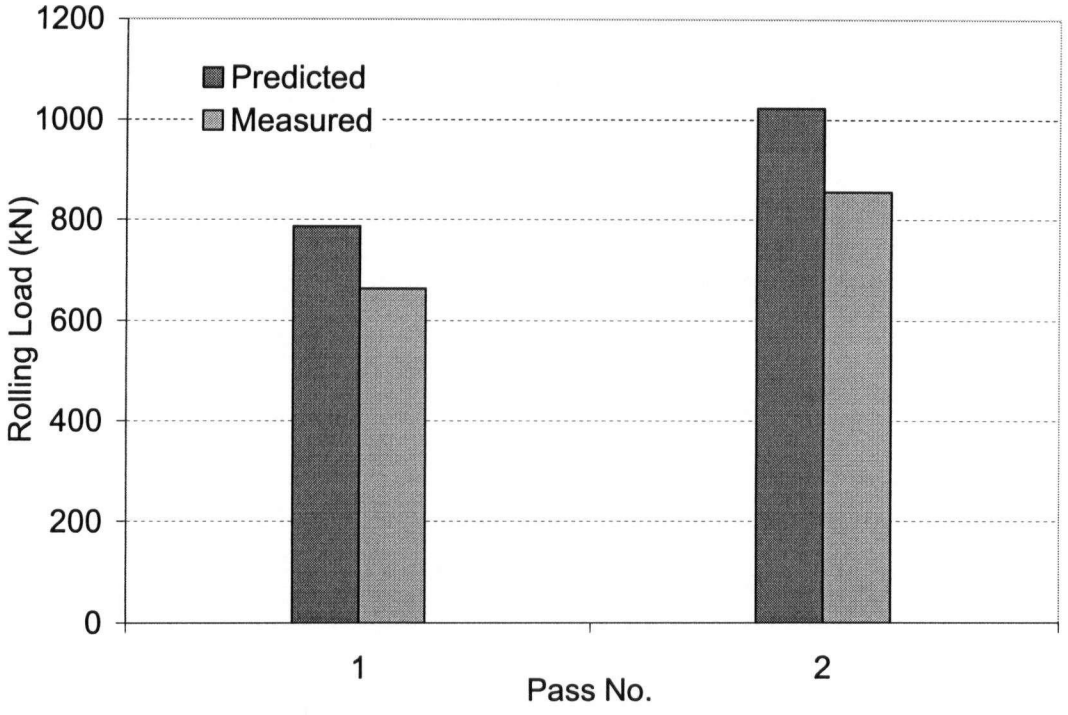

Figure C7.1 – Comparison of model predicted loads during rolling to experimental measurements for sample no. 7.

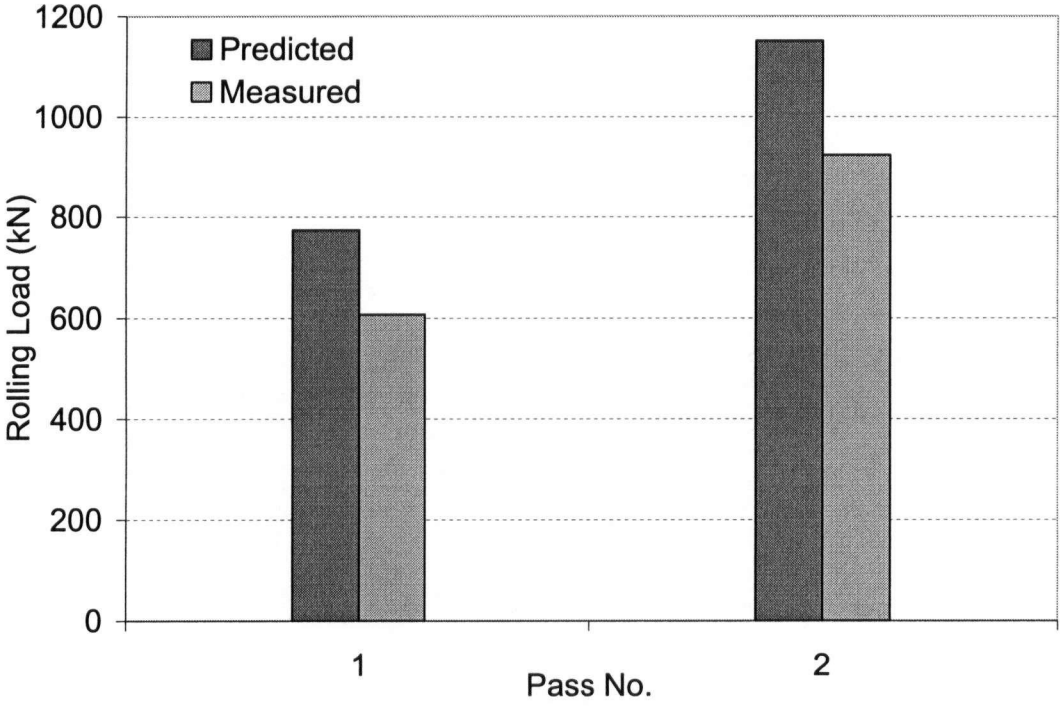

Figure C8.1 – Comparison of model predicted loads during rolling to experimental measurements for sample no. 8.

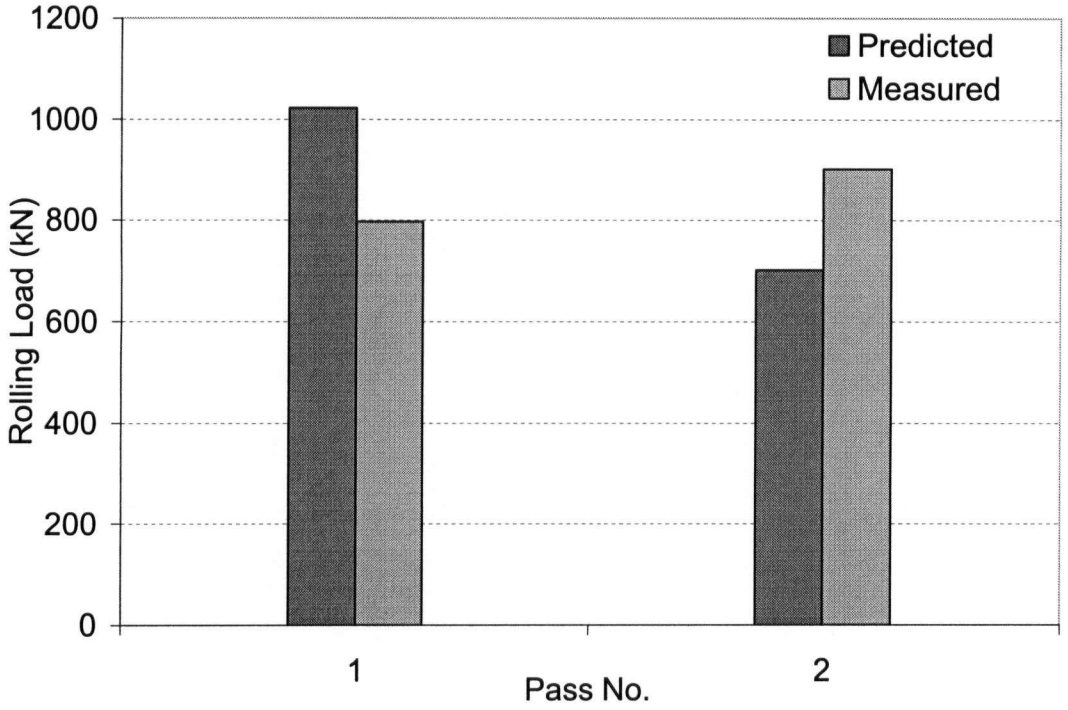

Figure C9.1 – Comparison of model predicted loads during rolling to experimental measurements for sample no. 9.

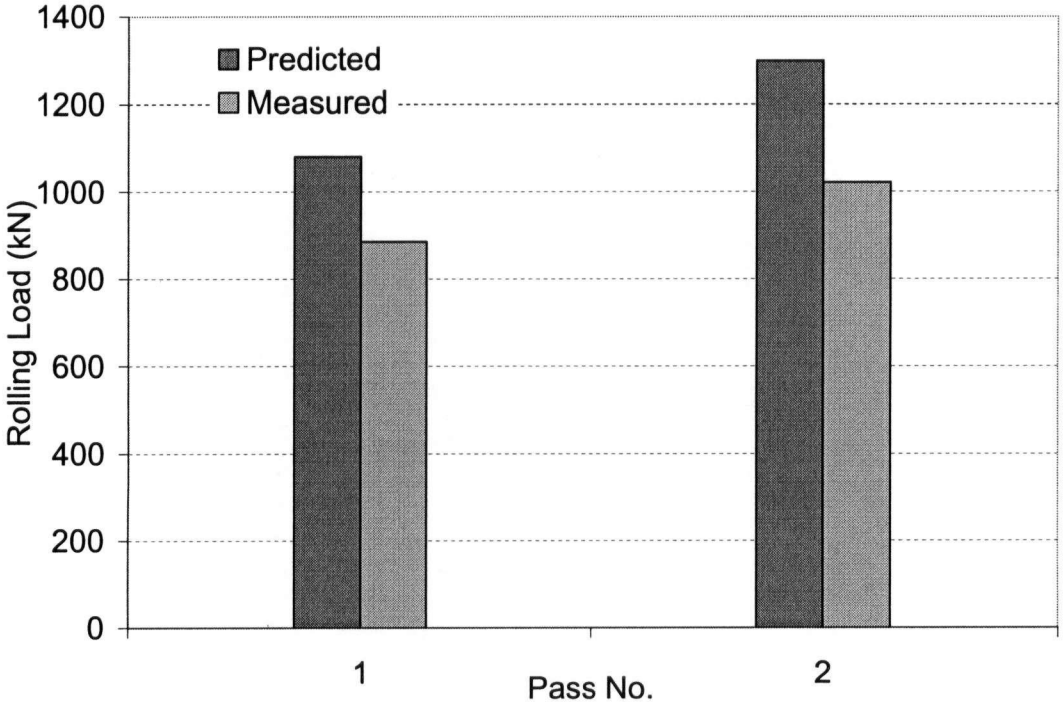

Figure C10.1 – Comparison of model predicted loads during rolling to experimental measurements for sample no. 10.

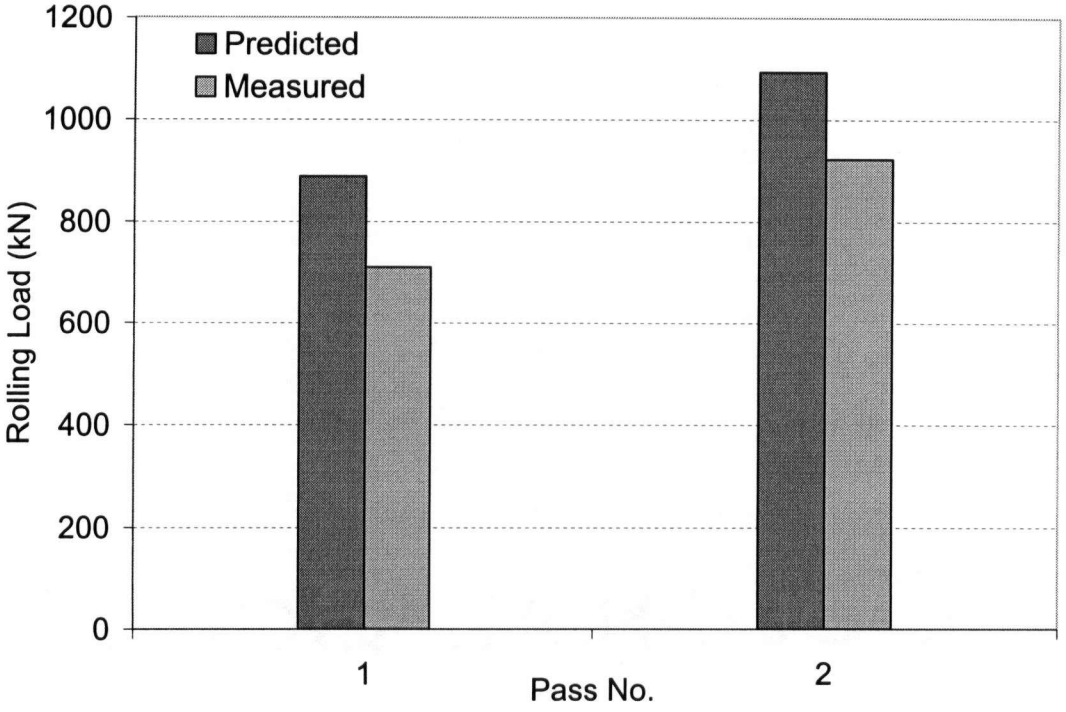

Figure C11.1 – Comparison of model predicted loads during rolling to experimental measurements for sample no. 11.

Appendix D

MICROSTRUCTURE VALIDATION

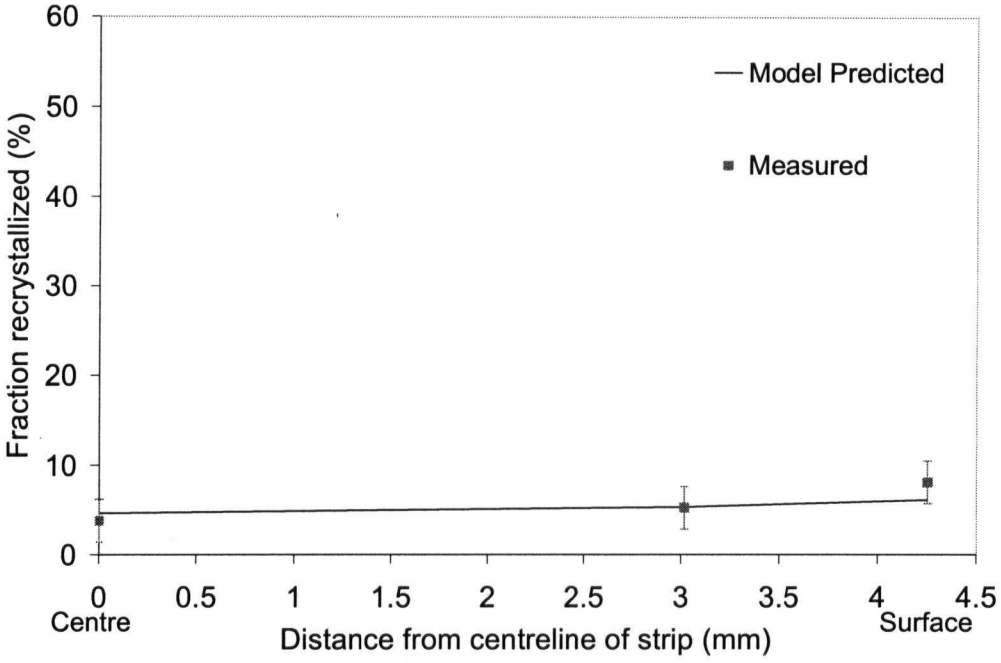

Figure D 1.1 – Comparison of internal state variable model predictions of fraction recrystallized through the thickness of the strip with experimental measurements for sample no. 1.

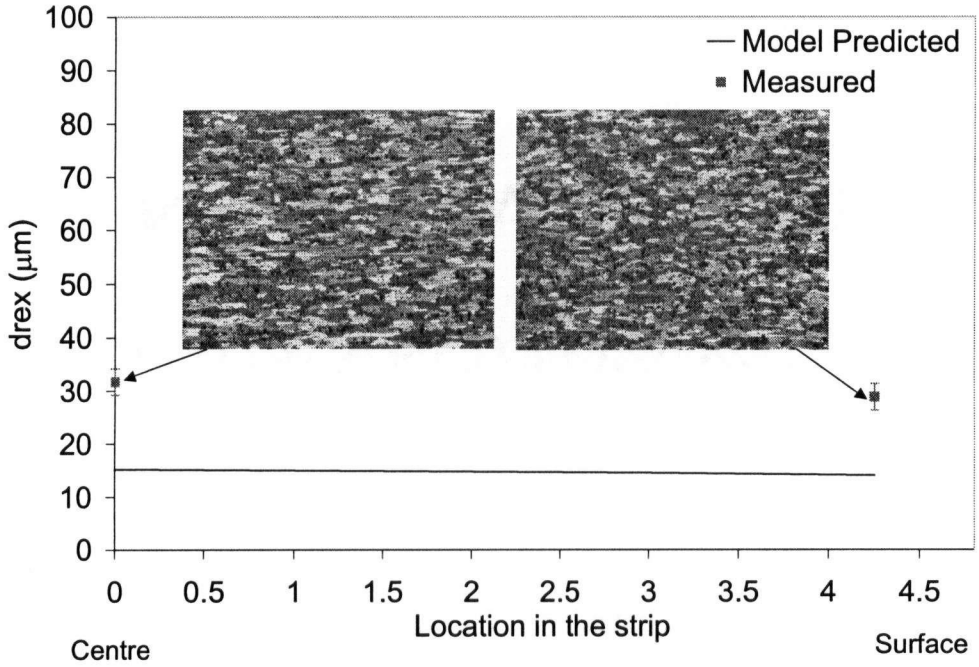

Figure D 1.2 – Comparison of internal state variable model predictions of recrystallized grain size through the thickness of the strip with experimental measurements using image analysis for sample no. 1.

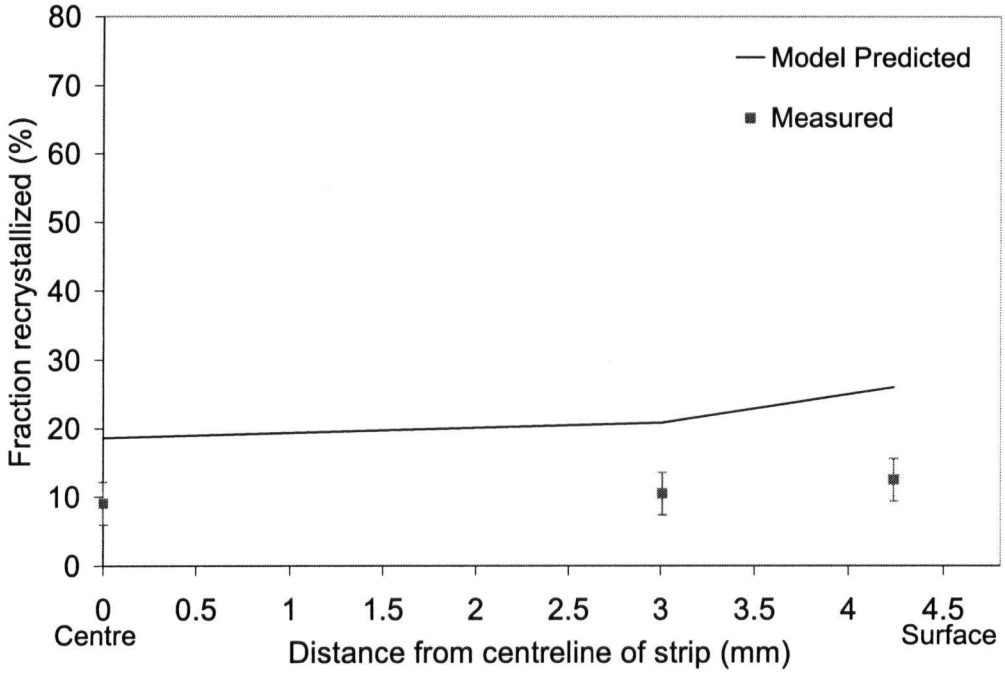

Figure D 2.1 – Comparison of internal state variable model predictions of fraction recrystallized through the thickness of the strip with experimental measurements for sample no. 2.

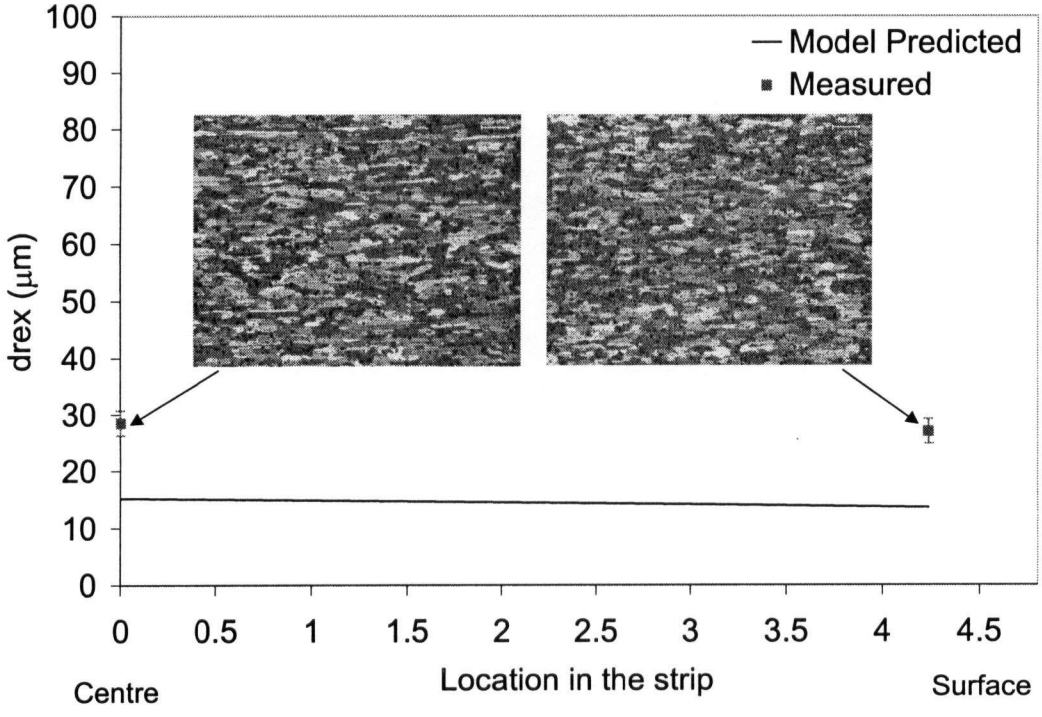

Figure D 2.2 – Comparison of internal state variable model predictions of recrystallized grain size through the thickness of the strip with experimental measurements using image analysis for sample no. 2.

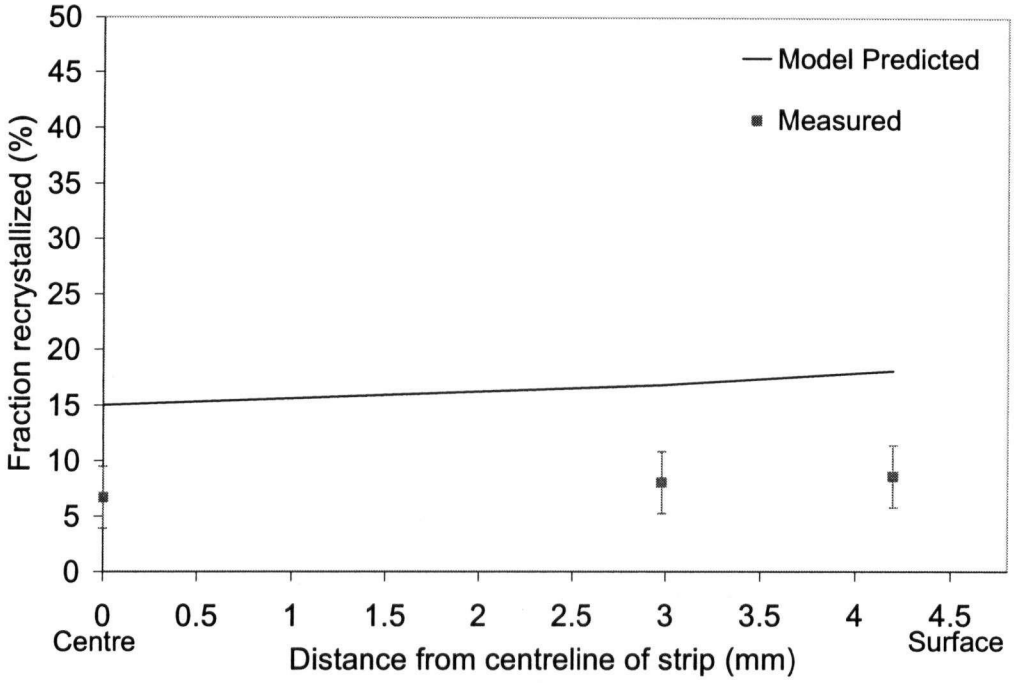

Figure D 3.1 – Comparison of internal state variable model predictions of fraction recrystallized through the thickness of the strip with experimental measurements for sample no. 3.

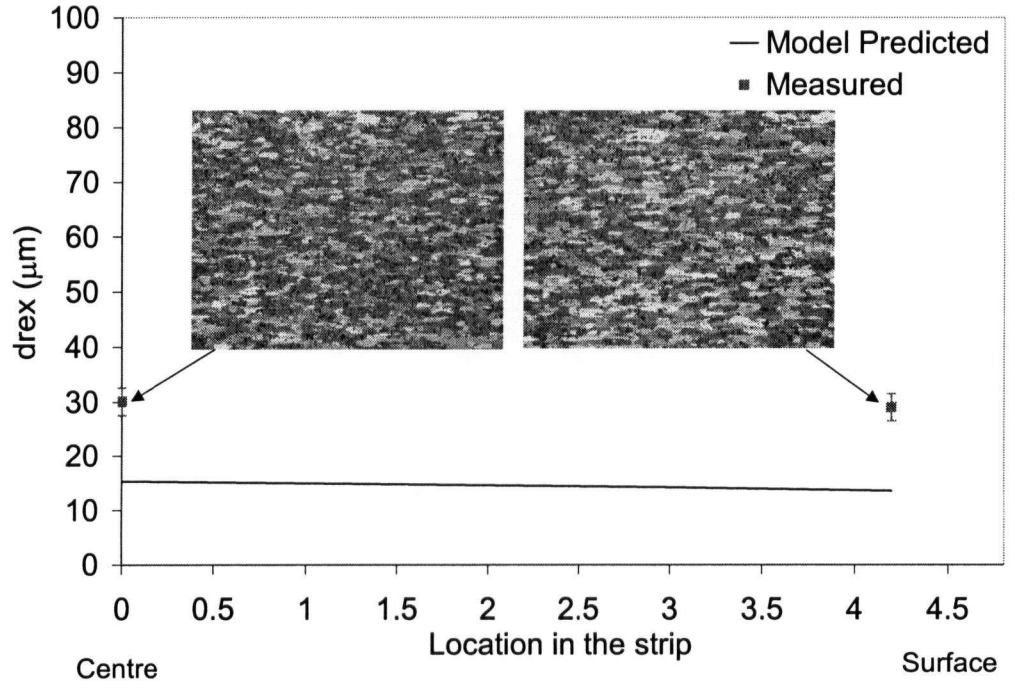

Figure D 3.2 – Comparison of internal state variable model predictions of recrystallized grain size through the thickness of the strip with experimental measurements using image analysis for sample no. 3.

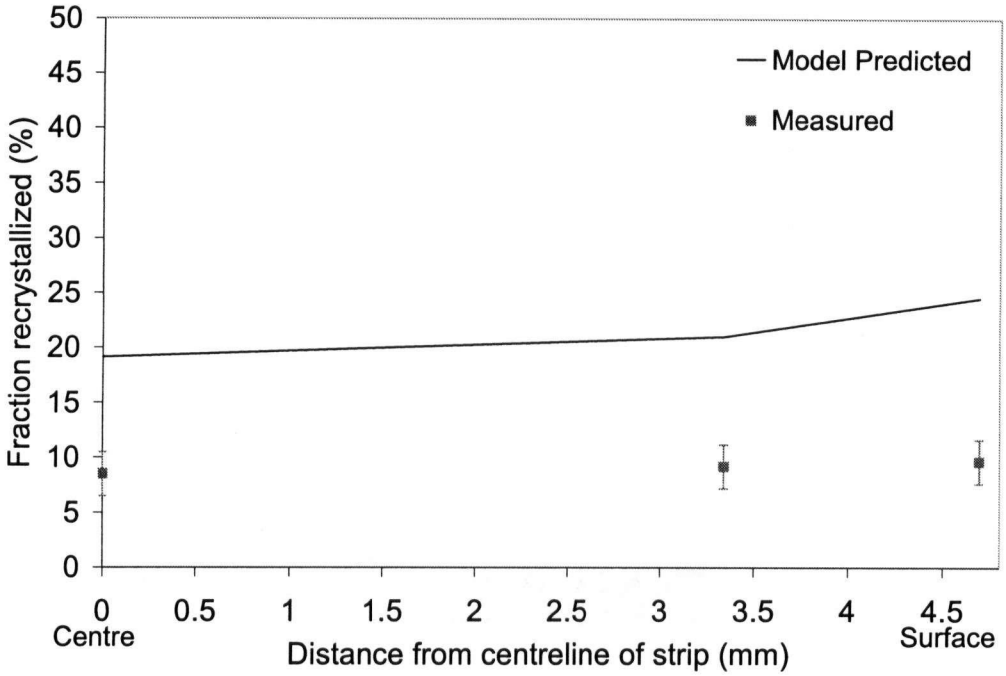

Figure D 4.1 – Comparison of internal state variable model predictions of fraction recrystallized through the thickness of the strip with experimental measurements for sample no. 4.

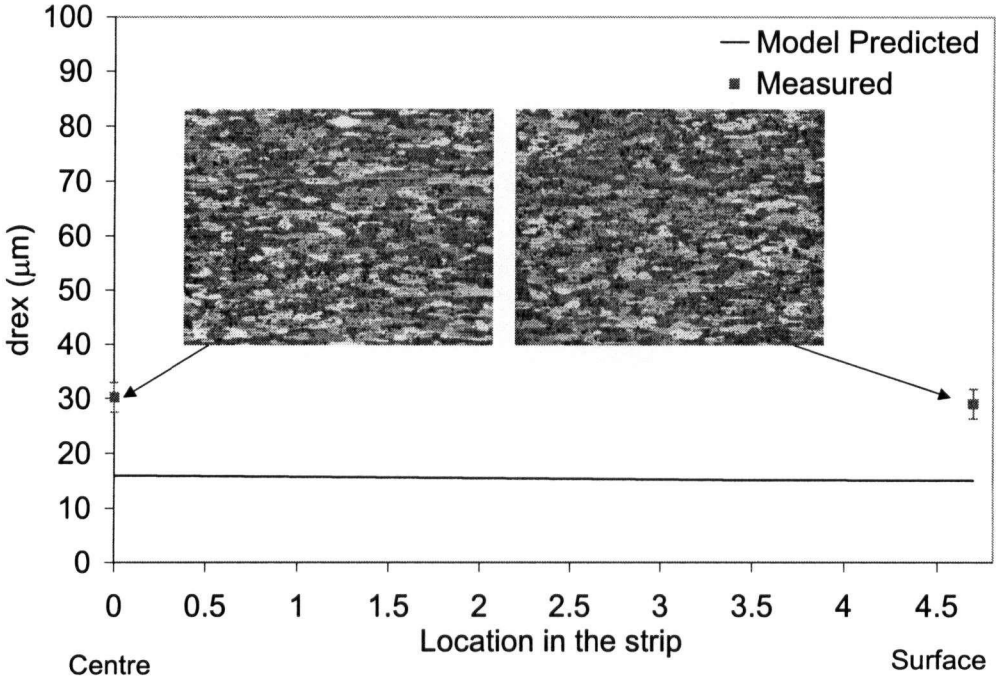

Figure D 4.2 – Comparison of internal state variable model predictions of recrystallized grain size through the thickness of the strip with experimental measurements using image analysis for sample no. 4.

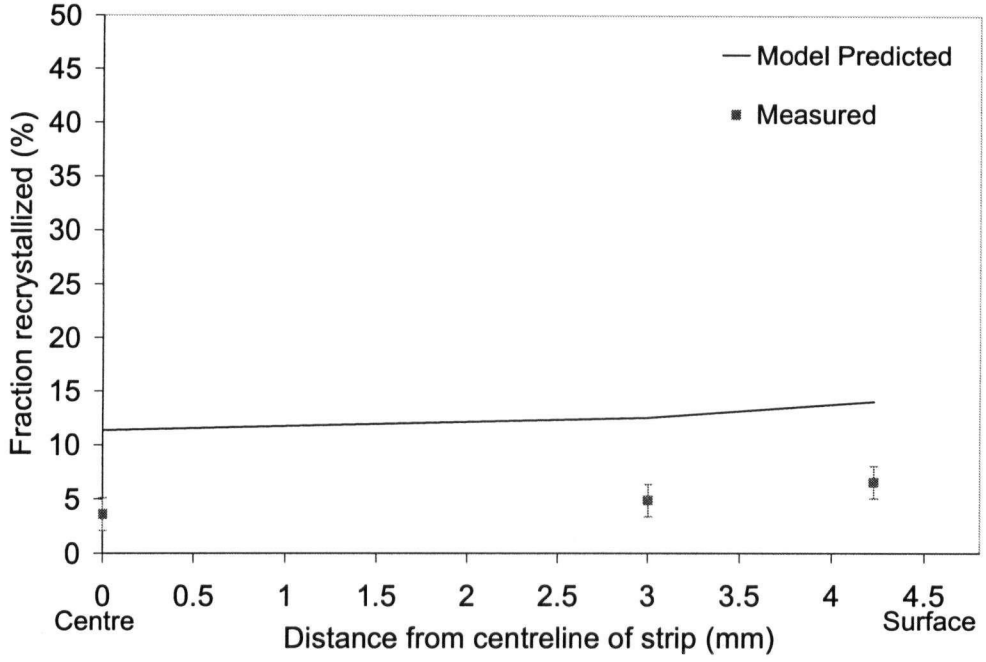

Figure D 5.1 – Comparison of internal state variable model predictions of fraction recrystallized through the thickness of the strip with experimental measurements for sample no. 5.

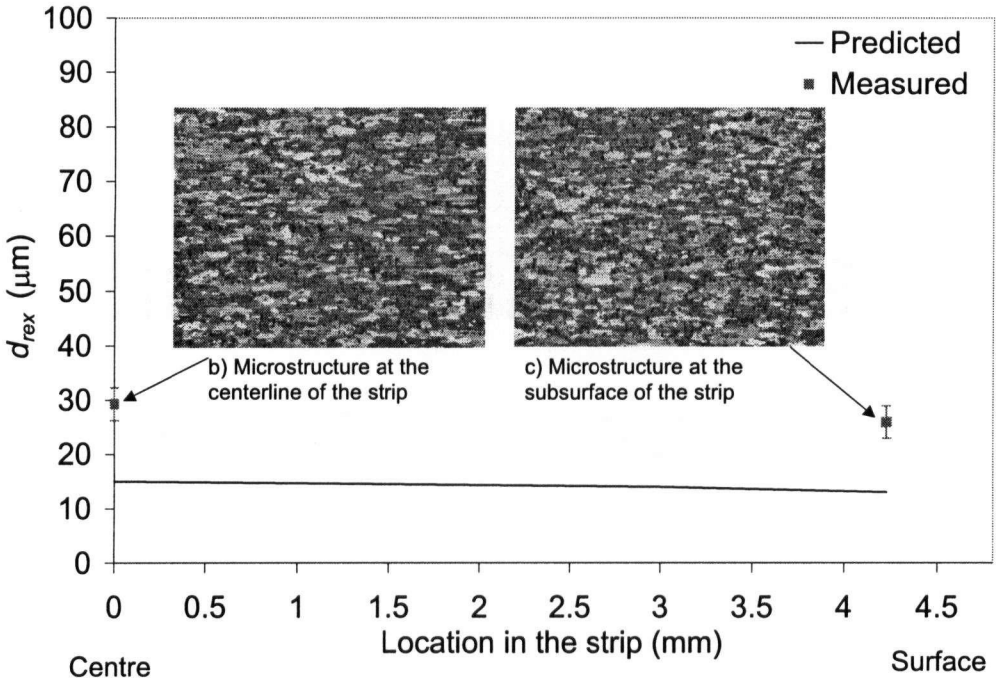

Figure D 5.2 – Comparison of internal state variable model predictions of recrystallized grain size through the thickness of the strip with experimental measurements using image analysis for sample no. 5.

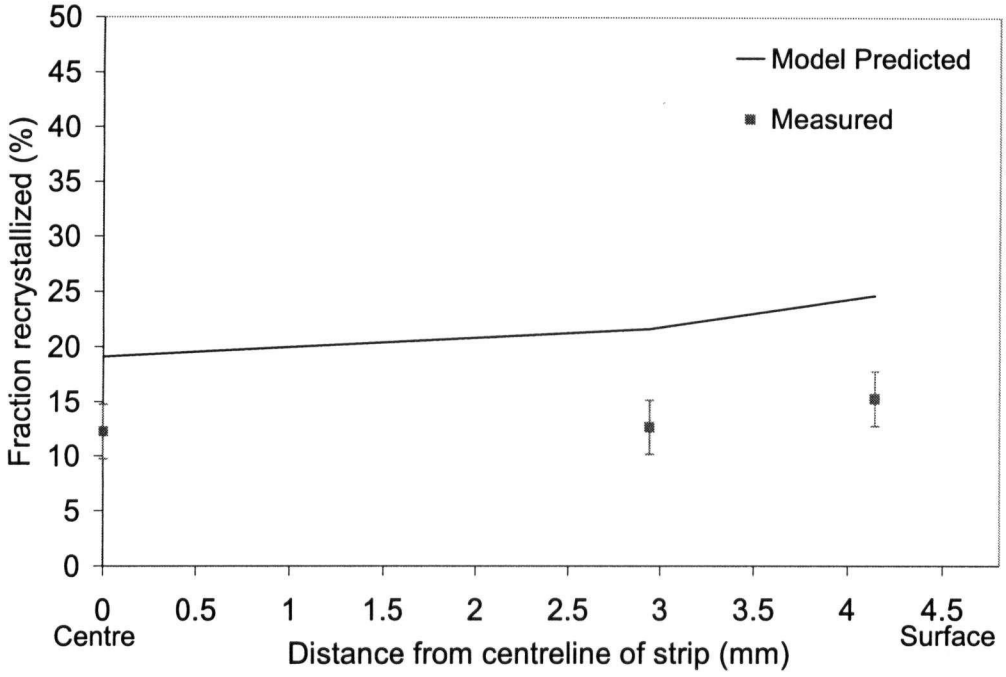

Figure D 7.1 – Comparison of internal state variable model predictions of fraction recrystallized through the thickness of the strip with experimental measurements for sample no. 7.

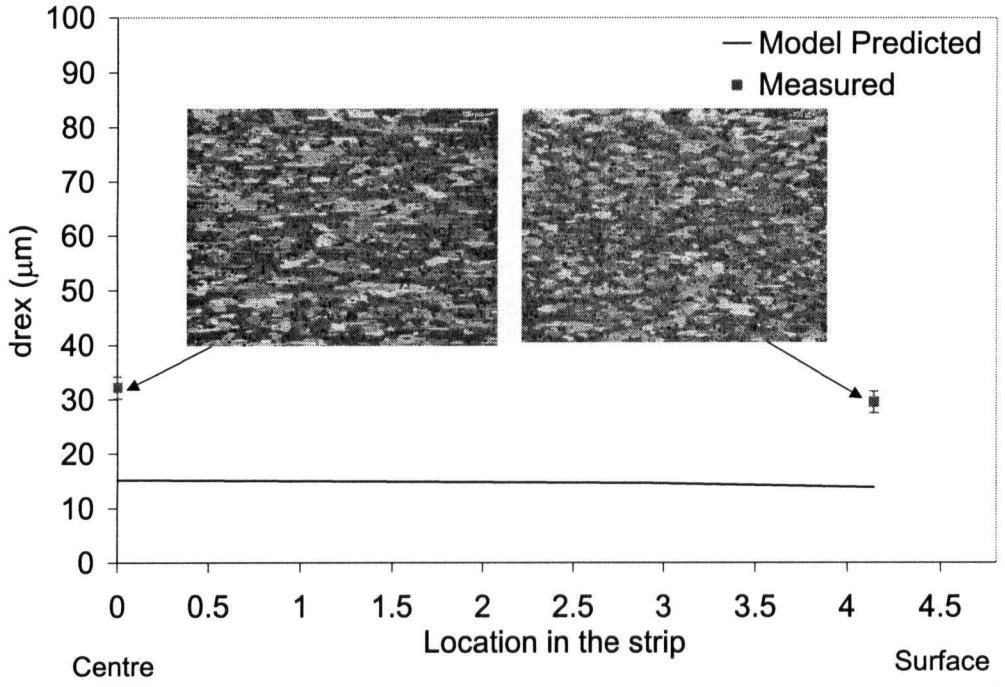

Figure D 7.2 – Comparison of internal state variable model predictions of recrystallized grain size through the thickness of the strip with experimental measurements using image analysis for sample no. 7.

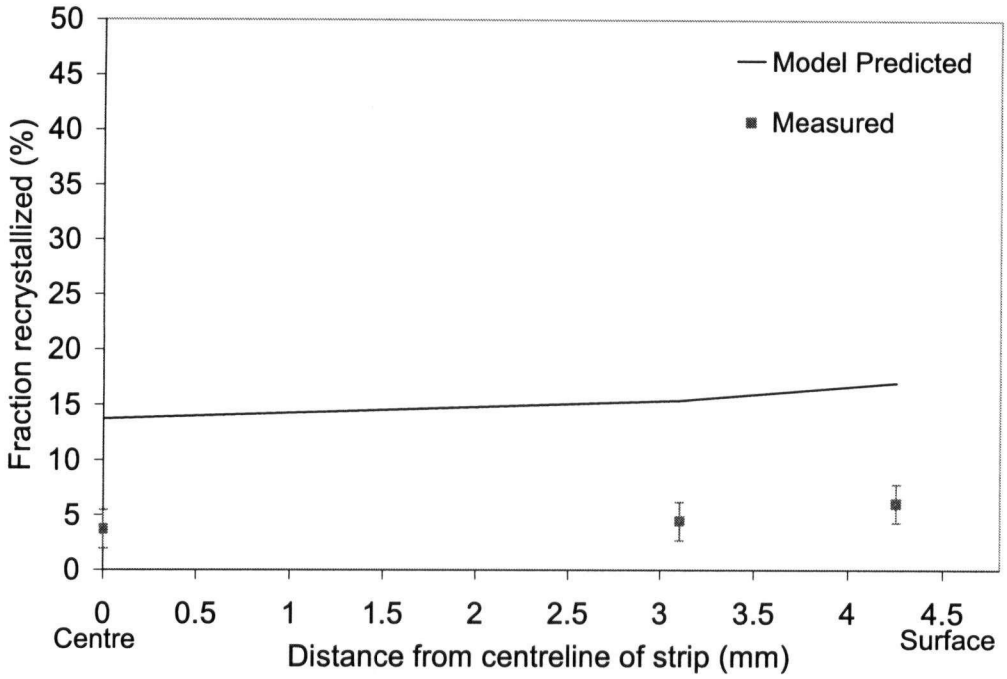

Figure D 8.1 – Comparison of internal state variable model predictions of fraction recrystallized through the thickness of the strip with experimental measurements for sample no. 8.

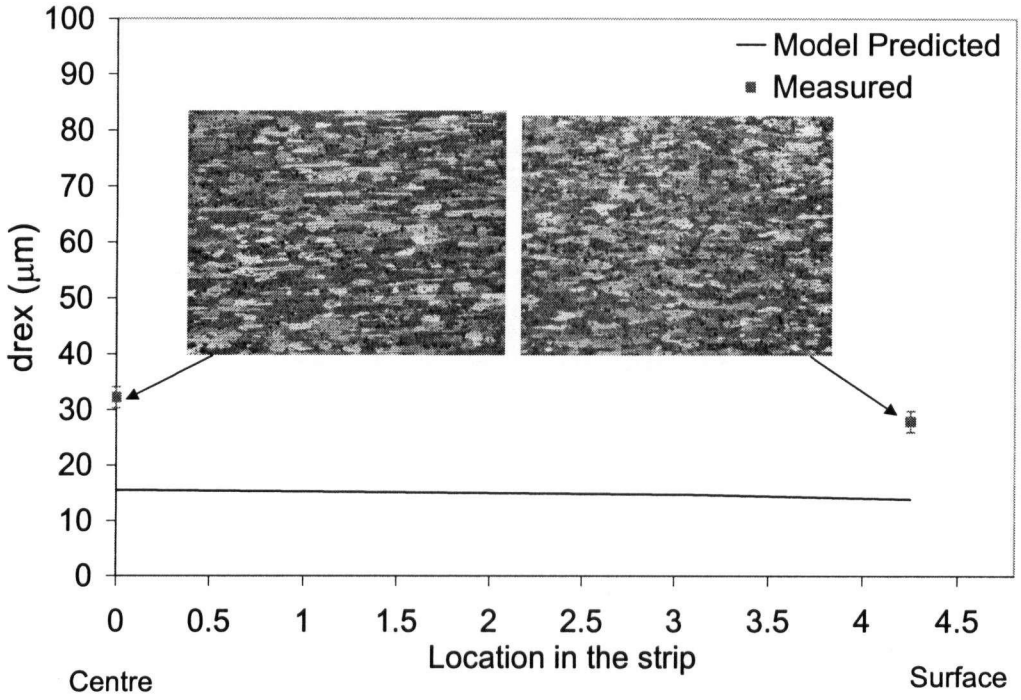

Figure D 8.2 – Comparison of internal state variable model predictions of recrystallized grain size through the thickness of the strip with experimental measurements using image analysis for sample no. 8.

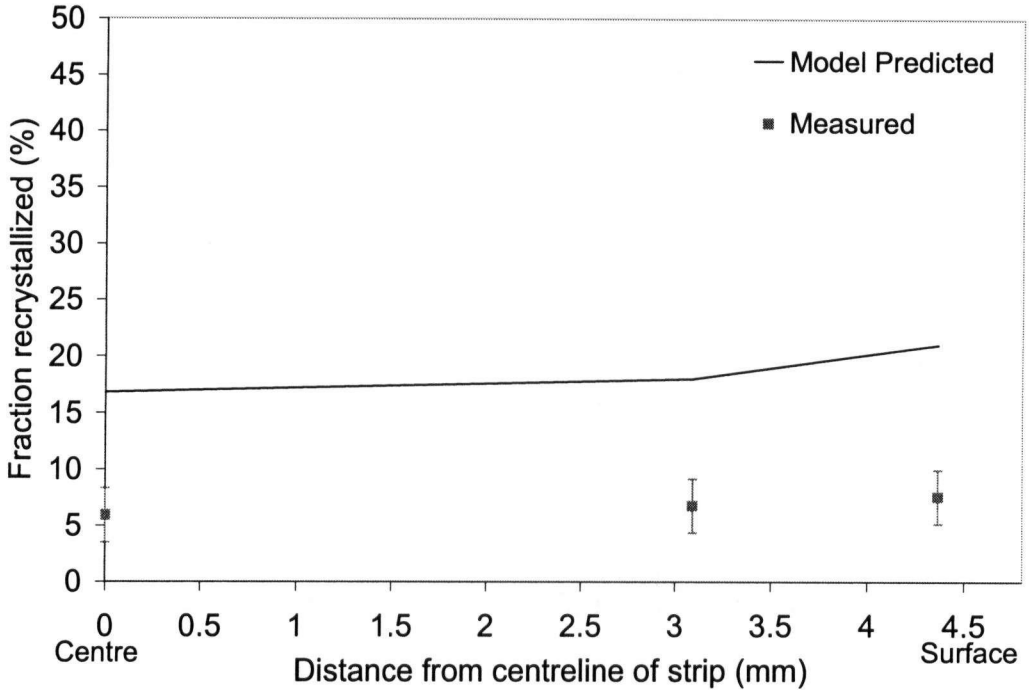

Figure D 9.1 – Comparison of internal state variable model predictions of fraction recrystallized through the thickness of the strip with experimental measurements for sample no. 9.

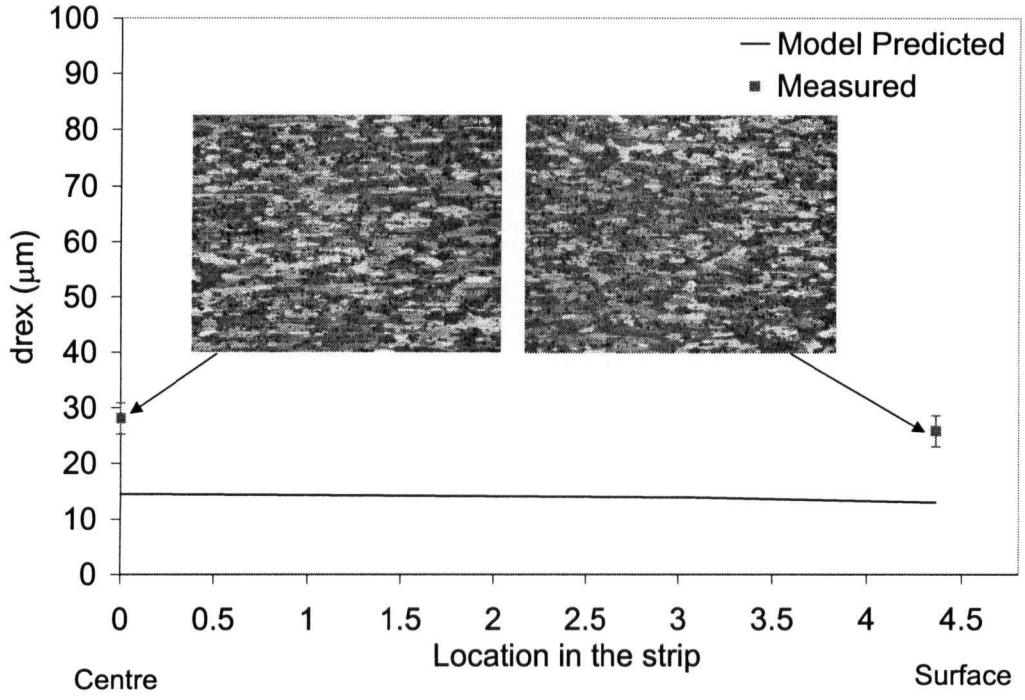

Figure D 9.2 – Comparison of internal state variable model predictions of recrystallized grain size through the thickness of the strip with experimental measurements using image analysis for sample no. 9.

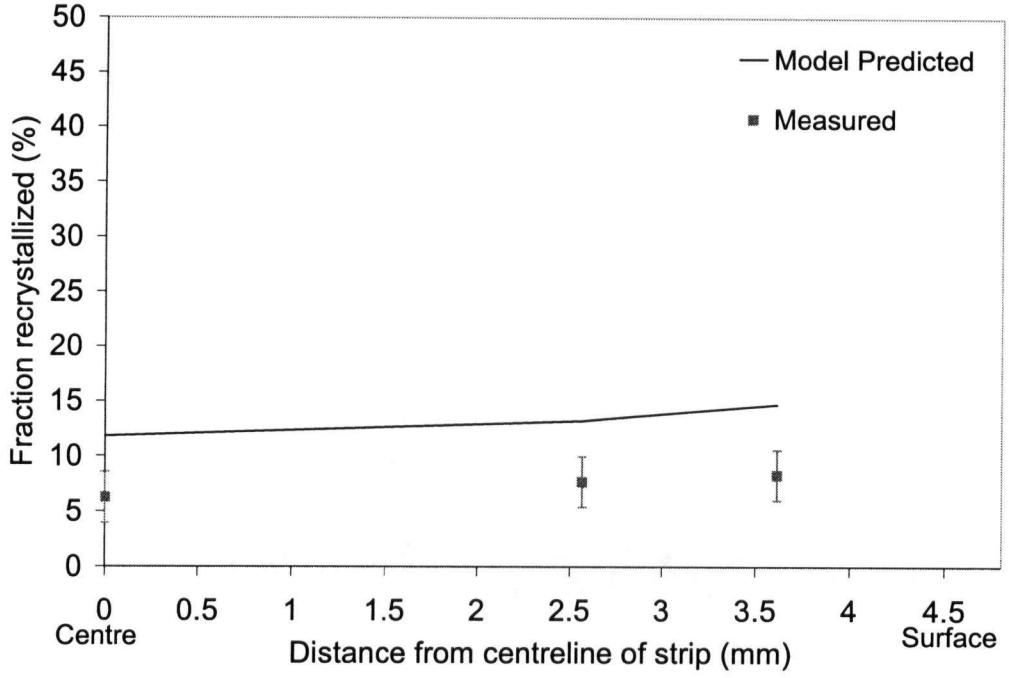

Figure D 10.1 – Comparison of internal state variable model predictions of fraction recrystallized through the thickness of the strip with experimental measurements for sample no. 10.

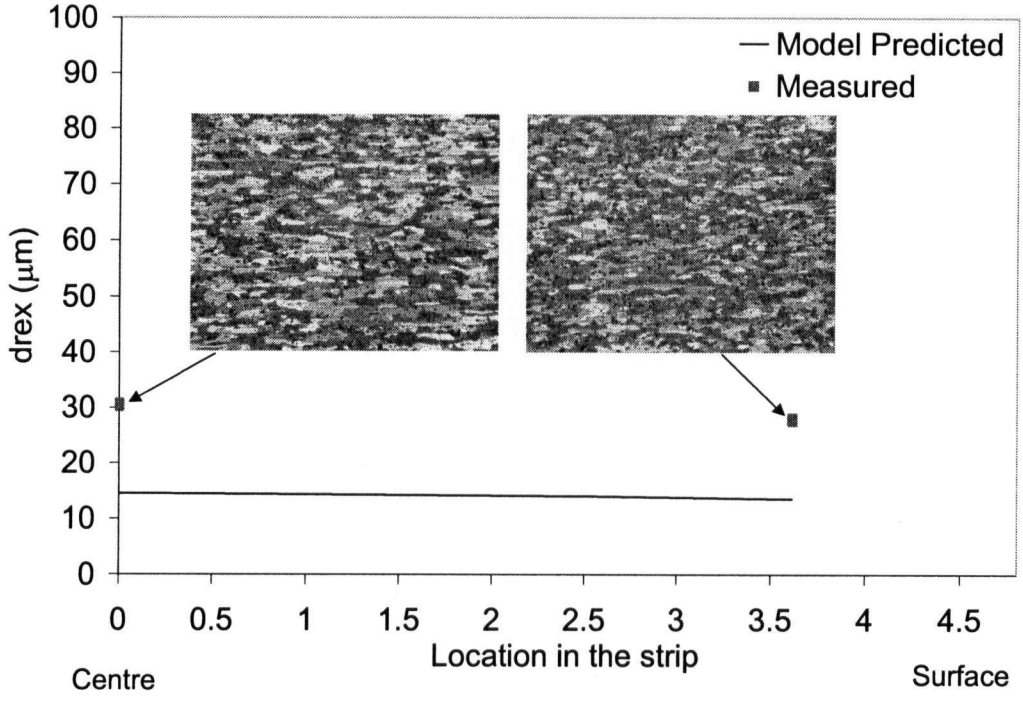

Figure D 10.2 – Comparison of internal state variable model predictions of recrystallized grain size through the thickness of the strip with experimental measurements using image analysis for sample no. 10.

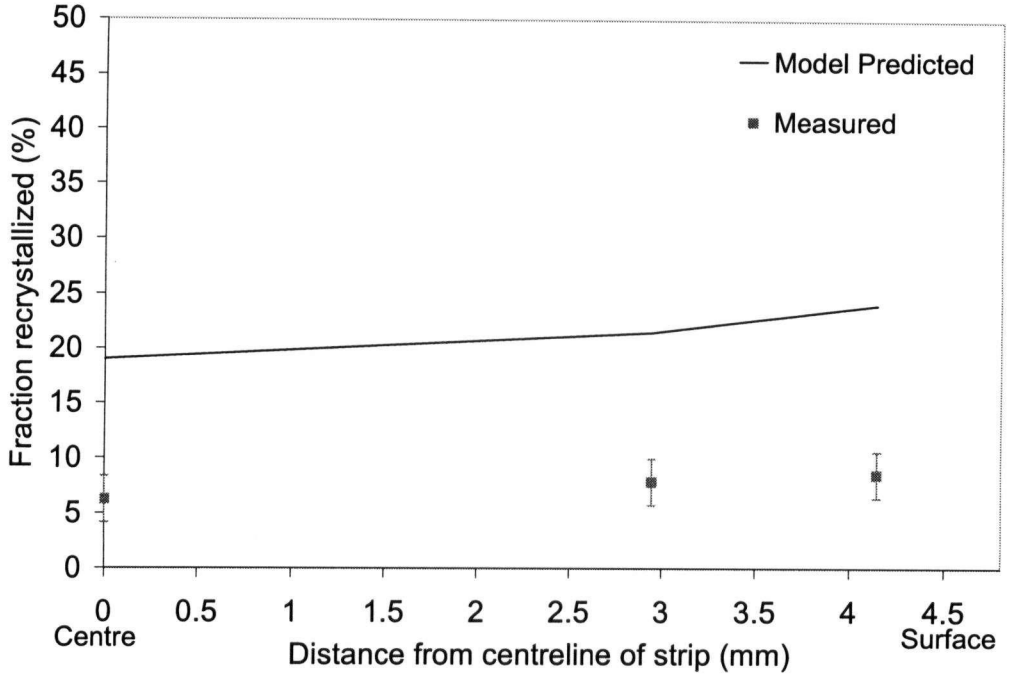

Figure D 11.1 – Comparison of internal state variable model predictions of fraction recrystallized through the thickness of the strip with experimental measurements for sample no. 11.

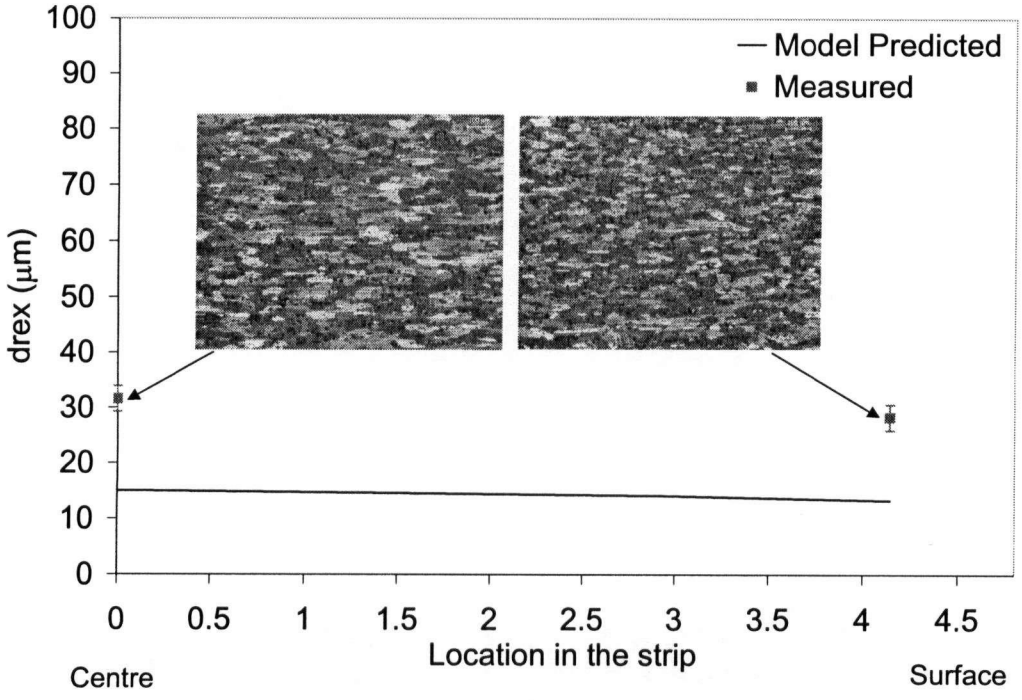

Figure D 11.2 – Comparison of internal state variable model predictions of recrystallized grain size through the thickness of the strip with experimental measurements using image analysis for sample no. 11.